

Exploring the mechanistic effects of life extending treatments on the mTOR network. A combined computational and experimental approach.

Neil William McDonald

Institute for Cell and Molecular Biosciences (ICAMB)

Newcastle University

A thesis submitted in partial fulfillment of the requirements for the degree of

Doctor of Philosophy

August 2018













"Remember to look up at the stars and not down at your feet. Try to make sense of what you see and wonder about what makes the universe exist. Be curious. And however difficult life may seem, there is always something you can do and succeed at. It matters that you don't just give up." – Professor Stephen Hawking
Your future has not been written yet. No one's has. Your future is whatever you make it.
So make it a good one –Doc Brown
Pick your battles and accept yourself for who you are – Chrissie Wellington

Acknowledgements

I would like to thank my supervisor Daryl Shanley for not only giving me the opportunity to carry out this research but also for all the help and support that he has offered me over the course of this project. It has been a pleasure to be part of your group over the last four years.

I would also like to express my gratitude to Ilaria Bellantuono for her continued advice and support throughout this project. Our conversations have always served to be a great source of motivation.

I will forever be grateful to the Centre for Integrated research into Musculoskeletal Ageing (CIMA) and in addition I would like to thank both the Medical Research Council (MRC) and Arthritis research UK for funding this PhD project.

Thank you to all those who helped me with the technical aspects of this project in particular to Juhi Misra, Philip Hall, Nan Wang and Andrew Filby.

A special thank you to all of the people that have made the last four years at Newcastle some of the best years of my life it has been an absolute privilege to know you. In particular a very special thank you goes to Alvaro Martinez Guimera, David Hodgson and Ciaran Welsh for all the laughter and joy that you brought to my life every day for the last four years. I cannot think of three people that I would rather have gone through this experience with.

I would like to thank my family for all the support that you have shown me over the years. In particular to my mum, there are no words of gratitude that can aptly describe what you have done for me. Thank you for always being there through the good and the bad, I could never have done this without you and as words fail me here all I can say is thank you.

Finally I would like to say thank you to my Deepali. When times were hard it was your belief in me that kept me going, you are the light of my life and every day you bring me a joy that cannot be described. I love you.

Abstract

Nitrogen containing bisphosphonates (N-BPs) such as Zoledronate are currently used to treat osteoporosis and act by disrupting the actions of osteoclasts responsible for bone resorbption by inhibiting prenylation. There is a growing body of evidence that these drugs have broader benefits including a reduction of mortality in patients treated with Zoledronate that exceeds the expected benefits conferred from reduced fracture risk alone. Further observations support a role for Zoledronate in longevity. Levels of cellular damage were reduced in a Hutchinson-Gilford progeroid mice model treated with a combination of Zoledronate and Statins. Interestingly, recent evidence that treatment of Zoledronate extends the lifespan of MSCs via inhibition of the mTOR pathway similarly to calorie restriction.

We apply an integrative systems modelling approach informed with data generated using Reverse Phase Protein Arrays to perform an in depth analysis of the response of the mTOR network to three life extending treatments. The hypothesis we test concerns the overlapping response we expect between Zoledronate and starvation-restimulation, whereas we would expect both MRC5 cells and MSC's to respond differently to Rapamycin treatment.

We show that a single model topology is capable of reproducing the data produced by RPPA for three separate life extending treatments in both MRC5 fibroblasts and MSCs. We identify that the activation of the AMPK-mTOR signalling axis is of primary importance in response to both nutrient deprivation and Zoledronate treatment. Furthermore we identify that the regulation of the mTOR network in response to these treatments occurs through two distinct mechanisms. In addition we demonstrate that in response to Rapamycin withdrawal it is the P70S6K negative feedback loop that is of primary importance with regards to mTOR regulation.

This work demonstrates the power of an integrative modelling-experimental approach and suggests that life extending treatments act through distinct mechanisms affecting similar sections of the mTOR network.

Contents

	1. Introduction	1
	1.1 The biology of ageing	3
	1.2 Why do we age?	3
	1.2.1 Evolutionary theories of ageing	4
	1.2.2 Molecular theories of ageing	5
	1.2.3 The hallmarks of ageing	6
	1.3 The mTOR network	7
	1.4 Ageing and the musculoskeletal system	11
	1.4.2 Mesenchymal stem cells and bone ageing	11
	1.4.3 Bisphosphonates, the mevalonate pathway and osteoporosis	12
	1.4.4 Bisphosphonates, cancer treatment and lifespan extension	15
	1.4.5 Role of AMPK in stem cell differentiation and ageing	15
	1.4.6 Osteogenesis links to the mTOR network	16
	1.4.6.1 C/EBPβ isoforms	16
	1.4.6.2 Wnt signalling	17
	1.5 The DNA damage response	18
	1.5.1 The DNA damage response and ageing	18
	1.5.2 Links between mTOR and the DNA damage response	19
	1.6 Systems biology	21
	1.6.1 Top down and bottom up	21
	1.6.2 Dynamic computational modelling	23
	1.6.3 Multiscale modelling	24
	1.6.4 Model simulation - deterministic and stochastic modelling	24
	1.6.5 Computational models of mTOR	25
	1.7 Objectives	27
2.	Materials and methods	29
	2.1 Experimental methodology	31
	2.1.1 General MRC5 cell culture	31
	2.1.2 Cell counting	31
	2.1.3 Thawing MRC5 cells	32
	2.1.4 Freezing and storage of MRC5 cells	32
	2.1.5 General mesenchymal stem cell culture	32
	2.1.6 Defrosting mesenchymal stem cell samples	34

	2.1.7 Freezing and storage of mesenchymal stem cell samples	34
	2.1.8 Lifespan extending treatments	34
	2.1.9 Flow cytometry methodology	38
	2.1.10 Cell fixation	38
	2.1.11 Cell permeabilisation	40
	2.1.12 Cell staining	40
	2.1.13 Cell permeabilisation imagestream	40
	2.1.14 Cell staining imagestream	41
	2.1.15 Reverse phase protein array preparation.	41
	2.1.15 Reverse phase protein array procedure	42
	2.2 Systems biology dynamic modelling	46
	2.2.1 SBGN and SBML	48
	2.2.2 Parameter estimation	48
	2.2.3 Pycotools	50
	2.2.4 Statistics	50
3.	A comparison of methodologies for the production of dynamic model calibration data	51
	3.1 Introduction	53
	3.2 Aims and objectives	54
	3.3 Reverse phase protein arrays	54
	3.4 Reverse phase protein array produces consistent time course data suitable for dynamic	
	modelling	55
	3.5 Intracellular flow cytometry	62
	3.6 Intracellular flow cytometry fails to provide consistent data suitable for dynamic	62
	modelling	
	3.7 Discussion	
1	3.8 Conclusions	
	A dynamical model of the mTOR signalling network reveals the kinetics of starvation and imulation in MRC5 fibroblasts and human bone marrow stem cells	
	4.1 Introduction	
	4.2 Aims	76
	4.3 Results	77
	4.3.1 Development of starvation-restimulation dynamic network model	77
	4.3.2 Reverse phase protein array provides a high quality calibration dataset	
	4.3.3 Parameter estimation	
	4.3.4 Constant AMPK activation prevents parameterisation of the model	84

4.3.5 Parameterisation of the 4E-BP1_pS65 observable requires a more in depth mTORC modelling approach	
4.3.6 Modelling the difference between MRC5 and MSC kinetics in response to starvation restimulation	
4.3.7 Fit results	97
4.4 Image flow cytometry fails to show correlation between DAPI –FOXO3A and Rheb-LAMP1	99
4.5 Discussion	104
A dynamical model of the mTOR signalling network reveals the kinetics of rapamycin an e-stimulation in MRC5 fibroblasts and human bone marrow stem cells	
5.1 Introduction	109
5.2 Aims	. 110
5.3 Results	. 111
5.3.1 Development of a rapamycin dynamic network model	. 111
5.3.2 Collection of MRC5 calibration dataset	. 113
5.3.3 Parameter estimation	. 116
5.3.4 Restimulation following rapamycin treatment is dependent upon P70S6K negative feedback	. 116
5.3.5 Restructured S6K feedback loop results in an improved fit	. 119
5.3.6 The removal of PDK1 dataset provides the closest fit between experimental and theoretical outputs	. 122
5.3.7 Parameterisation of the PTEN 4E-BP1_activity requires a more in depth mTORC1	
5.3.8 Modelling the difference between MRC5 and MSC kinetics in response to rapamyci	in-
5.3.10 Starvation-restimulation and rapamycin withdrawal lead to similar responses in MS but not MRC5 cells	SC
5.4 Image flow cytometry fails to show correlation between DAPI –FOXO3A and Rheb-LAMP1	. 137
5.5 Discussion	. 141
A dynamical model of the mTOR signalling network reveals the kinetics of zoledronate at	
6.4 Results	151
	Modelling approach

	6.4.1 Development of a zoledronate dynamic network model	151
	6.4.2 Utilising RPPA to produce a calibration dataset following zoledronate treatment	.155
	6.4.3 Zoledronate treatment of MRC5 cells results in cell death at 1μM	.155
	6.4.4 Treatment of MRC5 cells with 0.01 µM zoledronate followed by nutrient re-stimular results in clear dynamic signalling profiles.	
	6.4.5 Parameter estimation	.162
	6.4.6 Existing model is capable of fitting MRC5 dataset in response to zoledronate withdrawal	162
	6.4.7 Modelling difference in MRC5 and MSC	167
	6.4.8 Pycotools analysis reveals similar parameter constraints for both MRC5 and MSC parameter estimations	170
	6.4.9 Hooke and Jeeves	.174
	6.5 A comparison between zoledronate withdrawal and starvation-restimulation and rapamycin withdrawal.	178
	6.6 Image flow cytometry fails to show correlation between DAPI –FOXO3A and Rheb-LAMP1	
	6.7 Discussion	.187
7.	Discussion	.191
	7.1 Summary	.193
	7.1.1 Summary of key findings	.193
	7.2 Key study observations	.194
	7.2.1 Reverse phase protein arrays provide a high quality medium through-put alternative western blotting	
	7.2.2 Dynamic modelling reveals the importance of AMPK signalling in response to starvation-restimulation in MRC5 fibroblasts but not MSCs	195
	7.2.3 mTOR signalling following rapamycin withdrawal is dependent upon the P70S6K negative feedback loop	196
	7.2.4 Zoledronate withdrawal leads to an activation of the AMPK signalling pathway in MSCs but not MRC5 cells	. 197
	7.2.5 Imagestream	.198
	7.3 Limitations and future study	.199
	7.3.1 Technical	.199
	7.3.2 Computational	.200
	7.3.3 Biological	.201
	7.4 Research impact	.202
8.	Bibliography	.203

List of figures

- Figure 1.1: Schema representing the mTOR network.
- Figure 1.2: Stem cells and ageing.
- Figure 1.3: Schema representing the DNA damage response pathways interacting with FOXO3A.
- Figure 1.4: Schema representing Top down vs Bottom up in systems biology.
- Figure 2.1: Zeptosen Micro-Chip staining apparatus.
- Fig 2.2: System Biology dynamic modelling workflow.
- Figure 3.1: RPPA is capable of producing calibration time course data for a dynamic model.
- Figure 3.2: Alkaline phosphatase treatment reveals the level of non-specific binding for each antibody.
- _pS65.Figure 3.4 Alkaline phosphatase treatment can determine the level of non-specific binding between separate antibodies for the same protein. Figure 3.5 Treatment with 50μM of Torin1 leads to a reduction in mTORC1 pS2448 signalling.
- Figure 3.6 Intracellular flow cytometry is capable of producing calibration time course data for a dynamic model for S6_pS235/236.
- Figure 3.7 Insulin treatment enhances the capable of Intracellular flow cytometry to produce calibration time course data for a dynamic model for S6_pS235/236
- Figure 4.1: The mTOR network.
- Figure 4.2: Measuring the Kinetics of the mTOR Network in MRC5 Cells.
- Figure 4.3: Expanded Measurements of mTOR Network Kinetics in MRC5 Cells.
- Figure 4.4: Time course simulations from the model compared to re-stimulation data.
- Figure 4.5: Parameter time course simulations following the removal of ACC_pS79 from the MRC5 dataset.

- Figure 4.6: Parameter time course simulations following the removal of mTORC1_pS2448 from the MRC5 dataset.
- Figure 4.7: Time course simulations from the model compared to re-stimulation data with updated ACC starting concentration.
- Figure 4.8: Individual parameter estimation for the 4E-BP1 pS65 observable.
- Figure 4.9: A comparison of MRC5 vs MSC outputs for SS
- Figure 4.10 Time course simulations from the model compared to re-stimulation data utilizing the local Hooke and Jeeves algorithm.
- Figure 4.11 Genetic vs Hooke and Jeeves fit for MSC.
- Figure 4.12 AK Parameter time course simulations following the removal of AKT_pT308 from the MSC dataset.
- Figure 4.13: Image flow cytometry fails to show correlation between DAPI –FOXO3A and Rheb-LAMP1.
- Figure 4.14: Image flow cytometry time course correlation
- Figure 5.1: The mTOR network.
- Figure 5.2: Measuring the Kinetics of the mTOR Network in MRC5 Cells.
- Figure 5.3: Time course simulations from the model compared to re-stimulation data.
- Figure 5.4: Restructured PI3K-IRS1 topology.
- Figure 5.5: Time course simulations from the model compared to re-stimulation data using updated IRS1-PI3K topology.
- Figure 5.6: Akaike information criterion (AIC) score vs RSS.
- Figure 5.7: Parameter time course simulations following the removal of ACC_pS79 from the MRC5 dataset.
- Figure 5.8: Parameter time course simulations following the removal of PDK1_pS241 from the MRC5 dataset.

- Figure 5.9: Parameter time course simulations following the removal of mTORC1_pS2448 from the MRC5 dataset.
- Figure 5.10 Individual parameter estimations for the PTEN_pS380_T382_T383 and 4E-BP1_pS65 observables.
- Figure 5.11: Measuring the Kinetics of the mTOR Network in MSC Cells.
- Figure 5.12: A comparison of MRC5 vs MSC outputs following Rapamycin withdrawal.
- Figure 5.13: Time course simulations from the model compared to re-stimulation data utilizing the local Hooke and Jeeves algorithm.
- Figure 5.14: Genetic vs Hooke and Jeeves fit for MSC.
- Figure 5.15: A comparison of mTOR kinetics following Rapamycin withdrawal and starvation-restimulation in MRC5 and MSC cells.
- Figure 5.16: Image flow cytometry fails to show correlation between DAPI –FOXO3A and Rheb-LAMP1.
- Figure 5.17: Image flow cytometry time course correlation.
- Figure 6.1: Immuno-blotting data examining AKT phosphorylation.
- Figure 6.2: The mTOR network.
- Figure 6.3: The effect of Zoledronate on the mTOR network.
- Figure 6.4: Measuring the kinetics of the mTOR network in MRC5 cells.
- Figure 6.5: Imagestream flow cytometry reveals cell death in MRC5 cells.
- Figure 6.6: Zoledronate cell death assay.
- Figure 6.7: Measuring the dynamics of the mTOR network in MRC5 cells.
- Figure 6.8: Time course simulations from the model compared to Zoledronate withdrawal data in MRC5 cells.
- Figure 6.9: Time course ensemble for top 10 genetic algorithm parameter estimations in MRC5 cells.

- Figure 6.10: Parameter Variation in MRC5 Cells.
- Figure 6.11: Measuring the Kinetics of the mTOR Network in MSC Cells.
- Figure 6.12: A comparison of MRC5 vs MSC outputs following Zoledronate withdrawal.
- Figure 6.13: Time course ensemble for top 10 genetic algorithm parameter estimations in MSC cells.
- Figure 6.14: Parameter Variation in MSCs.
- Figure 6.15: Parameter variation between MRC5 and MSC cells.
- Figure 6.16: Time course simulations from the model compared to re-stimulation data utilizing the local Hooke and Jeeves algorithm.
- Figure 6.17: Genetic vs Hooke and Jeeves fit for MSC.
- Figure 6.18: A comparison of mTOR kinetics following Zoledronate withdrawal and starvation-restimulation in MRC5 and MSC cells.
- Figure 6.19: A comparison of mTOR kinetics following Zoledronate withdrawal and Rapamycin withdrawak in MRC5 and MSC cells.
- Figure 6.20: Image flow cytometry fails to show correlation between DAPI –FOXO3A and Rheb-LAMP1.
- Figure 6.21: Image flow cytometry time course correlation.

List of tables

- Table 2.1: Life extending treatment overview.
- Table 2.2: Timecourse data points for flow cytometry datasets.
- Table 2.3: Time course data points for Reverse Phase Protein Array datasets.
- Table 3.1: A comparison of possible protein analysis platforms
- Table 4.1: Reverse Phase Protein Array Antibodies.
- Table 4.2: Residual sum of squares value for each model.
- Table 4.3: Image flow cytometry time course correlation.
- Table 5.1: Reverse Phase Protein Array Antibodies.
- Table 5.2: Residual sum of squares value for each model.
- Table 5.3: Image flow cytometry time course correlation.
- Table 6.1: Reverse Phase Protein Array Antibodies
- Table 6.2: Residual sum of squares value for each model.
- Table 6.3: Image flow cytometry time course correlation

Abbreviations

TOR - Target of Rapamycin

mTOR - mammalian target of Rapamycin

mTORC1 - mammalian target of Rapamycin complex 1

mTORC2 - mammalian target of Rapamycin 2

IRS1 - Insulin receptor subunit 1

SH2 - src-homology-2

PI3K - Phosphoinosital kinase 3

PDK1 - phosphoinositide-dependent kinase 1

AKT/PKB – Protein kinase B

TSC1/2 - tuberous-sclerosis complex

P70S6K - Ribosomal protein S6 kinase beta-1

S6 – Ribosomal protein S6

FOXO3A - Forkhead box 03

RAPTOR - Regulatory-associated protein of mTOR

RICTOR - Rapamycin-insensitive companion of mammalian target of rapamycin

PTEN - Phosphatase and tensin homolog

PRAS40 - proline-rich Akt substrate of 40 kDa

GSK3ß - Glycogen synthase kinase 3 beta

GAP - GTPase activating protein

GDP - Guanosine-5'-diphosphate

GTP - Guanosine-5'-triphosphate

Rheb - Ras homolog enriched in the Brain

RAG A -Ras related GTPase A
RAG B -Ras related GTPase B
LRP1 - Low density lipoprotein receptor-related protein 1
SGK1 - serum- and glucocorticoid-induced protein kinase 1
C/EBP1 - CCAAT/enhancer binding protein
MSC - mesenchymal stem cells
FPP - farnesyl pyrophosphate
GGPP - geranyl-geranylpyrophosphate
AMPK - AMP activated protein kinase
ACC - acetyl-CoA carboxylase 1
LKB1 - Liver kinase B1
eIF-4E - eukaryotic translation initiation factor 4E
4E-BP1 - eukaryotic translation initiation factor 4E binding protein 1
DDR – DNA damage response
UV – Ultra violet radiation
ODE – ordinary differential equations
RSS - residual sum of squares
DMEM - Dulbecco's Modified Eagle Medium
PBS - phosphor buffered saline solution
DMSO - Dimethyl sulfoxide
PFA - para-formaldehyde

RPPA - reverse phase protein array

BB1 – Zeptosens blocking buffer 1

 $CLB1-Zeptosens\ spotting\ buffer\ 1$

CAB1 – Zeptosens assay buffer 1

SGBN - Systems Biology Graphical Notation

SBML - Systems Biology Mark-up Language

1. Introduction

1.1 The biology of ageing

Ageing is defined and characterised by the progressive decline of function of cells and tissues within an organism over time [1]. More people are living to old age and elderly people represent a greater proportion in our populations [2]. There is clearly a need to enhance our understanding of the biology of ageing and apply this knowledge to address the needs of the elderly and society as a whole. The field of ageing research is growing rapidly and our understanding of how we age and what mechanisms contribute to age related disease is increasing [3]. However there is a need to synthesis our fragmented knowledge and most importantly to establish ways to utilize both the knowledge we have already gathered and the knowledge we will gather in the future in order to ensure that we age healthier. Although ageing research is a field of interest in its own right the majority of applied research has focused on specific age-related diseases such as cancer and Alzheimer's [4, 5]. This research has focused on underlying mechanisms of these diseases their treatment rather than the prevention of the disease themselves. It is only in recent years with an increased understanding of ageing as a primary driver of these diseases that the focus has begun to shift towards prevention. By investigating how we age and how these various pathologies progress it is believed that we can identify interventions for each disease that may prevent or delay their onset allowing us to live healthier for longer [6, 7]. This chapter will present a summary of the main theories of ageing, the hallmarks of ageing and how they apply to the musculoskeletal system. It will also review the TOR network and its key role in the ageing process with a particular focus on its relationship to the pathogenesis of osteoporosis.

1.2 Why do we age?

This is a question that has interested scientists for thousands of years, why do we age? With the odd exception, organisms of all species show signs of ageing [8]. However how they age varies hugely. To understand this variation we must address fundamental questions such as why is it that a human has a lifespan of around 80 years whilst wild mice have an average lifespan of 1 year [9, 10]? Why have such differences evolved and why did they evolve in this way? A number of theories have been proposed to answer these questions with the most prominent being the Disposable Soma theory[11].

1.2.1 Evolutionary theories of ageing

There have been a number of theories proposed to explain why we age. One of the first theories proposed was that of 'programmed' ageing [3]. This theory is based on the principle that through the process of natural selection a 'biological clock' was developed in order to act as mechanism of death removing the elderly and infirm from the population [12]. This theory implies that it is the genetic code of an organism that is responsible for ageing, just as it is for development, and that our lifespan is therefore already at least in part pre-defined by our DNA [13]. This theory is however flawed as it relies upon the premise that natural selection is capable of exerting the same effect on the evolution of a species regardless of an organism's age. However as very few individuals live long enough in the wild for ageing to occur, there is therefore no opportunity for natural selection to act effectively and for genes to evolve that can induce programmed ageing [14-16]. Further to this whilst there have many genes found to have either a beneficial or deleterious effect on ageing, as in the nematode worm *C. elegans*, there are as yet no known gene combinations that result in the ablation of the ageing process [1, 7].

An early theory based on evolutionary principles was that of the mutation accumulation theory put forward by Peter Medawar [17]. Medawar proposed that whilst natural selection would be too weak to act on genes in aged individuals genetic mutations in an individual's germline could be inherited by future generations. If these mutations adversely affected the lifespan of a species and brought about the ageing phenotype, natural selection would not be able to act to eradicate these mutations. Huntington's disease is an age-related disease that fits the principles of mutation accumulation: carriers of a mutant huntingtin gene live normally through their reproductive lives and therefor the gene may be transmitted despite suffering serious neurological disease from mid-life [18]. A further theory proposed by George Williams is based on the pleiotropic activity of genes that have beneficial effects early in life but are harmful with age [19]. This is called the antagonistic pleiotropy theory. Williams proposed genes related to enhancing calcium availability as an example: in early life strong bones lead to higher vigour and evolutionary fitness but in later years can present problems with osteoarthritis. More recently genes such as p53 have been associated with antagonistic pleiotropy with benefits in early life to protect against unchecked growth but being proageing in late life by increasing levels of apoptosis.

The final and perhaps the most accepted evolutionary theory of ageing presented to date is the Disposable Soma theory [20]. The basis of the disposable soma theory is that an organism has a finite amount of metabolic resources available and in adult life must partition how much energy is spent on repair and maintenance compared to the amount of energy expended on reproduction. The organism is therefore faced with a 'trade-off' where an organism will sacrifice its ability to repair and maintain its genome in order to reproduce. Mice provide a clear example: as stated above 90% of wild mice die in the first year of their lives [21]. This is predominantly due to hyperthermia; it makes sense therefore for mice to allocate the majority of their energy resources into thermogenesis and reproduction instead of the energy demanding repair mechanisms in order to ensure the best chance of survival [22] [10]. Without sufficient repair mechanisms in place, damage will accumulate in the mouse leading to the onset of ageing [23]. Another disposable example used to support the soma theory is guppy predation/reproduction rates [24]. When observed in an environment with high levels of predation and subsequently a high extrinsic mortality rate guppy fish display faster maturation rates and increased neuromuscular performance at a young age when compared to low predation guppies [25]. A comparison of age related mortality between high predation guppy fish introduced into a low predation environment and those occurring naturally in a low predation environment revealed increased mortality at younger ages for the high predation population [26]. This suggests that in a high predation environment guppy fish have evolved to mature faster in order to ensure a maximum reproductive lifespan however this results in increased mortality at a decreased age compared to low predation guppy fish. This provides further support for the disposable soma theory by highlighting a trade-off in resources in guppy fish whereby high predation leads to increased reproduction at the expense of longevity.

1.2.2 Molecular theories of ageing

Evolutionary theories of ageing focus on the question of 'why we age'. The associated question of 'how we age' is addressed by theories which focus on the molecular mechanisms of ageing. These theories can often be used in conjunction with evolutionary theories (in particular the disposable soma theory). Many theories of molecular mechanisms of ageing have been proposed with the most prominent being, the somatic mutation theory, the telomere loss theory and the mitochondrial theory.

The somatic mutation theory is based on the idea that throughout an organism's life, cells are exposed to hazards that cause damage to constituent macromolecules such as DNA which if unrepaired will accumulate and it is this damage that drives ageing. This theory is in line with the disposable soma theory in that there is a direct link between the DNA repair ability within an organism and its lifespan. Indeed the better the repair mechanisms then the longer lived the organism [27].

The second of the molecular ageing mechanisms is the telomere loss theory. This theory is based on the end replication problem which results in the loss of base pairs from the telomeres following each cellular replication. The loss of telomeres leads to cellular senescence and apoptosis and is thought to be a key driver of ageing [28]. The loss of telomeres has been found to be exacerbated by levels of oxidative stress which cause lesions within telomeres promoting faster loss on division [29] [30]. Telomere shortening however is not so relevant in tissues where cells are largely post-mitotic and do not divide.

The third molecular mechanism is the mitochondrial theory. Mitochondria often described as the powerhouses of the cell as they provide the energy required for cellular processes [31, 32]. As with genomic DNA the number of mutations present in mitochondrial DNA increases with age resulting in dysfunction and a decrease in the production of energy for the cell with age [33, 34].

Each of these evolutionary and molecular theories have their merits and their flaws and it could be argued to some length which one is correct. For the purposes of what follows it will be assumed that the disposable soma theory provides the most comprehensive answer as to why we age. Whilst there is agreement and disagreement amongst ageing researchers as to what causes ageing it should be noted that there are some factors that are seen as being central to ageing biology theory. These have become known to ageing researchers as the 'Hallmarks of ageing' [35].

1.2.3 The hallmarks of ageing

The 'hallmarks of ageing' a set of nine occurances which nearly always correlate with ageing were first brought together by Lopez-Otin et al in 2013 in an important synthesis of ageing research [35]. These are genomic instability, telomere attrition, epigenetic alterations, loss of proteostasis, deregulated nutrient sensing, mitochondrial dysfunction, cellular senescence stem cell exhaustion and altered intra-cellular communication[36-

39]. There is strong evidence linking each of these hallmarks with the ageing phenotype however how they cause or result in the development of ageing remains the primary focus of many ageing researchers. Many of the hallmarks have strong links to the theories of ageing discussed above. Some are more obvious than others, for instance mitochondrial dysfunction, and telomere attrition have both contributed their own theories of ageing along with loss of proteostasis and genomic instability [34, 39, 40]. Deregulated nutrient signalling has strong links to the disposable soma theory whilst stem cell exhaustion and cellular senescence have many links between various theories of ageing.

Whilst it is prudent to keep in mind each of the hallmarks of ageing and how they link to the various theories of ageing, when investigating the mechanisms involved in any aspect of ageing it is not plausible to investigate all of them. It is therefore necessary to focus on one or two of the hallmarks and investigate how they interact within a given ageing phenotype. In the work presented in this thesis, the focus is on deregulated nutrient signalling, how these affect different cell types and how various treatments alter the response of the nutrient signalling network. The next section will look at this network in detail and summarise the key findings to date with regards to the nutrient sensing mTOR network and ageing.

1.3 The mTOR network

The target of Rapamycin (TOR) protein is a protein kinase which, in mammals, exists in two distinct multi subunit complexes, mTORC1 and mTORC2 (mammalian TOR complex 1 and 2). These complexes are part of a network that sense and integrate nutrient and amino acid availability, growth factor and hormonal signals [41, 42]. Depending upon the state of these inputs the TOR signalling pathway regulates cell growth, autophagy, protein production as well as energy stores around the body [43].

Activation of mTOR is controlled upstream by growth factors and hormones such as insulin. Binding of insulin to its receptor leads to autophosphorylation of the insulin receptor and the recruitment and tyrosine phosphorylation of insulin receptor subunit 1 (IRS1) [44, 45]. Tyrosine phosphorylation of IRS1 blocks its degradation and leads to increased interaction with proteins containing SH2 (src-homology-2) domains including Phosphoinosital kinase 3 (PI3K) leading to phosphorylation of its p110 domain [46-48]. Activated PI3K catalyses the production of phosphatidylinositol-3-phosphates via

phosphorylation which in turn are responsible for the regulation of different protein classes including the Rho family of GTPase proteins and the AGC protein kinases which include phosphoinositide-dependent kinase 1 (PDK1) [49, 50]. PDK1 is one of a number of proteins capable of phosphorylating the serine/threonine kinase AKT/PKB and interaction between the two results in the phosphorylation of AKT on its threonine 308 residue[51]. Phosphorylation of T308 acts an activator for AKT which is able to inhibit the action of the tuberous-sclerosis complex (TSC1/2) [52, 53]. Thus preventing TSC1/2 acting as a GTPase activating protein (GAP) for the Ras homolog enriched in the Brain (Rheb) protein and inhibiting the hydrolysis of Rheb bound GTP to GDP [54, 55]. In its GTP bound state Rheb is able to bind to FKBP38 resulting its disassociation from mTORC1 thus resulting in the activation of the mTORC1 complex [56]. The mTORC1 complex consists of the proteins TOR, RAPTOR, PRAS40 and mLST8. Phosphorylation of mTORC1 via the AKT pathway leads to the direct phosphorylation of downstream proteins including the ribosomal kinases S6K1 and S6K2 and the eIF4E binding proteins [41, 57, 58]. Phosphorylation of S6K1/2 and 4EBP1/2 regulate downstream mRNA translation as well as initiating cellular growth and proliferation [45, 59]. In addition to its activation of cell growth, the phosphorylation of S6K also acts to initiate a negative feedback loop which inhibits PI3K via direct phosphorylation of IRS1 on serines270/307/636/1001 [60]. Phosphorylation on these sites leads to the inability of IRS1 to associate correctly with the insulin receptor and the down regulation of PI3K/AKT signalling.

In addition to sensing energy levels through growth factor and insulin signalling mechanisms mTORC1 is also regulated by amino acids although the mechanisms behind this regulation are far from clear [41]. Whether all amino acids are required for full mTOR activation has yet be to be confirmed however it is known that leucine and arginine are both essential for mTORC1 to become active [61, 62]. What is known is that the Ras related GTPases (RAG A and RAG B) are involved directly in activating mTORC1 in response to amino acid stimulation [63, 64]. The RAG proteins are unusual amongst the Ras related proteins in that they don't rely on post translational protein modifications to achieve correct localisation within the cell [65]. In contrast they rely on a protein complex known as the Ragulator which acts as a lysosomal tether to lipid rafts on the lysosome [65, 66]. RAG A/B localisation to lysosome in turn acts to localise mTORC1 to the lysosome were it can be activated by Rheb [63]. Furthermore it has

been shown that v-ATPase components on the lysosome activate the Ragulator in the presence of amino acid although how amino acids are sensed and by what mechanism remains elusive[67]. Under low amino acid conditions the GATOR1 complex acts as a GAP protein for RAG proteins (RAG A/B) catalysing the conversion of GTP to GDP and inhibiting the activity of the RAG A/B heterodimer. Under high amino acid conditions the GATOR 2 complex acts to inhibit the GATOR 1 complex preventing its GAP action on RAG A/B [68, 69]. This allows the v-ATPase components to positively regulate the Ragulator and results in the binding of GTP to the RAG A/B heterodimer [41, 42].

Far less is known regarding the activation of the second TOR complex mTORC2. In addition to the TOR protein, mTORC2 consists of RICTOR, mSIN1, Proctor and Deptor with Rictor and mSIN1 required for structural integrity of the complex [42, 70, 71]. Whilst it has been termed a rapamycin insensitive complex its activity is inhibited by chronic exposure to rapamycin, likely brought about by decreased complex formation [72]. Upon growth factor stimulation mTORC2 localises to the endoplasmic reticulum where it becomes activated although the mechanisms behind this remain unclear however it is known that a PI3K is required for this activation [73-75]. Upon activation mTORC2 phosphorylates AKT on Ser473 either as a single phosphorylation or in addition to the phosphorylation on Thr308 further enhancing AKT's activation [76, 77]. Downstream functions of mTORC2 are also poorly defined although it is known to activate various PKC isoforms including protein Kinase C α and serum- and glucocorticoid-induced protein kinase 1 (SGK1) [77, 78]. The activation of PKCα is essential for cytoskeletal organisation whilst SGK1 is essential for cellular growth and ion transport [42]. In addition mTORC2 is possibly subject to negative regulation via mTORC1 activation [42]. It has been shown that active S6K1 phosphorylates mSIN1 on various serine residues leading to its disassociation from mTOR and the disassembly of the mTORC2 complex [79]. A representation of the mTOR network can be seen in figure 1.1.

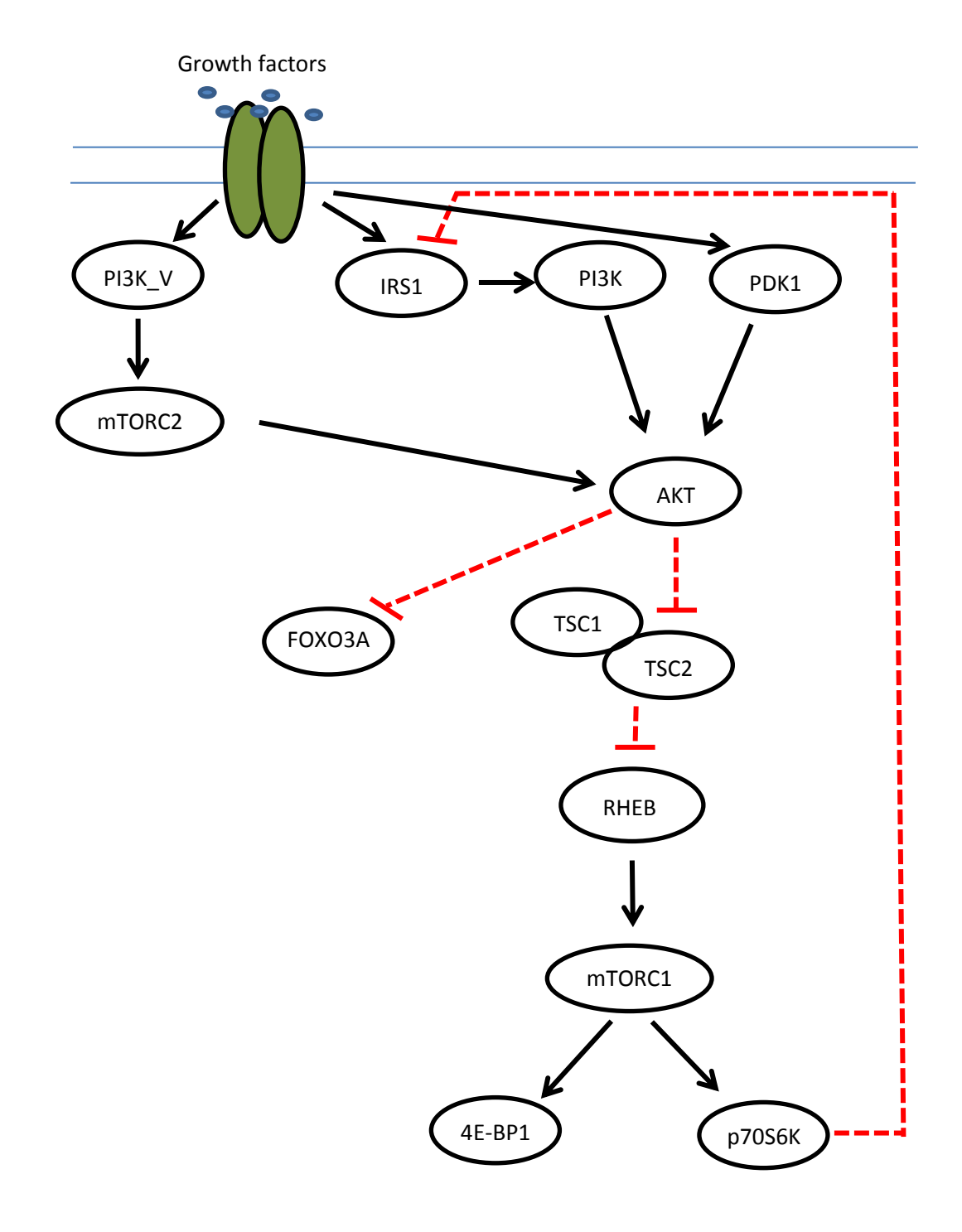


Figure 1.1: Schema representing the mTOR network. Adapted from [80]

1.4 Ageing and the musculoskeletal system

As previously described mTOR and its associated network plays an important role in ageing. In addition to the *C. elegans* mutants already described inhibition of mTOR leads to life extension in many other model organisms including *Drosophila melanogaster* and Mice [81]. As described above one of the hallmarks of ageing is a decline in stem cell number and function. There is increasing evidence that the inhibition of mTOR is beneficial in maintaining both stem cell number and function. Studies have shown that old mice treated with Rapamycin have better intestinal stem cell function than their untreated counterparts whilst Rapamycin has also been implicated in the rejuvenation of haematopoietic stem cells in old mice leading to enhanced protection from the influenza virus. In addition, inhibition of the mTOR network by Zoledronate (a nitrogen containing bisphosphonate) led to increased protection from DNA damage in mesenchymal stem cells [82]. Mesenchymal stem cells are precursor cells to the bone forming osteoblasts, with these findings suggesting a possible beneficial effect of mTOR inhibition with regards to bone formation and degradation.

Other ways in which mTOR inhibition is believed to extend lifespan include the inhibition of mRNA translation, increased activation of the stress response, increased mitochondrial respiration and reduction of inflammation [83].

Whilst the links between the mTOR network and ageing are well established far less is known regarding the links between stem cells and the ageing process. Stem cell ageing is of particular interest when investigating age related changes to the musculoskeletal system. Indeed there is now a significant focus on stem cells in both bone biology looking at mesenchymal stem cells (MSCs) with age and in muscle looking satellite cells with age. The following section will summarise what is known about the relationship between the musculoskeletal system and ageing with a focus on bone biology and MSCs.

1.4.2 Mesenchymal stem cells and bone ageing

As discussed above one theory of ageing suggests that with age our stem cell pool decreases and loses its ability to function correctly (figure 1.2 (A-B) [84-87]. Indeed there are multiple studies that show different stem cell groups each displaying a reduction in their ability to proliferate and differentiate correctly [88-91]. But it is of

interest whether this is a cause or a consequence of the ageing process and whether it would be altered so that various different tissues remain fully functional with increased age. Due to their regenerative potential both the importance and potential of stem cells in relation to ageing research is beginning to be understood and there is increased focus and attention being paid to this area of ageing research. One tissue at the centre of stem cell ageing biology is bone. It is well established that with increased age, bone remodelling homeostasis is affected with increased bone resorption and decreased bone formation (Figure 1.2 (C-D) [92-94]. Whilst we understand the biology behind both bone formation and bone resorption it is still poorly understood what drives the age related imbalance between the two processes. Is it a decrease in osteogenesis or an increase in bone resorption? Recent research in this area has focused on mesenchymal stem cell ageing and osteogenesis. Mesenchymal stem cells are capable of differentiating into three main types of cells: osteoblasts, chondrocytes and adipocytes [95]. With age there is a general decrease in the amount of differentiation coupled with a shift towards adipogenic differentiation (a process termed adipocyte switch) [96, 97]. The decrease in osteogenic differentiation eventually leads to reduced osteoblast numbers and may be responsible for the reduction in bone formation seen in old age although other factors may be involved [98]. Eventually the reduction in bone formation leads to age related diseases such as osteoporosis and increased risk of fractures and falls as a result of instability [99, 100]. The increase in falls and fractures, in particular hip fractures, often results in the development of other age related conditions brought about by long term inactivity [101]. The combination of such factors leads to an increased mortality rate amongst patients with hip fractures [102].

1.4.3 Bisphosphonates, the mevalonate pathway and osteoporosis

Currently osteoporosis is treated by targeting the bone resorption pathway as opposed to osteogenesis [103]. It is hypothesised that by reducing the amount of bone resorption that occurs the ratio of bone formation to bone resorption will be brought back into balance [104]. A class of drugs called Bisphosphonates have been developed that potently target bone resorption by inhibiting the formation and ability to function of mature osteoclasts [105]. The most potent class of bisphosphonates (nitrogen containing bisphosphonates) act by targeting the mevalonate pathway and inhibit prenylation [104, 106, 107]. The mevalonate pathway is a metabolic network that acts to synthesise isoprenoids and is responsible for the addition of Geranyl and Farnesyl groups to

proteins such as Ras and Rheb. The enzyme farnesyl pyrophosphate (FPP) synthase acts to catalyse the reaction of Geranyl pyrophosphate (GPP) to FPP which can then be inserted into the CAAX domain of specific proteins [108]. Nitrogen containing Bisphosphonates are a group of drugs used primarily in the treatment of osteoporosis and they act to inhibit FPP synthase by directly binding to its active site [109]. This disruption of the prenylation pathway leads to downstream disruption of osteoclastic signalling as protein prenylation is essential for vesicular trafficking, membrane ruffling, morphology and cytoskeletal arrangement [110, 111]. It has also been suggested that down-regulation of geranyl-geranylpyrophosphate (GGPP) (Enzyme responsible for the transference of a geranyl group to other proteins including small GTPase's) occurs during cell-cell contact induced during differentiation of the osteoblastic cell line MC3T3-E1 [112-114].

Whilst these drugs are very effective with regards to inhibiting bone resorption they often fail to bring the bone remodelling pathway back into balance as an increase in bone formation often does not occur [104]. Indeed recently it has been revealed that the prenylated proteins also play a role in osteogenesis [115, 116]. However even with the failure to increase osteogenesis bisphosphonates are considered a very effective treatment for osteoporosis and work is ongoing to attempt to unravel the mechanisms behind how they affect osteogenesis.

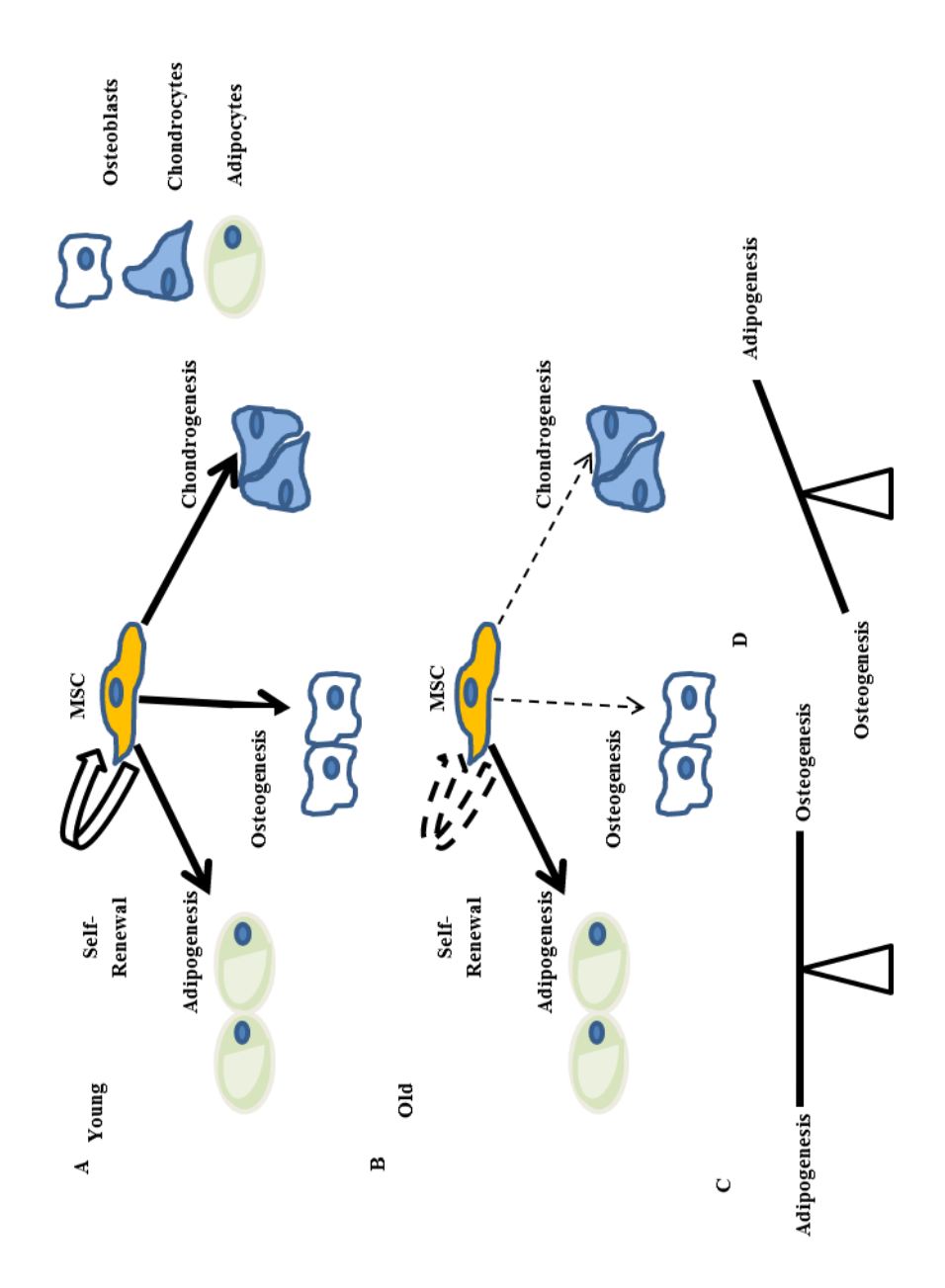


Figure 1.2: Stem cells and ageing. Schema representing how mesenchymal stem cell differentiation alters with age (A) Differentiation in young MSCs –differentiation is dependent upon tissue and cellular requirements, (B) Differentiation in old MSCs –adipogenesis becomes the primary differentiation pathway, Balance between adipogenesis vs osteogenesis in young MSCS (C) and Old MSCs (D).

1.4.4 Bisphosphonates, cancer treatment and lifespan extension

Over the last couple of decades there has been increased focus on the use of bisphosphonates as anti-cancer drugs [117]. Bone has long been the focus of cancer studies due to the frequency of bone metastases found in many different cancers including breast cancer and multiple myeloma [118, 119]. The treatment of these cancers and various different cancer cell lines with bisphosphonates has been shown to induce apoptosis and has been found to inhibit tumour growth in certain cases [117, 120]. The mechanisms behind these findings have never been fully elucidated. Recently even more novel findings have been published regarding the use of bisphosphonates in cancer and ageing studies. It was found, for example, that patients with hip fractures being treated with the Bisphosphonate Zoledronate showed a 28% decreased mortality rate compared to untreated controls[121]. There have been several other studies that have observed increased lifespan, decreased mortality rates, decreased cardiovascular events and decreased cancer incidence in osteoporotic patients undergoing bisphosphonate treatment [122, 123]. Additionally, when treated with a combination of statins and Zoledronate a mouse model of Hutchinsons-Gilford progeroid syndrome displayed decreased cellular DNA damage, reduced progeroid symptoms and an extended lifespan [124].

Following on from these results, work carried out at the University of Sheffield has investigated how Zoledronate treatment affects MSCs and to identify the mechanisms behind these actions. They have shown that treatment of MSCs in culture extends their proliferative lifespan as well as decreasing the amount of cellular DNA damage within cell cultures undergoing high numbers of passages compared to controls [82]. Upon further examination they observed that there was inhibition of the mTOR network due to the de-prenylation of the proteins Ras and Rheb. Following Zoledronate treatment a decrease in phosphorylated mTORC1, mTORC2 and S6K lead to increased nuclear localisation of FOXO3A which in turn enhanced the DNA damage response following irradiation.

1.4.5 Role of AMPK in stem cell differentiation and ageing

AMP activated protein kinase (AMPK) is a highly conserved regulator of cellular energy status and tightly controls energy consuming process within a cell. AMPK acts by inhibiting anabolic processes and activating catabolic processes [125]. It has recently been implicated in mesenchymal stem cell differentiation by down-regulating adipocyte

genes and inducing osteoblastic genes [96]. In a study from 2012, Kim et al showed that the level of AMPK increased during osteoblastic differentiation of MSCs as well as there being an increase in the phosphorylated state of AMPK [96]. However, this does not align with other research carried out on MC3T3-E1 cells which showed that the levels of AMPK decreased with osteoblastic differentiation [126]. This could be explained by the fact that MSC are progenitor cells whereas MC3T3-E1 cells are partially differentiated cells. In support of this suggestion another study showed that AMPK signalling was a time co-ordinated process which was upregulated during the early stages of osteoblastic differentiation and then down-regulated during the later stages of osteogenesis [98]. Interestingly, the early increase in AMPK signalling leads to a feedback mechanism activating the AKT-mTOR network. These studies were carried out in adipose derived and dental pulp derived MSC and it is not known if the results are entirely transferable to bone marrow derived MSC or if some of their observations are tissue specific. For instance it has been observed that adipocyte derived MSCs are more likely to differentiate in adipocytes than osteoblasts with the opposite being true for bone marrow derived MSCs (bmMSCs).

1.4.6 Osteogenesis links to the mTOR network

There are several key pathways involved in osteogenesis each of which can be linked back to the mTOR network; these include the Wnt signalling pathway and signalling through C/EBP isoforms.

1.4.6.1 C/EBPβ isoforms

C/EBP-β transcription is activated by eukaryotic translation initiation factor 4E (eIF-4E) which is repressed by eukaryotic translation initiation factor 4E binding protein 1 (4EBP) [57]. Upon activation of TOR signalling 4EBP is phosphorylated resulting in its release from eIF-4E and the transcription of C/EBP-β. There are three distinct C/EBPβ isoforms, the full length LAP, short length LIP and the extended length LAP* isoforms [127]. During osteogenesis the expression of all three isoforms increases however they do not all act to induce osteogenesis [128]. LAP and LIP both act to enhance expression of RUNX2 and increase its interaction with the osteocalcin promoter (both of RUNX2 and Osteocalcin are crucial for osteogenesis along with osterix)[129, 130] . The extended isoform acts to inhibit osteogenesis by inhibiting transcription. Both the LAP and LIP isoforms also directly interact with ATF4 which in addition to RUNX2 binds to the promoter region of osteocalcin activating its transcription [129]. ATF4 also appears

to facilitate amino acid transport within pre-osteoblasts another requirement in osteogenesis [131]. Each of the C/EBPβ isoforms has a different role in osteogenesis as already mentioned the extended form appears to inhibit osteoblast formation by recruitment of the SWI/SNF chromatin remodelling complex which may help to keep the osteoblasts in an immature state [132]. The standard length isoform enhances the expression of osteogenic genes and the short isoform LIP enhances osteoblast differentiation and maturation [95, 128, 133, 134]. It is interesting to note that in the absence of the long isoforms overexpression of LIP has been shown to inhibit terminal osteoblast differentiation [135]. This suggests that LIP may compensate for the lack of long isoforms in the cell and act to recruit certain complexes which keep the cell in an immature state. It seems therefore that C/EBPβ isoforms act in a dual role. Initially acting to keep the cells in an immature state when conditions are unfavourable and then to activate osteogenic genes and terminal differentiation once the correct conditions are present. Once osteogenic differentiation is initiated SMAD3 binds to C/EBPβ and abrogates its inhibitory function on RUNX2 driving further osteogenesis.

1.4.6.2 Wnt signalling

It is well known that Wnt signalling is required for correct bone development with many studies establishing that ablation of Wnt signalling leads to bone deformities and decreased bone formation [136]. The Wnt proteins Wnt3a and Wnt10b bind to the Fizzled receptors and recruit the LRP5/6 co-receptors and lead to the inhibition of Glycogen synthase 3 which is also inhibited by AKT and in turn when active can activate the TSC1/2 complex [137]. Once GSK3 is inhibited β-catenin becomes stabilised and translocates to the nucleus where it regulates the T-cell factor/lymphoid enhancer factor (TCL/LEF). LRP5/6 binding to Frizzled receptors is inhibited by DKK1 which recruits Kremen to the LRP5/6 receptors inactivating them [97]. Overexpression of either Wnt3a or Wnt10b or inhibition of DKK1 leads to increased osteogenesis with a reduction in trabecular bone formation being seen upon Wnt inhibition [138, 139]. In addition to these observations it has also been observed that the adipogenic protein PPARy is inhibited by Wnt10b [140]. PPARy is one of the key proteins that drive Adipogenesis as it inhibits RUNX2 activity Wnt10b prevents this inhibition from occurring however active PPARγ has also been shown to directly induce β-catenin proteasomal degradation preventing osteogenesis. As Wnt signalling appears to be key in regulating osteogenesis it may be interesting to investigate this pathway further in

order to assess how the inhibition of the mTOR network by bisphosphonates affects β -catenin driven osteogenesis.

There are a number of other proteins and transcription factors involved in osteogenesis and that are affected by both of these pathways, these include Smad2 and Smad5 which interact with Runx2 following its activation and appear to be required in vivo to induce osteogenesis. Osterix is another protein that is absolutely required for osteogenesis and acts downstream of Runx2. It appears to act together with Satb2 to enhance bone regeneration and formation. The exact roles of C/EBPβ in osteogenesis have yet to be confirmed however the effect of bisphosphonate treatment (or indeed mTOR inhibition) on these isoforms may well prove interesting to explore. In addition the effect of mTOR inhibition on osteogenesis and how inhibition of mTORC1 alone differs from dual inhibition in terms of the downstream effects of osteogenesis could also prove extremely interesting to study.

1.5 The DNA damage response

The DNA Damage response (DDR) is a set of pathways which are heavily implicated in the ageing process. As the DDR is not the main focus of this work this section will present a summary of the theoretic links between the DDR and ageing as well as summarising the links between the mTOR network and the DDR.

1.5.1 The DNA damage response and ageing

The links between the DDR and various diseases such as cancer are well established. However how the DDR relates to ageing is a far more complicated and involves the interplay between numerous different factors both environmental and genetic. As all molecules within an organism can essentially be replaced with the exception of DNA any lasting damage to the DNA of an organism can result in many adverse effects including early onset ageing [141]. It is therefore unsurprising early onset ageing environmental factors include many practices that result in DNA damage with smoking and alcohol consumption often cited as two possible environmental factors that result in premature ageing [37, 142]. The most common form of DNA damage in humans is as a result of ultra-violet radiation (UV) from the sun. It is believed that such stresses result

in an increase in oxidative molecules which in turn cause DNA damage [143]. How such damage in turn advances the ageing phenotype is as yet unknown. In order to ascertain the links between the DDR and ageing a number of models have bene employed, including progeroid models of ageing [141]. One of the characteristics of these models is that they show decreased DNA damage repair ability resulting in the early onset of age related diseases. Indeed mouse models lacking the ability to carry out DNA damage repair display increased age related symptoms compared to wild-type controls. Anti-ageing models such as rodents fed a calorie restricted diet results in the preservation of the DDR over time compared with wild-type controls [144]. In addition to preserving the DDR caloric restriction has also been shown to reduce the levels of reactive oxygen species as well as reducing the rates that mutations occur within the DNA [145].

1.5.2 Links between mTOR and the DNA damage response

Several studies have shown that FOXO3A activates the DNA damage response although the exact mechanism by which is does so remains unknown (Figure 1.3)[146]. One recent report suggests that FOXO3A interacts with the ATM-Chk2-P53 complex by phosphorylating ATM [147]. The same group has recently followed up this work by revealing that ovarian and breast cancer cell lines can be reprogrammed to non-cancerous cells by inducing the nuclear translocation of FOXO3A by metformin [148]. They again showed that ATM and p53 were both activated by FOXO3A during this process providing support for their previous work. Some of the data that the UoS have produced appears to support this hypothesis. They showed that silencing FOXO3A using siRNA resulted in a complete lack of ATM phosphorylation in irradiated cells compared to controls. Further to this they also showed that silencing of FOXO3A results in an increase in the number of DNA damage foci in MSCs which have been irradiated; this was true for both control cells and cells treated with Zol.

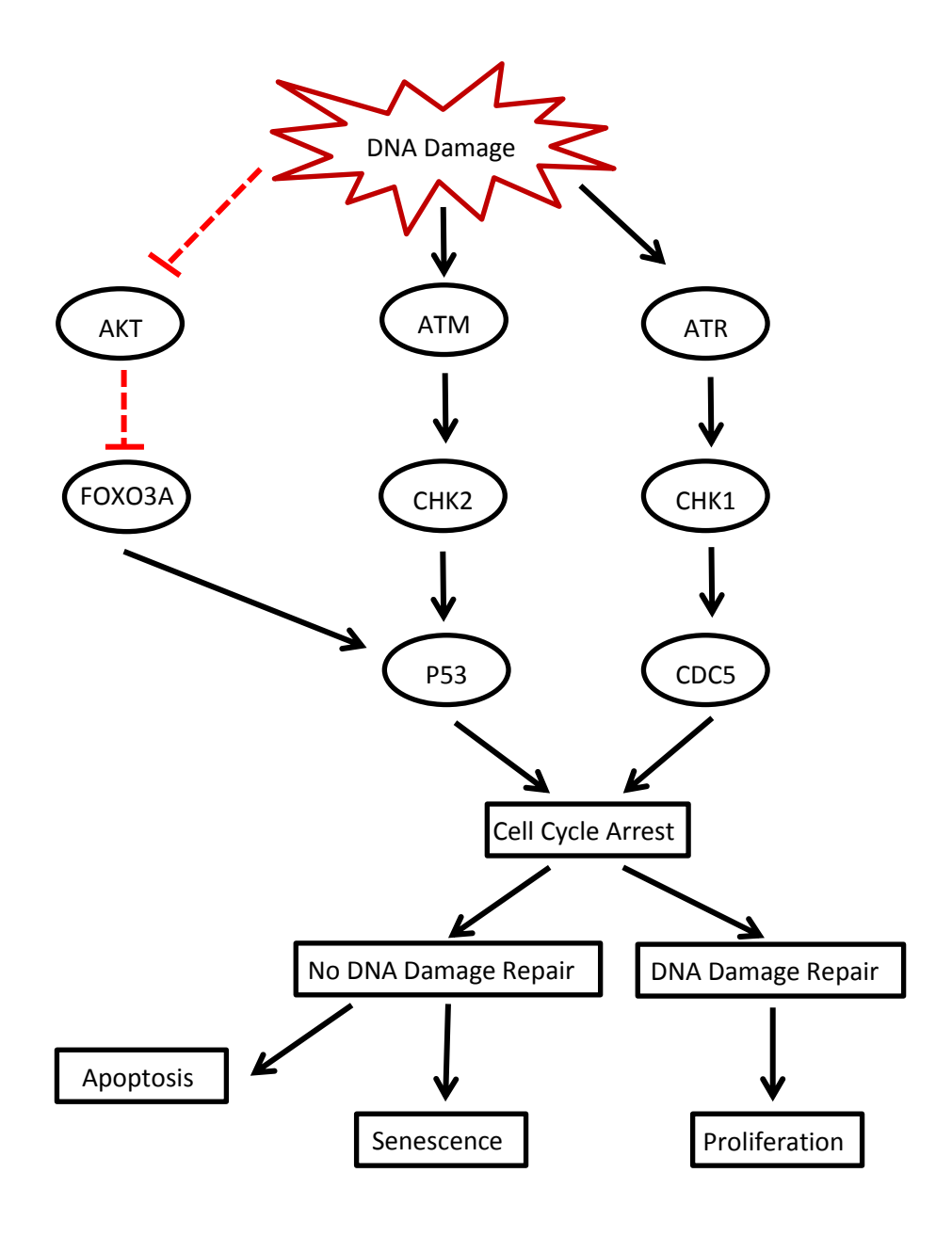


Figure 1.3: Schema representing the DNA damage response pathways interacting with FOXO3A. Adapted from [149]

1.6 Systems biology

Each of the systems discussed above present a large degree of complexity and exploring the interconnectivity of the networks would not be possible using a purely experimental approach. A solution to this is to apply a systems biology approach whereby the networks are modelled computationally informed by experimental data [150]. The field of systems biology is extremely broad and as such it lacks a definitive definition [151]. However all definitions of systems biology essentially include computational analysis of biological data at different scales whether that be at the organism or cellular level. The interconnectedness of these scales and the individual components within them is what interests systems biologists, with the aim of all systems biologists to assess and gain a better understanding of how a system as a whole functions. Under the definitions above systems biology encompasses not just 'dry lab' computational work but also 'wet lab' experimental work which can work either independently or in cohesion with each other.

1.6.1 Top down and bottom up

Classically there are two approaches that are used in computational modelling. These are termed 'top down' and 'bottom up' (Figure 1.4) [152]. In the top down approach at first there is no definition of sub systems or indeed mechanistic detail or a system [153]. In this case a particular question is not defined by a particular mechanistic observation but from a large set of observations. Microarrays are the primary source of data for top down modelling in computational biology [154]. Experiments will be performed testing the action of particular perturbation and mRNA measured using microarrays allowing for the analysis of thousands of genes. From this analysis the gene regulatory networks that are affected by a particular perturbation can be identified leading to a more detailed representation of the system. The bottom up approach is essentially the opposite of top down. This is a reductionist approach whereby a reaction or a small sub system is analysed and the remaining system built up around it in order to obtain the full system to be analysed [152, 155]. Traditionally biology has focused on this type of approach with the reaction of individual molecules measured and then a question posed from the result as to what else may be happening to the system. Dynamic modelling is most closely associated with a bottom up approach but in a full systems biology project the focus will be informed from the outcome of a top down analysis.

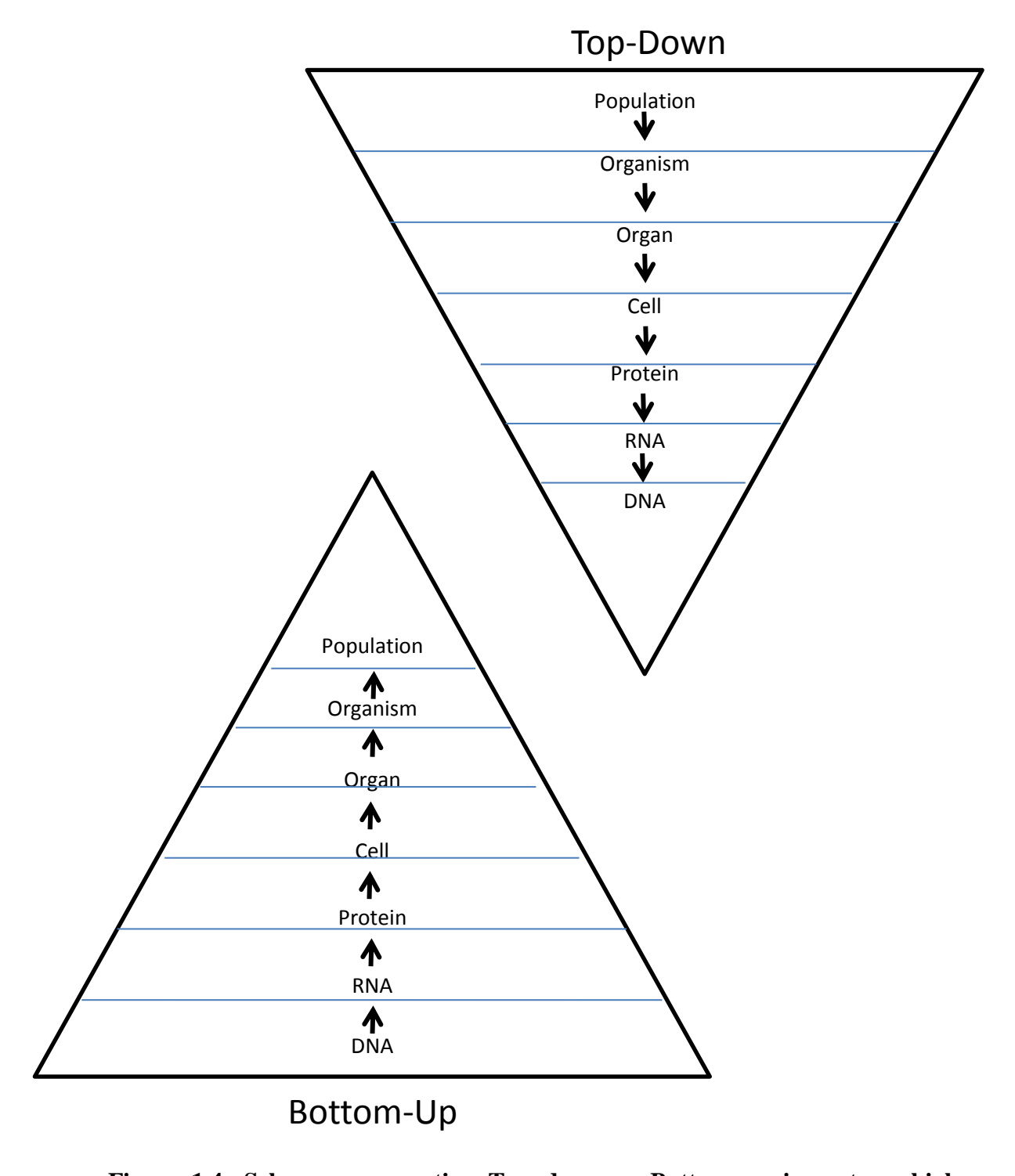


Figure 1.4: Schema representing Top down vs Bottom up in systems biology. Adapted from [156].

1.6.2 Dynamic computational modelling

Computational modelling is an important component of systems biology [157]. Models are represented by a set of mathematical equations (normally ordinary differential equations). The information contained within each equation governs how it interacts with other equations within a model framework in addition defining the behaviour of the specific biological event (for instance a phosphorylation event) which the equation represents. This allows for the abstraction of an overall biological concept into a mathematical framework governed by mathematical rules of the equations within the model structure [158]. The advantage of this is that due to the ability to solve these mathematical equations a model can be used to define, simulate and predict outcomes based on inputted knowledge. Indeed slight variations to the mathematical model structure (topology) of a model can allow a user to determine which topology provides the closest match to a given prediction. Or indeed can provide an entirely new prediction based on what was already previously known. The attribute that defines a dynamic model from a non-dynamic model is that it can be said to have 'memory' [159]. In the case of most dynamic this 'memory' is commonly referred to as the 'state' in which the model exists. As most models are designed to have an 'initial state' or an initial set of conditions from which the model acts to predict the outcome of a relevant situation. As the simulation progresses the model goes through a number of different 'states' and may eventually establish a 'steady state'. The behaviour of a model are governed by the mathematics of the equations used in the building of a model (usually ordinary differential equations). There is an established nomenclature used to represent the model structure based on species, reactions and parameters [160]. A species within the model represents a particular node within the network this could be a particular mRNA, protein, cell or even organ or individual. A reaction is the connection between each of the nodes within the model and these can be governed by numerous different kinetic laws. In the work presented in this thesis the reaction type used is that of mass action [161, 162]. Here, the rate of reaction is proportional to the product of the reacting substrates. Parameters encompass both species and reactions within a model as they are the values assigned to either a species or the rate at which a reaction occurs within the model.

1.6.3 Multiscale modelling

As previously stated systems biology involves the study of large networks over varying scales. This poses various challenges that must be overcome in order to correctly model a system. For instance the process of a transcription factor takes seconds whilst the subsequent activation of that protein takes milliseconds. This can be followed up through the cellular levels to macromolecules such as hormones that can take hours to exert an effect. The question therefore is how these different scales can be measured [163]. This is of particular importance in drug pharmacology where a drug may target a genetic component which leads to macromolecular event [164]. This is what multi-scale modelling attempts to solve. One way to solve this problem is to abstract the 'lower scale' networks to a point where there is a loss of dynamic function (they cease to be dynamic models and remain at a constant). This allows for the development of the 'higher scale' model with a singular input from the 'lower scale' [159]. Whilst the focus of this work will not be on the multiscale nature of the signalling networks involved it is important that this is kept in mind when the results are interpreted. For instance whilst the focus of this work is on the microscopic scale the effect of the treatments tested will each have an effect on the macroscopic level of cellular signalling in particular when focusing on stem cell biology.

1.6.4 Model simulation - deterministic and stochastic modelling

Before discussing the basis of deterministic and stochastic modelling it is necessary to first define both what an algorithm is and how an algorithm works to form a model simulation [165]. An algorithm can be defined as a set of rules performed in steps to achieve an output [166]. Using this definition it is therefore possible to define a model simulation as the process of using an algorithm to reproduce the problem presented by the model in question. There are primarily three types of algorithm: deterministic, stochastic and hybrid (a combination of deterministic and stochastic) [167]. The majority of dynamic models are presented in a deterministic form. This is to say that the variables contained within their simulations are considered not to be random. This is not always the case however as biological systems are inherently stochastic in nature [168]. It is therefore often necessary to model certain systems using stochastic modelling. This means that whilst the overall network reactions and variables remain the same as in a deterministic model they are not only governed by time but also by a probability distribution [162, 167]. The primary focus of such a modelling process is usually

governed by the abundance of a particular species within the model. A low species value inherently lends itself to stochastic simulations whereas a large species value is more likely to be deterministic in nature. Due to the random probability distributions within stochastic models it is possible that they can give an entirely different outcome to a modelling problem and it is therefore appropriate to correctly choose which type of modelling is to be performed [169]. Whether or not deterministic or stochastic modelling is used dynamic modelling is primarily data driven as discussed above with data forming a hypothesis which ultimately drives the development of a model. How data is collected and which variables within the model that are measured are dependent upon both the ability to collect the data experimentally and the question that is being addressed. These data are used to inform the model by optimising the parameters within the model via a process termed parameter estimation [170]. This process involves the identification of a parameter set which is approximates the 'best fit' of a model in the context of experimental data. This is usually presented within a statistical format (in many cases the residual sum of squares (RSS)) whereby a parameter value results in a simulation within the confines the error (either standard deviation, standard error of the mean or confidence intervals) of the experimental data. The parameter set with the overall smallest deviation from this mean is considered the 'best fit'.

1.6.5 Computational models of mTOR

As previously discussed due to its complexity the ageing process naturally lends itself to a systems biology approach. However the question remains with so many factors involved how do you model a process as complicated as ageing? This has mainly been tackled to date using abstract large scale network models without looking in-depth at the molecular interactions of the molecules or else abstracting a particular network connected with ageing such as the mTOR network, the DDR or reactive oxygen species and their effect on cellular processes. This section will focus on the models of the mTOR network that have previously been published. Over recent years our group and others have had made substantial progress in dynamic modelling related to the mTOR network. The following is a summary of the key work and dynamic models produced to date: in 2012 Dalle Pezze et al developed a dynamic model of the mTOR network to analyse the activation and regulation of mTORC2. By exploring different model topologies with different regulatory options upstream of mTORC2 they were able to disseminate that mTORC2 activation occurs independently of the TSC1/2 complex and

is dependent on a PI3K variant [80]. In 2012 Sonntag et al extended this model to explore the relationship between AMPK and mTOR. In this study, they also used different model topologies to represent different modes of regulation of AMPK by the TOR network (a total of 6 models were explored). Upon calibrating these models to AMPK and mTOR related timecourse data they were able to select a model that correctly predicted the experimental outcomes. They showed that IRS1 is the most likely activator of AMPK within the mTOR network and that this in turn can be regulated by a negative feedback loop involving downstream factors [171]. More recently in 2016 Dalle Pezze et al examined the effect that amino acids have directly on the mTOR network. As discussed above it is known that amino acids act to activate the mTORC1 complex however it is not known as to whether there are other kinases within the pathway which are also activated by amino acids. By combining computational modelling with text-mining advanced proteomics it proved possible to delineate that amino acids act to activate PI3K, AMPK and mTORC2 in an mTORC1 independent manner [172]. Whilst each of these studies have focused on the short term effects of perturbations on the mTOR network work has also been carried out investigating the long term effects of perturbations on the mTOR network. In 2013 Smith et al investigated the long term relationship between reactive oxygen species, the mTOR network and FOXO transcription factors. They showed that long term nutrient deprivation led to the upregulation of anti-oxidant defence systems however this also lead to the loss of IRS1 receptors and FOXO over time. In contrast under higher oxidative stress conditions the protective effect could be lost [173]. In addition to work carried out by our group in collaboration with others a number of researchers have also utilised computational modelling to investigate the mTOR network. In 2009 Jain and Bhalla investigated the role of the mTOR network in protein synthesis within dendritic cells. They showed that brain derived neurotrophic factor gate activated mTOR and protein synthesis with the model not demonstrating bi-stability [174]. Also in 2009 Borisov et al investigated the crosstalk between the insulin signalling and epidermal growth factor signalling networks using a dynamic modelling approach. Using this approach they were able to identify key nodes within the networks that could be used as possible drug combination targets in future studies [175]. Other dynamic models of the mTOR network include Araujo et al who investigated the dynamic states of the mTOR network in cancer and non-cancer phenotypes in addition to Caron et al who used a large scale modelling approach to identify all of the networks and crosstalk linked to the two mTOR complexes [176, 177].

1.7 Objectives

The aim of this project is to compare and contrast the response of the mTOR network to three separate life extending treatments with the following hypothesis.

Zoledronate and caloric restriction act upon both mTOR complexes. Therefore both Zoledronate and starvation-restimulation should affect the mTOR network in similar ways and elicit a similar response to one another following withdrawal and restimulation in both MRC5 and MSCs. As acute rapamycin treatment only affects mTOR complex 1 the effect of treatment withdrawal should produce a separate response. The response of the mTOR network following rapamycin withdrawal should differ to that of the other treatments however it should not differ between cell types.

This will be achieved by focusing on the following objectives:

- 1. To identify potential new methodologies capable of producing timecourse data required for the calibration of dynamic models
- To design and build a dynamic model capable of representing the response of the mTOR network following serum-starvation, Zoledronate withdrawal and Rapamycin withdrawal
- 3. To produce timecourse data measuring key components of the mTOR network in response to each treatment in both MRC5 cells and Mesenchymal stem cells
- 4. To calibrate the dynamic model in objective 2 using the timecourse data produced in objective 3
- 5. To compare the response of MRC5 cells and MSCs in response to each treatment

2. Materials and methods

2.1 Experimental methodology

2.1.1 General MRC5 cell culture

MRC-5 fibroblasts were grown in Dulbecco's Modified Eagle Medium (DMEM) high Glucose (Sigma-Aldrich, Dorset, UK D5796) supplemented with 10% foetal bovine serum (FBS; Biosera, Ringmer, UK), 1% of L-Glutamine (Sigma-Aldrich, Dorset, UK G7515) and 1% of Penicillin-Streptomycin (Sigma-Aldrich, Dorset, UK P4333). Cells were cultured in 75cm² cell culture flasks (Fisher Scientific, Corning, vented cap, NY, USA, 430641U) and incubated (Binder Incubators) in a humidified atmosphere at a constant temperature of 37°C, 20% oxygen and 5 % CO². Once cells reached 80% confluence they were removed from incubation and counted and split as follows, media was aspirated off (Integra Vacusafe) and cells washed with 10ml of phosphor buffered saline solution (PBS)(Sigma-Aldrich, Dorset, UK D5773). The PBS was removed by aspiration as before and 2ml of Trypsin-EDTA 1x (Sigma-Aldrich, Dorset, UK T3924) was added and the cells placed back into the incubator for two minutes. Following two minutes incubation the cells were removed and trypsin effectiveness checked using a Nikon TMS Microscope (Nikon UK, Kingston Upon Thames, UK). 8ml of Pre-heated (37°C) DMEM (made as described above) was added to the cells to end trypsinisation. Cells were then removed from flasks and added to a 50ml Falcon tube using 10ml (Sarstedt AG&Co.Sarstedtstraße 1,51588 Nümbrecht GERMANY, 86.1254.001). For the purposes of cell counting 15µl was taken from the cell suspension and the remaining solution centrifuged at 850rpm for five minutes (Jouan CR3). The supernatant was then removed using an aspirator and cells resuspended using DMEM as above with 2ml of DMEM added per one million cells. Cells were then re-plated onto 75cm² cell culture flasks as above with 1 million cells per flask (2ml of cell solution) and 18ml of DMEM added to each flask to make a total of 20ml of DMEM per flask.

2.1.2 Cell counting

Cells were counted as follows: the $15\mu l$ taken from the Falcon tube was placed on a haemocytometer (Brand, Fuchs-Rosenthal, 97861 Werthiem, Germany, 719805) and the number of cells per square of the haemocytometer was counted for a minimum of three squares. A calculation to ascertain an estimate for the number of cells within the Falcon tube was then carried out as follows: The dimensions of each square of the haemocytometer are $0.1 \times 0.1 \times 0.02$ mm equalling a volume of 0.0002m l. Therefore the

number of cells present in each square of the haemocytometer is equal to the number of cells per 0.0002ml of media. This number was then multiplied by 5000 in order to ascertain the number of cells per ml and then by the dilution factor to ascertain the total number of cells present in the Falcon tube. Cells were then centrifuged for 5 minutes at 2000 rpm and the supernatant removed via aspiration.

2.1.3 Thawing MRC5 cells

Prior to culturing, MRC5 cells were removed from -200°C storage in liquid nitrogen and allowed to thaw completely. Cells were then removed from cyrotubes (Sarstedt AG & Co.

Sarsted, tstraße 1,51588 Nümbrecht, GERMANY, 86.1254.001) and placed into a 50ml Falcon tube and 9ml of DMEM (pre-heated to 37°C and made as above) per vial of cells added to the Falcon tube. Cells were then centrifuged at 850rpm for 5 minutes and the supernatant aspirated. Cells were then resuspended in 10ml of DMEM per million cells and then 10ml of cell suspension added to 75cm2 cell culture flasks as above. 10ml of DMEM was the added to each flask to make a total volume of 20ml per flask. Cells were then incubated for 24 hours following which DMEM was removed and replaced.

2.1.4 Freezing and storage of MRC5 cells

MRC5 cells were prepared for storage as follows: Following a cell count any cells to be stored were resuspended in DMEM as above however following the re-plating of any cells still being grown, Dimethyl sulfoxide (DMSO) (Sigma-Aldrich, Dorset, UK D5418) was added to make a 10% DMSO solution with 1 million cells per 1ml of solution. 1ml of this freezing mixture was then added to Cyrotubes and stored at -80°C for 24 hours before being transferred into liquid nitrogen storage at -200°C.

2.1.5 General mesenchymal stem cell culture

Primary MSC's (kindly supplied by Juhi Misra, the University of Sheffield, UK) were grown in Dulbecco's Modified Eagle Medium (DMEM) high glucose, GlutaMAX supplement (Thermofisher, Atley Way, Cramlington NE23 1WA 61965-026) containing 10% HyClone™ Foetal Bovine Serum (U.S.), Human Mesenchymal Stem Cell Screened (Fisher Scientific, NY, USA SH-30070.03M). MSC's were cultured in 25cm² Falcon tissue culture treated flasks (Fisher Scientific, Corning incorporated, NY, USA, 353109) for one passage at a density of ~500,000 cells per flask until cells

reached 80 % confluency. For the duration of cell culture, cells were incubated in a humidified atmosphere at a constant temperature of 37°C, 20% oxygen and 5 % CO². Upon reaching 80% confluency, cells were counted and plated out into 150cm² Falcon tissue culture treated flasks (Fisher Scientific, Corning incorporated, NY, USA, 355001) at a density of ~ 500,000 cells per flask. The procedure for splitting MSC cell cultures was carried out as follows: Flasks were removed from incubation, culture media was removed by aspiration with (Integra Vacusafe) and washed with PBS at room temperature. The PBS was then removed by aspiration and Trypsin-EDTA (0.05%), Phenol red (Fisher scientific, Gibco, NY, USA, 25300-054) (pre-heated to 37°C) added for a duration of two minutes - the cells were placed back into the incubator during this time. Once two minutes had elapsed, cells were taken out of the incubator and checked under a microscope to make sure that they had detached prior to the addition of culture medium (pre-heated to 37°C) to the cells resulting in the inhibition of the trypsin. Cells were then transferred using Starstedt pipettes (Sarstedt AG & Co, Sarstedt, straße, 151588 Nümbrecht, GERMANY, 25ml 86.1885.001, 10ml 86.1254.001, and 5ml 861253.001) to 50ml Falcon tubes. A volume of 15µl was taken from the 50ml falcon tubes and used to perform a cell count as described above for MRC5 cells. Cells were then re-suspended in culture medium (at a dilution of 2ml per million cells) prior to being re-plated into 150cm2 Falcon tissue culture flasks as previously described at ~ 500,000 cells per flask and a further 18ml of culture medium added to each flask. To ensure an even coating of cells over the surface of the flask, each flask was swirled in a figure of eight shape and then incubated as previously described. All cell culture medium was pre-heated to 37°C in a water bath prior to use)

2.1.6 Defrosting mesenchymal stem cell samples

Prior to culturing, MSC samples were removed from storage in liquid nitrogen at -200°C and allowed to thaw until the sample was in solution but still in a semi-solid state. The MSC sample was then transferred into a 15ml Falcon tube and 4ml of culture medium added per 1ml of sample. Cells were then plated as previously described onto 25cm² Falcon tissue culture flasks at a density of ~500,000 cells per flask and culture medium added to each flask to create a total of 10ml of culture medium per flask. After a duration of 24 hours the culture medium was removed from each flask and replaced with fresh medium to remove any DMSO (Sigma-Aldrich, Dorset, UK, D5879) from each flask.

2.1.7 Freezing and storage of mesenchymal stem cell samples

MSCs frozen in cyrotubes (Sarstedt AG & Co. were Sarstedt, straße 1,51588 Nümbrecht, GERMANY, 86.1254.001) containing ~500,000 cells in a volume of 1ml. Following the splitting of cells (as detailed above), any cells that were to be frozen down and stored were resuspended in culture medium and centrifuged again at 2000 rpm for 5 minutes and the supernatant then removed. Cells were then resuspended in a freezing solution containing 10% DMSO (Sigma-Aldrich, Dorset, UK D5879) in HyCloneTM Foetal Bovine Serum (U.S.), Human Mesenchymal Stem Cell Screened red (Fisher scientific, Gibco, NY, USA, SH-30070.03M). This was made up prior to cell culture in batches of 50ml and stored at 4°C (freezing solution was used at this temperature to aid freezing process). Cyrotubes were then stored at -80°C for a minimum of 24 hours prior to storage in liquid nitrogen at -200°C.

2.1.8 Lifespan extending treatments

Following a period of cell culture (as above), cells were plated, split and counted prior to being plated onto 10cm plates for flow cytometry and onto six well plates for Reverse Phase Protein Arrays. The details for this can be found in each methodologies respective section (sections 2.1.9 and 2.1.15). Following a period of 24 hours after splitting, cells were treated in the following ways: For Starvation-Restimulation culture medium was aspirated and for MRC5 cells (DMEM) high Glucose (Sigma-Aldrich D5796) supplemented with 1% of Penicillin-Streptomycin (Sigma-Aldrich P4333) were added. For MSCs DMEM high glucose, GlutaMAX supplement (Thermofisher, 61965-

026) was added to the cells. Following a period of 24 hours this treatment was stopped by aspirating all culture medium from the cells and adding DMEM high Glucose (Sigma-Aldrich D5796) supplemented with 10% foetal bovine serum (Supplier), 1% of L-Glutamine (Sigma-Aldrich G7515) and 1% of Penicillin-Streptomycin (Sigma-Aldrich P4333) to the MRC5 cells and DMEM high glucose, GlutaMAX supplement (Thermofisher, 61965-026) containing 10% HyCloneTM Foetal Bovine Serum (U.S.), Human Mesenchymal Stem Cell Screened (Fisher Scientific, SH-30070.03M) to the MSCs. For Rapamycin treatment, both cell types had their cell culture medium removed and were treated with 10nM of Rapamycin (Enzo Life Sciences, Exeter, U.K.) diluted into either DMEM high Glucose (Sigma-Aldrich D5796) supplemented with 10% foetal bovine serum (Supplier), 1% of L-Glutamine (Sigma-Aldrich G7515) and 1% of Penicillin-Streptomycin (Sigma-Aldrich, P4333) (MRC5) or DMEM high glucose, GlutaMAX supplement (Thermofisher, 61965-026) containing 10% HyCloneTM Foetal Bovine Serum (U.S.), Human Mesenchymal Stem Cell Screened (Fisher Scientific, SH-30070.03M) (MSCs). Following a period of 24 hours the Rapamycin treated cell media was aspirated and replaced with either DMEM high Glucose (Sigma-Aldrich D5796) supplemented with 10% foetal bovine serum (Supplier), 1% of L-Glutamine (Sigma-Aldrich G7515) and 1% of Penicillin-Streptomycin (Sigma-Aldrich P4333) (MRC5) or DMEM high glucose, GlutaMAX supplement (Thermofisher, 61965-026) containing 10% HyClone™ Foetal Bovine Serum (U.S.), Human Mesenchymal Stem Cell Screened (Fisher Scientific, SH-30070.03M) (MSCs). For Zoledronate cells were treated with 1µM of Zoledronate (Kindly provided by Mellanby bone Research Group, University of Sheffield). This was carried out as follows, after a period of 24 hours cell culture medium was aspirated and replaced with either DMEM high Glucose (Sigma-Aldrich D5796) supplemented with 10% foetal bovine serum (Supplier), 1% of L-Glutamine (Sigma-Aldrich G7515) and 1% of Penicillin-Streptomycin (Sigma-Aldrich P4333) (MRC5) or DMEM high glucose, GlutaMAX supplement (Thermofisher, 61965-026) containing 10% HyCloneTM Foetal Bovine Serum (U.S.), Human Mesenchymal Stem Cell Screened (Fisher Scientific, SH-30070.03M) (MSCs) containing 1µM of Zoledronate. After a period of 72 hours this was aspirated and replaced with either DMEM high Glucose (Sigma-Aldrich D5796) supplemented with 10% foetal bovine serum (Supplier), 1% of L-Glutamine (Sigma-Aldrich G7515) and 1% of Penicillin-Streptomycin (Sigma-Aldrich P4333) (MRC5) or DMEM high glucose, GlutaMAX supplement (Thermofisher, 61965-026) containing 10%

HyClone™ Foetal Bovine Serum (U.S.), Human Mesenchymal Stem Cell Screened (Fisher Scientific, SH-30070.03M) (MSCs). Details for each treatment are shown in Table 2.1.

<u>Table 2.1: Life extending treatment overview.</u> An overview of how each lifespan extending treatment was carried out for both MRC5 and MSC cells. Both the treatment details and restimulation details are shown.

Treatment	Treatment Methodology	Restimulation Methodology	
Starvation-	MRC5 – DMEM high	MRC5 – DMEM high Glucose,	
Restimulation	Glucose supplemented with	supplemented with 10 % foetal	
	1% Penicillin-Streptomycin	bovine serum, 1% L-Glutamine and	
	MSC- DMEM high Glucose,	1% Penicillin-Streptomycin	
	GlutaMAX	MSC – DMEM high glucose	
		supplemented with 10 % Hyclone	
		foetal bovine serum	
Rapamycin	MRC5 – 10nM Rapamycin	MRC5 - DMEM high Glucose,	
	diluted in DMEM high	supplemented with 10 % foetal	
	Glucose supplemented with	bovine serum, 1% L-Glutamine and	
	1% Penicillin-Streptomycin	1% Penicillin-Streptomycin	
	MSC- 10nM Rapamycin	MSC – DMEM high glucose	
	diluted in DMEM high	supplemented with 10 % Hyclone	
	Glucose, GlutaMAX	foetal bovine serum	
Zoledronate	MRC5 - 1µM Zoledronate	MRC5 – DMEM high Glucose,	
	diluted in DMEM high	supplemented with 10 % foetal	
	Glucose supplemented with	bovine serum, 1% L-Glutamine and	
	1% Penicillin-Streptomycin	1% Penicillin-Streptomycin	
	MSC- 1µM Zoledronate	MSC – DMEM high glucose	
	diluted in DMEM high	supplemented with 10 % Hyclone	
	Glucose, GlutaMAX	foetal bovine serum	

2.1.9 Flow cytometry methodology

Prior to the following protocol, cells were cultured as above until the required number of cells was obtained for each experiment. The protocol below was used for both MSC and MRC5 cells except were specified. Following culturing, cells were removed from incubation and split and counted as above. Following a cell count, cells were plated out on 10cm (Fisher Scientific, Corning, vented cap, NY, USA, 430167) at a density of 500000 cells per plate, with a 6ml of DMEM culture media (see above) added to make a total of 8ml per plate and incubated at 37°C, 5% CO² for 24 hours. Following this incubation period the culture media was removed from each plate and replaced with DMEM containing Zoledronate, Rapamycin or DMEM containing only 1% of Penicillin-Streptomycin for starvation-Restimulation (Sigma-Aldrich P4333) made as in 2.1.8. Timecourse experiments were then carried out for each of the three treatments (Table 2.2).

2.1.10 Cell fixation

Cells were fixed as follows: Replicates were removed from incubation and treatment media removed. Each replicate was then washed using 5ml of ice cold PBS which was then removed and 1ml of Trypsin added to each plate (Trypsin specific to each cell type see above). Cells were then incubated for two minutes before 4ml of ice cold DMEM was added to end trypsinisation and each replicate removed from their plates and added to a 15ml Falcon tube. Cells were then centrifuged to remove the supernatant. This step and all wash steps that follow were specific to each cell type. For MRC5 cells centrifugation was carried out 850 rpm for 5 minutes whilst for MSC's centrifugation was carried out 2000 rpm for 5 minutes. Following centrifugation the supernatant for each replicate was removed by tipping the supernatant into a waste tube (this process was used following each wash step carried out) and cells resuspended in 1 ml of paraformaldehyde (PFA)(Thermoscientific, Rockford, IL 61101, USA, 28908). Each replicated was then incubated in a water bath at 37°C for 10 minutes after which cells were centrifuged and the PFA removed as above. Following PFA removal cells were the resuspended in PBS and centrifuged to wash off the PFA (henceforth this will process will be referred to as a wash step). The PBS was then removed as above and the wash process repeated before cells were suspended in 0.1% sodium Azide (Sigma-Aldrich, Dorset, UK S8032) and stored until staining.

<u>Table 2.2: Timecourse data points for flow cytometry datasets.</u> The time points for the imagestream flow cytometry experiments are shown here for both during treatment and post re-stimulation for each treatment.

Timecourse	Treatment		
During	Starvation-Restimulation	Rapamycin	Zoledronate
Treatment			
0 Minutes	X	X	X
30 Minutes	X	X	
60 Minutes	X	X	
24 Hours	X	X	X
48 Hours			X
72 Hours			X
Following			
Restimulation			
0 Minutes	X	X	X
5 Minutes	X	X	X
15 Minutes	X	X	X
30 Minutes	X	X	X
60 Minutes	X	X	X
2 Hours	X	X	X
4 Hours	X	X	X
8 Hours	X	X	X
24 Hours	X	X	X

2.1.11 Cell permeabilisation

Cells were removed form storage in Sodium Azide by washing as above and then resuspended in 2ml of PBS and a second wash step performed. Following the second wash the PBS was removed by pouring it into a waste container and cells resuspended in 2ml of blocking buffer (49ml PBS, 1ml FBS) for a period of 1 hour at room temperature following which samples were centrifuged and the supernatant removed as above. A further wash was then carried out using 2ml of PBS before cells were resuspended in 2ml of 0.1% Triton-X 100 (Sigma-Aldrich, Dorset, UK T8787) for a period of 15 minutes at room temperature following which the Triton-X 100 was removed by centrifugation as above. Cells were then washed with 2ml of PBS.

2.1.12 Cell staining

Immediately following permeabilisation primary antibodies were added to each replicate and incubated for 12 hours. For each step, antibodies were diluted to their required concentration using PBS in a total volume 100µl. Following primary antibody staining cells were washed as above and second wash with 2ml of PBS carried out. Cells were then incubated with secondary antibodies in the same way as for primary antibodies for a period of 1 hour in the dark. After this incubation cells were washed as above with a second wash with 2ml of PBS carried out. Cells were then resuspended in 1ml of PBS and transferred to 2ml flow cytometry tubes. Samples were then fed through a BD FACSKANTO2 flow cytometer (BD Biosciences, San Jose, CA 95131) and results analysed using Flowing Software 2 (Cell Imaging Core of the Turku Centre for Biotechnology, Finland).

2.1.13 Cell permeabilisation imagestream

Cells were removed form storage in Sodium Azide by washing as above and then resuspended in 200µl of PBS. Cells were then transferred to a 96 well plate for permeabilisation and staining. Following transfer to the 96 well plate cells were resuspended in 200µl of staining buffer (49ml PBS, 1ml FBS) and washed by centrifugation at 350G (this is the wash stage for all further imagestream work). The supernatant was then flicked off and cells were resuspended in 100µl of permeabilisation buffer (0.05ml Triton-X 100 Sigma-Aldrich T8787, 49ml PBS, 1ml FBS) for a period of 5 minutes at room temperature following which another 100µl of staining buffer was added to the cells before the Triton-X 100 was removed by centrifugation as above. Cells were then washed with 200µl of staining buffer.

2.1.14 Cell staining imagestream

Immediately following permeabilisation primary antibodies were added to each replicate and incubated for 1 hour. For each step, antibodies were diluted to a 1:100 concentration using staining buffer. Following primary antibody staining 100μl of staining buffer was added to each well and cells washed as above and second wash with 200μl of staining buffer carried out. Cells were then incubated with secondary antibodies in the same way as for primary antibodies for a period of 30 minutes in the dark. After this incubation 100μl of staining buffer was added to each well and cells washed as above with a second wash with 200μl of staining buffer carried out. Cells were then resuspended in 60μl of staining buffer and transferred to 1.5ml Eppendorf tubes (Starlab, Milton Keynes, MK14 5BU, S1615-5550). Samples were then fed through an Imagestream flow cytometer (Amnis Imagestream 2, Merck-Millipore, Frankfurter, Straβe, 250 64293, Darmstadt, Germany) and results analysed using (Ideas 6.2 Merck-Millipore, Frankfurter, Straβe, 250 64293, Darmstadt, Germany).

2.1.15 Reverse phase protein array preparation

Cells were cultured as above prior to reverse phase protein array (RPPA) being carried out. Time courses were generated for each of the three treatments as shown in Table 2.3. Prior to the following protocol, cells were cultured as above until the required number of cells was obtained for each experiment. The protocol below was used for both MSC and MRC5 cells except where specified. Following culturing, cells were removed from incubation and split and counted as above. Following a cell count, cells were plated out on six well plates (Fisher Scientific, Corning, NY, USA, 07-200-80) at a density of 200000 cells per plate for MRC5 cells and 100000 cells per plate for MSCs, with a 3ml of DMEM culture media (see above) added to make a total of 4ml per plate and incubated at 37°C, 5% CO² for 24 hours. Following this incubation period the culture media was removed from each plate and replaced with DMEM containing Zoledronate, Rapamycin or DMEM containing only 1% of Penicillin-Streptomycin for starvationrestimulation (Sigma-Aldrich P4333) made as in 2.1.8. Following treatment, cell culture medium was aspirated and replaced with either DMEM high Glucose (Sigma-Aldrich D5796) supplemented with 10% foetal bovine serum, 1% of L-Glutamine (Sigma-Aldrich G7515) and 1% of Penicillin-Streptomycin (Sigma-Aldrich P4333) (MRC5) and DMEM high glucose, GlutaMAX supplement (Thermofisher, 61965-026) containing 10% HyCloneTM Foetal Bovine Serum (U.S.), Human Mesenchymal Stem

Cell Screened (Fisher Scientific, SH-30070.03M) (MSCs) for the remainder of the time course. For each time point cell culture medium was aspirated and 1ml of ice cold PBS added to each well. This was then aspirated and a further 1ml of ice cold PBS added and aspirated. Following the PBS washes 40µl of RPPA lysis buffer (Kindly supplied by Nan Wang, Newcastle University) was added to each sample. Cells were then scraped using a cell scrapper until all cells had been lifted from the plate surface and the cells and lysis buffer transferred from each well into a 1.5ml Eppendorf tube. Samples were then sonicated for a period of 15 mins. This was carried out as three sets of 5 minutes, with 10 sonication cycles of 15 seconds of sonication followed by 15 seconds of no sonication at a temperature 4°C. Samples were then stored at -20 °C until transfer to the Newcastle University Proteins and proteomics unit (NUPPA) RPPA facility.

2.1.15 Reverse phase protein array procedure

Samples were centrifuged at 13000 rpm for 5 minutes and the supernatant collected into 1.5ml Eppendorf tubes and the pellet discarded. 10ul of supernatant was then transferred to a 96 well plate and diluted with 15µl of RPPA lysis buffer (Kindly supplied by Nan Wang, Newcastle University) and 100µl of spotting buffer (Zeptosens Spotting Buffer CSBL1, Zeptosens Ltd). Serial dilutions of 100%, 75%, 50% and 25% were then made using a Beckmans Coultier BioMEK liquid handler, a 1:5 solution of lysis buffer and spotting buffer (Zeptosens Spotting Buffer CSBL1) and plated into a 384 well plate. Samples were then stored overnight at -20°C prior to plating. Samples were plated on to Zeptosens Protein Micro-ArrayChips (Zeptosens Protein MicroArray-Chips, Zeptosens Ltd) using a SIM Nano plater 2.1 (SIM) alongside a reference plate. Following printing the micro-chips where placed inside a vaporiser loaded with BB1 Blocking buffer (Zeptosens blocking buffer BB1, Zeptosens Ltd) for a period of one hour after which they were submerged in distilled water for 1 second six times. Microchips were then centrifuged at 300 rpm to remove any excess water this wash step was then repeated a further two times after which any remaining water was removed and the micro-chips loaded onto a staining rack. Each individual sample set was then washed three times by pipetting 100µl of CAB1 assay buffer (Zeptosens Assay buffer CAB1, Zeptosens Ltd) into each slot ensuring that no air bubbles remaining on the microchips. 80µl of each primary antibody were added to their designated sample set and staining for 16 hours. Figure 2.1 displays a representative staining rack set up. Primary antibodies were removed and each individual sample set was then washed three times

by pipetting 100µl of CAB1 assay buffer into each slot. 80µl of secondary antibody were then added to every sample set and left to stain for a period of two hours after which the antibody was removed and a further three washes with blocking buffer carried out. Following the final wash the CAB1 assay buffer was not removed from the sample sets. The staining rack was then placed inside a Zeptosens imager and each sample set imaged and quantified for their respective antibody.

<u>Table 2.3: Time course data points for Reverse Phase Protein Array datasets.</u> The time points for the RPPA time courses are shown here for both during treatment and post re-stimulation for each treatment.

Timecourse	Treatment		
During	Starvation-Restimulation	Rapamycin	Zoledronate
Treatment			
0 Minutes	X	X	X
30 Minutes	X	X	
60 Minutes	X	X	
24 Hours	X	X	X
48 Hours			X
72 Hours			X
Following			
Restimulation			
0 Minutes	X	X	X
1 Minutes	X	X	X
3 Minutes	X	X	X
5 Minutes	X	X	X
10 Minutes	X	X	X
20 Minutes	X	X	X
30 Minutes	X	X	X
60 Minutes	X	X	X
2 Hours	X	X	X
4 Hours	X	X	X
8 Hours	X	X	X
24 Hours	X	X	X

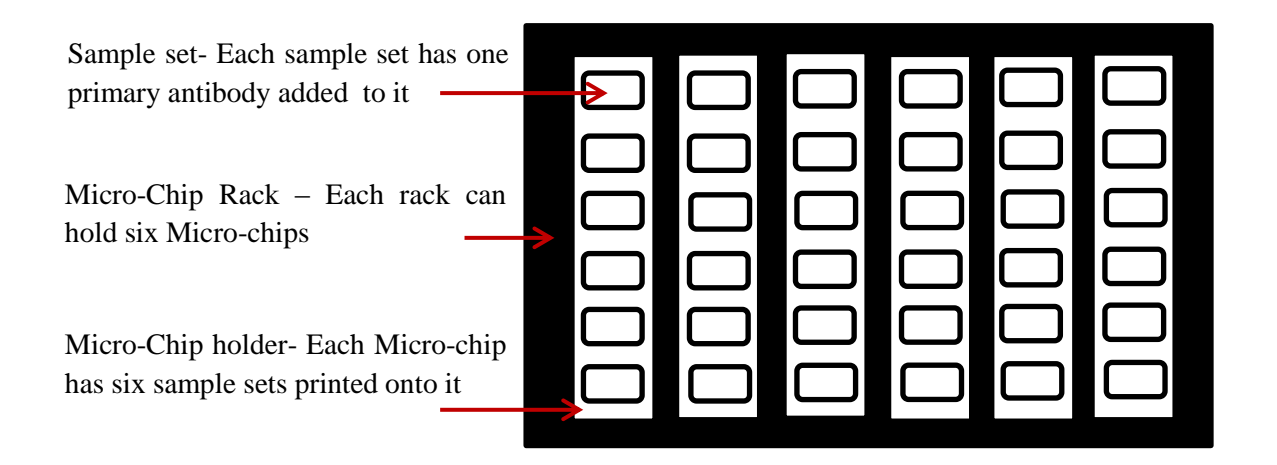


Figure 2.1: Zeptosen Micro-Chip staining apparatus an overview of the staining apparatus used during the RPPA process. Each micro-chip has six sample sets printed onto it allowing for six different antibodies per micro-chip. Each rack has room for six micro-chip holders which hold the microchips in place and form a seal around each sample set preventing contamination.

2.2 Systems biology dynamic modelling

Throughout this work a systems biology approach was used. A dynamic computational model based on previous research was constructed and used to design, plan and carry out experimental procedures aimed to inform the model. The dynamic modelling approach carried out was as follows; firstly a computational model was defined using previous literature knowledge and data. Secondly the model topology is simplified to represent a network capable of answering the question of interest and ODE's used to define the reactions within the model. Thirdly the model was parameterised using timecourse data. Once the model is calibrated it can then be used as a tool with which to further investigate the network of interest. It is often the case that that a dynamic model is produced to simulate the response of a network to a specific perturbation for example the effect of Rapamycin on the mTOR network. Following calibration it is possible to perturb the network further by increasing or decreasing the relative expression of a particular species within the model. This, for example, is often carried out in models investigating the effect of cancer on different biological networks where oncogenic proteins become dysregulated. Further analysis of the dynamic model predictions can be used to plan further experiments. If these experiments fail to support the model predictions then a change in network topology is performed and the model recalibrated. The general procedure for systems biology dynamic modelling is shown in figure 2.2. The dynamic modelling approach was chosen for this work as it allowed a direct comparison of a single model reacting to three separate perturbations and in addition the mTOR network has already been proven to be an ideal target for this systems biology approach.

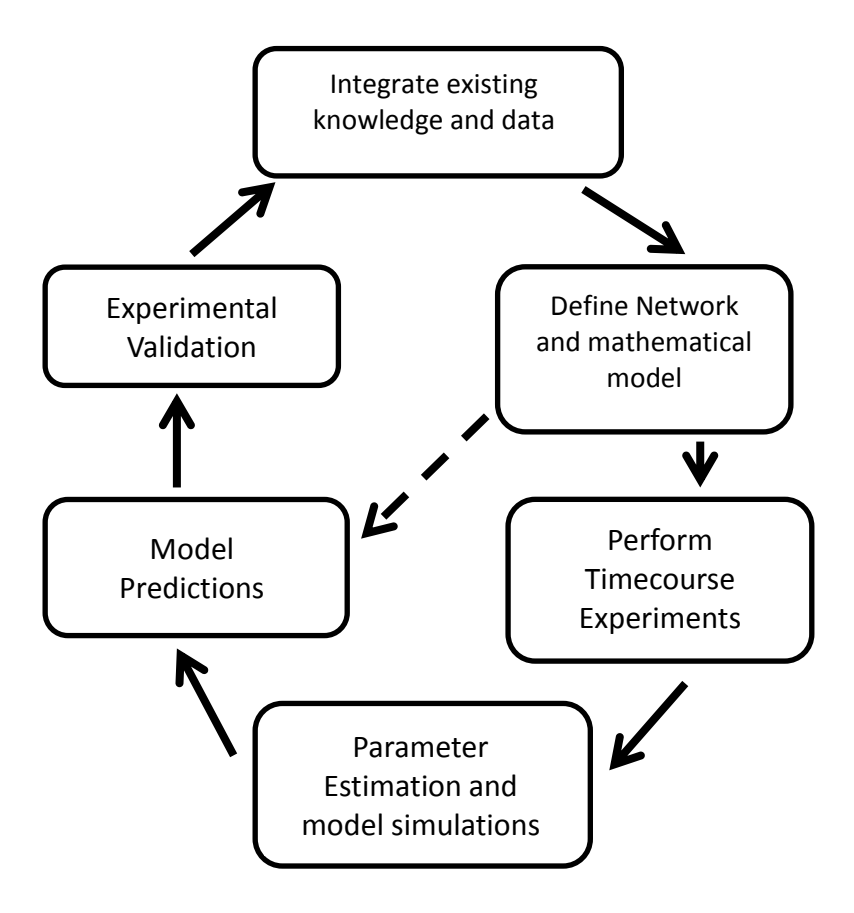


Fig 2.2: System Biology dynamic modelling workflow. An overview of the systems biology dynamic modelling work flow is shown here. Following the integration of existing knowledge and data a computational network is defined and time course experiments carried out. Parameter estimation is carried out and predictions made which are validated with experimental data and reviewed using previously published molecular biology. Alternatively following model definition model predictions can be made and experimentally validated.

2.2.1 SBGN and SBML

In order to construct the original model topology the program CellDesigner 4.4 was used [178]. This allowed for the creation of model in Systems Biology Graphical Notation (SBGN) a language that represents networks visually [179]. The advantage of using SBGN is that it was specifically designed for this purpose and provides an industry standard for the production of dynamic models. Following the original definition of the network topology the model was exported in Systems Biology Mark-up Language (SBML) and imported into COPASI (4.15-4.20) [160]. As with SBGN, SBML provides a standard computational language for dynamic modelling that is compatible with a large number of different modelling platforms. Whilst in this work COPASI was used to perform simulations and to refine the network structure the final model was exported as SBML in order to allow for the submission to peer reviewed journals.

2.2.2 Parameter estimation

Parameter estimation is the process of estimating a given parameter set based on experimental data. Parameter estimation was performed using Copasi's parameter estimation function [162, 167]. Initial parameter estimations were carried out on a local PC using the following settings, Randomised start values, lower limit 1E⁻⁶ and upper limit 1E⁻⁴. The genetic algorithm was selected to perform the initial parameter estimations as this method provided a global deterministic algorithm which was neither computationally or processor time demanding. Initial parameter estimations were used to inform and refine the model topology prior to full calibration. Once a final model topology was in place, a full calibration was performed utilising a computational cluster. The parameter estimation was set up as described using the genetic algorithm (Number of generations = 300, Population size =150, Random number generator = 1, Seed = 0), in addition the parameter scan function was utilised as follows, executable = yes, Repeat number of iterations = 20, sub task = parameter estimation. This was then submitted to a computer cluster and a Python script (Kindly provided by Ciaran Welsh) used to perform 10000 estimation repeats.

Following successful completion of 10000 parameter estimations each repeat, the python package PyCotools was used to rank each parameter fit by its chi-squared value. The chi-squared statistical test is used to determine whether or not the observed difference between two sets of data occurs due to chance. Using this measure it is

possible to analyse which set of simulated parameter values provides the closest fit to the measured data. For each model the parameter set with the lowest chi-squared value inserted into the model and analysed using the parameter estimation task in Copasi. For this estimation the current solution statistic algorithm was used and data collected for each of the measured variables within the model.

Following successful parameter estimation using the genetic algorithm the updated parameter set was transferred back to a computer cluster for further refinement using the Hooke and Jeeves algorithm. As this algorithm is a local search algorithm it only searches the parameter space around the previously defined parameters. This repeat was carried out as above with the following changes, randomised start values = no, Hooke and Jeeves (Iteration limit = 50, Tolerance = $1E^{-5}$, Rho = 0.2), and 2000 parameter estimations carried out.

2.2.3 Pycotools

Pycotools is python package developed at Newcastle University by Ciaran Welsh. It allows a user to programmatically control the Copasi program to achieve their desired objectives. Pycotools was used throughout this work in chapters 4 and 5 to run multiple parameter estimations and then to extract the parameter estimation with the lowest residual sum of square score in order to analyse the model fit achieved. In chapter 6 an updated version of Pycotools was then used to carry out in depth analysis of the model fits including time course ensembles and parameter variation analysis.

2.2.4 Statistics

Normalised experimental data are shown as the mean value with error bars of plus and minus the standard error of the mean calculated in Microsoft Excel (2010). All graphs were plotted using Sigmaplot 12.5 (Systat Software Inc; San Jose, CA, USA). Quantification of protein expression for RPPA samples was carried out using Zeptoview 3 (Zeptosens Ltd). The Pearsons χ^2 value was obtained and the residual sum of squares value for all observables calculated using Copasi. A p-value was calculated for the model analysed in chapter 4 using the RSS obtained by each model and the degrees of freedom calculated from the data as follows (N columns -1)* (N Rows -1). In chapter 6 a t-test was performed using Microsoft excel (2010) and a P-value obtained with a value of below 0.05 considered significant.

3. A comparison of methodologies for the production of dynamic model calibration data

3.1 Introduction

The production of quantitative time course data for calibration and validation of computational models is a key aspect of dynamic modelling. A range of experimental methodologies are available for generating such data at both the RNA and protein levels. In the case of RNA, microarrays or RNA-seq are the two high-throughput methodologies most commonly used to generate large data sets and qPCR for data sets with a smaller scope. The choice depends on whether the data is to be used for modelling gene regulatory networks or to calibrate a model where a particular RNA plays a role. In the case of proteins, mass spectrometry methods are available for highthroughput measurement but have not been commonly used for the calibration of dynamic models. The majority of computational modelling studies do not require such large datasets and low throughput methods such as western blotting are usually sufficient. Western blotting is generally accepted as a reliable and repeatable method for producing protein level measurements. It is however time consuming and potentially error prone and therefore not ideally suited to the production of data sets required for calibrating sets of dynamic models as in this work. Experience within our research group has shown that it would take around one person year to develop a model for one treatment using western blotting for data generation. This project requires the development of six calibrated models so it was necessary to investigate alternative methodologies that could replicate the quality of results produced by western blotting but which would be more time efficient. A number of alternatives to western blotting exist for protein level quantification. These include Reverse Phase Protein Arrays (RPPA), Intracellular Flow cytometry, Simple Western, mass cytometry and mass spectrometry. From these it was decided that RPPA and flow cytometry provided the most likely alternatives to western blotting. In addition to the possibility of being more time efficient than western blotting both methodologies were considered reliable and robust and had both previously been successfully used in systems modelling studies [180, 181].

3.2 Aims and objectives

- To provide an overview of two alternative methodologies to western blotting
- 1. To analyse two pilot studies investigating the quality of data produced by each method
- 2. To analyse which technique should be taken forward to produce complete a data set with which a dynamic model of the mTOR network can be calibrated

3.3 Reverse phase protein arrays

Developed in 2001 by Paweletz et al the Reverse Phase Protein array technology is based on gene expression microarrays widely used transcriptional research, its creation followed previous attempts to create a protein microarray [182] [183]. Previous iterations were designed using glass slides with recombinant proteins or antibodies bound to them (in the same way that mRNA strands are bound to a microarray chip) prior to the sample of interest being added to the chip allowing for the detection of protein-protein interactions or protein-antibody interactions. RPPA differs to these early protein microarrays in that it works in the opposite way to a microarray, hence the 'reverse phase' in its title [184]. In RPPA the samples of interest are printed directly onto the slide prior to incubation with primary antibodies. A secondary antibody conjugated to a fluorophore is then used as a read out for protein activity. Using this method it is in principle possible to perform measurements of hundreds of proteins and samples. RPPA is however dependent on highly specific antibodies and it is this requirement that has thus far slowed the uptake of RPPA as a major analytical methodology for protein analysis. There are currently several efforts underway to create a library of validated antibodies for RPPA that can be accessed by researchers worldwide [185].

To date RPPA has proved a useful tool in several areas such as profiling of dysregulated protein networks in tumour samples from cancer patients and for validation of biomarker discoveries [186]. A primary of example of its use to date has been its use as one of the platforms used in a multi-omic molecular profile study investigating personalised treatment in breast cancer progression [187]. This study utilised RPPA to study the relative protein activation, phosphorylation and expression in

metastatic breast cancer patients. From the data generated by RPPA in combination with transcriptional methodologies the authors were able to suggest personalised therapeutic targets for each of the 25 patients in the study. Whilst the use of RPPA in the calibration of dynamic network models is not yet wide spread there are some notable examples. In 2012 Peng et al used RPPA to examine differences in protein levels in myelodysplastic syndromes compared to control samples. The authors compared 179 different antibodies across 10 samples and five time points. They used a subset of this extensive dataset to parameterise a dynamic model of the p38 mitogen-activated protein kinase (MAPK) pathway which enabled them to identify a shift in regulation for the degradation of key proteins from JNK to p38 pathways [180]. In addition RPPA has also been utilised in the development of a computational model of the HER-2 targeting receptor tyrosine kinase (RTK) inhibitor Trastuzumab a common anti-cancer therapeutic. Following calibration of a dynamic model with RPPA generated data the authors showed that PTEN protein expression was the key factor in resistance to HER-2 targeting therapeutics such as Trastuzumab [188]. Due to its previous use in the development of dynamic models it was decided that RPPA could offer the medium-throughput alternative to western blotting required for this project.

3.4 Reverse phase protein array produces consistent time course data suitable for dynamic modelling

To test the suitability of RPPA for the production of time course data sets relevant to this work a time course experiment was carried out using MRC5 cells. For this initial study cells were treated using the starvation-restimulation protocol described in section 2.1.8. A timecourse of 60 minutes following restimulation was chosen consisting of six time points (0, 5, 10, 20, 30 and 60 minutes post restimulation) (figure 3.1). As a first examination of RPPA's suitability to produce time course data for the mTOR network a set of six antibodies relating to both mTORC1 and mTORC2 were selected. These consisted of mTORC1_pS2448, AKT_pS473, P70S6K_pT389, S6_pS235/236, 4E-BP1_pT37/46 and 4E-BP1_pS65. The initial run of RPPA proved successful at producing consistent time course data of a high standard for the antibodies tested (figure 3.1). Of particular note was the consistent data between mTORC1_pS2448 and its downstream read out S6_pS235/236 (figure 3.1 A+D). In contrast measurement for the two 4E-BP1 residues differ in their profile when compared to the upstream mTORC1_pS2448 output, but when compared against each other they display similar

expression profiles (figure 3.1 E+F). Whilst five of the antibodies produced similar outputs the P70S6K_pT389 profile differs significantly from each of the other profiles (figure 3.1 C). In addition for the majority of data points tested displayed low standard deviations with the exception of the sixty minute time point.. The exception to this was the S6K_pT389 antibody which had a very low standard deviation for the sixty minute time point (figure 3.1 C).

As mentioned in section 3.3 one of the main drawbacks of RPPA is its dependence on specific antibodies. In order to address this it was necessary to carry out a series of quality control experiments on the antibodies currently being examined. As part of the initial time course a single repeat was treated with alkaline phosphatase as a means to remove all phosphorylation events within each sample, this repeat was processed alongside the experimental repeats. As the alkaline phosphatase acts to remove phosphate groups bound to proteins it can be assumed that any fluorescence detected during the imaging of these samples is either auto-fluorescence or non-specific binding of the antibody in question. The alkaline phosphatase repeat can then be compared to the experimental results to help reveal the specificity of a particular antibody (figure 3.2). In the case of four of the antibodies (mTOR_pS2448, AKT_pS473, S6_pS235/236 and 4E-BP1_pS65) whilst there is some fluorescence detected in the alkaline phosphatase repeat these values are significantly lower than those of the corresponding experimental repeats (figure 3.2 A, B, D, F). This therefore suggests that these four antibodies are suitable for use with RPPA especially in the case of S6_pS235/36. However two of the antibodies display high fluorescence even when treated with alkaline phosphatase (4E-BP1_pT37/46 and S6K_pT389) (figure 3.2 C+E). For both of these antibodies their RFI is of a similar value whether or not they have been treated with alkaline phosphatase suggesting that these particular antibodies have a high amount of non-specific binding. Neither of these antibodies are therefore suitable for further analysis with RPPA. This may also explain why the profile for S6K_pT389 differs from all of the other antibodies tested.

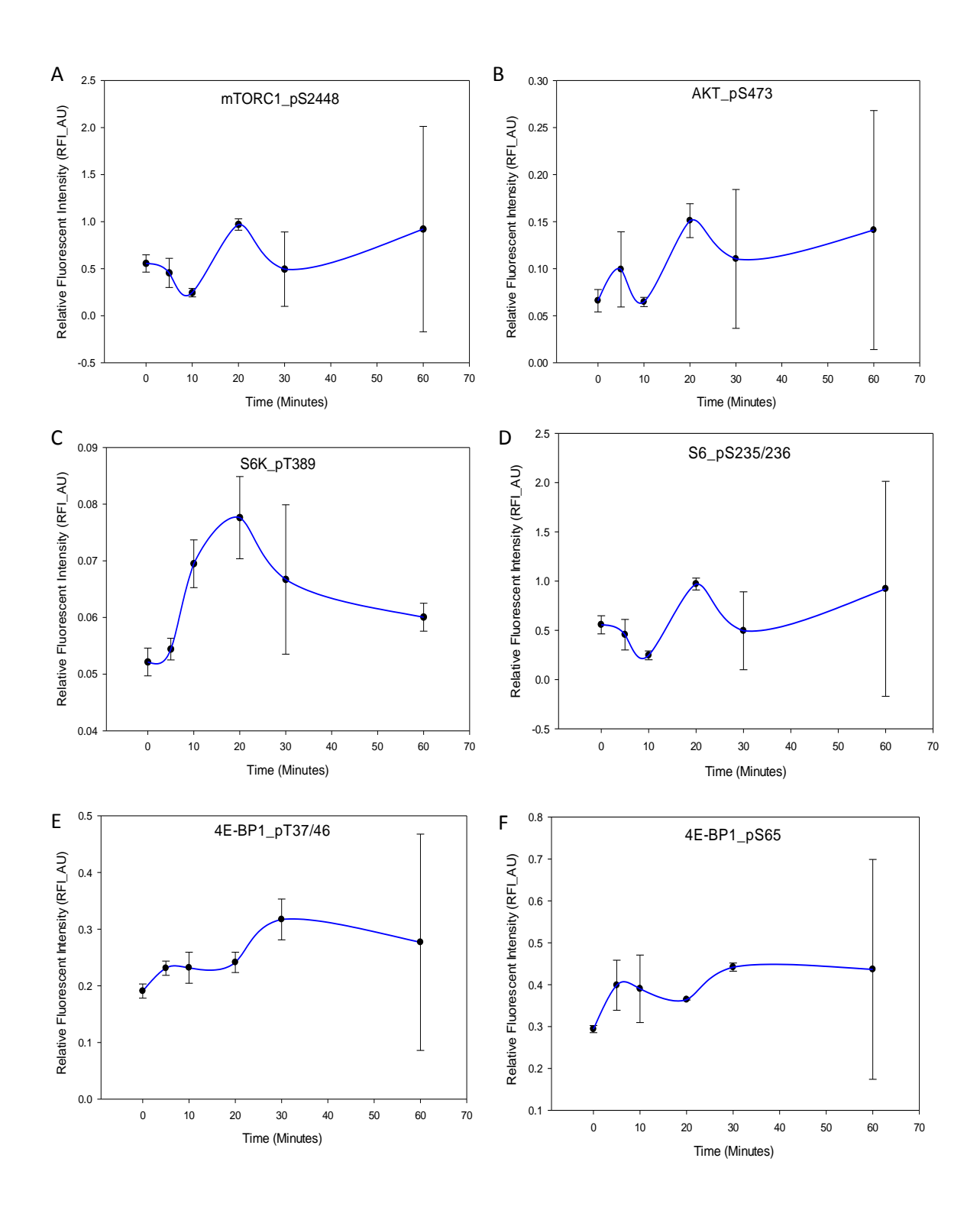


Figure 3.1: RPPA is capable of producing calibration time course data for a dynamic model. Sixty minute time course following a 24 hour starvation period. Cells were restimulated at 0 hours and relative fluorescent intensity measured at each time point (n=2) (Mean +/-SEM). (A) mTORC1_pS2448, (B) AKT_pS473, (C) P70S6K_pT389, (D) S6_pS235/236, (E) 4E-BP1_pT37/46 and (F) 4E-BP1_pS65.

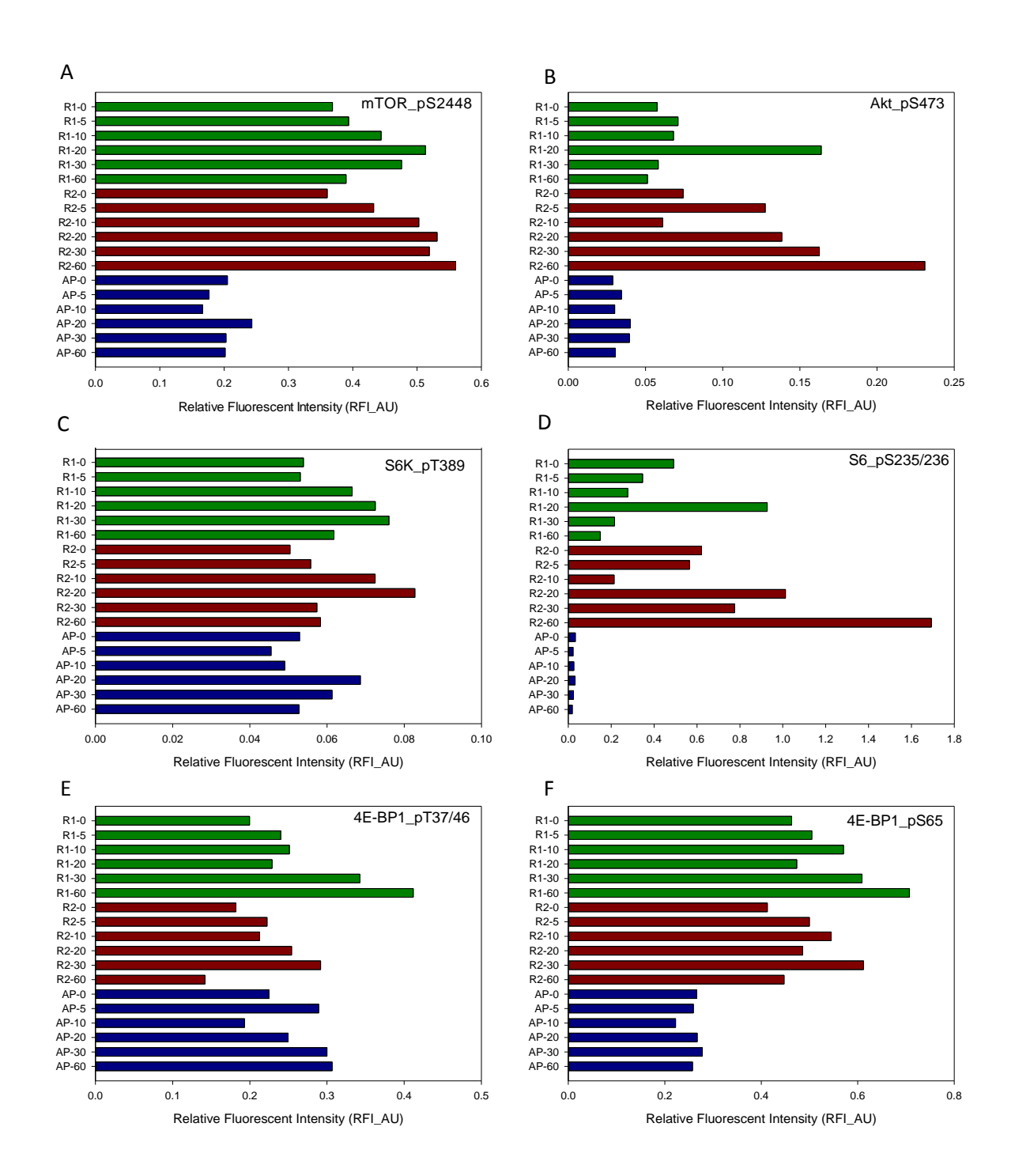


Figure 3.2: Alkaline phosphatase treatment reveals the level of non-specific binding for each antibody. Level of relative fluorescent intensity for two experimental repeats (R1-Green, R2- Red) compared to alkaline phosphatase treatment (Blue). Antibodies measured were as follows (A) mTORC1_pS2448, (B) AKT_pS473, (C) P70S6K_pT389, (D) S6_pS235/236, (E) 4E-BP1_pT37/46 and (F) 4E-BP1_pS65.

In addition to performing alkaline phosphatase treatment it was thought prudent to assess the reliability of RPPA not just between replicates but also between different antibodies for the same phospho-site. An additional three antibodies for AKT_pS473, S6_pS235/236 and 4E-BP1_pS65 from different sources were tested (Figure 3.3). The second antibodies tested for both AKT_pS473 and S6_pS235/236 displayed lower RFI values to the original antibodies whilst the second 4E-BP1_pS65 antibody displayed increased RFI to the original (Figure 3.3 B, D, E). However whilst the RFI values between antibodies differs the overall profile remains the same with similar standard deviations for each time point being observed between related antibodies and as with the original antibodies the sixty minute time point had the largest standard deviation in all three of the new antibodies (Figure 3.3 A-F).

As with the original set of six antibodies it was necessary to investigate if the new antibodies being tested showed non-specific binding when treated with alkaline phosphatase. A comparison was therefore carried out against the respective antibodies from the original six antibodies tested (Figure 3.4). In the case of AKT_pS473 both antibodies displayed similar levels of RFI in the alkaline phosphatase treated repeat when compared to the RFI of the experimental repeats (figure 4.4 A+B). Whilst the second antibody for S6_pS235/236 showed lower variation between repeats it had a much lower RFI than the first antibody tested (figure 3.4 C+D). This meant that although the level of RFI was low in the alkaline phosphatase repeat for this antibody it still represented a significant amount of the overall RFI in the experimental results suggesting that for further RPPA the original antibody for S6_pS235/236 should continue to be used (figure 3.4 C+D). In contrast the second 4E-BP1_pS65 antibody tested showed lower RFI values in the alkaline phosphatase repeat when compared to the original antibody (figure 3.4 E+F). Therefore in any subsequent RPPA analysis the second antibody tested should be the antibody used to detect the levels of expression for this protein. Following these experiments it can be concluded that RPPA is capable of producing consistent and reliable time course data for the purpose of calibrating dynamic models.

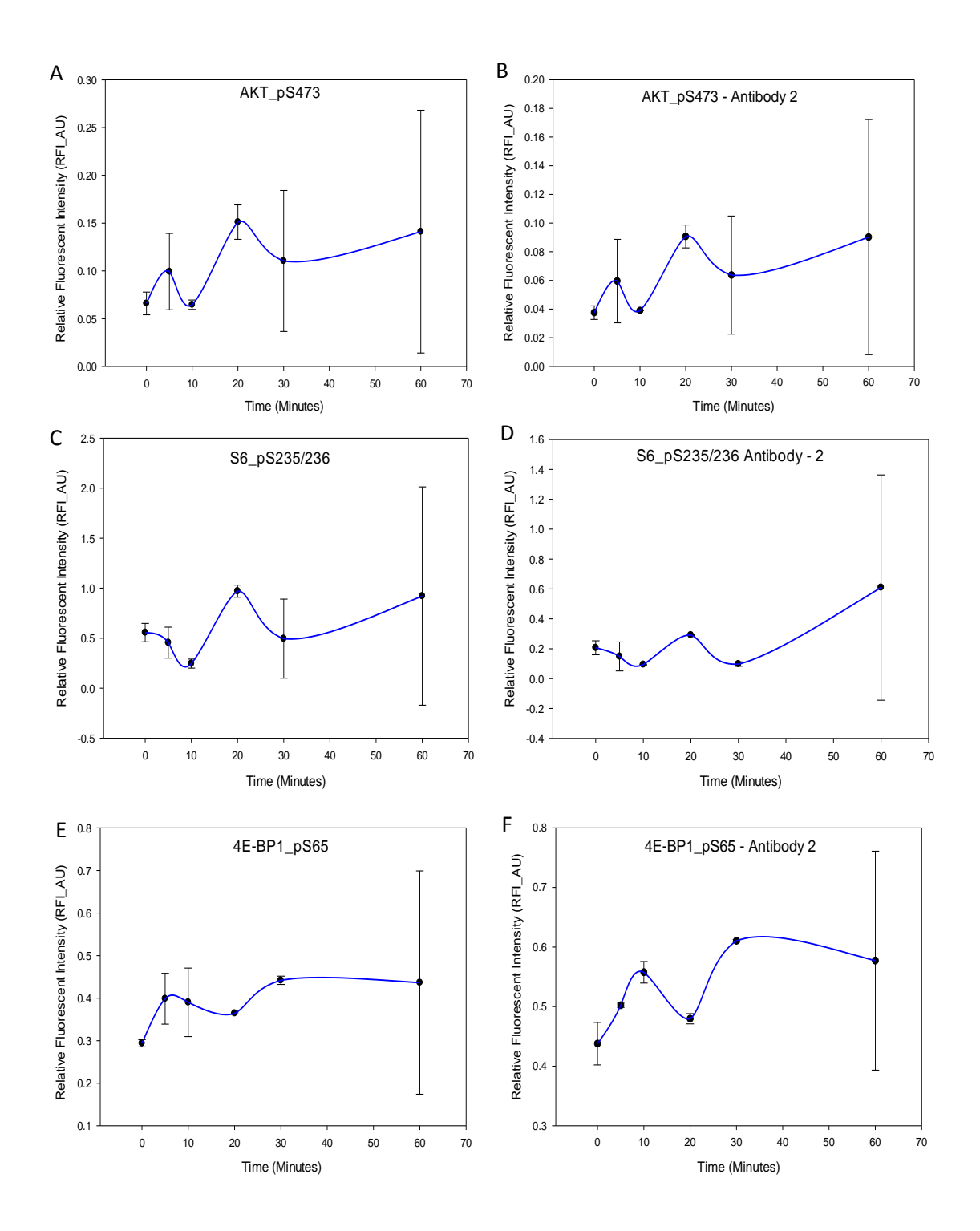


Figure 3.3: RPPA output remains consistent between different antibodies for the

same protein. Sixty minute time course following a 24 hour starvation period. Cells were restimulated at 0 hours and relative fluorescent intensity measured at each time point (n=2) (Mean +/- SEM). The following outputs for two antibodies for the same protein but form separate sources are compared. (A-B) AKT_pS473, (C-D) S6_pS235/236, (E-F) 4E-BP1_pS65.

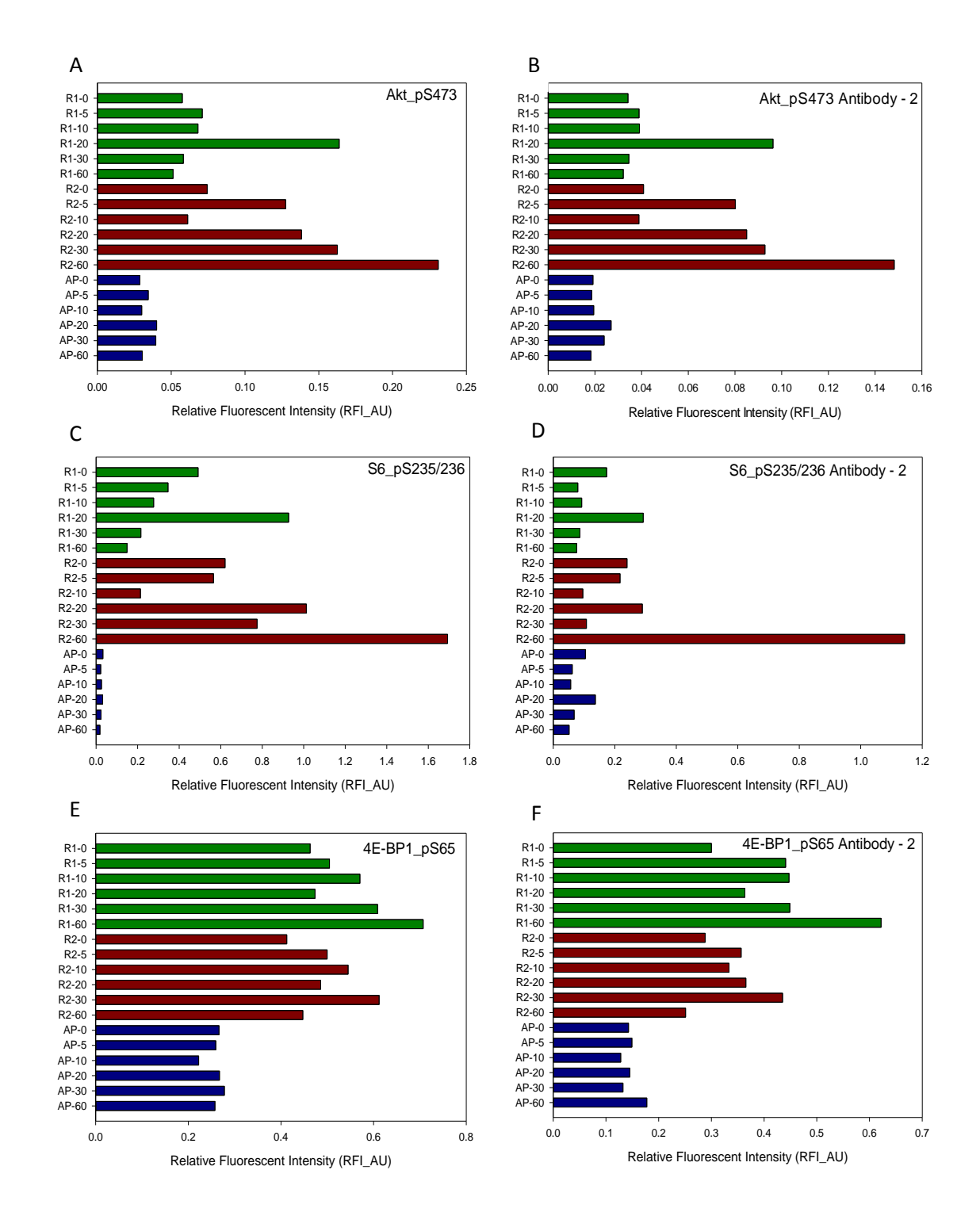


Figure 3.4: Alkaline phosphatase treatment can determine the level of non-specific binding between separate antibodies for the same protein. Level of relative fluorescent intensity for two experimental repeats (R1-Green, R2- Red) compared to alkaline phosphatase treatment (Blue). The following outputs for two antibodies for the same protein but form separate sources are compared. (A-B) AKT_pS473, (C-D) S6_pS235/236, (E-F) 4E-BP1_pS65.

3.5 Intracellular flow cytometry

Classically the core focus of flow cytometry has been the measurement of extracellular cell markers, however over the last decade there has been major advancements in the development of flow cytometers, antibodies and staining procedures [189]. This has led to the increased ability to measure the activation or inhibition of intracellular proteins using flow cytometry [190, 191]. Intracellular flow cytometry involves the permeablisation of fixed cells prior to detection of intracellular protein-epitopes using antibodies. Antibodies are either conjugated directly to a fluorophore or a primary antibody followed by a secondary antibody conjugated to a fluorophore is used. Cells are then passed through a flow cytometer which excites the flourophores using lasers to generate different wavelengths of light. This light emitted from the fluorphores then passes through a series of opitcal filters optics which separate the light emission based on wavelengths allowing for the detection of different flurophores in the same sample. The number of different antibodies and fluorophores that can be detected is determined by the flow cytometry system however as a standard it should be possible to analyse up to eight serparate antibodies on a standard instrument. Whilst the ability of intracellular flow cytometry to produce time course data capable of calibrating intracellular based dyanmic models has yet to be explored the use of flow cytometry in systems modelling is well documeted. Flow cytometry provided the principle technique for the analysis of microbial cell population dynamics and is commonly used in cancer research to identify cell population dynamics [181, 192]. It has also previously been shown to be capable of producing intracellular time course data for protein networks including the mTOR network [193, 194]. With the ability to analyse multiple proteins within each sample it is possible that intracellar flow cytometry could provide a viable alternative to western blotting for the produciton of calibration data for dynamic modelling. Here we present a pilot experiment with the aim of testing intracellular flow cytometrys ability to produce time course data for the mTOR network.

3.6 Intracellular flow cytometry fails to provide consistent data suitable for dynamic modelling

In order to test the ability of intracellular flow cytometry to produce time course data suitable for calibrating dynamic models a pilot experiment was designed. An initial study was carried out using MRC5 cells treated with 50µM of the mTOR inhibitor Torin1 for a period of 24 hours. For the purposes of this study only two time points were examined with samples generated at time 0 hours prior to Torin1 treatment and following 24 hours Torin1 treatment. As this was a preliminary study it was not felt necessary to fully test the capabilities of the flow cytometry systems by testing a large number of antibodies with varying conjugated fluorophores and so it was decided that only two antibodies should be tested. The two antibodies being studied consisted of AKT_pT308 conjugated to alexa-488 and mTORC1_pS2448 conjugated to PECY7, with the antibodies chosen to minimise the requirement for compensation between the conjugated fluorophores. Following treatment with Torin1 for 24 hours there was a slight decrease in mTORC1_pS2448 fluorescence (figure 3.5 A-D) whilst control cells showed no decrease in PECY7 fluorescence (figure 3.5 E-H). Due to limited fluorescence from the AKT_pT308 antibody used it was not possible to determine if there was any change in AKT_pT308 activity (Appendix A). Whilst there was an indication from this study that flow cytometry could provide time course data suitable for dynamic model calibration the results were inconclusive and therefore it was necessary to carry out further experiments to fully explore its capabilities.

A time course was carried out using MRC5 cells following the starvation-restimulation protocol described in section 2.1.8 and measurements were taken at 0, 5, 15 and 30 minutes post-stimulation. As this was to be a more rigorous test of intracellular flow cytometry's capabilities four separate antibodies were examined (mTORC_pS448-PECY7, AKT_pT308-Alexa 488, AKT_pS473-APC and S6_pS235/236-V450). As with the previous experiment it was not possible to obtain a read-out for AKT_pT308 alexa-488 (data not shown) and as such this antibody was not tested again. Following restimulation there was no change in the level of mTORC_pS2448 activity over the first three time points (0, 5, 15 minutes) and a decrease in activity after 30 minutes of restimulation (Appendix A). AKT_pS473 showed an increase in activity at 5 minutes following restimulation with a decrease at 15 minutes following restimulation.

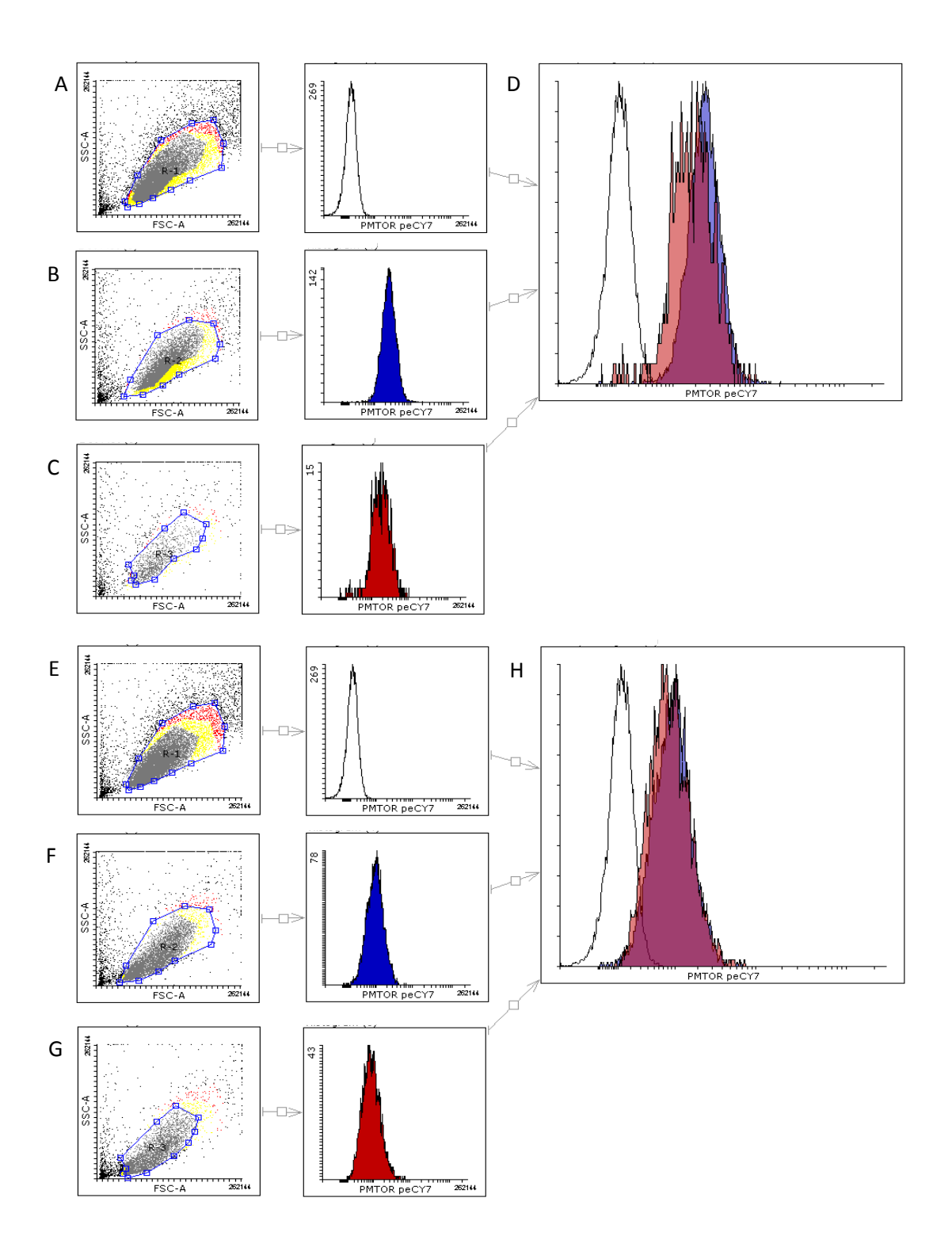


Figure 3.5: Treatment with 50μM of Torin1 leads to a reduction in mTORC1 pS2448 signalling. MRC5 cells were treated with 50μM Torin1 for 24 hours with samples taken at 0 hours and 24 hours. (A+E) unstained sample (B) 50μM Torin1 0 hours, (C) 50μM Torin1 24 hours, (D) Overlay histogram displaying a comparison for each time point, (F) Untreated sample 0 hours, (G) Untreated sample 24 hours, (H) Overlay histogram displaying a comparison for each time point.

A further increase in activity was seen at 30 minutes (Appendix A). Of the antibodies tested only the output for S6_pS235/236-V450 activity was consistent with the expected behaviour of the S6_pS235/236 phosphorylation site following serum starvation-restimulation. Following restimulation there was a significant increase in S6_pS235/236 activity between the 5 minutes and 15 minute time points with a slight decrease in activity observed between the 15 minute and 30 minute time points (figure 3.6 A-G).

Due to the S6_2325/236-v450 antibody displaying behaviour consistent with that expected following serum starvation-restimulation it was decided that a further study should be carried out using insulin to increase the effect of restimulation. MRC5 cells were treated as in section 2.1.8 with 100nM of insulin (Sigma-Aldrich, Dorset, UK) added to DMEM high Glucose supplemented with 10% foetal bovine serum, 1% of L-Glutamine and 1% of Penicillin-Streptomycin prior to restimulation. The addition of insulin to the restimulation cell culture media had no effect on the overall behaviour displayed by AKT_pS473-APC with increased activity at 5 minutes post restimulation followed by decreased activity at 15 minutes post restimulation before a final increase in activity at 30 minutes post restimulation (Appendix A). The overall output for mTORC1_pS2448-PECY7 displayed at small increase in activity following insulin restimulation. However as opposed to the other antibodies being examined it failed to produce consistent results across repeats with each of three separate repeats displaying different behaviour throughout the time course (Appendix A). As with the previous experiment the S6_2325/236-v450 antibody displayed behaviour consistent with that expected. Following insulin enhanced restimulation S6_2325/236-v450 activity increased over the first 15 minutes of the time course with a decrease in activity observed following 30 minutes post restimulation (figure 3.7 A-G). Following these experiments it can be concluded that whilst intracellular flow cytometry can produce time course data for particular proteins within the mTOR network it fails to do so in a consistent manner for many of the required read-outs. It is therefore not be suitable for further examination as an alternative to western blotting. A comparison of the three possible protein analysis platforms is provided in table 3.1.

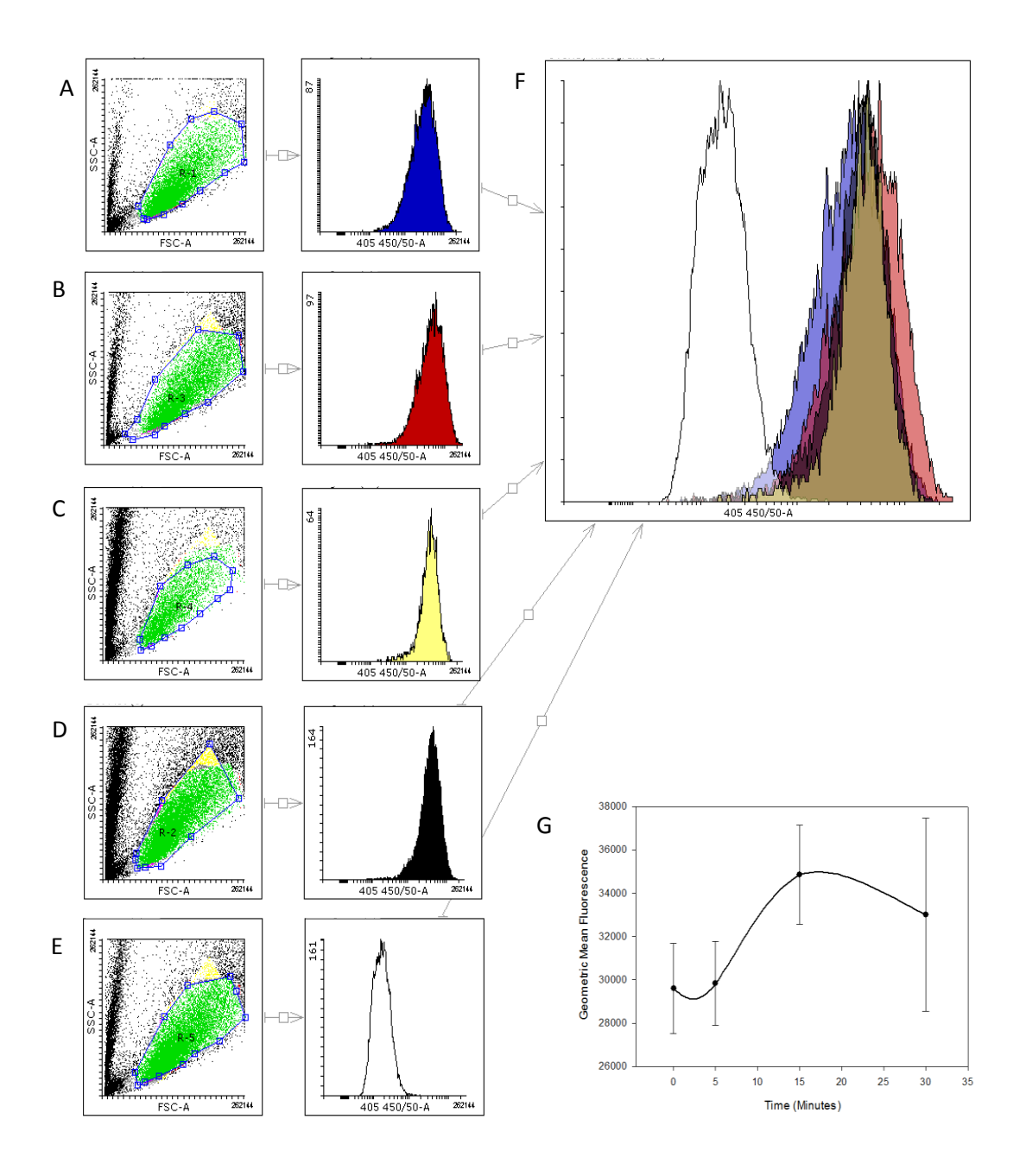


Figure 3.6: Intracellular flow cytometry is capable of producing calibration time course data for a dynamic model for S6_pS235/236. Cells were serum starved overnight and then re-stimulated with FBS and L-Glutamine containing media with time points collected after (A) 0 minutes, (B) 5 minutes, (C) 15 minutes and (D) 30 minutes (n=3) representative of 1 repeat shown. (F) Overlay histogram displaying a comparison for each time point. (G) The average Geometric mean for each time point plotted against time (Mean +/- SEM).

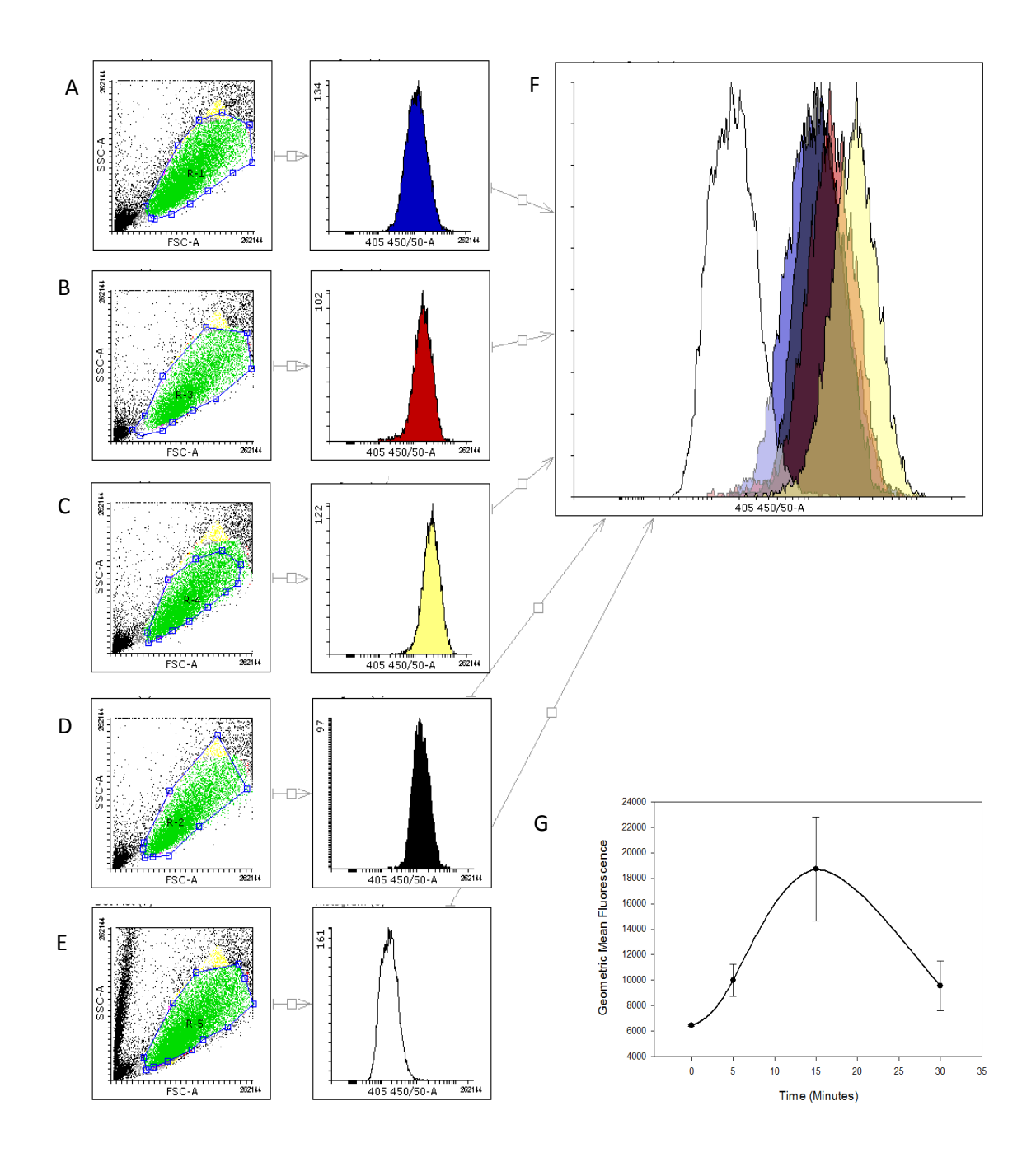


Figure 3.7: Insulin treatment enhances the capable of Intracellular flow cytometry to produce calibration time course data for a dynamic model for S6_pS235/236.

Cells were serum starved overnight and then re-stimulated with FBS and L-Glutamine media supplemented with 100nM insulin with time points collected after (A) 0 minutes, (B) 5 minutes, (C) 15 minutes and (D) 30 minutes (n=3) representative of 1 repeat shown. (F) Overlay histogram displaying a comparison for each time point. (G) The average Geometric mean for each time point plotted against time (Mean +/- SEM).

Table 3.1: A comparison of possible protein analysis platforms

Analysis Platform	Advantages	Disadvantages
Western Blotting	 Separates proteins based on molecular weight Analysis platform is already commonly used so comparisons with previous work can be carried out No Specialist equipment required 	 Work intensive High amount of lysate is required per run Only one antibody can be analysed per gel per run Low – medium throughput
Reverse Phase Protein arrays	 Medium – high throughput Multiple antibodies can be tested for per run Low volume of lysate required 	 Requires specialist equipment Requires highly specific antibody for each protein analysed
Intracellular Flow Cytometry	 Multiple antibodies can be tested for per run Medium throughput Specialist facilities in place 	 Can only analyse cell sample once Antibodies cannot be reused Requires careful matching of primary antibodies to secondary antibodies Compensation must be applied for each antibody making it impractical to measure many antibodies at once

3.7 Discussion

The purpose of this work was to determine whether reverse phase protein arrays or intracellular flow cytometry could provide an alternative method to western blotting for the purpose of producing time course data in order to calibrate a dynamic model. Whilst both methodologies proved capable of producing time course data the quality of this data differed greatly between each technique. Flow cytometry proved capable of replicating the expected output for the mTOR network but only for one of the three antibodies tested (S6_pS235/236-v450). This technology appears to be hampered by the same problems encountered when performing western blots. It is possible to analyse up to eight antibodies per sample with the technique which is a greater number than with western blotting however samples cannot be retested once they have been stained. Ultimately this means that many more replicates will be required for the same time course to achieve the coverage required to fully calibrate a dynamic model and therefore little time would be saved when compared to western blotting. As this was the principle reasoning behind this study it can be said that flow cytometry failed to meet our criteria. In addition the use of eight antibodies within the system being used would lead to numerous compensatory issues with regards to the overlap of spectral output of fluorophores being tested. Meaning that whilst this could be carried out in theory it is unlikely that all eight antibodies could be used in practise. If these tests had proved to be successful then it may have been possible to proceed using a higher throughput flow cytometry machine or indeed to analyse samples utilising mass cytometry a technique that combines the principles of both flow cytometry and mass spectrometry. This would have allowed for the analysis of a much larger set of antibodies however it was decided that when the output from the RPPA was taken into account that there was no requirement to carry out further experiment utilising this type of flow cytometry. During these experiments it was noted that flow cytometry may be of use for a more specific application. Within the mTOR network both FOXO3A and Rheb are dependent on their cellular localisation for correct activity. It was decided that the cellular localisation of these proteins should be measured using imagestream flow cytometry a technique that photographs cells as they pass through the flow cytometer allowing for analysis of colocalisation properties between fluorophores. In the case of FOXO3A a comparison with the nuclear stain DAPI could be used and for Rheb a comparison with the lysosomal marker LAMP-1 could be used to analyse the localisation of these proteins following each of the different treatments.

RPPA proved capable of producing high quality time course data sets capable of calibrating a dynamic model. It has also been possible to answer the question of whether or not RPPA is more time effective than western blotting. As it takes the same amount of time to produce the time course lysates for both methodologies this is a question of how quickly each sample can be analysed. For this experiment a total of nine antibodies were tested however it is noteworthy that this time course was carried out alongside another experiment with the total number of antibodies measured numbering eighteen. With the possibility of printing a total number of sixty-four samples onto a single RPPA chip this allows for the measurement of a total of three replicates plus reference proteins on one chip. As one RPPA slide contains six chips with the possibility to analyse 64 samples per chip it is possible to assay either 384 samples with one antibody per slide or 64 samples with 6 antibodies per slide. In addition as it is possible to print multiple slides at once these figures can be multiplied by the number of slides required. As mentioned earlier this has been carried out measuring 179 antibodies on only ten samples [180]. The entire RPPA measurement process takes one week to complete meaning that following the production of the cell lysates it is possible to analyse the reaction of a huge number of proteins making this process far more time effective than western blotting. Theoretically therefore RPPA appears to be an extremely effective substitute for western blotting in the production of calibration data for dynamic models. The main limitation to this process is the requirement for highly specific antibodies and therefore it is possible that some proteins within the mTOR network such as P70S6K_pT389 may not be measureable with RPPA it will therefore be necessary to use alternative readouts of mTORC1 activity such as the 4E-BP1 and ribosomal S6 antibodies assayed above (figure 3.2 C).

Since these experiments were performed there have been further examples of RPPA being utilised in the field of dynamic modelling. Tan et al used RPPA to measure the activation of osteoblastic protein markers during osteoblast differentiation. Combining this data with a dynamic model the authors were able to test how different cytokines combined to activate osteogenesis and provide a potential therapeutic tool for patients of osteoporosis [195]. With the data available we can conclude that RPPA can provide an effective and time efficient method for producing time course data for dynamic modelling and therefore this methodology was taken forward in this work.

3.8 Conclusions

- Reverse Phase Protein arrays are capable of producing reliable time course data suitable for the calibration of dynamic models
- RPPA is both time efficient and high-throughput in comparison to western blotting
- Intracellular flow cytometry was capable of producing time course data for the calibration of dynamic models
- This method was however not as reliable as RPPA nor as time efficient
- RPPA will used to produce the time course data required for this work
- Imagestream flow cytometry will be investigated as a method for studying intracellular localisation of FOXO3A and Rheb

4. A dynamical model of the mTOR signalling network reveals the kinetics of starvation and restimulation in MRC5 fibroblasts and human bone marrow stem cells

4.1 Introduction

A key role for a reduction in of nutrient signalling in ageing is well established. The first systematic genetic screen to identify genes involved in ageing were conducted in C. elegans which identified individuals with mutations directly linked to the mTOR network [7, 196-198]. The Daf-2 and Daf-16 mutants (*C. elegans* homologues for mammalian IGF-1R and FOXO) were found to live up twice as long as their wild type counterparts [199]. Mutations in homologues in other model species such as *Drosophila* and mice are also long-lived and provide evidence for evolutionary conservation. There is now an extensive body of research on the connection between nutrient signalling and the ageing process [197, 198].

The mTOR network is activated in a number of ways including nutrient signalling and amino acid stimulation. Caloric restriction (also referred to as dietary restriction) was one of the first interventions identified as being able to extend lifespan in a number of model organisms and remains the 'gold standard' in lifespan extension interventions. Caloric restriction is defined as a reduction in calorie intake without malnutrition. This leads to a reduction in the activation of the insulin/IGF-1 signalling and a downregulation of both mTORC1 and mTORC2 [200]. Although the exact mechanisms of how caloric restriction works have yet to be fully established it is believed that the down regulation of mTORC1 leading to an increase in autophagy plays a major role [201]. One proposed explanation is that the shift in the balance between the anabolic mTORC1 processes and catabolic autophagy processes results in increased longevity [202]. Autophagy is responsible for the recycling of amino acids during periods of caloric restriction. It also removes damaged organelles from cells. As we age the autophagic response declines whilst mTOR signalling increases. It is believed that by maintaining a higher autophagic response for longer that there will be increased clearance of damaged components within cells. This in turn could possibly delay the ageing process, however this has so far proved difficult to quantify[83].

As caloric restriction provides the most well characterised method for lifespan extension it was an obvious choice for us to study in detail the mechanistic reaction of the mTOR network following a period of starvation. Currently, there is no methodology for performing caloric restriction *in vitro* therefore in order to examine the effect of caloric restriction a method mimicking its effect was sought. Previous work carried out by our own group utilising serum starvation has proved largely successful in the study of the

mTOR network and caloric restriction. It was therefore decided that this method for mimicking caloric restriction in vitro should be used for this study [171, 172].

The computational model described in this section provides the main framework for all of the dynamic models that follow. Previous work in our group has used dynamic modelling to study the wiring of the mTOR network and the various effects of insulin and amino acid signalling [80, 171, 172, 203]. These models provide the building blocks upon which the development of this model was based. It was decided that for our control cell line we should use MRC5 fibroblasts as again previous research by our group has shown these cells to be a reliable model cell line with which to investigate the mTOR network [203]. In addition having used these cells previously it allows for the comparison with previous experiments carried out by our group and further validation of the RPPA systems for production of time course data. Finally as we wish to compare this output to that from bone marrow derived stem cells we will be able to do so with confidence.

4.2 Aims

This study aims at examining the effect of re-stimulation following serum starvation on the mTOR network. We aim to define using a computational dynamic model how the mTOR network responds in MRC5 fibroblasts and how the mTOR network response differs in human mesenchymal stem cells.

4.3 Results

restimulation.

4.3.1 Development of starvation-restimulation dynamic network model In order to investigate the response of the mTOR network to serum starvationrestimulation (SSR) a static model was designed and built as described in section 3.2. As a basis for the initial model a dynamic model previously described in the literature produced by our group was used to inform the core structure of the model [171]. With the core model structure in place additional reactions were added to the model based on key literature findings. The focus when expanding the network was to add reactions relevant to two particular areas, amino acid stimulation of the mTOR network and proteins known to be affected by Zoledronate treatment. In addition to altering the existing core structure to include further relevant proteins, proteins no longer relevant to the current study were removed from the model structure. This resulted in an expanded network incorporating proteins related to Zoledronate treatment and amino acid stimulation that would be capable of simulating to the response of starvation-

The network used throughout this chapter is shown in Figure 4.1 and all reactions can be found in appendix B. It includes both insulin/growth factor (GF) and amino acid activation of mTORC1 in addition to insulin/GF activation of mTORC2. Insulin/GF stimulates mTORC1 through activation of PI3K and subsequent activation of PDK1 and AKT on threonine 308. This results in the phosphorylation of the TSC1/2 complex inhibiting its GAP activity on Rheb. Rheb in its GTP bound active state is then able to activate mTORC1. For the purposes of this work amino acids are deemed to activate mTORC1 directly and lead to its phosphorylation of serine 2448. Once activated mTORC1 directly activates both P70-S6K and 4E-BP1 with P70-S6K feeding back upstream to inhibit the phosphorylation and activation of IRS1 and PI3K.

As mentioned in section 1.3 very little is known regarding mTORC2 upstream activation and therefore in this study mTORC2 is activated by a PI3K species distinct from the PI3K upstream of PDK1 and mTORC1 [80]. Once activated mTORC2 leads to phosphorylation of AKT on serine 473. Within the model, phosphorylation on serine 473 can occur both before and after threonine 308 phosphorylation with the same being true for threonine 308 phosphorylation. Once activated AKT_pS473 is then capable of phosphorylating FOXO3A leading to its inhibition. The exact mechanism by which

AKT phosphorylates and inhibits FOXO3A is still disputed within the literature and it is not fully understood if phosphorylation on either threonine 308 or serine 473 is required or if phosphorylation on both sites is required [204]. Recent findings however have suggested that mTORC1 inhibition alone is not sufficient to lead to FOXO3A inhibition [205]. Therefore in this study only AKT phosphorylated on serine 473 either on its own or in addition to threonine 308 phosphorylation can phosphorylate FOXO3A.

4.3.2 Reverse phase protein array provides a high quality calibration dataset

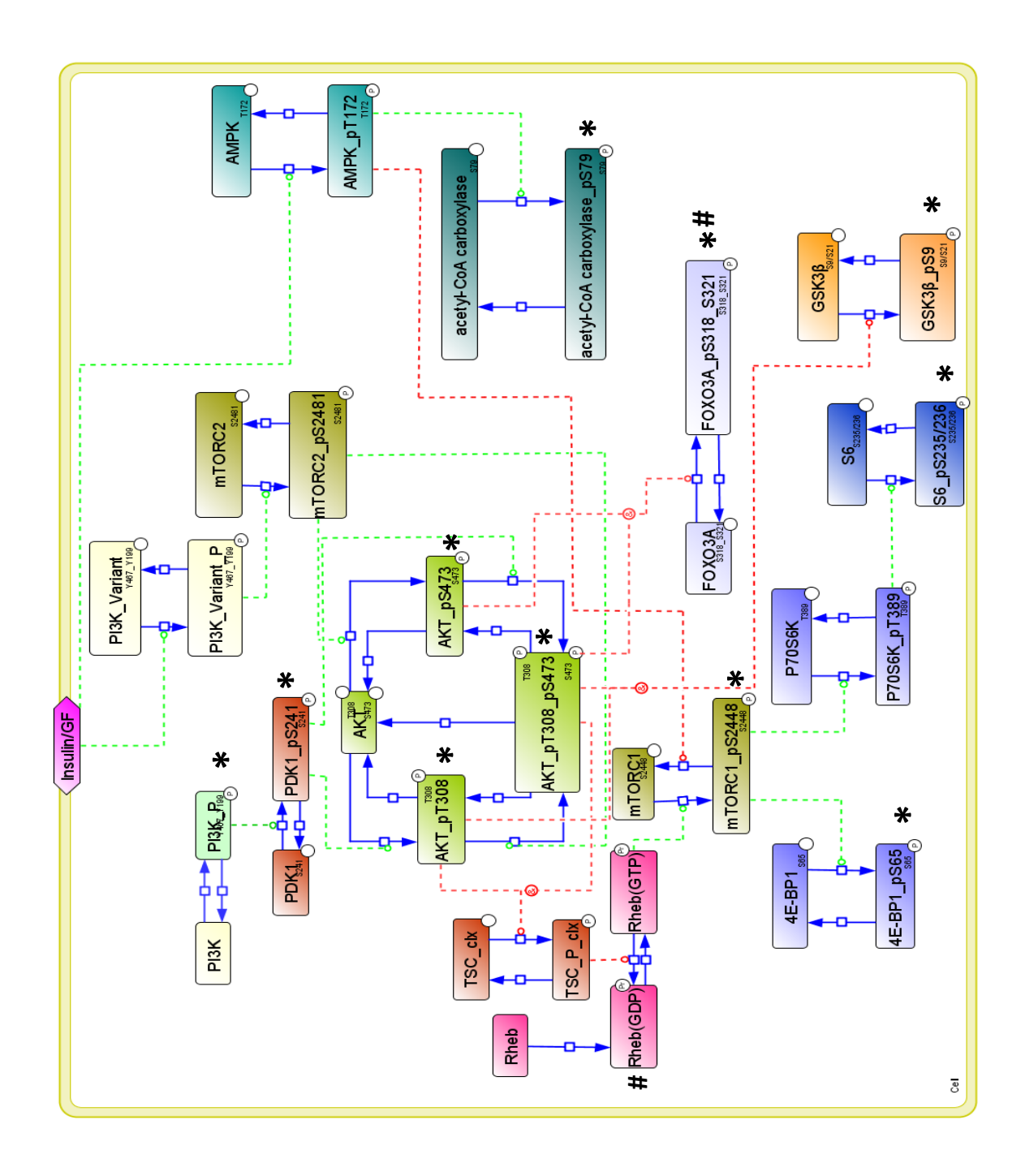
Once the topology of the network model had been decided a calibration dataset was required. As discussed in the previous chapter the method chosen for the production of this data set was reverse phase protein arrays (RPPA). It was decided that a 24 hour time course should be carried out with increasing intervals between the time points as described in section 2.1.15. This would allow us to capture the rapid response of the mTOR network to re-stimulation in addition to allowing the study of the longer term effects. A group of 7 proteins were initially assayed and their initial response to restimulation analysed over a period of 60 minutes. Figure 4.2 shows the results of the initial run of these samples with the expected response seen in all metabolites except mTORC1_pS2448 which initially decreases following re-stimulation (Figure 4.2-B). However for AKT_pS473, S6_235/236 and S6_240/244 (Figure 4.2-A, E, F) an overall increase is observed over the 60 minutes. For 4EBP1_pS65 an initial increase up to 30 minutes is observed followed by a decrease between 30-60 minutes (Figure 4.2-C). Whilst this behaviour is also observed in the P70S6K_pT389 antibody tested, the alkaline phosphatase control for this antibody again displayed non-specific binding. This output could not therefore be validated as P70S6K_pT389 phosphorylation (Figure 4.2-D).

With the initial time course proving to be successful the antibody coverage was expanded to include a further 11 antibodies providing good cover across the mTOR network for both total and phospho proteins (Figure 4.3). With a larger number of proteins measured it was possible to examine why the output from the previously measured mTORC1_pS2448 decreased following re-stimulation, indeed this behaviour could be seen throughout the upstream PI3K network with PI3K p85_pY467_Y199, PTEN_pS380_T382_T383 and PDK1_pS241 all displaying similar behaviour (Figure 4.3-B, C, D). Whilst it was not possible to measure AMPK_pT172 it was possible to

assay acetyl-coA carboxylase - a downstream effector of AMPK (Figure 4.3-A). Importantly this protein displayed the expected behaviour observed following amino acid deprivation previously seen with western blotting [172]. This could explain the decrease in PI3K and MTORC1 signalling observed across the first 30 minutes of the time course. A list of all Antibodies assayed can be found in Table 4.1.

<u>Table 4.1: Reverse Phase Protein Array Antibodies.</u> A list of all antibodies assayed during starvation-restimulation experiments

Antibody	Antibody	Source
ACC	AKT_pS473	Cell Signalling Technology
ACC_pS79	mTOR	Cell Signalling Technology
PI3K p85_pY467_Y199,	mTOR_pS2448	Cell Signalling Technology
PTEN	4E-BP1	Cell Signalling Technology
PTEN_pS380_T382_T383	4E-BP1_pS65	Cell Signalling Technology
PDK	S6_pS235/236	Cell Signalling Technology
PDK1_pS241	S6_pS240/244	Cell Signalling Technology
AKT	FOXO3A	Cell Signalling Technology
AKT_pT308	FOXO3A_pS318_S321	Cell Signalling Technology
A-tubulin		Cell Signalling Technology



<u>Figure 4.1: The mTOR network.</u> A SBGN network model diagram displaying the effect of amino acids on the mTOR network. Asterisks mark phospho proteins measured for starvation-restimulation RPPA experiments whilst hashtags mark proteins assayed by imagestream flow cytometry.

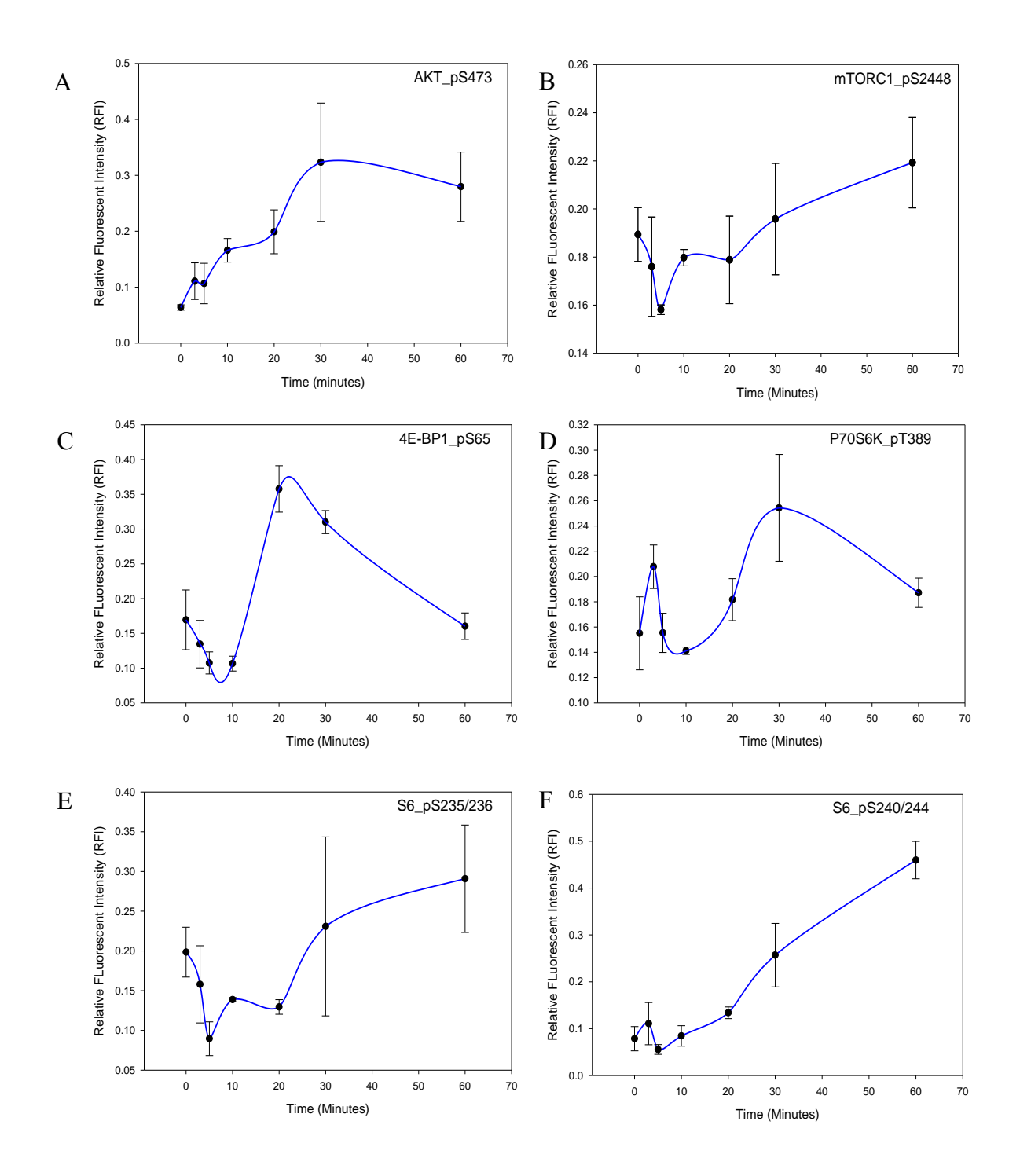


Figure 4.2: Measuring the Kinetics of the mTOR Network in MRC5 Cells. A sixty minute time course following 24 hour serum starvation. Cells were re-stimulated at 0 hours and relative fluorescent intensity measured at each time point (n=3) (Mean +/- SEM). (A) AKT_pS473, (B) mTORC1_pS2448, (C) 4E-BP1_pS65, (D) P70S6K_pT389, (E) S6_pS235/236, (F) S6_pS240/244.

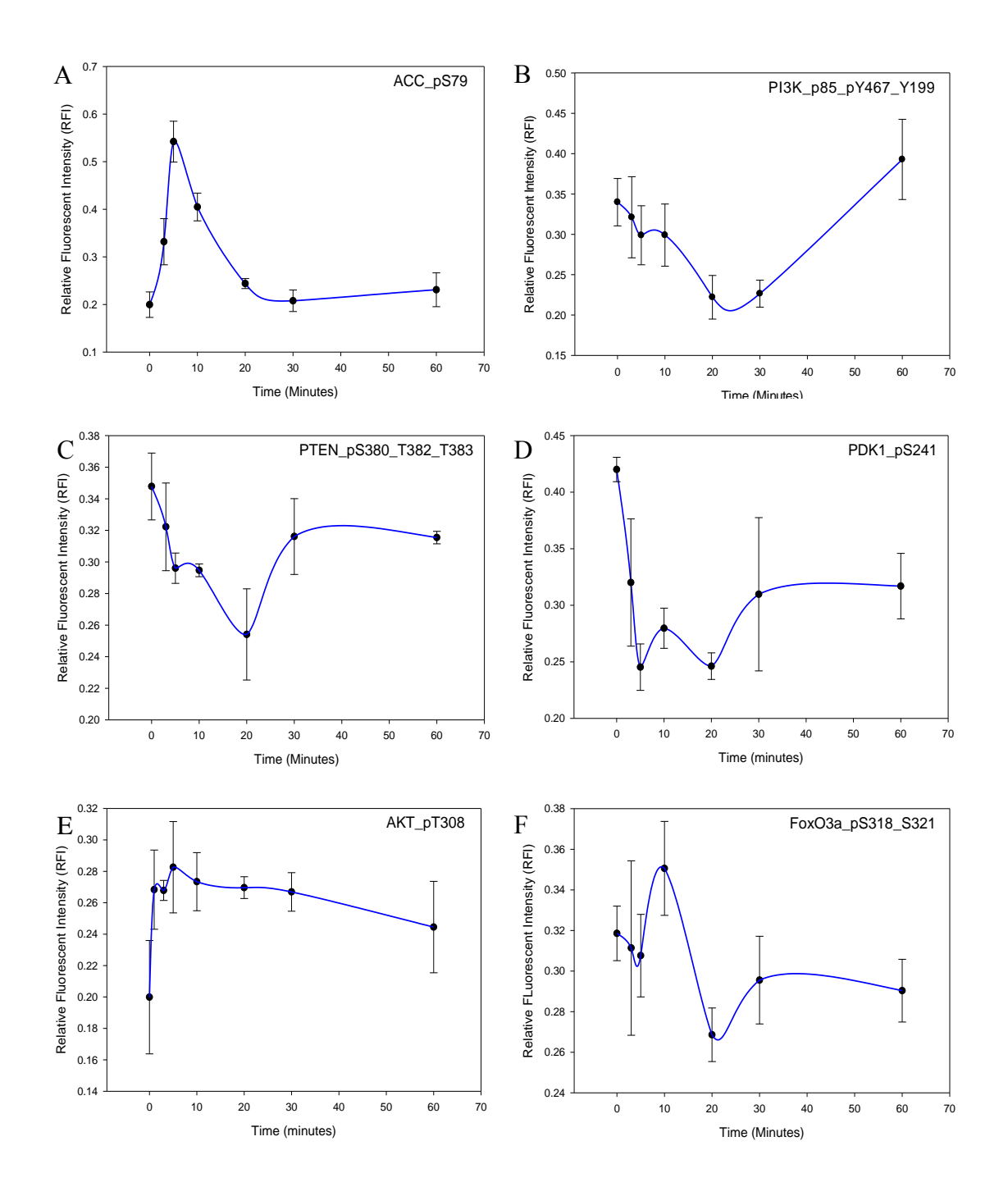


Figure 4.3: Expanded Measurements of mTOR Network Kinetics in MRC5 Cells.

A sixty minute time course following 24 hour serum starvation. Cells were re-stimulated at 0 hours and relative fluorescent intensity measured at each time point (n=3) (Mean +/- SEM). (A) ACC_pS79, (B) PI3K_p85_pY467_pY199, (C) PTEN_pS380_pT382_pT383, (D) PDK1_pS241, (E) AKT_pT308 (F) FOXO3A_pS318_pS321.

4.3.3 Parameter estimation

In order to calibrate the model using the data generated by RPPA, parameter estimation was carried out for the first 60 minutes of the time course. The data was first normalised to the housekeeping protein α-tubulin and then the control time point 0 set to a value of 1 and all subsequent time points divided by this value. Whilst not crucial at this stage this would allow for a later direct comparison between the MRC5 and MSC datasets. A total number of 10000 runs were then performed using a computational cluster. The time length for these runs was variable as they were dependent on how the cluster was being used on a given day by multiple users. As the residual sum of squares (RSS) outputted by Copasi is dependent on the scale of the data used it was not possible to test a "goodness of fit" using a p-value (data with value between 10-100 will produce a higher RSS than data with values between 0.1 and 1 however the same level of "fit" will be achieved). Therefore whilst this test was performed for all model fits it was not taken as a measurement of "goodness of fit".

4.3.4 Constant AMPK activation prevents parameterisation of the model

Parameter estimations using the genetic algorithm over 10000 runs were carried out. The initial findings for the parameter estimations are shown in figure 4.4. Whilst it proved possible to attain expected fits between the experimental data and model simulations for ACC_pS79, AKT_pT308, PTEN_pS380_pT382_pT383, PDK1_pS241 and mTORC1_pS2448 it was not possible to attain reasonable fits to all other observables. Given the clear flow of information through the network seen within the experimental data it was unlikely that the data itself was at fault for the inability of the model to achieve a reasonable fit for the majority of observables. It was therefore reasonable to assume that a part of the module topology itself was at fault. As such it was necessary to examine each section of the network in order to ascertain where the network topology was incorrect. Two areas of particular note were immediately identified as possible problem areas within the model. The first section of the model topology to undergo testing was AMPK-ACC activation by nutrients. Whilst the experimental output was as expected when compared to recent literature reports this section of the model was also the least well defined in terms of how AMPK interacts with the mTOR network. The second section of the network that was analysed was the mTORC1_pS2448 output. Whilst the experimental output for this variable followed the

experimental outputs for upstream mTORC1 effecters it differed significantly from its downstream effector 4E-BP1_pS65. In addition it is disputed within the literature as to whether mTORC1_pS2448 is an acceptable read-out for mTORC1 activation [206]. In order to test which of these outputs has the largest effect on model fitting the experimental data for each variable was removed from the model and parameter estimations carried out. For this round of estimations a total of 2500 parameter estimations were performed and the resultant residual sum of squares (RSS) values compared. With removal of the ACC_pS79 dataset the model was incapable of fitting the remaining variables to the model (RSS = 2758.46) suggesting that this variable is crucial to performing parameter estimations on this model (Figure 4.5). In contrast whilst removal of the mTOR_pS2448 also decreased the ability of the model to fit the remaining variables (RSS = 15.06 compared to original model RSS = 3.52) the effect of removing this variable was far less dramatic. It was therefore decided that the AMPK-ACC section of the network should be altered in order to achieve a closer fit between the model simulation and experimental dataset.

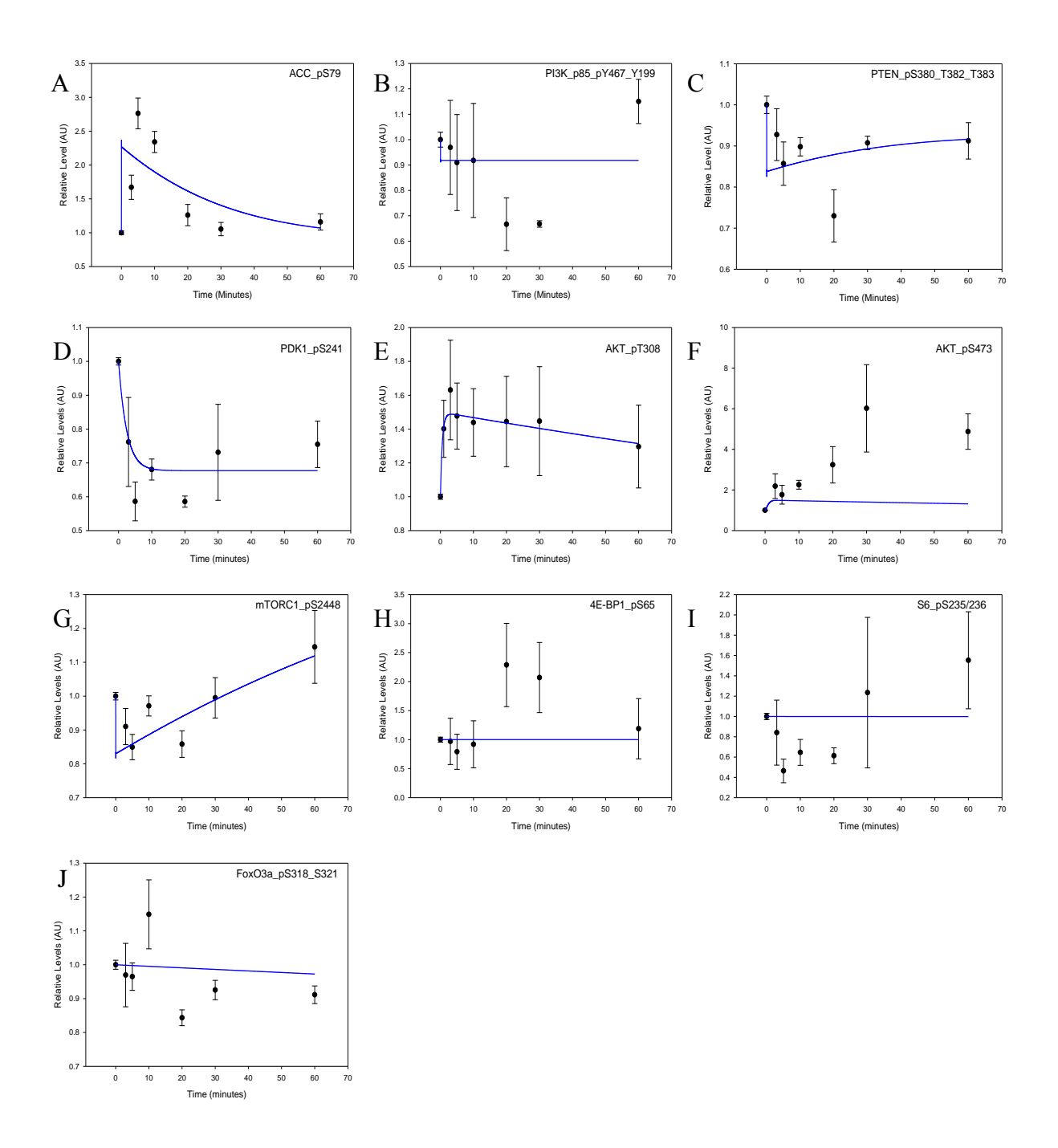


Figure 4.4: Time course simulations from the model compared to re-stimulation

data. The model displayed in figure 4.1 was calibrated using the RPPA data shown in figures 4.2 and 4.3. A parameter estimation consisting of 56 parameters in total was performed using the genetic algorithm (10000 runs). The Residual sum of squares between the experimental data (Black \pm -SEM) and the simulated data (Blue) was calculated as 3.52 with a reasonable fit achieved (P-value = 0.99).

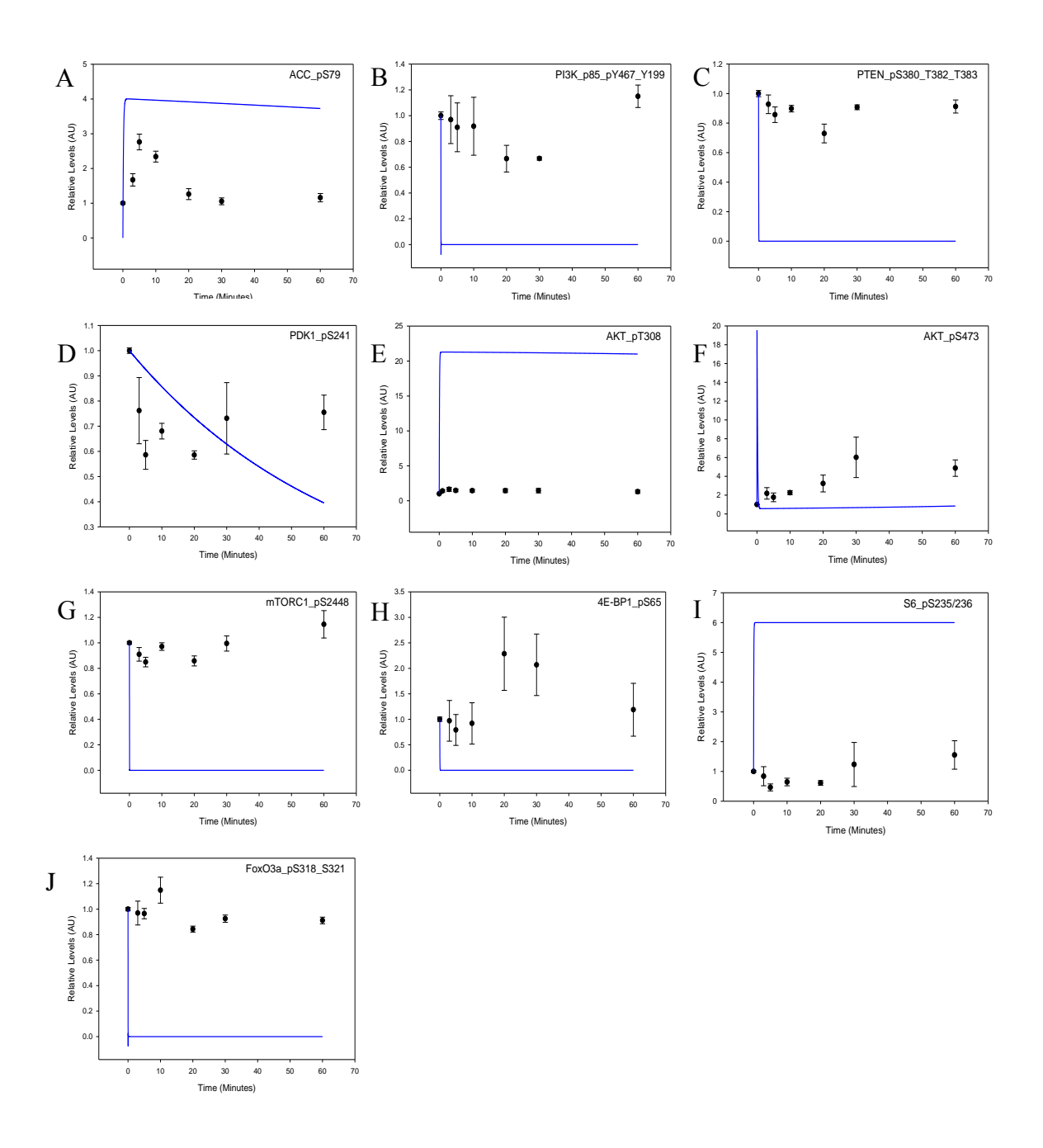


Figure 4.5: Parameter time course simulations following the removal of ACC_pS79 from the MRC5 dataset. The model displayed in figure 4.1 was calibrated using the RPPA data shown in figures 4.2 and 4.3. A parameter estimation consisting of 56 parameters in total was performed using the genetic algorithm with the experimental data for ACC_pS79 removed from the dataset (2500 runs). The Residual sum of squares between the experimental data (Black +/- SEM) and the simulated data (Blue) was calculated as 2758.46 with no fit achieved (P-value = 0.0001).

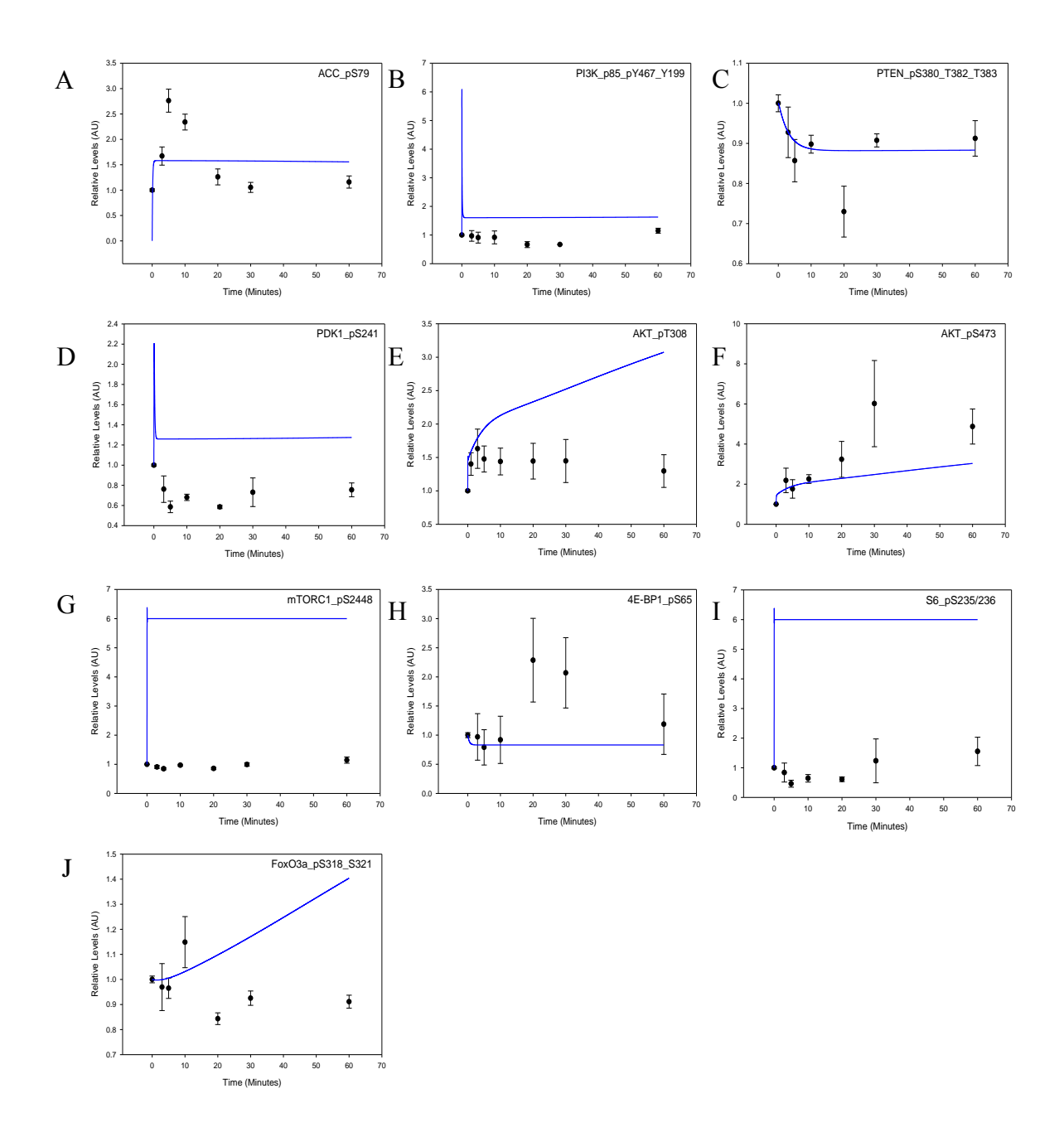


Figure 4.6: Parameter time course simulations following the removal of mTORC1 pS2448 from the MRC5 dataset. The model displayed in figure 4.1 was calibrated using the RPPA data shown in figures 4.2 and 4.3. A parameter estimation consisting of 56 parameters in total was performed using the genetic algorithm with the experimental data for mTORC1_pS2448 removed from the dataset (2500 runs). The Residual sum of squares between the experimental data (Black +/- SEM) and the simulated data (Blue) was calculated as 15.06 with a poor achieved (P-value = 0.058).

Following the finding that removing the ACC_pS79 experimental data dramatically decreased the overall fit of the model it was decided that further investigation should be carried out into how the AMPK-ACC section of the model impacted the model outputs. Upon removal of the ACC_pS79 dataset from the parameter estimations the model predicts a constant level of ACC_pS79 (figure 4.6 A). This is opposed to the transient activation observed in the experimental data. The initial concentration for the AMPK_pT172 and ACC_pS79 variables within the model is set to 1 representing a baseline activation following serum starvation. As AMPK acts to inhibit PI3K and mTORC1 it was hypothesized that this could occur whilst AMPK_pT172 was present at only baseline concentrations leading to constant PI3K and mTORC1 inhibition. The mechanism for activation of AMPK following amino acid restimulation is still being investigated however as there has been reports that following stress induction (such as the influx of nutrients following starvation) AMPK localises from the nucleus into the cytoplasm. It is feasible therefore that this is what is being observed within our dataset with phosphorylation and cytoplasmic localisation following re-stimulation followed by localisation to the nucleus as the cell adapts to the nutrient rich environment. It was therefore decided that AMPK should be set to decay following phosphorylation leading to a transient expression of AMPK_pT172 and ACC_pS79 representing an unknown mechanism triggering nuclear localisation. The ACC_pS79 dataset was therefore recalibrated with the initial concentration of AMPK_pT172 and ACC_pS79 set to 0. A set of 10000 parameter estimations were then carried out with the new topology. As can be observed in figure 4.7 with the new topology in place the model is capable of fitting all of the dependent variables with the exception of 4E-BP1_pS65 (RSS = 0.15).

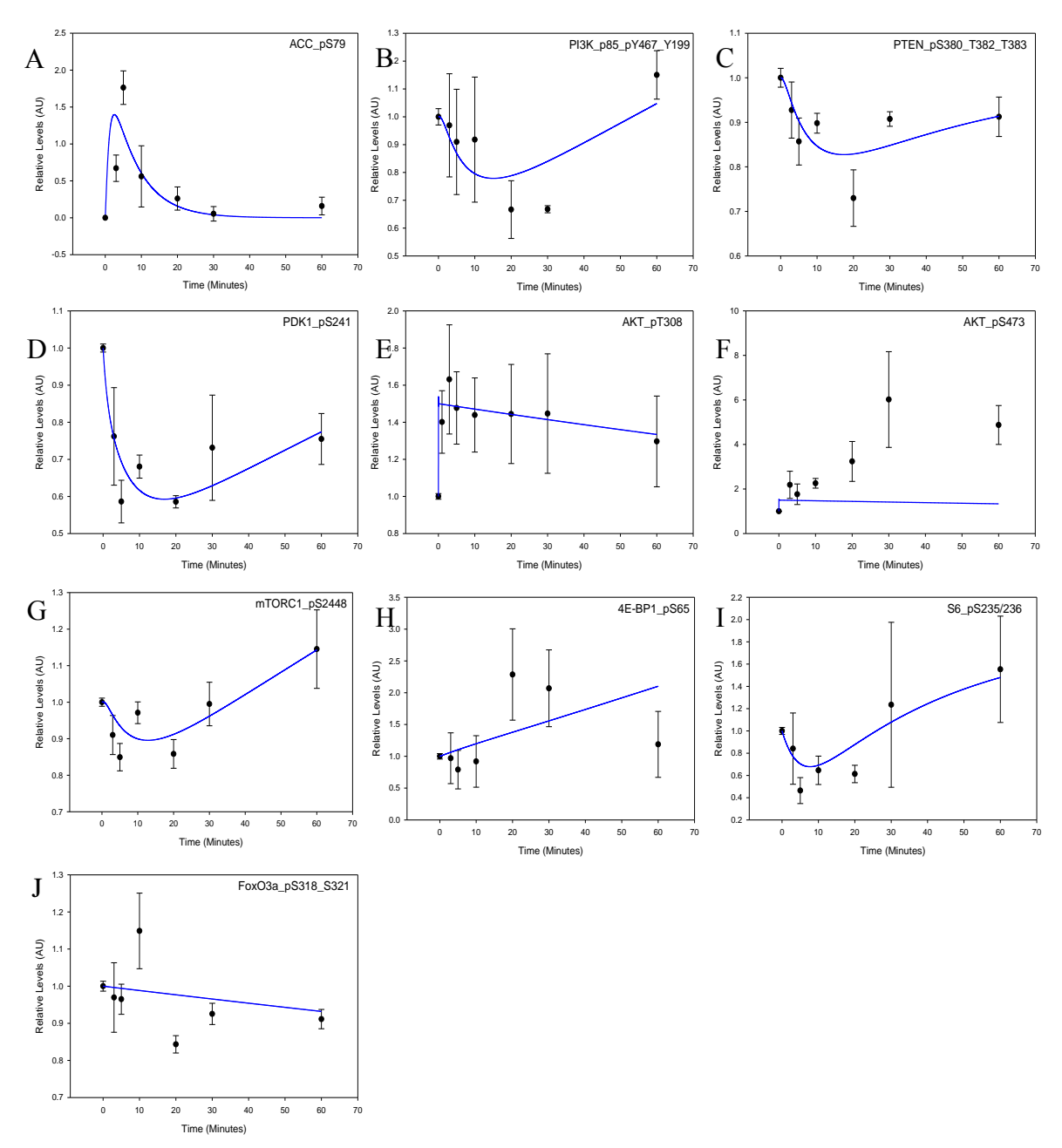


Figure 4.7: Time course simulations from the model compared to re-stimulation data with updated ACC starting concentration. The model displayed in figure 4.1 was calibrated using the RPPA data shown in figures 4.2 and 4.3. A parameter estimation consisting of 56 parameters in total was performed using the genetic algorithm (10000 runs). The residual sum of squares between the experimental data (Black +/- SEM) and the simulated data (Blue) was calculated as 0.23 with a good fit achieved (P-value = 1).

4.3.5 Parameterisation of the 4E-BP1_pS65 observable requires a more in depth mTORC1 modelling approach

In order to test whether the model was capable of fitting the 4E-BP1 pS65 data it was proposed that a further set of parameter estimations should be carried out using just the 4E-BP1_pS65 data. For this experiment the model shown in figure 4.1 was used with a total of 2500 parameter estimations were performed using the genetic algorithm. In addition all initial reaction parameters were set to a randomized value as in previous parameter estimations. As can be seen in figure 4.8 once the model is given only the 4E-BP1_pS65 data it is possible to fit the experimental observations to the computational simulations. As previously discussed it is possible that the output for mTORC1_pS2448 may not represent a true activation of the mTORC1 complex. Therefore without further modelling of mTORC1 and its regulatory reactions it may not be possible to correctly model this output. In addition whilst it is impossible to fully analyse the output form the P70S6K_pT389 antibody used for the initial RPPA in this section due to non-specific binding it should be noted that for both antibodies tested, the output for this protein is very similar in behaviour to that of the 4E-BP1 antibody. This allows for the possibility that both 4E-BP1 and P70S6K behave in a similar manner following re-stimulation. As modelling the in depth regulation of both 4E-BP1 and P70S6K by mTORC1 would represent a large scale modelling process it was decided that the output for 4E-BP1_pS65 should be left as seen in figure 4.7.

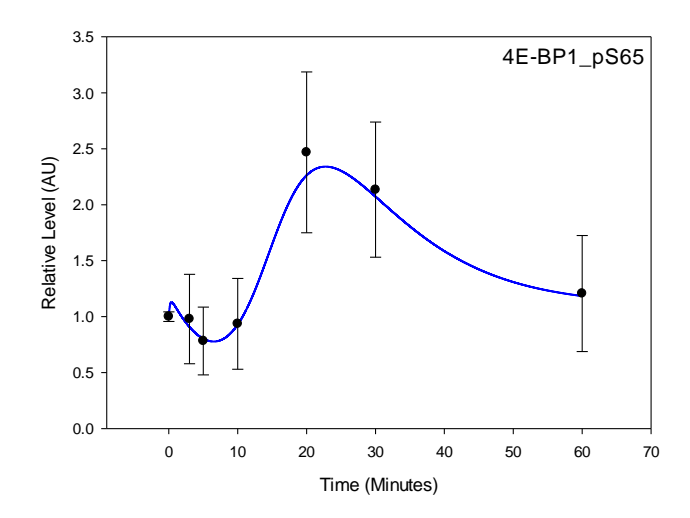


Figure 4.8: Individual parameter estimation for the 4E-BP1_pS65 observable. The model displayed in figure 4.1 was calibrated using the re-simulated RPPA data shown in figure 4.2 for 4E-BP1_pS65 only. A parameter estimation consisting of 56 parameters in total was performed using the genetic algorithm (2500 runs). The Residual sum of squares between the experimental data (Black +/-SEM) and the simulated data (Blue) was calculated as 0.0047 with a very good fit achieved (P-value = 1).

<u>Table 4.2: Residual sum of squares value for each model.</u> The residual sum of squares for each model fitted to the experimental data for both MRC5 and MSC datasets. The lower the RSS value, the closer the fit between the model simulations and the corresponding dataset. Corresponding figure number also shown.

Parameter Estimation	Residual Sum of	Figure No.		
Squares				
MRC5 Genetic Fit 1	3.52	4.4		
MRC5 ACC	2758.46	4.5		
MRC5 mTOR	15.06	4.6		
MRC5 Genetic Fit 2	0.23	4.7		
MRC5 4E-BP1_pS65	0.0047	4.8		
MRC5 Hooke and Jeeves	0.15	4.10		
MSC Genetic Fit	0.16	4.11		
MSC Hooke and Jeeves	0.20	4.11		
MSC AKT_pT308	0.15	4.12		

4.3.6 Modelling the difference between MRC5 and MSC kinetics in response to starvation-restimulation

Having calibrated the model to an MRC5 dataset it was then necessary to produce a second dataset representing the response of MSCs to serum starvation-restimulation. This was carried out as previously described for the MRC5 cells. A comparison between the MRC5 and MSC outputs are shown in figure 4.9. Having performed RPPA experiments using MSCs and compared the outputs to the MRC5 dataset our next question was how well our original model could fit the new dataset and to investigate which sections of the model differed the most. There were two possible methods which could be used to perform this comparison: firstly we could perform a full parameter estimation as previously carried out for the MRC5 dataset and then compare the best RSS values from each of the models or secondly we could program the calibrated model with the MSC dataset and then perform parameter estimations using the already calibrated values as the starting values (in the original parameter estimation these values were randomised). Whilst the second option was favoured for these experiments as it would be a more direct comparison between two parameter sets (as opposed to examining at changes between two separate optimization problems) it was felt necessary to also carry out the first option. The purpose of this was to obtain an RSS value which would serve as a reference point for a 'best fit' which could then be compared to an RSS value obtained using the previously calibrated model. The parameter estimation was carried out as previously described for the MRC5 dataset with an RSS value of 0.15943 obtained (Table 4.2) (Figure 4.11).

Following the calibration shown in figure 4.7 the MRC5 dataset was removed and replaced with the MSC dataset. A set of 100 parameter estimations using the Hooke and Jeeves algorithm was then performed using the reaction parameter values obtained by the best fit to the MRC5 dataset as the initial reaction parameter values. A set of 100 parameter estimations was also carried out in this way with the MRC5 dataset.

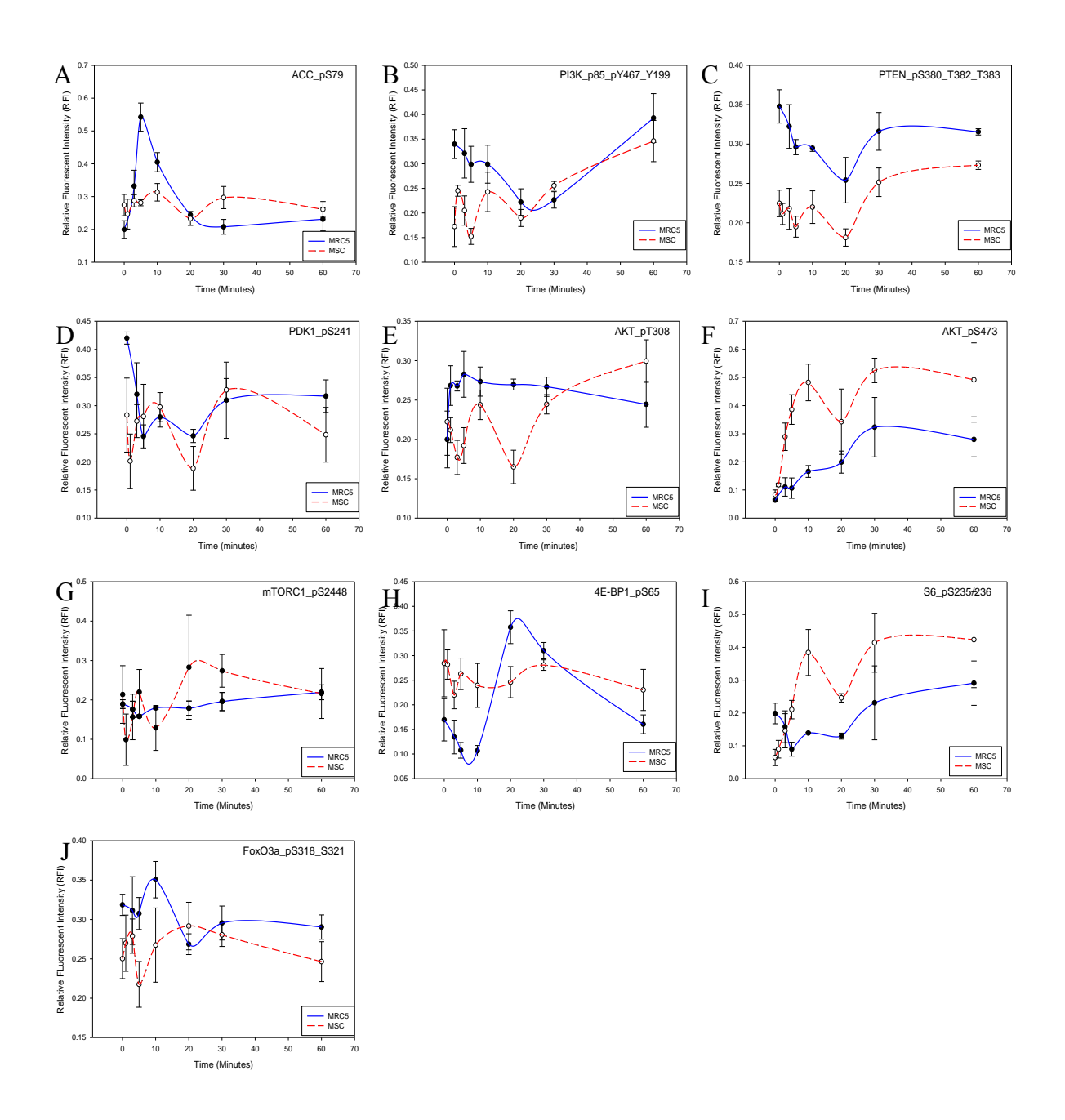


Figure 4.9: A comparison of MRC5 vs MSC outputs for SS. A sixty minute time course following 24 hour serum starvation for both MRC5 (Blue) and MSC (Red) cells. Cells were re-stimulated at 0 hours and relative fluorescent intensity measured at each time point (n=3) (Mean +/- SEM). (A) ACC_pS79, (B) PI3K_p85_pY467_pY199, (C) PTEN_pS380_pT382_pT383, (D) PDK1_pS241, (E) AKT_pT308, (F) AKT_pS473, (G) mTORC1_pS2448, (H) 4E-BP1_pS65, (I) S6_pS235/236 and (J) FOXO3A_pS318_pS321.

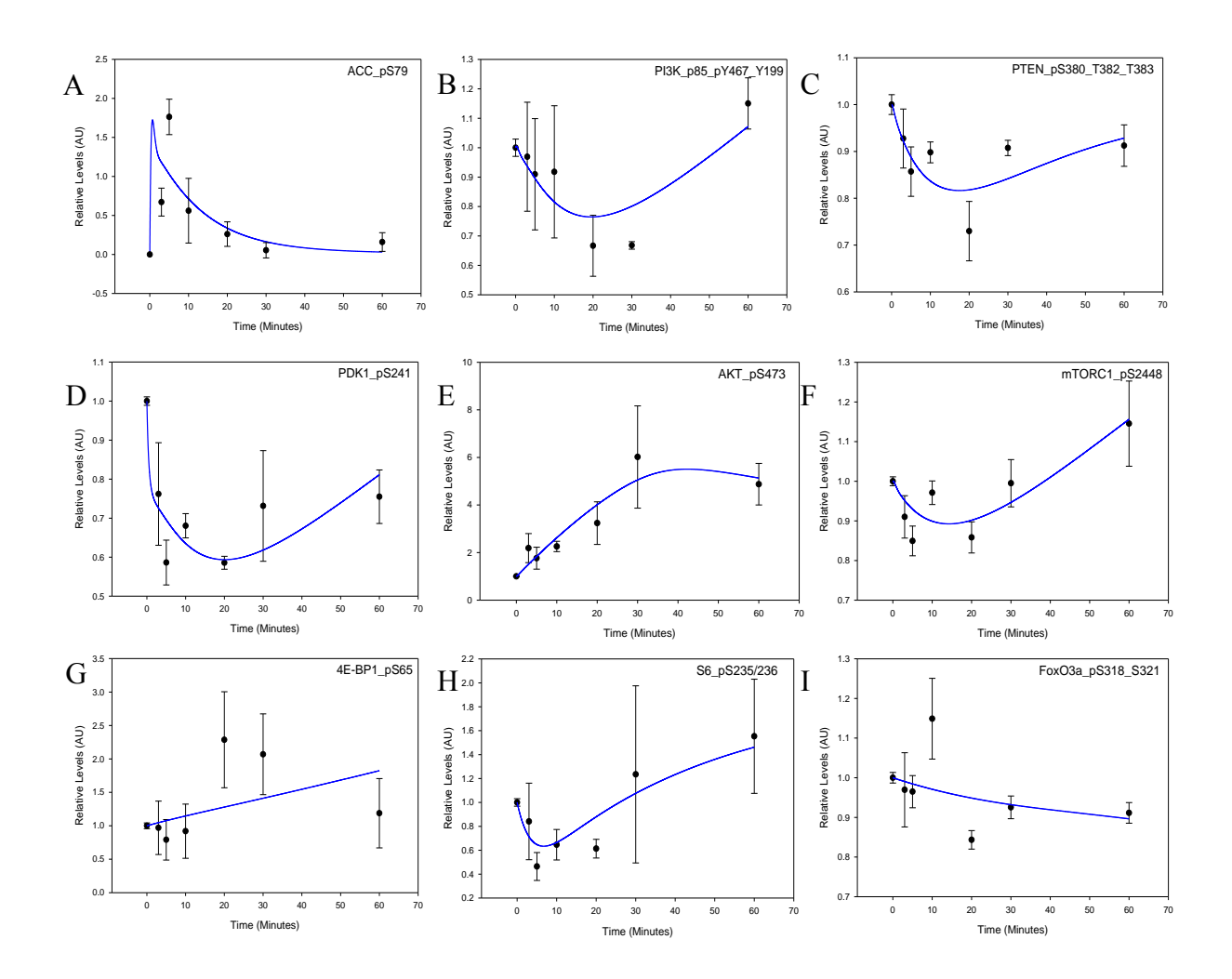


Figure 4.10 Time course simulations from the model compared to re-stimulation data utilizing the local Hooke and Jeeves algorithm MRC5 cells. The model displayed in figure 4.1 was calibrated using the re-simulated RPPA data shown in figures 4.2 and 4.3. A parameter estimation consisting of 56 parameters in total was performed using the local algorithm Hooke and Jeeves (100 runs). The Residual sum of squares between the experimental data (Black +/- SEM) and the simulated data (Blue) was calculated as 0.15 with a very good fit achieved (P-value = 1).

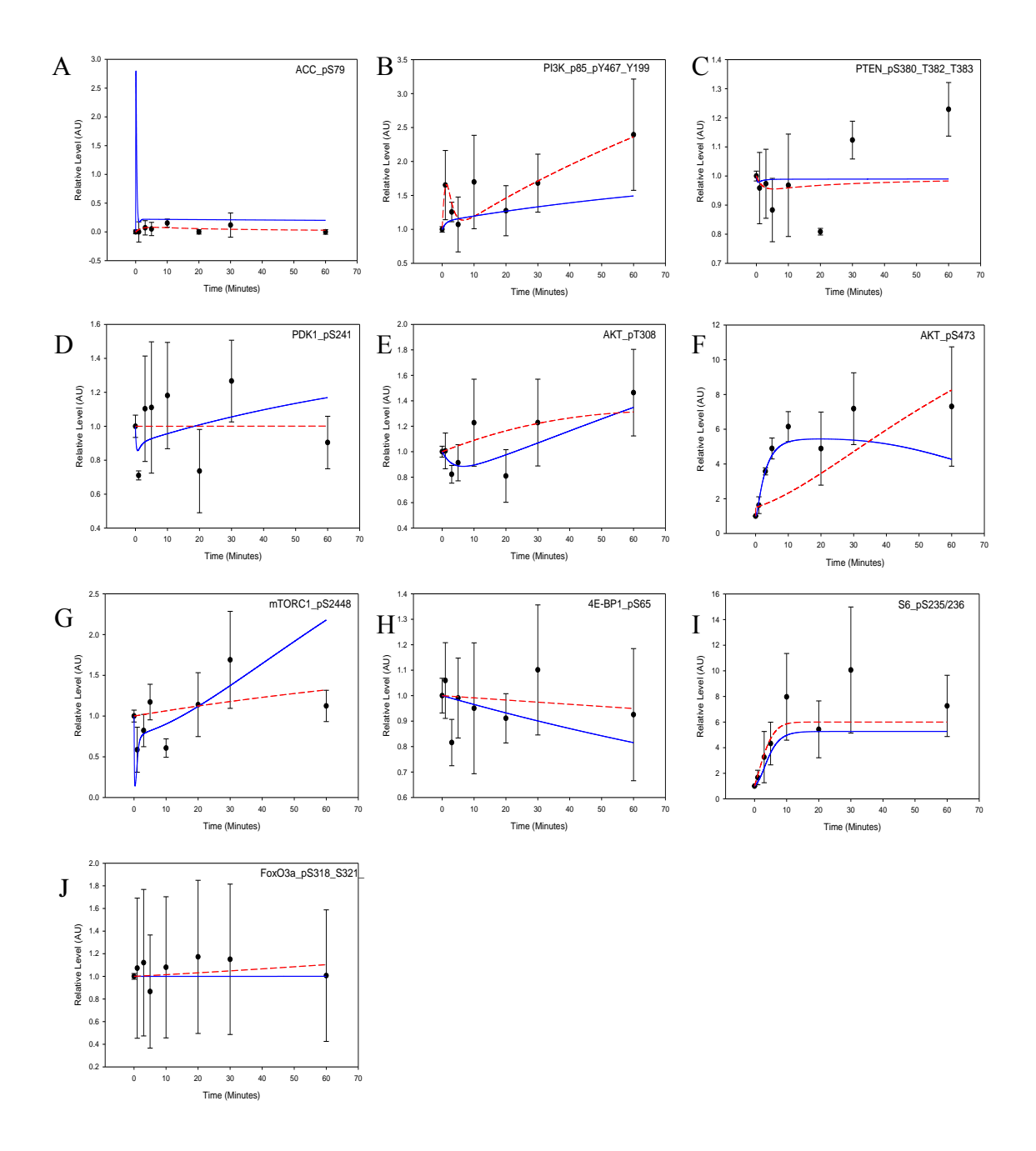


Figure 4.11 Genetic vs Hooke and Jeeves fit for MSC. The model displayed in figure 4.1 was calibrated using the RPPA data shown in figure 4.9. A parameter estimation consisting of 56 parameters in total was performed using the genetic algorithm (10000 runs) (Blue) randomising the initial parameter values and the Hooke and Jeeves algorithm (100 runs) (Red) using previously obtained parameter values form the MRC5 data fit. The Residual sum of squares between the experimental data (Black +/- SEM) and the simulated data (Genetic-Blue, Hooke and Jeeves-Red) was calculated as 0.16 (genetic) and 0.20 (Hooke and Jeeves) with a good fit achieved for both (P-value = 1 (Both)).

4.3.7 Fit results

As predicted subjecting the MRC5 calibrated model to the local algorithm Hooke and Jeeves enhanced the fit (0.153) (Figure 4.10). As described above parameter estimations were carried out using both Hooke and Jeeves and the genetic algorithm for the MSC dataset and the fits compared. The RSS value obtained from the genetic algorithm randomised parameter estimation was 0.15943. Whilst the Hooke and Jeeves algorithm parameter estimations failed to reach this value (RSS = 0.203398) as can be seen in figure 4.11 this set of parameter estimations was capable of fitting certain datasets more closely than the genetic algorithm parameter estimation. Interestingly the genetic algorithm fit for ACC_pS79 attempted to fit a very transient peak upon restimulation in the MSC similar to that in the MRC5 cells however this was not seen in the Hooke and Jeeves parameter set (Figure 4.11). Whilst this may be an artefact of this particular fitting estimation it is noteworthy that in the MSC dataset the ACC_pS79 peak following re-stimulation does not occur as it does in other cell types. For most of these estimations there is very little difference between each of the two fitting methods with the main exception being AKT_pS473. The genetic algorithm fit was capable of finding a fit for both AKT phosphorylation sites however the Hooke and Jeeves algorithm provided a different fit for AKT_pT308 which given the variation in the dataset can be said to be a reasonable fit. As this part of the model is possibly the most complex it was theorised that the model may struggle to fit data for both AKT_pT308 and AKT_pS473. Therefore a further Hooke and Jeeves parameter estimation was performed with the AKT_pT308 dataset removed. This resulted in the correct fitting of the AKT_pS473 parameter (figure 4.12).

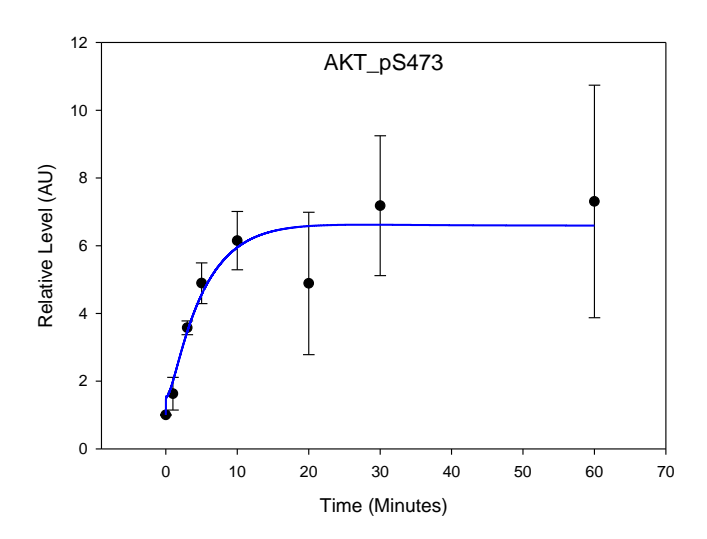


Figure 4.12 AK Parameter time course simulations following the removal of AKT_pT308 from the MSC dataset. The model displayed in figure 4.1 was calibrated using the re-simulated RPPA data shown in figure 4.9. A parameter estimation consisting of 56 parameters in total was performed using the Hooke and Jeeves algorithm (100 runs) without the dataset for AKT_pT308. The residual sum of squares between the experimental data (Black +/- SEM) and the simulated data (Blue) was calculated as 0.15 with a very good fit achieved (P-value = 1).

4.4 Image flow cytometry fails to show correlation between DAPI – FOXO3A and Rheb-LAMP1

In addition to performing RPPA time course experiments to measure the response of both MRC5 and MSC cells to starvation-restimulation it was decided that further information could be gained using flow cytometry. In contrast to the results presented in chapter 4 an alternative method of flow cytometry was used for these experiments in the form of Imagestream flow cytometry. Imagestream flow cytometry differs from standard flow cytometry in that in addition to measuring the intensity of fluorophores excitation by lasers it also contains cameras which image the cells as they pass through the machine. This allows for the analysis of various aspects of protein activation including cellular localisation. In the case of the mTOR network there are two proteins of particular interest in this study namely FOXO3A and Rheb. Whilst FOXO3A phosphorylation was measured by RPPA it is known that the phosphorylation of FOXO3a does not always correspond to its inhibition and that phosphorylated FOXO3A can enter the nucleus and act as a transcription factor, therefore analysing its cellular localisation is the only way of accurately measuring FOXO3A activity. Rheb is a small GTPase that localises to the lysosome and acts upstream of mTORC1 and is inhibited by the TSC1/2 complex. It was not expected that starvation-restimulation should have an effect on Rheb localisation however Zoledronate treatment as discussed in chapter 7 does affect its localisation and therefore it was felt necessary to measure the reaction of Rheb to each treatment preformed. In order to carry out a localisation comparison two separate antibodies were also used in this test with 4',6-diamidino-2-phenylindole (DAPI) used as a nuclear stain and Lysosomal-associated membrane protein 1 (LAMP-1) conjugated to Alexa-488 used as a lysosomal stain. In order to account for any compensation required (false positive due to overlapping excitation spectrums) between each of the fluorophores (Alexa-488, PE and Alexa-647) single repeats stained using only one of the antibodies were performed allowing for a compensation matrix to be set up. Time course experiments were then carried out following restimulation (Figure 4.13). For each time point the single cell population was selected and then the images obtained for these cells selected in order to obtain only those images in focus (figure 4.13 A +B). Analysis was them carried out using the nuclear localisation wizard within Ideas 6 and the co-localisation wizard in order to identify those cells positive for FOXO3A and DAPI (nuclear localisation) and RHEB and LAMP1 (co-localisation) (figure 4.13 C + D). Selecting these populations allowed for the analysis of co

localisation between the proteins of interest (Pearson's correlation co-efficient) (figure 4.13 E). A representative image of untreated cells is shown in figure 4.13. It did not prove possible in this analysis to obtain the number of cells required to analyse the localisation of interest (Pearson's correlation co-efficient) (figure 4.14). However it can be inferred from the data obtained that there is no correlation between either FOXO3A and DAPI or between Rheb and LAMP1 throughout the time course (Table 4.3).

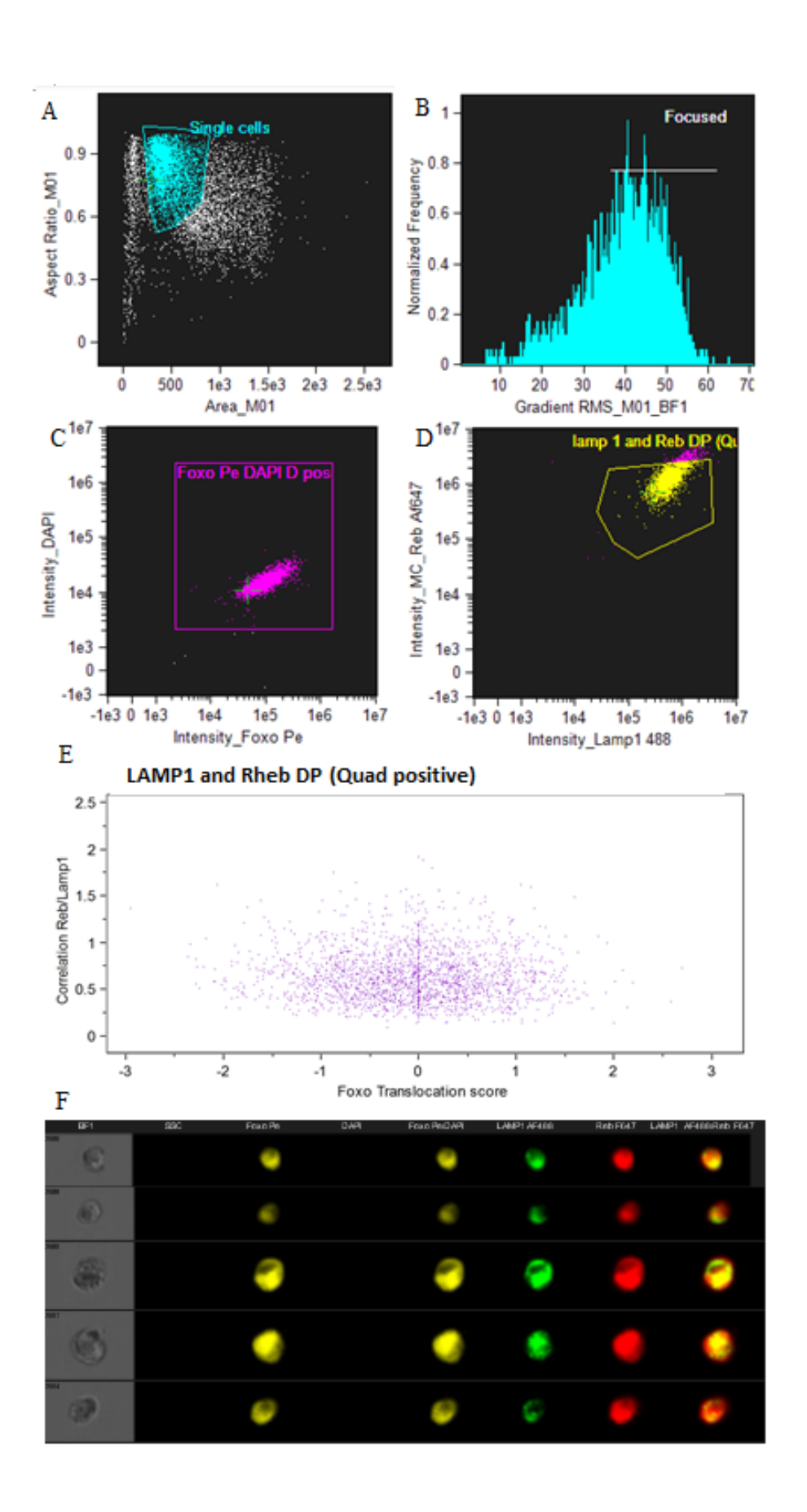


Figure 4.13: Image flow cytometry fails to show correlation between DAPI – FOXO3A and Rheb-LAMP1. Representative image displaying image flow cytometry analysis of untreated cells prior to serum starvation. (A) A single cell population was selected, (B) followed by the removal of images that were not in focus. (C) Nuclear localisation correlation was analysed for FOXO3A and DAPI, in addition to (D) correlation analysis of RHEB and LAMP1. (E) Population analysis displaying correlation between DAPI-FOXO3A and Rheb-LAMP1. (F) Representative image of in focus single cell population for 0 hour untreated cells.

<u>Table 4.3: Image flow cytometry time course correlation</u>. Correlation values for each time point assayed for FOXO3A-DAPI (FD) and Rheb-LAMP1 (RL) (Pearson's correlation co-efficient; all values are non-significant P>0.05).

Time Point	FOXO3A-DAPI	Rheb-LAMP1	P-value
	Pearson's correlation	Pearson's correlation	FD/RL
	co-efficient	co-efficient	
0 hours	-0.01483	0.6018	0.99/0.59
30 minutes starved	0.439	0.5776	0.67/0.61
60 minutes starved	0	0.05805	1/0.97
24 hours starved	-0.1342	0.671	0.91/0.53
5 minutes restimulated	-0.1014	0.6737	0.94/0.53
15 minutes restimulated	-0.08476	0.6458	0.95/0.55
30 minutes restimulated	-0.101	0.674	0.94/0.53
60 minutes restimulated	0	0.6302	1/0.57

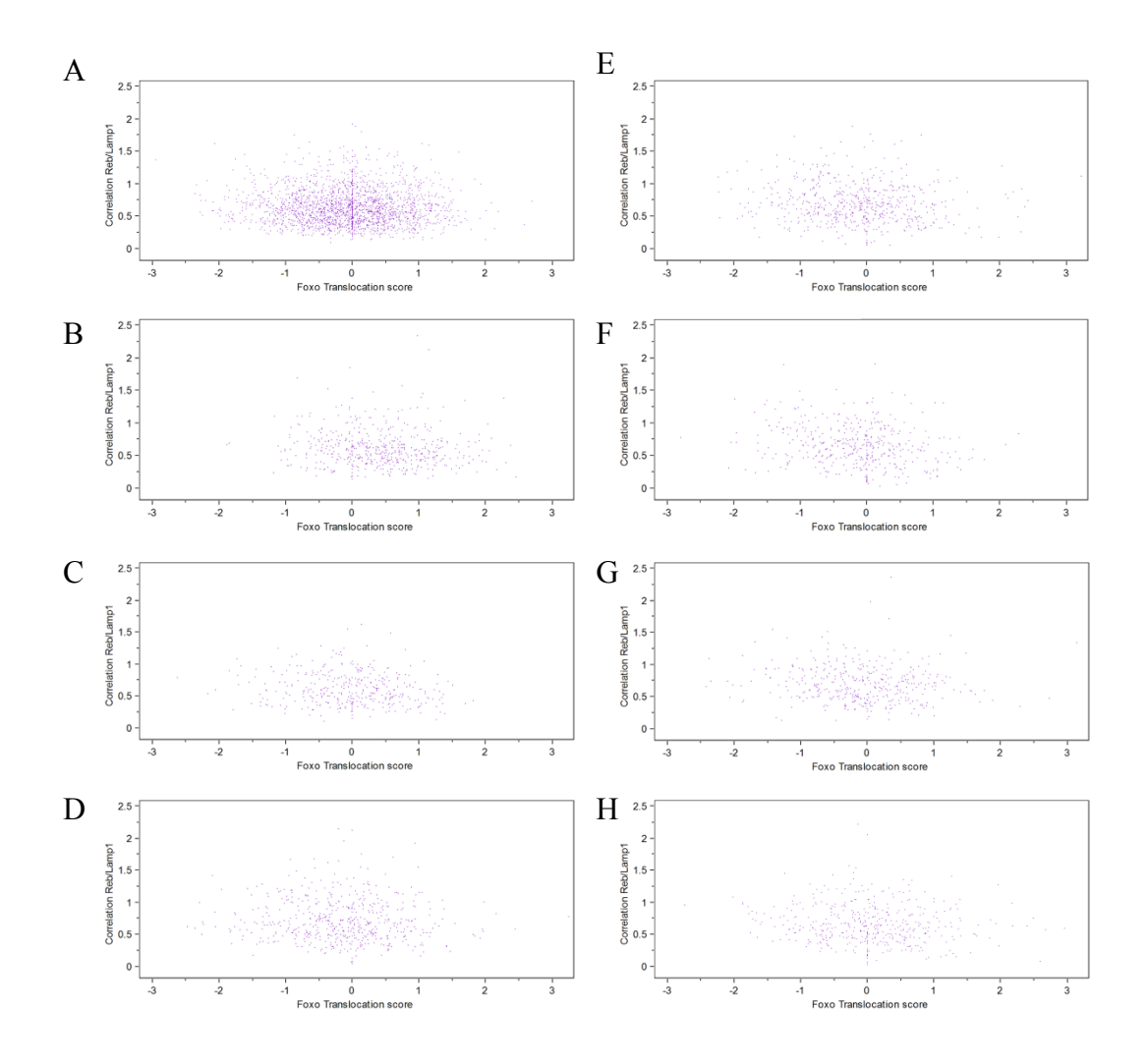


Figure 4.14: Image flow cytometry time course correlation. Population analysis displaying correlation between DAPI-FOXO3A and Rheb-LAMP1, (Pearson's correlation co-efficient) (A) 0 hour untreated cells, (B) 30 minutes serum starved cells, (C) 60 minutes serum starved cells, (D) 24 hour serum starved cells, (E) 5 minutes re-stimulated cells, (F) 15 minutes re-stimulated cells, (G) 30 minutes re-stimulated cells, (H) 60 minutes re-stimulated cells.

4.5 Discussion

The aims of the work presented here were to define a dynamic model capable of representing the mTOR networks response to starvation-restimulation. To calibrate this model in both MRC5 and MSCs using reverse phase protein arrays. To use imagestream flow cytometry to analyse the cellular localisation of key proteins within the mTOR network. And to identify how MRC5 fibroblasts and MSCs differ in their response to starvation-restimulation. Through the computational dynamic modelling approach described above this has been achieved. The model presented above proved capable of simulating the response of both MRC5 and MSCs in response to restimulation following a period of serum starvation.

Reverse phase protein arrays were used throughout this work and proved to be an excellent alternative to western blotting, producing high quality calibration datasets for both MRC5 and MSCs. Upon expansion of the work carried out in the previous chapter it proved possible to measure a total of eighteen proteins within the mTOR network and upon inspection of the data it was possible to follow the flow of information through the network with related proteins displaying similar kinetic profiles. As was discussed previously one of the main problems with RPPA is the availability of specific antibodies to proteins. However due to the amount of research carried out on the mTOR network this was not a hindrance to this work as there are large number of extremely specific antibodies available covering large sections of the mTOR network. There are a couple of proteins within the network that could not be analysed, specifically the TSC proteins, P70S6K and AMPK. Given their importance to the network in addition to validating the results shown above using western blotting it would be beneficial to analyse these proteins and include them in future parameter estimations.

Following starvation-restimulation there was an increase in the phosphorylation of ACC_pS79 in MRC5 cells that was not present in the corresponding MSC dataset. The increase in phosphorylation in ACC_pS79 in MRC5 cells corresponds directly with previous data investigating the response of AMPK activity following starvation-restimulation [172]. Whilst the model presented above proved capable of fitting this activation it was incapable of fitting the large section of the remaining observables. The removal of the baseline activation of this observable led to the ability of the model to fit all of the remaining observables bar the 4E-BP1_pS65 observable. This finding suggests that there are mechanisms governing the activity of the AMPK-ACC axis that

are absent from our model. It has been shown that the AMPK cellular localisation is dependent upon a number of different factors including environmental stress [207, 208]. It is therefore feasible that the increase in phosphorylation observed in ACC_pS79 is dependent upon the cellular localisation of active AMPK_pT172 to the cytoplasm upon restimulation following serum starvation. To test this theory further studies would be required investigating the following. Firstly confirmation western blots should be carried out to ascertain if the kinetics observed using RPPA is representative of the response of the mTOR network. As previously mentioned the kinetic profile of ACC_pS79 follows the same profile previously observed for AMPK following restimulation. In addition to this comparison of the kinetic profiles for both AKT_pT308 and AKT_pS473 reveals similar activation profiles following restimulation to previously published observations [172]. Secondly analysis of AMPK cellular localisation should be performed, this could be done as above using imagestream flow cytometry or other techniques such as nuclear fractionation.

A comparison of the responses of MRC5 fibroblasts to MSCs showed that there is a significant difference between the response of ACC_pS79 to restimulation between the cell types. Whilst the response observed in MRC5 cells is similar to the profile of AMPK observed in previous observations this is not the case for the MSCs with no overall change in signalling observed. An explanation for this is that AMPK is a key protein in MSC differentiation and is therefore placed under more stringent control in the MSCs compared to the differentiated MRC5 cells. Indeed recent research has shown that AMPK can act to bypass the inhibition of mTORC1 activity by caloric restriction in intestinal stem cells thus protecting these stem cells from the effects of caloric restriction [209]. As this study was carried out in mice caution needs to be used when applying the results to the *in vitro* work shown here. However it would be of interest to investigate if a similar mechanism exists in MSCs which could possibly explain why there is no ACC_pS79 peak observed in the MSC dataset.

Whilst imagestream flow cytometry has shown itself to be an extremely powerful analysis tool it did not prove possible in this experiment to obtain a time course that could be used in the calibration of a dynamic model. In order to be confident of making predictions regarding the localisation of a cellular population with this technology it is necessary that the cellular population analysed following the removal of out of focus images and the selection of single cell population number over 500 cells [191]. This was

not the case here with population sizes varying between 300-500 cells. It was therefore not possible to analyse the co-localisation of either FOXO3A and DAPI or Rheb and LAMP1.

Overall the aims of this work have been met with a dynamic model capable of reproducing the response of both MRC5 cells and MSCs to serum starvation restimulation. RPPA has proved to be a reliable and efficient methodology for the production of calibration time courses required for this work however further work is required to validate the outputs observed above. The dynamics of the mTOR network observed could be simulated using the model with the assumption that AMPK baseline activity does not affect mTOR signalling. In addition it proved possible to use a MRC5 calibrated model to reproduce kinetics observed in MSCs. However this analysis still attempted to fit a transient peak to the ACC_PS79 observable suggesting that the response of this observable differs between the two cell types examined and should be investigated further.

5. A dynamical model of the mTOR signalling network reveals the kinetics of rapamycin and restimulation in MRC5 fibroblasts and human bone marrow stem cells

5.1 Introduction

Rapamycin is a macrocyclic antibiotic isolated from the bacteria *Streptomyces hygroscopicus* and discovered in the soil on Easter Island in 1975 [210, 211]. Despite initially being employed as an immunosuppressant Rapamycin also displayed antigrowth properties and was therefore analysed as an anti-cancer compound [212, 213]. Following the discovery that Rapamycin inhibited growth in multiple cancer cell lines further research subsequently discovered that Rapamycin inhibited cell growth across multiple model organisms including Drosophila and C. elegans in addition to human cell lines [213-215]. Rapamycin targets a complex of proteins which differs in its make up across species however its core proteins are highly conserved. This complex became known as the target of Rapamycin complex (TORC) with mTORC being the mammalian set of target proteins. It is from these initial discoveries that the field of mTOR research developed with the pathway now considered one of the key pathways in molecular biology. As such since the discovery of Rapamycin and its target complex, Rapamycin and its homologues have been of interest in the field of ageing research.

The precise mechanism of action for Rapamycin has remained elusive despite extensive research utilizing the compound. Rapamycin is able to quickly penetrate the plasma membrane of cells and bind to the FK506 binding protein (FKBP12) [216]. This leads to a gain of function complex that is capable of binding the mTOR complex 1(mTORC1) leading to its inhibition. As previously discussed in section 1.3, mTOR is present in two distinct complexes mTORC1 and mTORC2. Whilst mTORC1 is Rapamycin sensitive the second TOR complex mTORC2 is classed as Rapamycin insensitive. However, in certain cell types chronic Rapamycin inhibition leads to mTORC2 inhibition [72]. Again the mechanism for this inhibition has not been established but it is believed to be due to the sequestering of unbound mTOR by the Rapamycin FKBP12 complex preventing further formation of the mTORC2 complex. The insolubility and poor pharmokinetics of Rapamycin has led to the development of other Rapamycin derived compounds termed Rapalogs which include, Temsirolimus, Deforolimus and Everolimus [217-219].

The ability of Rapamycin to increase lifespan in mammals was first reported in 2009 when Harrison et al showed that Rapamycin was capable of extending the lifespan of mice regardless of sex [220-222]. They also showed that the lifespan extension did not differ between early and late life treatment. Lifespan extension following treatment with

Rapamycin has also been observed in *Drosophila melanogaster* [223]. *Drosophila* flies treated with Rapamycin display a lifespan extension that is directly comparable to the lifespan extension observed through caloric restriction and anti-ageing mutants.

Rapamycin is currently one of the best characterised drugs in the study of lifespan extension and ageing and has also being implicated as having a positive impact in osteoporosis. Rapamycin was therefore included in this study as a reference drug with which to compare the response of both MRC5 and mesenchymal stem cells (MSC) cell types. In addition, Rapamycin was found not to exhibit the same beneficial effect on MSCs as Zoledronate [82].

The computational model described in this section builds on that described in chapter 5. As described previously MRC5 cells are used as a control cell line with MSCs also used to determine the kinetic effects that Rapamycin exerts on the mTOR network.

5.2 Aims

The aim was to examine the effect of re-stimulation following Rapamycin treatment on the mTOR network. We aim to define using a computational dynamic model how the mTOR network responds in MRC5 fibroblasts and how the mTOR network response differs in human mesenchymal stem cells.

5.3 Results

5.3.1 Development of a rapamycin dynamic network model

The model used throughout this section is described in section 4.3.1 and displayed in figure 5.1 (all reactions can be found in appendix B). As described previously the amino acid/nutrient activation of the model will remain as before with a constant level of nutrients available to the cells. Nutrients activate the model in three separate points with PI3K, mTORC1 and AMPK all being activated by nutrient inputs. As before PI3K activation leads to the activation of PDK1 and subsequent activation of AKT on threonine 308. This in turn phosphorylates and inhibits the TSC1/2 complex leading to activation of Rheb(GTP). Rheb in its GTP bound form is then free to activate the mTORC1 complex leading to the activation of the downstream effectors P70S6K_pT389, S6_pS235/236 and 4E-BP1_pS65 with a P70S6K_pT389 feedback loop inhibiting further activation of PI3K by nutrient signalling. In addition, an additional species was added to the model to represent the interaction of mTOR with Rapamycin which acts to destabilise the mTORC1 complex. This was represented by a single mass action reaction in which unphosphorylated mTORC1 is converted to mTOR by Rapamycin. A reverse mass action reaction was also included with mTOR being converted to mTORC1. The treatment time with Rapamycin in this section was 24 hours. As chronic Rapamycin inhibition is normally classed as 3 days is was decided that the mTORC2 branch of the model should not be altered with regards to Rapamycin inhibition and as such the mTORC2 section of the model is as described in section 4.3.1.

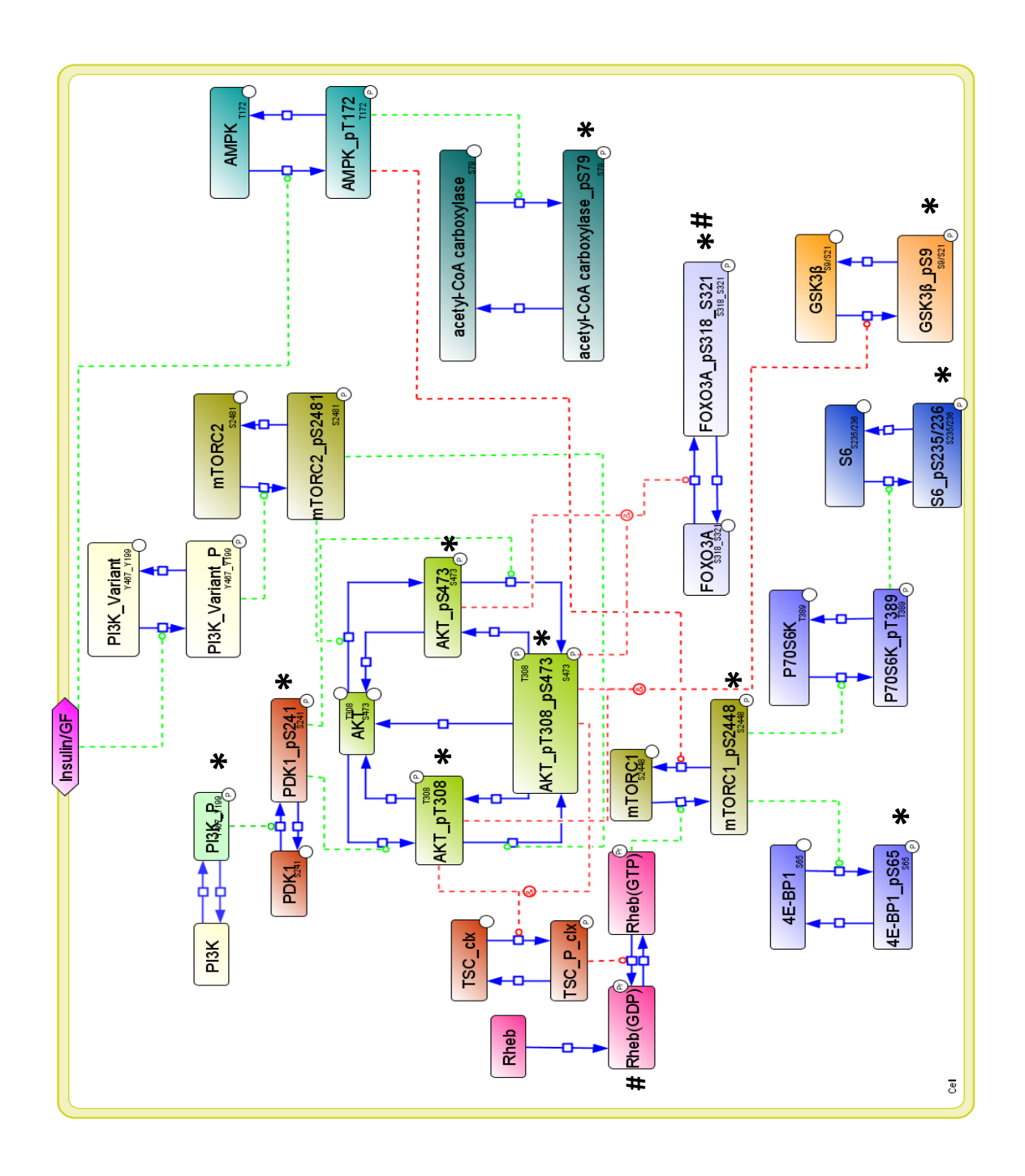


Figure 5.1: The mTOR network. A SBGN network diagram displaying the effect of amino acids on the mTOR network. Asterisks mark phospho proteins measured for starvation-restimulation RPPA experiments whilst hashtags mark proteins assayed by imagestream flow cytometry.

5.3.2 Collection of MRC5 calibration dataset

As with the previous chapter once the topology of the model was established a calibration dataset was collected using RPPA. In this case a 24 hour time course was carried out as described in section 2.1.15. As with the starvation re-stimulation dataset the time course was designed to allow for the capturing of the immediate dynamics of the mTOR network following removal of Rapamycin. A total of 17 proteins were analysed consisting of 9 phosphoproteins, 8 total proteins and the house keeping protein α-tubulin (Table 5.1). As each of the proteins being measured had been analysed previously it was decided to fully utilise RPPA's ability to produce time course data on a large scale with all of the antibodies analysed at the same time as opposed to the smaller separate runs carried out for the starvation re-stimulation dataset. As can be seen in figure 5.2 there was very clear response observed within the mTOR network. In contrast to starvation re-stimulation there is no AMPK/ACC peak following restimulation. This appears to support recent work showing that the AMPK activation peak is directly related to amino acid availability. Following Rapamycin withdrawal ACC_pS79 decreases rapidly over the first 5 minutes of the time course and remains low throughout (Figure 5.2 A). The response of PI3K p85_pY467_pY199, PTEN_pS380_pT382_pT383 and AKT_pT308 all follow the same dynamics with an initial decrease over the first 3 minutes followed by an increase in phosphorylation at 5 minutes (Figure 5.2 B, C, E). Phosphorylation levels then decrease back to initial levels at 10 minutes followed by a second increase on 20 minutes post re-stimulation. Phosphorylation decrease between 20 and 30 minutes with an increase in activity seen between 30 and 60 minutes. Whilst PDK1_pS241, mTORC1_pS2448 and 4E-BP1 pS65 follow the same dynamics as the three proteins mentioned above for 5 minutes onwards, they differ in their initial response with an increase in signalling occurring immediately following re-stimulation followed by a decrease at the 3 minute time point (Figure 5.2 D, G, H). The response of AKT_pS473 following Rapamycin withdrawal is very similar to the response of AKT_pT308 with an initial decrease followed by an increase in phosphorylation at the 5 minute time point. However it differs in that this increase remains lower than the initial 0 time point and that there is no increase in signalling seen at the 60 minute time point (Figure 5.2 F). Following Rapamycin withdrawal there is a very clear dynamic displayed by the FOXO3a phosphorylation site measured with an increase in phosphorylation occurring up to the 3 minute time point at which point phosphorylation remains consistent (Figure 5.2 I).

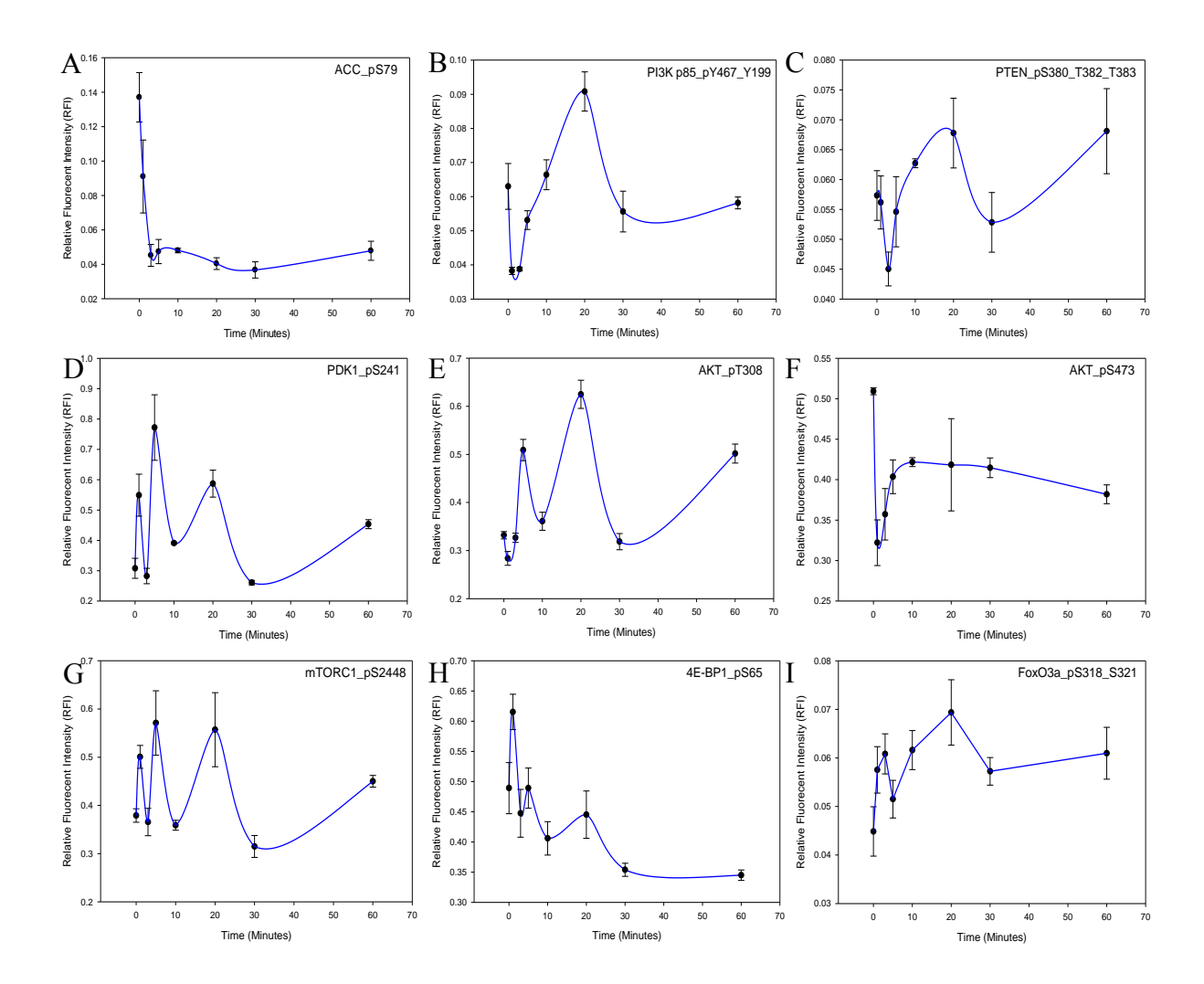


Figure 5.2: Measuring the Kinetics of the mTOR Network in MRC5 Cells. A sixty minute time course following 24 hour Rapamycin treatment (10nM). Cells were re-stimulated at 0 hours and relative fluorescent intensity measured at each time point (n=3) (Mean +/- SEM). (A) ACC_pS79, (B) PI3K_P85_pY467_Y199, (C) PTEN_pS380_T382_T383, (D) PDK1_pS241, (E) AKT_pT308, (F) AKT_pS473, (G) mTORC1_pS2448, (H) 4E-BP1_pS65 and (I) FOXO3A_pS318_S321.

<u>Table 5.1: Reverse Phase Protein Array Antibodies.</u> A list of all antibodies assayed during starvation-restimulation experiments

Antibody	Antibody	Source
ACC	AKT_pS473	Cell Signalling Technology
ACC_pS79	mTOR	Cell Signalling Technology
PI3K p85_pY467_Y199,	mTOR_pS2448	Cell Signalling Technology
PTEN	4E-BP1	Cell Signalling Technology
PTEN_pS380_T382_T383	4E-BP1_pS65	Cell Signalling Technology
PDK	FOXO3A	Cell Signalling Technology
PDK1_pS241	FOXO3A_pS318_S321	Cell Signalling Technology
AKT	AKT_pT308	Cell Signalling Technology
A-tubulin		Cell Signalling Technology

5.3.3 Parameter estimation

As with the starvation re-stimulation model, following generation of a calibration dataset using RPPA, parameter estimations were carried out for the first 60 minutes of the timecourse. The data was first normalised to the housekeeping protein α -tubulin and then the control time point 0 set to a value of 1 and all subsequent time points divided by this value. This would allow for a direct comparison between the MRC5 and MSC datasets. As with the previous model, a total number of 10000 runs were then performed using a computational cluster with the genetic algorithm used as described in section2.2.2. The time length for these runs was variable as they were dependent on how the cluster was being used on a given day by multiple users. As described in section 4.3.3 the residual sum of squares (RSS) value was used to determine a "goodness of fit" due to the scale of the data being used.

5.3.4 Restimulation following rapamycin treatment is dependent upon P70S6K negative feedback

As in the previous chapter, 10000 parameter estimations were performed using the Genetic algorithm and the results analysed (figure 5.3). As can be observed in figure 5.3 acceptable fits were achieved for the observables, ACC_pS79, AKT_pS473 and FOXO3A_pS318_pS321. For each of the other observable read outs the model failed to fit the data. For this dataset there is no clear flow of information through the network as was observed in the previous chapter. Instead there is a clear break between the downstream and upstream read outs. This is likely due to the fact that Rapamycin targets the mTORC1 complex only within the network as opposed to the network wide effect observed in serum starvation. For the purposes of this model it can therefore be assumed that the upstream regulators PI3K and PTEN may be in an active and inactive state respectively at the 0 hour time point whereas the downstream effectors mTORC1 and 4E-BP1 can be said to be in a downregulated state. As such one possible explanation for the lack of fit is the simplified S6K negative feedback loop within the model topology. In the current iteration upon phosphorylation S6K acts to dephosphorylate PI3K directly with IRS1 not included within the model. To address this it was decided to alter the model topology to include IRS1 and its PI3K activation. The new topology is summarised in Figure 5.4.

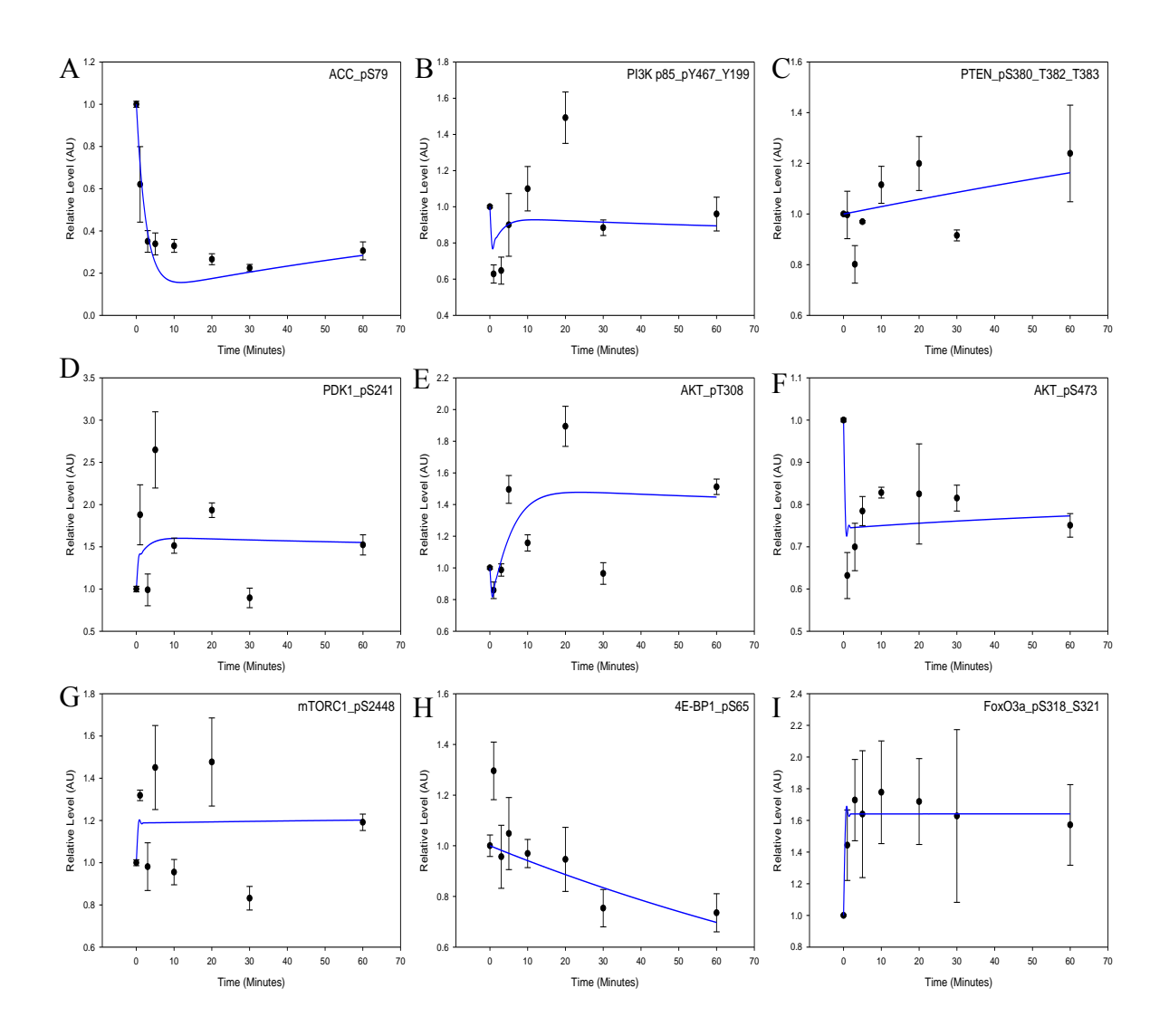


Figure 5.3: Time course simulations from the model compared to re-stimulation

data. The model displayed in figure 5.1 was calibrated using the RPPA data shown in figures 5.2. A parameter estimation consisting of 59 parameters in total was performed using the genetic algorithm (10000 runs). The Residual sum of squares between the experimental data (Black +/- SEM) and the simulated data (Blue) was calculated as 0.65.

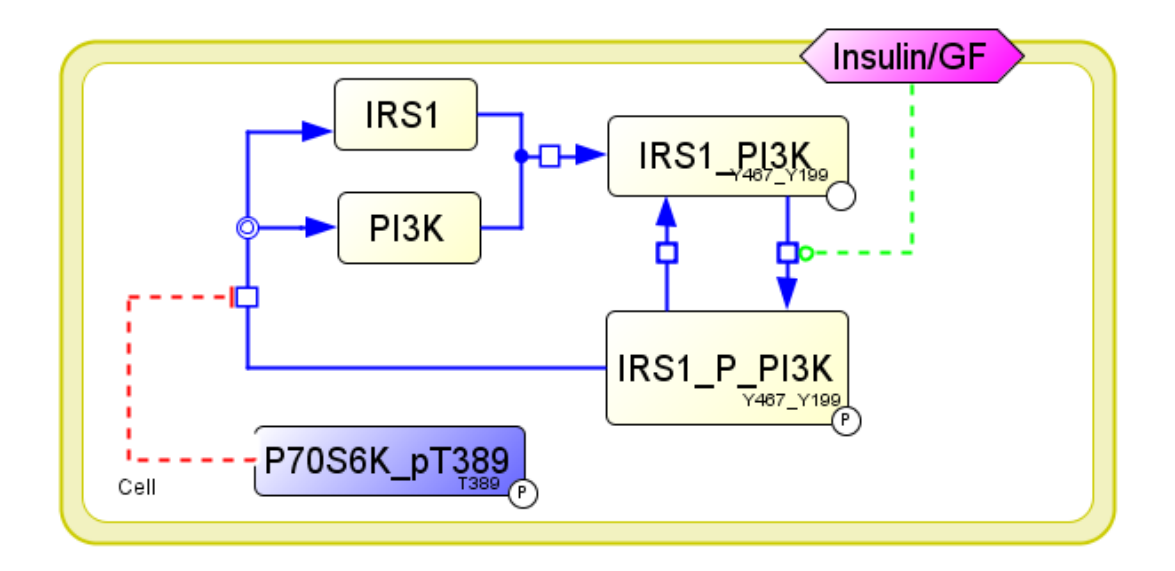


Figure 5.4: Restructured PI3K-IRS1 topology. A SBGN dynamic model diagram displaying the new PI3K-IRS1 network topology. All other reactions remain as seen in figure 5.1.

5.3.5 Restructured S6K feedback loop results in an improved fit

With the new topology established a further parameter estimation run was performed as above. As can be seen in figure 5.5 although there is a decrease in the RSS value with the IRS1-PI3K topology in place the decrease is not significant (0.642177 compared to 0.657493)(figure 5.5). Due to the increase in the number of reactions within the model however it was decided that the Akaike information criterion (AIC) should be calculated for both models. The AIC method takes into account model complexity and is a more suitable comparison method between two different models to the same dataset. Upon calculation of the AIC it was clear that whilst there is no difference between the old and new topology when comparing RSS scores there is a clear difference between the two topologies when the AIC scores are compared (figure 5.6). As the new topology provided a lower AIC score it was decided that from this point this topology would be used.

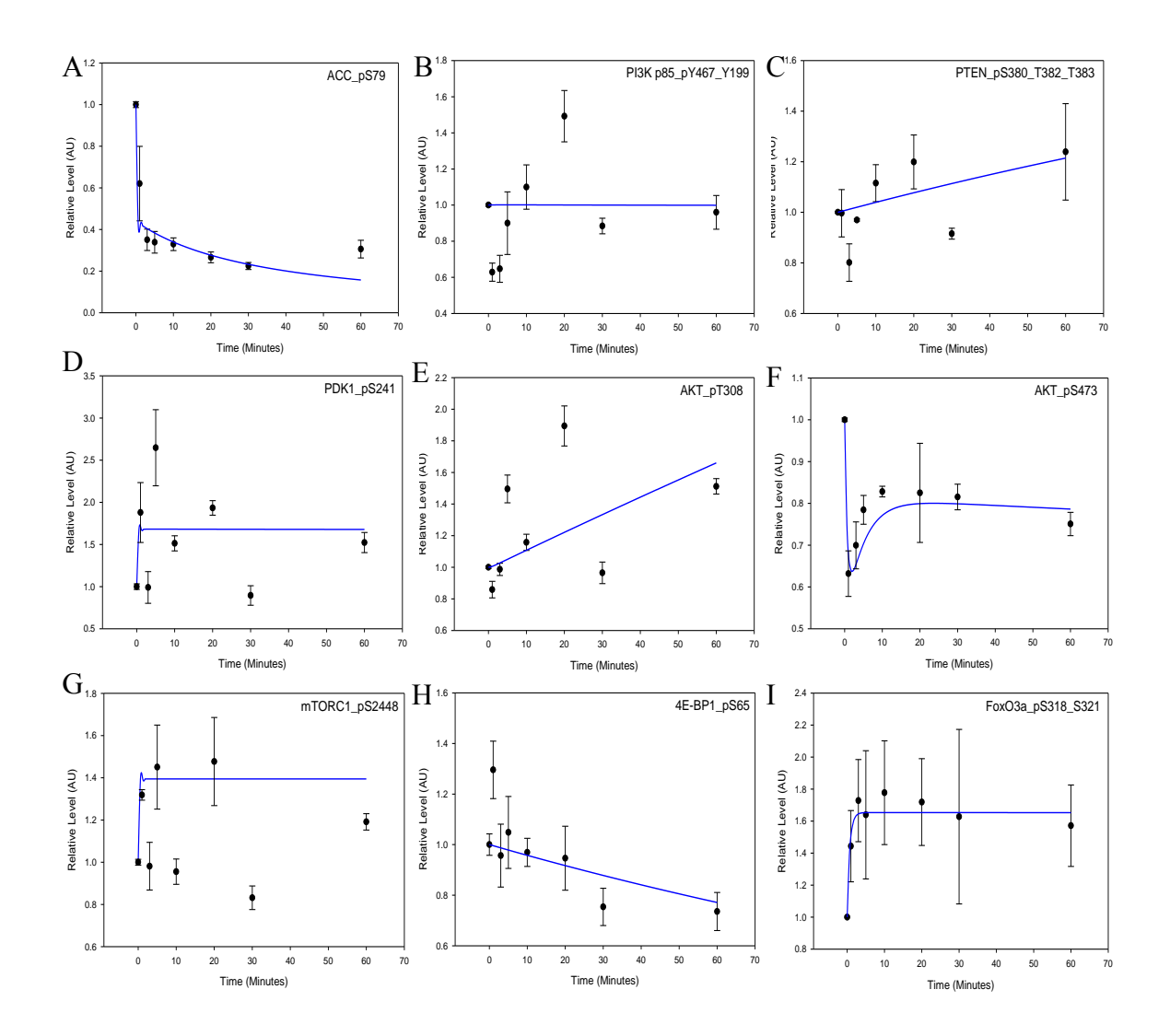


Figure 5.5: Time course simulations from the model compared to re-stimulation data using updated IRS1-PI3K topology. The model displayed in figure 5.1 was calibrated using the RPPA data shown in figures 5.2. A parameter estimation consisting of 59 parameters in total was performed using the genetic algorithm (10000 runs). The Residual sum of squares between the experimental data (Black +/- SEM) and the simulated data (Blue) was calculated as 0.64.

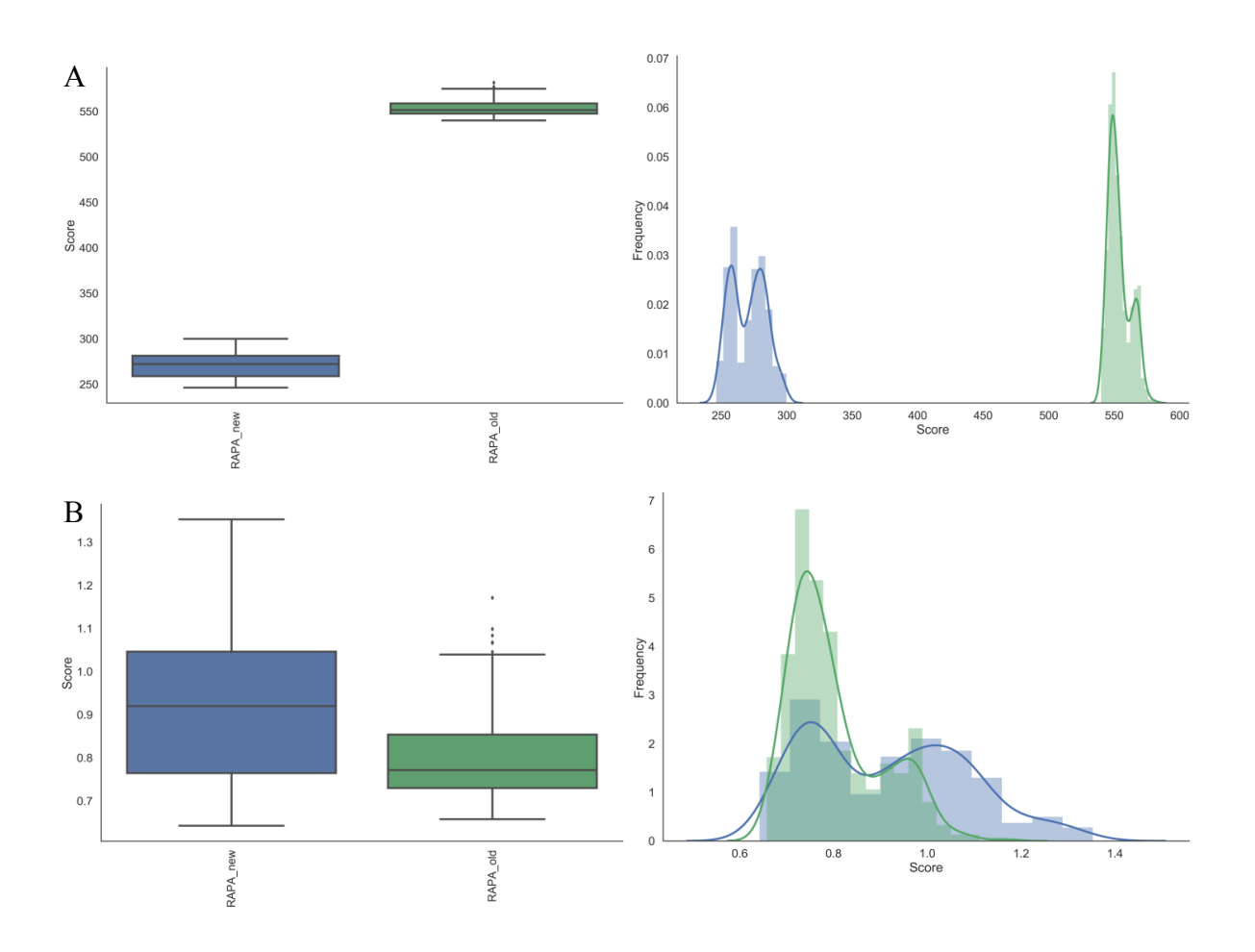


Figure 5.6: Akaike information criterion (AIC) score vs RSS. The AIC score (A) and RSS values (B) were calculated for all 10000 parameter sets and plotted as both boxplots and histograms for the original topology (Green) and the updated IRS1-PI3K topology (Blue).

5.3.6 The removal of PDK1 dataset provides the closest fit between experimental and theoretical outputs

Although the AIC score for the new topology is lower than the old network topology the model fit obtained was still not acceptable. As such it was decided that as with the previous chapter datasets should be removed and the subsequent model fit analysed to assess which dependent variable has the most impact on model fitting. Following analysis of the data it was decided that the following datasets should each be removed from the model, ACC_pS79, PDK1_pS241 and mTORC1_pS2448. The reasoning behind this decision was as follows: 1) For ACC_pS79 very little is known regarding how AMPK is affected following Rapamycin withdrawal and whilst the model has been designed based on the current understanding of the mTOR network the majority of that knowledge is based upon serum starvation data. As such the impact and role of AMPK and ACC within the model may very well differ between Rapamycin withdrawal and serum starvation. Following withdrawal of the ACC_pS79 dataset no difference was observed with regards to the RSS score of the models with and without ACC_pS79 (0.642177 and 0.632724). This suggests that following Rapamycin withdrawal the AMPK-ACC axis has far less impact on the relevant kinetics of the mTOR network (figure 5.7). 2) The second dependant variable to be removed from the parameter estimation datasets was that of PDK1_pS241. As with ACC_pS79 there is very little research into the impact of Rapamycin treatment on PDK1 activation. Indeed whilst it is known that PDK1 activation and phosphorylation on serine 241 is dependent upon an autophosphorylation loop, the mechanism for PDK1 activation and its relationship to mTOR activation remains elusive. Upon removal of the PDK1 dataset from the model there is a clear decrease in the RSS value (0.326863 compared to 0.642177) (figure 5.8). 3) The third dependent variable that was removed from the dataset was mTORC1_pS2448. As discussed in the previous chapter it is largely agreed that the phosphorylation site on serine 2448 on the mTORC1 complex does not always correspond to mTORC1 activation. As such it was thought prudent to remove this dataset in order to determine whether or not with an absence of this mTORC1 dataset the model would be able to correctly predict the action of the S6K negative feedback loop. As can be seen in figure 5.9 although the removal of mTORC1_pS2448 from the dataset decreased the RSS value to a similar degree as the removal of PDK1 (0.341805 and 0.326863), the model was unable to correctly predict the response of PI3K.

Whilst the best overall fit for this dataset is obtained by removing PDK1_pS241 there was very little difference in terms of RSS values between this dataset and the removal of mTORC1_pS2448. Indeed both sets of experimental data display inconsistent behaviour when compared to their upstream or downstream regulators and effectors. For the purposes of this study however as the removal of PDK1_pS241 provided the best fit between experimental and theoretical data it was decided that the model should be taken forward with this dataset removed for subsequent parameter estimations.

5.3.7 Parameterisation of the PTEN 4E-BP1_activity requires a more in depth mTORC1 modelling approach

As in section 4.3.5 it was decided that further investigation should be carried out regarding the models inability to fit both the PTEN_pS380_T382_T382 and 4E-BP1_pS65 outputs. As in the previous chapter it was decided that parameter estimations should be carried out using only the data of particular interest. In this case the model was parameterised as above with 500 parameter estimations being carried out as these were exploratory parameter estimations. As can be seen in figure 5.10 when the model is presented with only the single datasets it is capable of finding a fit for both observables. The issues surrounding 4E-BP1_pS65 fitting have been discussed previously in section 4.3.5 and will not be covered here. PTEN activity however provides a different problem to fitting 4E-BP1. Whereas the relationship between 4E-BP1 and the mTOR network is well defined the relationship between PTEN and the mTOR network is less clear. It is known that dephosphorylation of PTEN leads to the inhibition of PI3K activation however what drives PTEN dephosphorylation and how this relates to Rapamycin is very poorly understood. It would therefore be necessary to investigate this mechanism in further detail in order to correctly model this output.

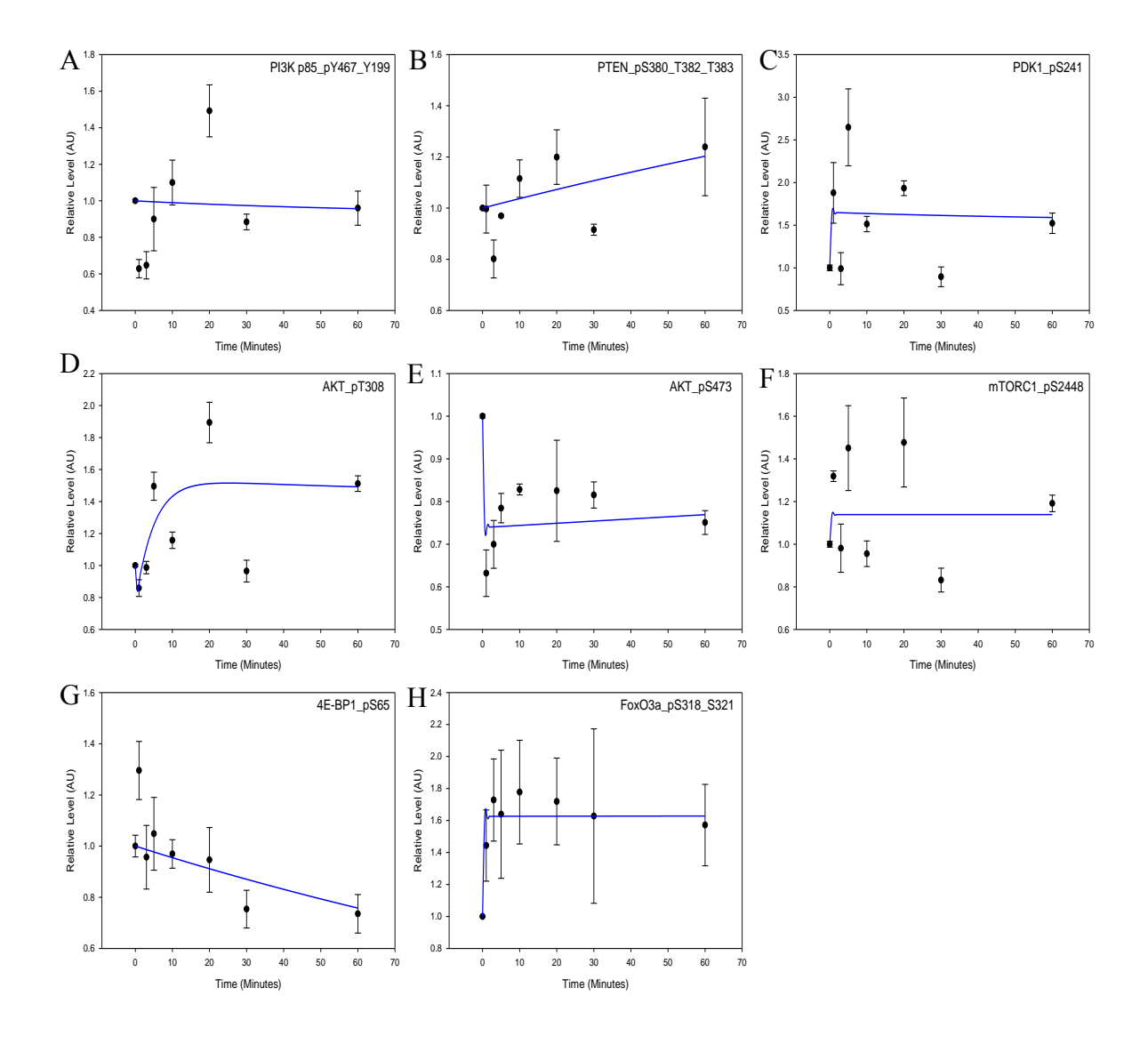


Figure 5.7: Parameter time course simulations following the removal of ACC_pS79 from the MRC5 dataset. The model displayed in figure 5.1 was calibrated using the RPPA data shown in figures 5.2. A parameter estimation consisting of 59 parameters in total was performed using the genetic algorithm with the experimental data for ACC_pS79 removed from the dataset (1000 runs). The Residual sum of squares between the experimental data (Black +/- SEM) and the simulated data (Blue) was calculated as 0.63.

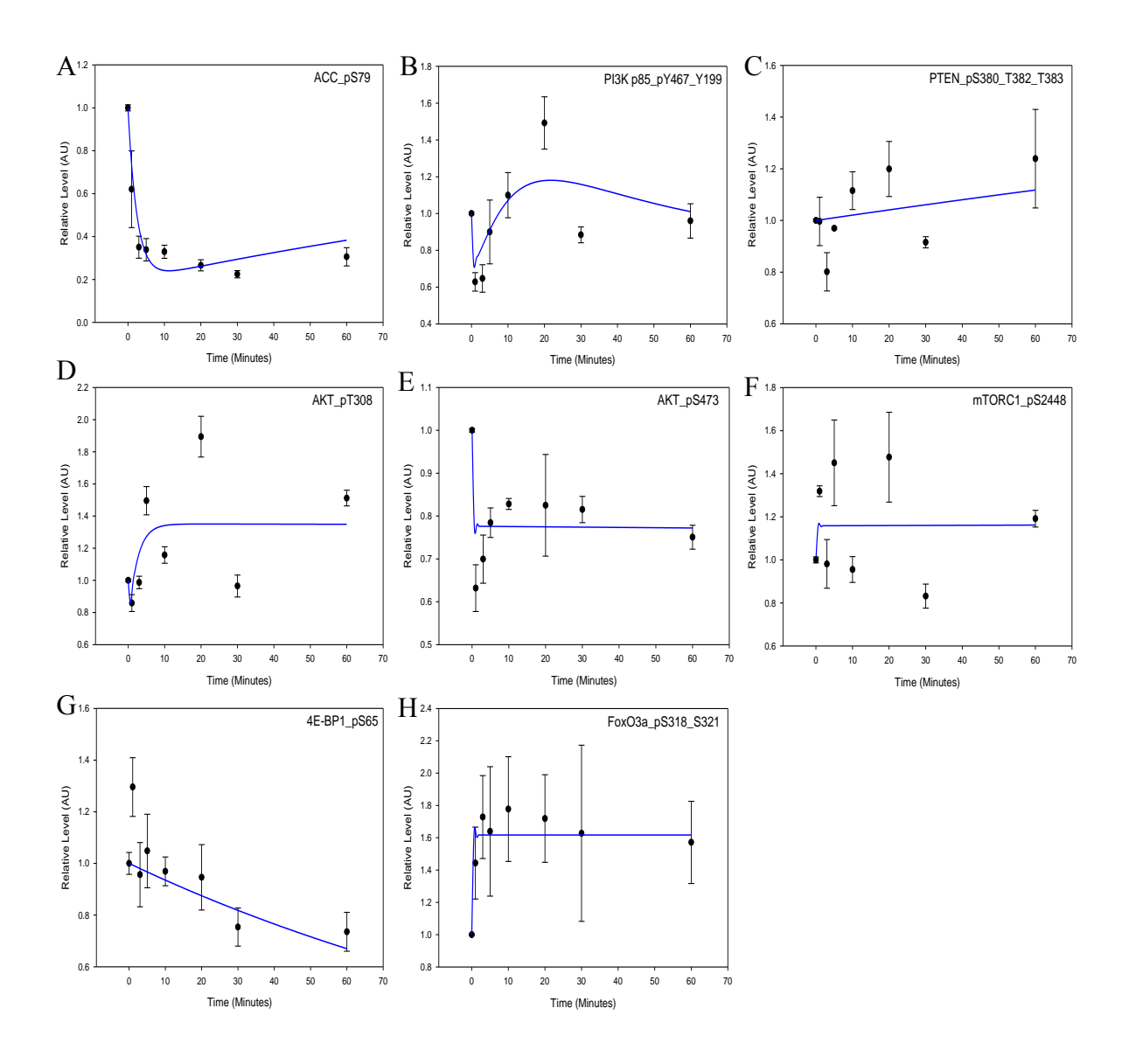


Figure 5.8: Parameter time course simulations following the removal of PDK1_pS241 from the MRC5 dataset. The model displayed in figure 5.1 was calibrated using the RPPA data shown in figures 5.2. A parameter estimation consisting of 59 parameters in total was performed using the genetic algorithm with the experimental data for PDK1_pS241 removed from the dataset (1000 runs). The Residual sum of squares between the experimental data (Black +/- SEM) and the simulated data (Blue) was calculated as 0.32.

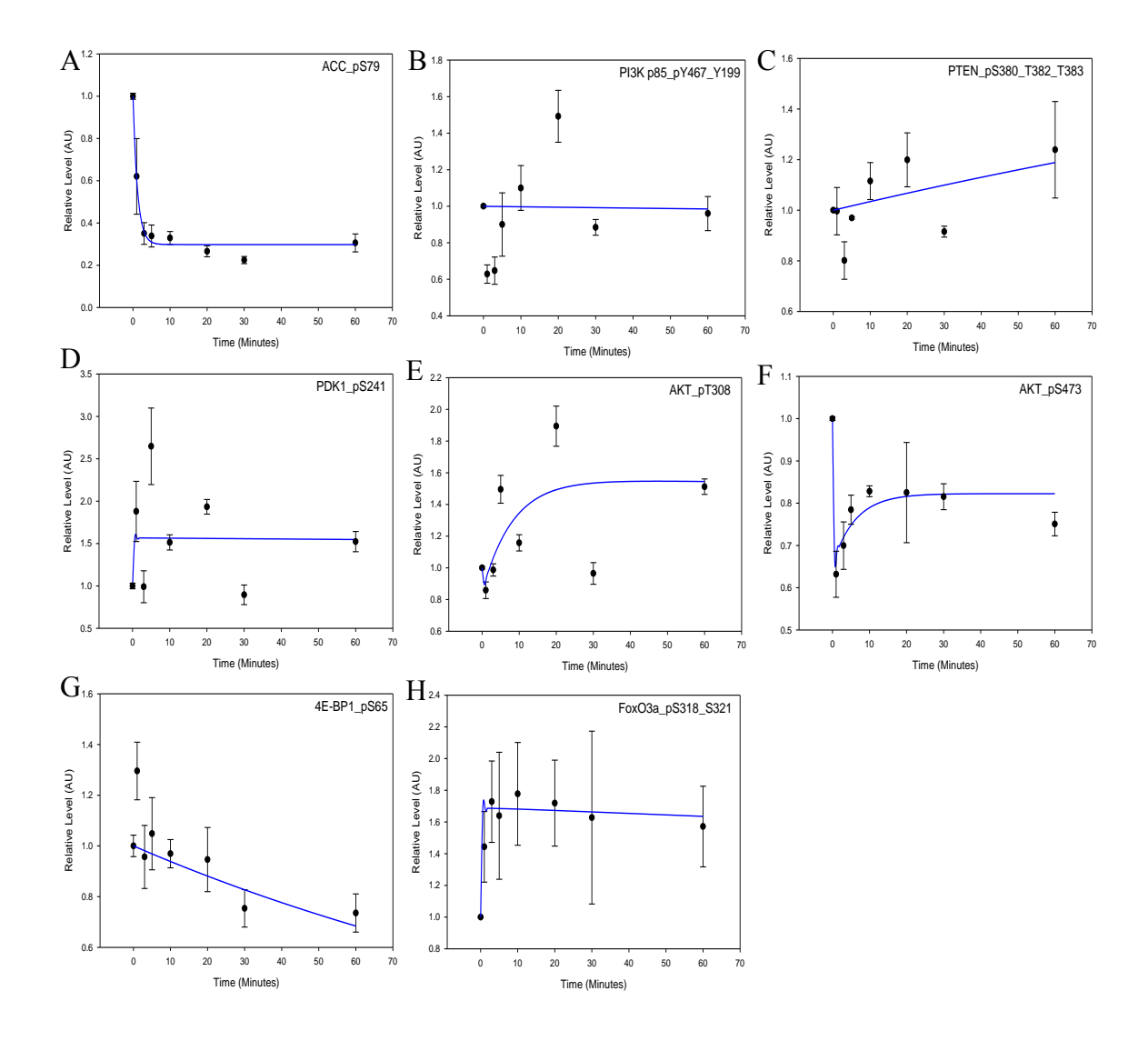
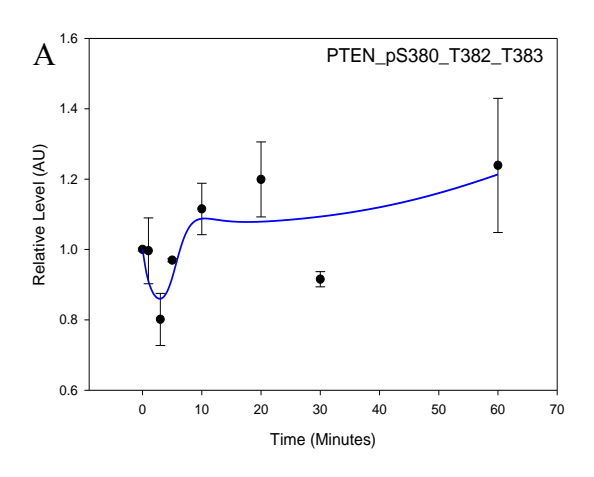


Figure 5.9: Parameter time course simulations following the removal of mTORC1_pS2448 from the MRC5 dataset. The model displayed in figure 5.1 was calibrated using the RPPA data shown in figures 5.2. A parameter estimation consisting of 59 parameters in total was performed using the genetic algorithm with the experimental data for mTORC1_pS2448 removed from the dataset (1000 runs). The Residual sum of squares between the experimental data (Black +/-SEM) and the simulated data (Blue) was calculated as 0.34.



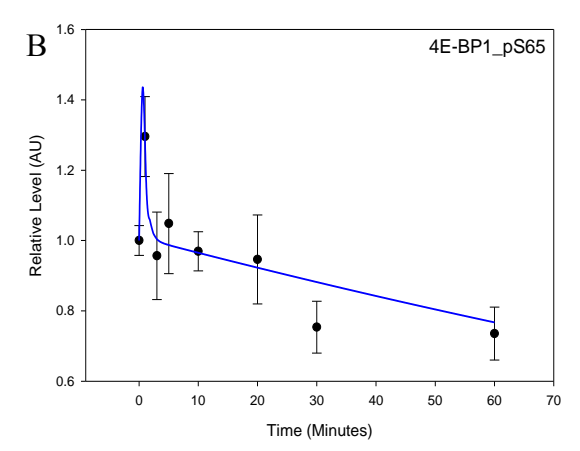


Figure 5.10: Individual parameter estimations for the PTEN_pS380_T382_T383 and 4E-BP1_pS65 observables. The model displayed in figure 5.1 was calibrated using the resimulated RPPA data shown in figure 5.2 for both PTEN_pS380_T382_T382 (A) and 4E-BP1_pS65 (B) individually. A parameter estimation consisting of 59 parameters in total was performed using the genetic algorithm (1000 runs). The Residual sum of squares between the experimental data (Black +/- SEM) and the simulated data (Blue) was calculated as 0.06 (A) and 0.03 (B).

<u>Table 5.2: Residual sum of squares value for each model.</u> The residual sum of squares for each model fitted to the experimental data for both MRC5 and MSC datasets. The lower the RSS value, the closer the fit between the model simulations and the corresponding dataset. Corresponding figure number also shown.

Parameter Estimation	Residual Sum of	Figure No.
	Squares	
MRC5 Original Topology	0.65	5.3
MRC5 New Topology	0.64	5.5
MRC5 ACC	0.63	5.7
MRC5 mTOR	0.34	5.8
MRC5 PDK1	0.32	5.8
MRC5 PTEN	0.06	5.10
MRC5 4E-BP1	0.03	5.10
MRC5 Hooke and Jeeves	0.30	5.13
MSC Genetic Fit	0.35	5.14
MSC Hooke and Jeeves	0.99	5.14

5.3.8 Modelling the difference between MRC5 and MSC kinetics in response to rapamycin-restimulation

Having calibrated the model to the MRC5 dataset a second time course dataset was created for the MSCs. This time course was carried out using the same time points as in the MRC5 dataset and is shown in figure 5.11 with a comparison between MRC5 and MSC response to Rapamycin withdrawal shown in figure 5.12. In comparison to the MRC5 dataset the MSC dataset is highly consistent with a clear flow of information through the network. The exception to this was for PDK1_pS241, where the profile shows an increase in activation following 10 minutes restimulation followed by a decrease in signalling between 10-30 minutes prior to further increase in signalling at 60 minutes. The inconsistency of PDK1 behaviour in response to Rapamycin withdrawal provides further evidence that there are mechanisms governing its activation that have not currently included with regards to Rapamycin treatment. For the purposes of calibration with the MSC dataset with the Genetic algorithm it was decided that the PDK1 dataset should be included in the parameter estimation and the output analysed as carried out above in the MRC5 dataset.

As in the previous chapter a comparison testing the ability of the calibrated MRC5 model to fit the MSC data was carried out. The MRC5 dataset was removed and replaced with the MSC dataset. A set of 100 parameter estimations using the Hooke and Jeeves algorithm was then performed using the reaction parameter values obtained by the best fit to the MRC5 dataset as the initial reaction parameter values. In addition a set of 100 parameter estimations was also carried out as above for the MRC5 dataset.

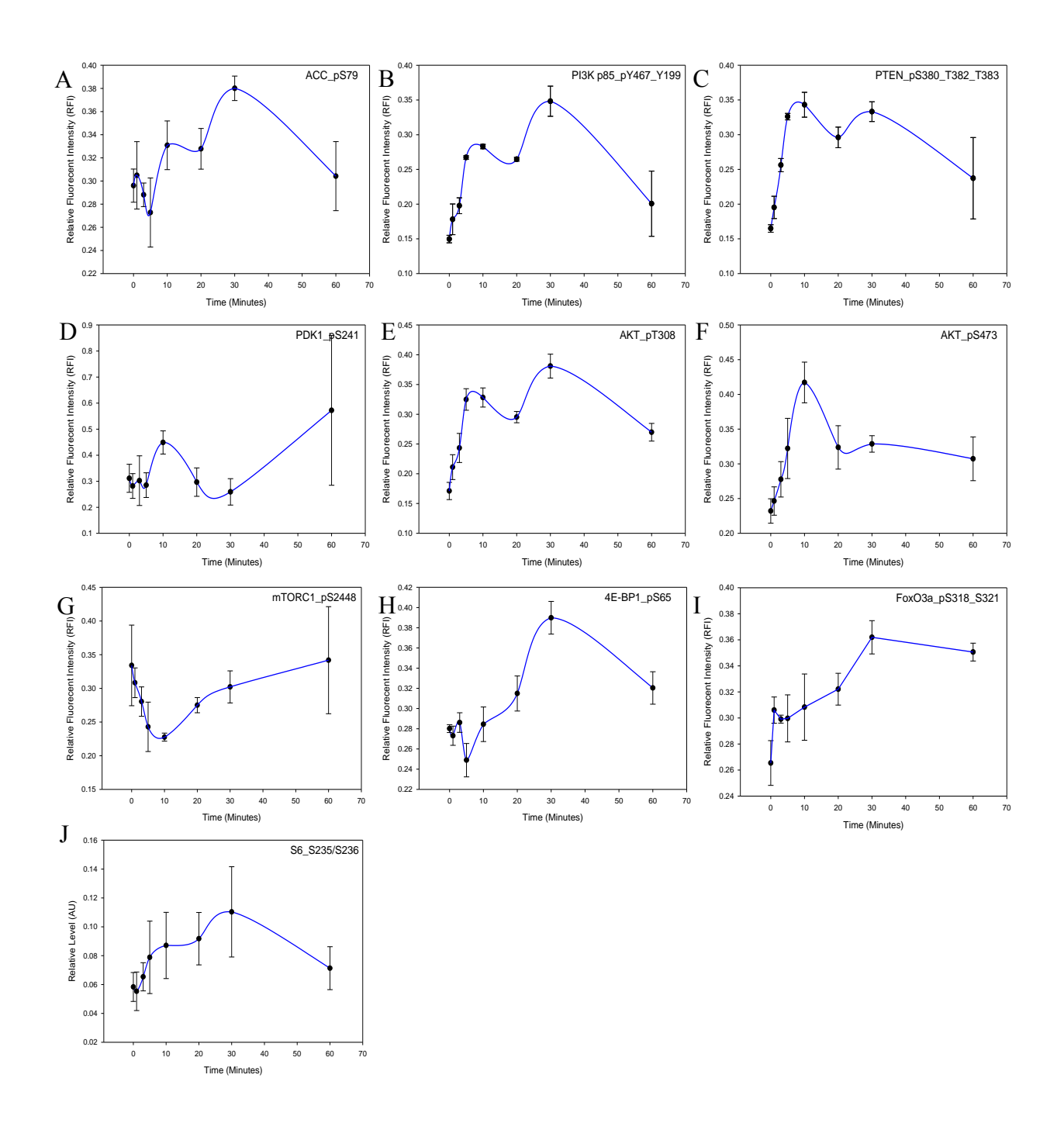


Figure 5.11 : Measuring the Kinetics of the mTOR Network in MSC Cells. A sixty minute time course following 24 hour Rapamycin treatment (10nM). Cells were re-stimulated at 0 hours and relative fluorescent intensity measured at each time point (n=3) (Mean +/- SEM). (A) ACC_pS79, (B) PI3K_P85_pY467_Y199, (C) PTEN_pS380_T382_T383, (D) PDK1_pS241, (E) AKT_pT308, (F) AKT_pS473, (G) mTORC1_pS2448, (H) 4E-BP1_pS65, (I) FOXO3A_pS318_S321 and (J) S6_pS235/236.

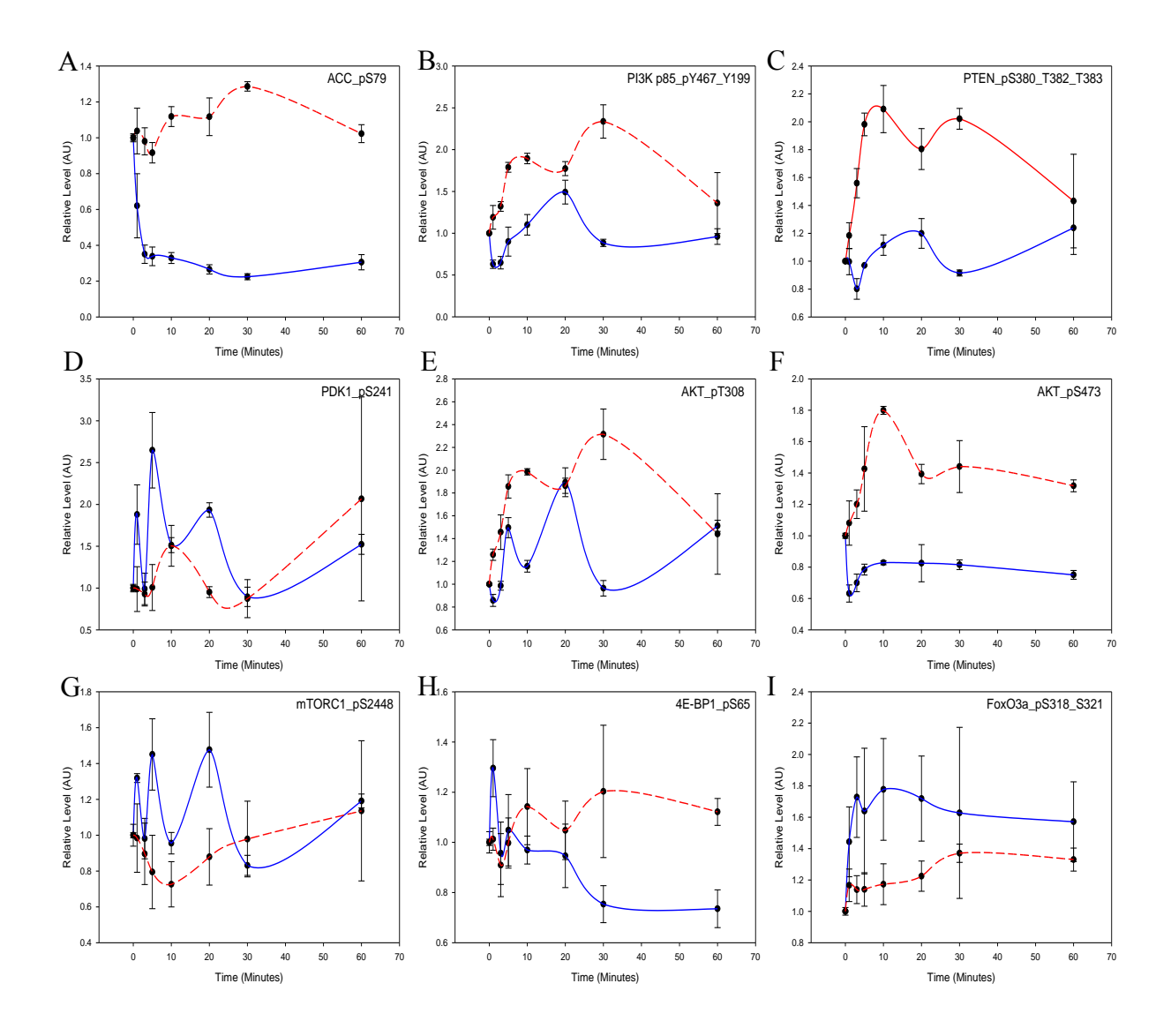


Figure 5.12: A comparison of MRC5 vs MSC outputs following Rapamycin withdrawal. A sixty minute time course following 24 hour Rapamycin treatment for both MRC5 (Blue) and MSC (Red) cells. Cells were re-stimulated at 0 hours and relative fluorescent intensity measured at each time point (n=3) (Mean +/- SEM). (A) ACC_pS79, (B) PI3K_p85_pY467_pY199, (C) PTEN_pS380_pT382_pT383, (D) PDK1_pS241, (E) AKT_pT308, (F) AKT_pS473, (G) mTORC1_pS2448, (H) 4E-BP1_pS65 and (I) FOXO3A_pS318_pS321.

5.3.9 Parameter estimation results MSC

Following calibration with the genetic algorithm the MRC5 model was subjected to 100 runs using the Hooke and Jeeves algorithm (figure 5.13). This resulted in a slight improvement in the ability of the model to fit the data provided (RSS=0.30 compared to 0.32). This improvement of 0.02 was significantly less than that achieved in the previous chapter using the starvation restimulation dataset (0.08). Upon comparison between the MSC datasets parameterised using the Hooke and Jeeves and genetic algorithm it became apparent that there was a large difference between the ability of the models to fit the data (figure 5.14). The target RSS obtained using the genetic algorithm for the MSC dataset was 0.35, whilst this value is larger than value of 0.32 obtained using the MRC5 dataset, there was also a larger number of variables measured (9 compared to 8). As can be seen in figure 5.14 the genetic algorithm was capable of fitting 7 out of 9 of the variables measured with PDK1 pS241 FOXO3A_pS318_pS321 failing to be fitted (figure 5.14 D + I). The Hooke and Jeeves algorithm using the previously calibrated MRC5 model was capable of fitting 4 out of the 9 variables measured. As with the genetic algorithm fit it was unable to fit the PDK1 dataset. This provides further evidence that Rapamycin treatment and withdrawal results in alterations to PDK1 regulation (figure 5.14 D). The Hooke and Jeeves model also failed to provide a fit to either AKT phosphorylation sites (figure 5.14 E + F).

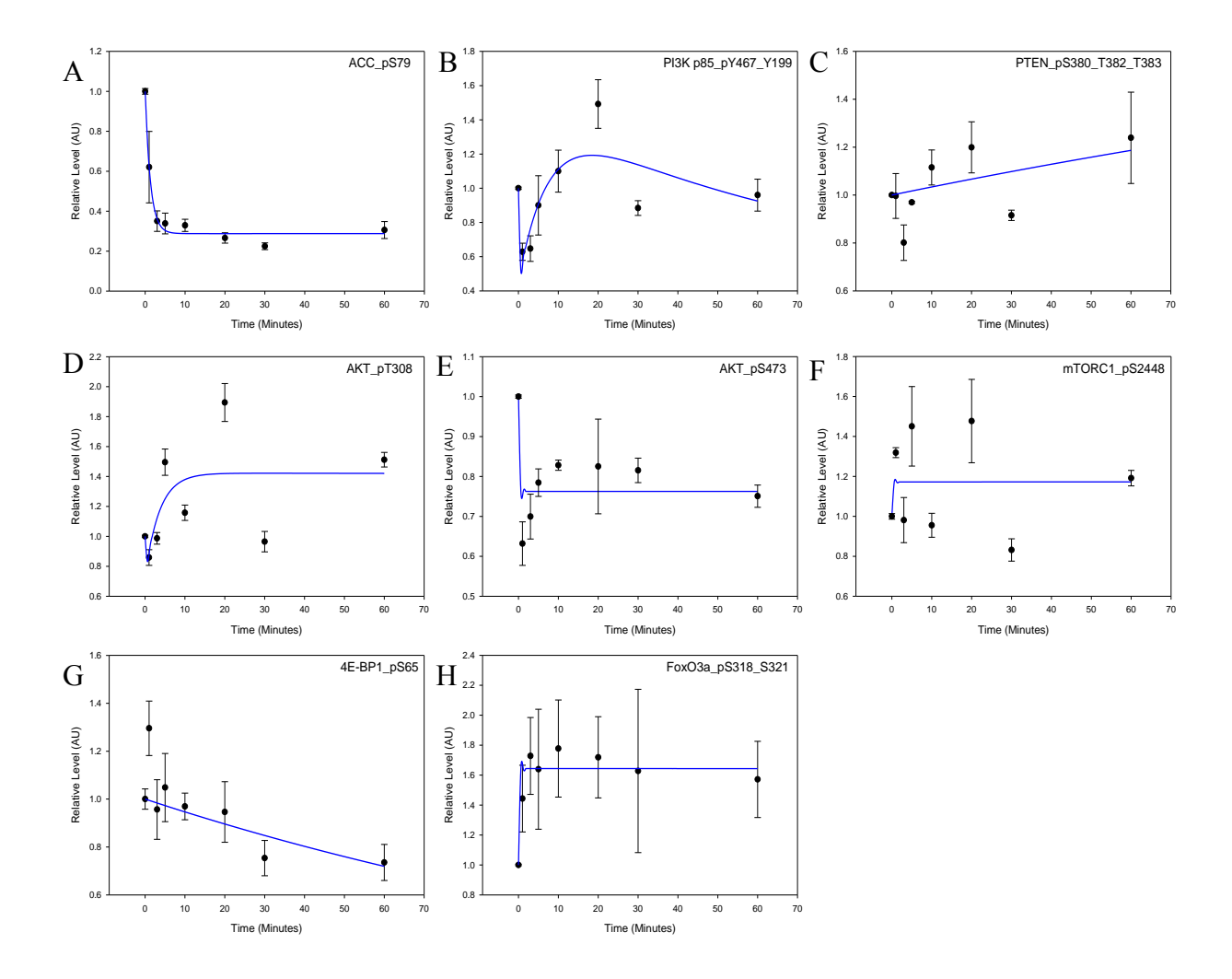


Figure 5.13: Time course simulations from the model compared to re-stimulation data utilizing the local Hooke and Jeeves algorithm. The model displayed in figure 5.1 was calibrated using the re-simulated RPPA data shown in figures 5.2 A parameter estimation consisting of 59 parameters in total was performed using the local algorithm Hooke and Jeeves (100 runs). The Residual sum of squares between the experimental data (Black +/- SEM) and the simulated data (Blue) was calculated as 0.30.

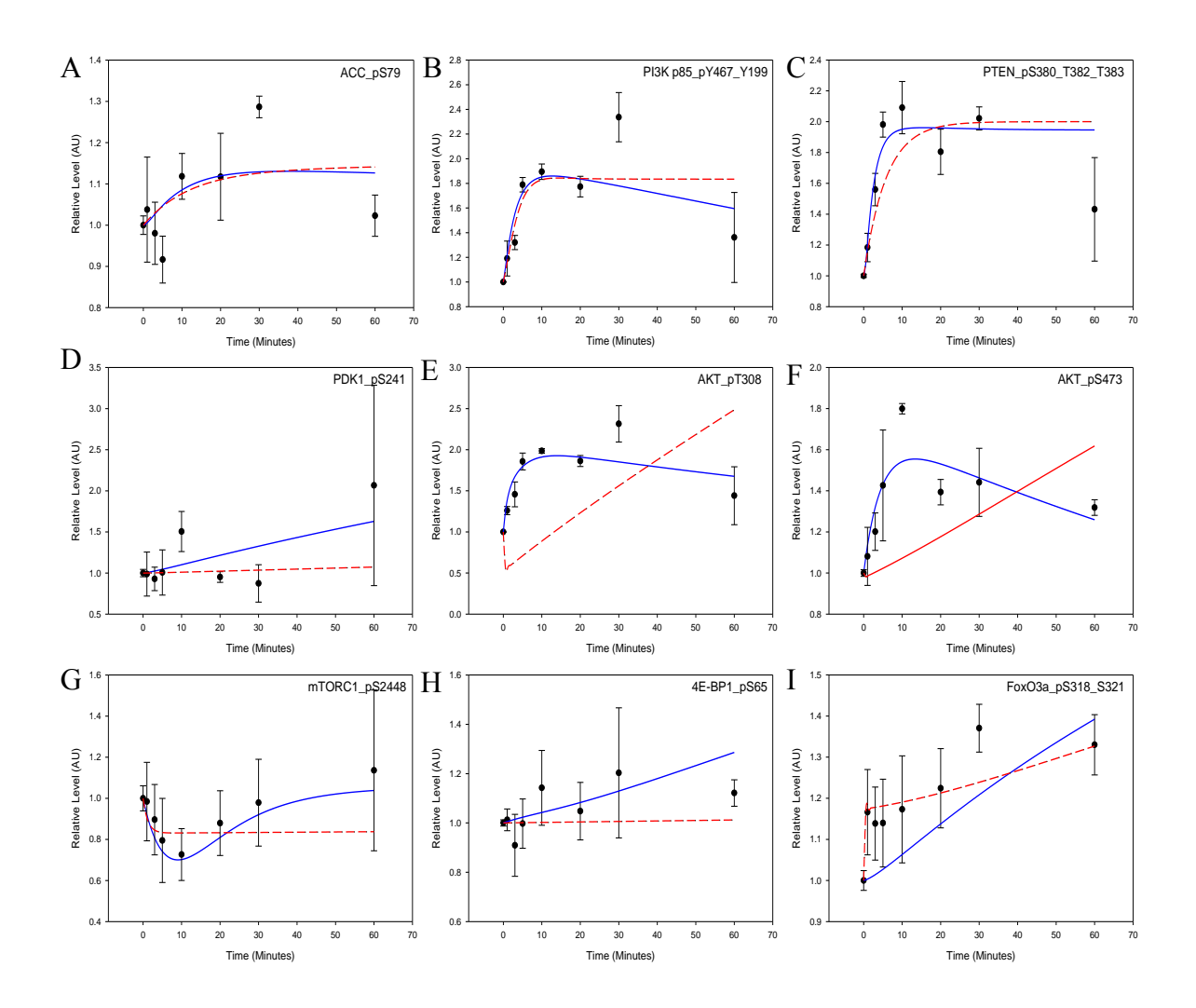


Figure 5.14: Genetic vs Hooke and Jeeves fit for MSC. The model displayed in figure 5.1 was calibrated using the RPPA data shown in figure 5.11. A parameter estimation consisting of 59 parameters in total was performed using the genetic algorithm (10000 runs) (Blue) randomising the initial parameter values and the Hooke and Jeeves algorithm (100 runs) (Red) using previously obtained parameter values form the MRC5 data fit. The Residual sum of squares between the experimental data (Black +/- SEM) and the simulated data (Genetic-Blue, Hooke and Jeeves-Red) was calculated as 0.35 (genetic) and 0.99 (Hooke and Jeeves).

5.3.10 Starvation-restimulation and rapamycin withdrawal lead to similar responses in MSC but not MRC5 cells

Following serum starvation-restimulation there is a clear kinetic response by the mTOR network as can be seen in figure 5.15 for both MRC5 and MSC cells. However following Rapamycin treatment and withdrawal MRC5 cells show no clear dynamic response (figure 5.15 A-I). In comparison, MSCs display a very clear dynamic response following Rapamycin withdrawal (figure 5.15 J-R). In terms of the response to the mTOR network this difference also holds true with very little similarity observed between the two treatment responses in MRC5 cells. The MSCs however display similar behaviour to both treatments in a number of variables measured. Of note the response of ACC_pS79 (figure 5.15 A) displays an almost identical profile. Across all of the variables measured in can be concluded that 7 profiles display similar kinetic profiles and only the two AKT phosphorylation sites display significantly different kinetics. In both cases this appears to be due to a difference in the scale of the response by the variable in question. Following Rapamycin withdrawal there is a more significant increase in the level of AKT_pT308 phosphorylation compared to starvationrestimulation (figure 5.15 N). The opposite can said for the AKT_pS473 phosphorylation site with a far greater increase observed in response to starvationrestimulation (figure 5.15 O).

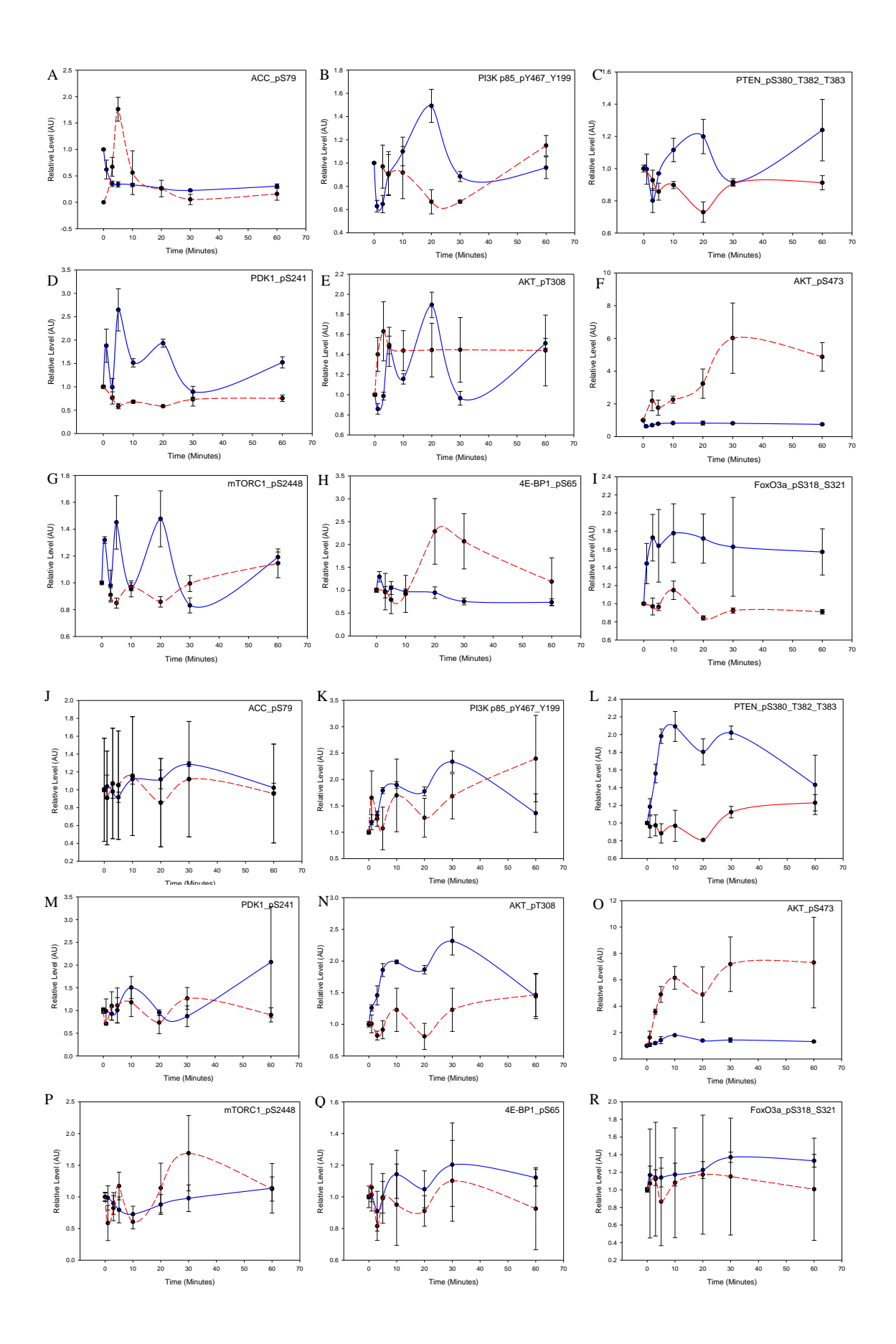


Figure 5.15 A comparison of mTOR kinetics following Rapamycin withdrawal and starvation-restimulation in MRC5 and MSC cells. A sixty minute time course following 24 hour Zoledronate treatment (Blue) and starvation-restimulation (Red). Cells were restimulated at 0 hours and relative fluorescent intensity measured at each time point (n=3) (Mean +/-SEM) in MRC5 cells (A) ACC_pS79, (B) PI3K_p85_pY467_pY199, (C) PTEN_pS380_pT382_pT383, (D) PDK1_pS241, (E) AKT_pT308, (F) AKT_pS473, (G) mTORC1_pS2448, (H) 4E-BP1_pS65 and (I) FOXO3A_pS318_pS321. In MSCs (J) ACC_pS79, (K) PI3K_p85_pY467_pY199, (L) PTEN_pS380_pT382_pT383, (M) PDK1_pS241, (N) AKT_pT308, (O) AKT_pS473, (P) mTORC1_pS2448, (Q) 4E-BP1_pS65 and (R) FOXO3A_pS318_pS321. (Previous page).

5.4 Image flow cytometry fails to show correlation between DAPI – FOXO3A and Rheb-LAMP1

As in the previous chapter imagestream flow cytometry was used to analyse the response of FOXO3A and Rheb cellular localisation following Rapamycin treatment and withdrawal. The timecourse used during the imagestream flow cytometry assays differed from those obtained using the RPPA with time points taken at the following times 0 hour (untreated), 30 minutes post treatment, 60 minutes post treatment, 24 hours post treatment, 5 minutes post restimulation, 15 minutes post restimulation, 30 minutes post restimulation, and 60 minutes post restimulation. LAMP1-Alexa-488 and DAPI were also stained for in order to allow for lysosomal and nuclear localisation comparison as in the previous chapter. One of the advantages of the Ideas software used during this analysis is that once a template for an experiment has been created it is possible to apply the same template along with the same compensation matrix to multiple experiments. This allowed for the analysis of all Imagestream experiments undertaken without changing any parameters within the analysis and removing individual bias that can be inserted in confocal microscopy. A representative image of cells following 24 hours Rapamycin treatment in shown in figure 5.16. As in the previous chapter a single cell population was selected and out of focus cell images removed from the analysis prior to analysi of co-localisation between FOXO3A- DAPI and Rheb-LAMP1 (figure 5.16 A-D). Unfortunately whilst the Rapamycin samples analysed contained more cells in the final analysis (post focus, single cell identification) this total was still lower than required to perform analysis of sub-cellular localisation (Pearson's correlation co-efficient) (figure 5.17). In addition whilst DAPI was present in both the starvation-restimulation and Rapamycin data it did not show up in the final population (Pearson's correlation co-efficient) (figure 5.16 E). Therefore whilst the data shown in table 5.3 indicates a slight increase in both FOXO3A-DAPI and Rheb-LAMP1 correlation it is not possible to say with any certainty that this is the case.

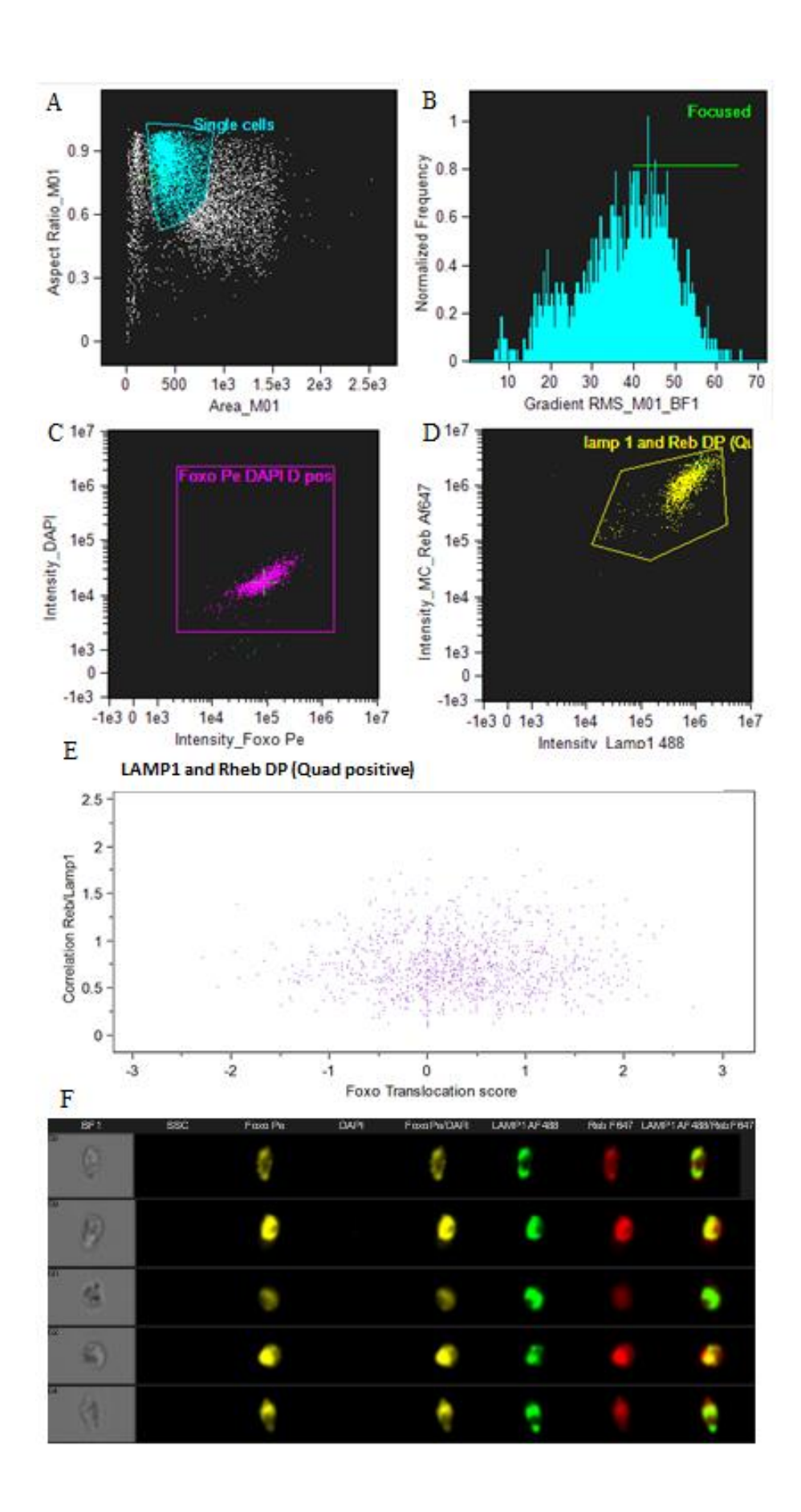


Figure 5.16: Image flow cytometry fails to show correlation between DAPI – FOXO3A and Rheb-LAMP1. Representative image displaying image flow cytometry analysis of untreated cells following 24 hour Rapamycin treatment (10nM)(A) A single cell population was selected, (B) followed by the removal of images that were not in focus. (C) Nuclear localisation correlation was analysed for FOXO3A and DAPI, in addition to (D) correlation analysis of RHEB and LAMP1. (E) Population analysis displaying correlation between DAPI-FOXO3A and Rheb-LAMP1. (F) Representative image of in focus single cell population for 0 hour untreated cells.

<u>Table 5.3: Image flow cytometry time course correlation</u>. Correlation values for each time point assayed for FOXO3A-DAPI (FD) and Rheb-LAMP1 (RL) (Pearson's correlation co-efficient; all values are non-significant P>0.05).

Time Point	FOXO3A-DAPI	Rheb-LAMP1	P-value
	Pearson's correlation	Pearson's correlation	FD/RL
	co-efficient	co-efficient	
0 hours	-0.01483	0.6018	0.99/0.59
30 minutes treated	-0.5771	0.6628	0.61/0.54
60 minutes treated	-0.2335	0.6377	0.85/0.56
24 hours treated	0.277	0.7108	0.82/0.50
5 minutes restimulated	0.6233	0.7556	0.57/0.45
15 minutes restimulated	0.3694	0.7627	0.76/0.45
30 minutes restimulated	0.4967	0.7499	0.67/0.46
60 minutes restimulated	0.794	0.7519	0.42/0.46

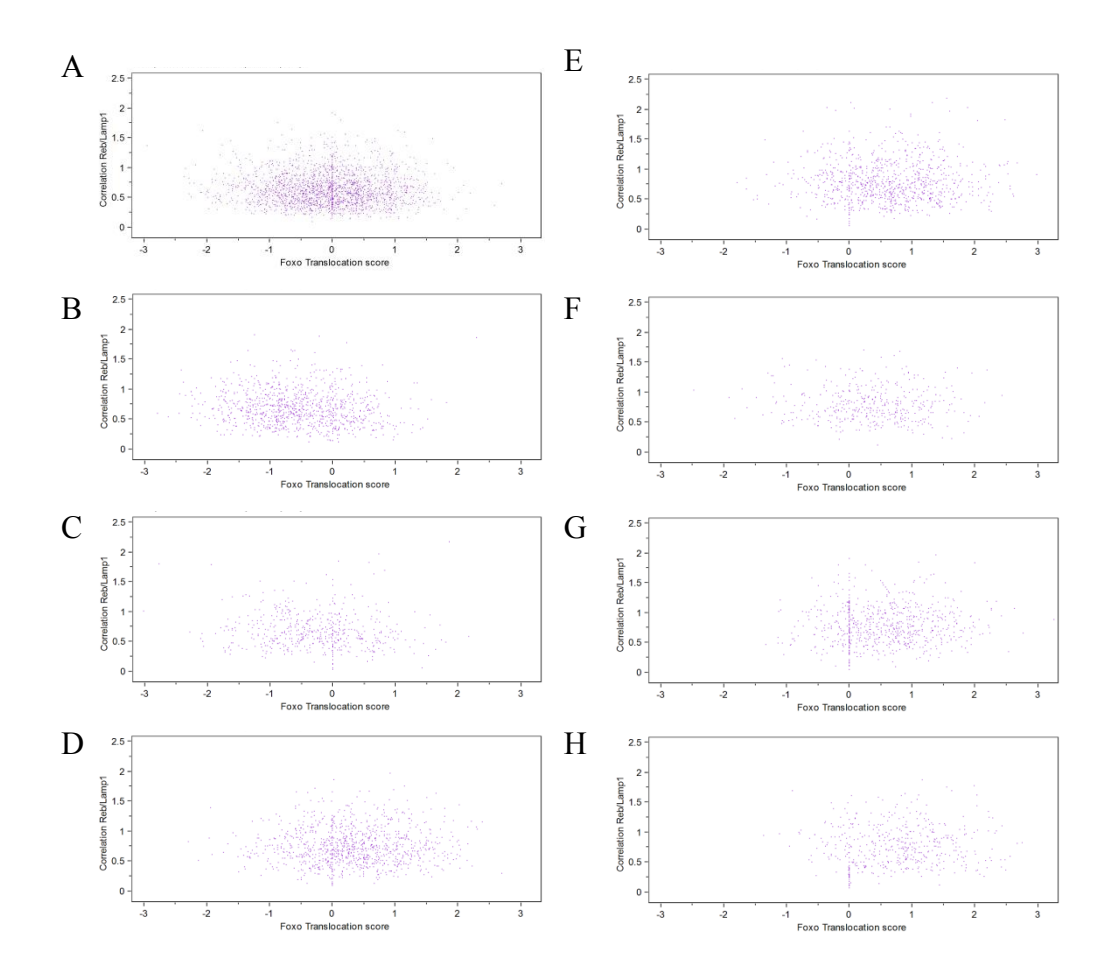


Figure 5.17: Image flow cytometry time course correlation. Population analysis displaying correlation between DAPI-FOXO3A and Rheb-LAMP1, (Pearson's correlation co-efficient) (A) 0 hour untreated cells, (B) 30 minutes Rapamycin treated cells, (C) 60 minutes Rapamycin treated cells, (D) 24 hour Rapamycin treated cells, (E) 5 minutes re-stimulated cells, (F) 15 minutes re-stimulated cells, (G) 30 minutes re-stimulated cells, (H) 60 minutes re-stimulated cells.

5.5 Discussion

The aims of the work presented here were: 1) to define a dynamic model capable of representing the mTOR networks response to Rapamycin withdrawal; 2) to calibrate this model in both MRC5 and MSCs using reverse phase protein arrays; 3) to use imagestream flow cytometry to analyse the cellular localisation of key proteins within the mTOR network and; 4) to identify how MRC5 fibroblasts and MSCs differ in their response to Rapamycin withdrawal. Through the computational dynamic modelling approach described above this has been achieved. The model presented proved capable of simulating the response of both MRC5 and MSCs in response to restimulation following a period of Rapamycin treatment.

As with the previous chapter RPPA was used to produce calibration data with measurements taken for a total of 16 proteins across the mTOR network. In contrast to the data produced in the previous chapter the data presented here for MRC5 cells produced a large amount of variation. In addition upon analysis of this data whilst parts of the network displayed a clear flow of information as expected a number of observables displayed behaviour not consistent with the rest of the time course. In contrast the data produced for the MSCs displayed a clear flow of information throughout the time course with the exception of PDK1_pS241.

One possible explanation for the variation observed in the MRC5 dataset is that Rapamycin is considered a very messy drug with many off target effects [221]. However a key part of the network that was consistently affected by Rapamycin was identified as the P70S6K negative feedback loop. A model topology alteration within this section of the network led to a reduced AIC score and a similar RSS value despite having a larger number of reactions within the model. Whilst it was not possible to measure P70S6K activation or inhibition of IRS1 following Rapamycin withdrawal using RPPA it is possible using western blotting. Further validation experiments should therefore be performed focusing on the analysis of this section of the network. As opposed to caloric restriction which feeds into numerous sections of the mTOR network, Rapamycin is known to primarily feed into mTORC1. The identification of the P70S6K negative feedback loop therefore makes biological sense. In the previous chapter the removal of particular datasets allowed for the identification of ACC_pS79 as the dataset whose removal lead to the largest decrease in fitting ability. Although a similar methodology was followed above it was not possible to identify a single set of

data whose removal either negatively or positively affected the models ability to achieve a fit. The removal of PDK1_pS241 led to the largest reduction in RSS value amongst the datasets analysed however little difference was observed upon removing either PDK1_pS241 or mTORC1_pS2448 data from the parameter estimations. The failure to fit PDK1_pS241 for either the MRC5 or MSC data however suggests that there are mechanisms governing PDK1 activation not included within the model. As PDK1 is phosphorylated on serine 241 through an autophosphorylation loop it is possible that Rapamycin treatment interferes with this process. There are no studies to date however investigating the effect of Rapamycin treatment on PDK1 activation.

Previously this work has shown that an MRC5 calibrated model was capable of fitting data from MSCs following starvation-restimulation. This however was not achieved in response to Rapamycin withdrawal with a number of observables failing to achieve an acceptable fit to the MSC data within the MRC5 calibrated model. Given the large differences observed between the two cell types responses to Rapamycin withdrawal this is to be expected. As to why such differences exist in response to identical treatments is more difficult to answer. However one explanation is that stem cells are stringently regulated in order to prevent differentiation, self-renewal and cellular growth under sub optimal conditions [36, 224]. A number of these mechanisms act as cancer preventions therefore it is possible that regulation of the mTOR network is more rigid in MSCs than in MRC5 cells resulting in the differences observed.

A comparison of the reaction of MRC5 cells to starvation-restimulation and Rapamycin withdrawal revealed very few similarities across the observables assayed. In contrast a comparison of the reaction of MSCs to starvation-restimulation and Rapamycin withdrawal revealed a number of similar kinetic responses. Given the importance of AMPK in starvation-restimulation it is of particular interest that the readout used (ACC) for this protein displays extremely similar behaviour in response to both treatments. This is further evidence supporting tight regulation of AMPK in MSCs. The two observables which display differential behaviour between the two treatments in MSCs are the two AKT phosphosites. As Rapamycin acts to inhibit mTORC1 activity only in MSCs the difference in their profiles is to be expected. Indeed following Rapamycin withdrawal AKT_pT308 activity increases to a far larger extent than following starvation-restimulation. Whilst the mTORC2 dependent AKT_pS473 displays a far

greater increase in activity following starvation-restimulation compared to Rapamycin withdrawal.

As in the previous chapter it did not prove possible to obtain time course data capable of calibrating a dynamic model using imagestream flow cytometry. In addition in the final analysis DAPI does not appear despite being present (cells not positive for DAPI would be excluded from the final cell population being analysed following nuclear localisation analysis). This is also the case for the starvation-restimulation dataset however as DAPI is added immediately prior to analysis on the Imagestream flow cytometer and both the starvation-restimulation and Rapamycin datasets were analysed at the same time this is not unexpected. This is also the reason as to why both treatments appear to have a limited number of cells appearing in the final analysis. A possible explanation for this is that during the permeabilisation step cells were placed into 0.1% Triton-x 100 for longer than the optimal time period leading to cell lysis.

The dynamic model presented here was able to reproduce the response of Rapamycin withdrawal in both MRC5 and MSCs. Due to the variation observed in the MRC5 dataset a number of problems arose during the fitting process. These included the requirement for a more detailed P70S6K feedback loop and the removal of the PDK1_pS241 data from the final parameter. Further work is therefore required investigating the impact of Rapamycin treatment on PDK1 activation. A comparison between the response of MSCs to starvation-restimulation and Rapamycin withdrawal revealed similar kinetic profiles excluding the two AKT observables analysed. However the reaction of each phosphorylation site on AKT makes biological sense when placed in the context of the treatment being analysed.

6. A dynamical model of the mTOR signalling network reveals the kinetics of zoledronate and re-stimulation in MRC5 fibroblasts and human bone marrow stem cells

6.1 Introduction

Zoledronate is a nitrogen containing bisphosphonate (N-BP) used in the treatment of osteoporosis primarily in post-menopausal women [115]. N-BPs were designed to inhibit bone resorption by targeting the maturation process of the bone resorbing osteoclasts. Mechanistically N-BPs act by inhibiting the mevalonate network responsible for the post-translational prenylation modification. They do so by inhibiting the farnesyl diphosphate synthase (FPP) enzyme. Prenylation of a protein is a key posttranslational modification that primarily governs their appropriate localisation within the cell. Prenylation involves the addition of either a farnesyl (c15) or a geranyl-geranyl (c20) group being added to a protein at a CAAX motif at the c-terminus of the protein [108, 225]. Due to its role in protein localisation and modulating function prenylation is a key step in many signal transduction pathways [226]. The mechanistic effect of FPP synthase inhibition is discussed in section 1.4.3. In recent years off target effects of N-BPs have been observed, particularly in the case of Zoledronate and cancer treatment. Due to the well-established links between the mTOR network and cancer a number of studies have been undertaken to investigate the effect of Zoledronate on the mTOR network. Two mTOR network linked proteins are affected by prenylation: firstly the Gprotein Ras is farnesylated leading to its activation and localisation at the plasma membrane; and secondly the Ras homolog enriched in the brain (Rheb) is also farnesylated which leads to its association with various membranes within a cell and its ability to bind to GTP [227, 228]. In healthy cells, membrane localisation and activation of Ras leads to its binding with GTP and allows it to interact with PI3K on its p110 subunit [118]. This interaction with RAS facilitates the activation of PI3K that occurs via the binding of insulin to the insulin receptor. Activation of PI3K leads to a downstream cascade resulting in the conversion of PIP2 to PIP3 and the activation of AKT via its phosphorylation on tyrosine 308. Once phosphorylated AKT can interact with the TSC1/2 complex resulting in its phosphorylation and inhibition [43]. The TSC1/2 complex regulates the activity of Rheb by maintaining it in its GDP bound state, phosphorylation of TSC1/2 results in Rheb associating with GTP to form its active state which can then interact with FKBP38 resulting in its disassociation from within the mTORC1 [55, 58]. Rheb interaction with FKBP38 and its subsequent disassociation from mTORC1 activates the complex resulting in the phosphorylation of S6K and the activation of several downstream transcription factors. Once activated S6K also initiates a negative feedback loop inhibiting the insulin receptor [60].

Far less is known regarding the second TOR complex mTORC2. However, it is known that active mTORC2 phosphorylates AKT on serine 473 and that mTORC2 is inhibited by S6K activation [43]. Activation of mTORC2 appears to be Rheb independent and it is disputed whether or not the phosphorylation of S473 on AKT is required for its full activation [52].

There are several parallels between the effects seen on the mTOR network when cells are treated with Zoledronate and when they are subjected to caloric restriction. Zoledronate treatment leads to an increased DNA damage response and the inhibition of mTORC1[82]. This also occurs in calorie restriction as there is a decrease in insulin levels and therefore a decrease in signalling from the insulin receptor resulting in decreased AKT activity [197]. In addition to this a decrease in glucose leads to a lower level of ATP in the cell altering the ration of AMPK-ATP with the result being increased AMPK activity and further mTORC1 inhibition [229]. It has also been shown that stem cell numbers can be preserved by calorie restriction and that this was due to mTORC1 inhibition [230, 231]. Furthermore calorie restriction appears to protect the proliferative and differentiation capacity of MSC in skeletal muscle, although the mechanisms behind this are currently unknown. Recently it was shown that Rheb inhibition extended lifespan in *C.Elegans* in a pattern that mimicked intermittent fasting and highlights the possibility that inhibition of Rheb prenylation could extend lifespan [232].

6.2 Modelling the effect of zoledronate on the mTOR network

To date there is no published work using dynamic modelling investigating the effect of Zoledronate on the mTOR network. However previous work carried out prior to this study in collaboration with Ilaria Bellantuono's group at the University of Sheffield attempted to explain the mechanisms observed in MSCs following Zoledronate treatment [82]. The key findings of this work form the basis of the model produced within this chapter and are summarised here. Initial predictions generated by the model were unable to reproduce the observations reported in Misra et al 2016 as the removal of prenylated species within the model occurred too rapidly. Whilst the inhibition of FPP synthase occurs over a matter of minutes the effect of Zoledronate is not observed until three days post treatment. Due to this, an alternative hypothesis was proposed suggesting that the rate of inhibition of Zoledronate is not dependent upon the rate of inhibition of FPP synthase but rather the turnover of prenylated proteins within the cell.

This alteration resulted in a slow three day reduction in the number of prenylated proteins within the model. In the initial simulations of this work Ras was not included upstream of PI3K as previous models had proved successful in replicating mTOR network dynamics without the inclusion of Ras e.g. Dalle Pezze et al 2012 and 2016 [172, 233]. Initial predictions by the dynamic model suggested that following Zoledronate treatment there was an increase in the activity of AKT_pT308. This increase in activity was due to the inhibition of mTORC1 activity and S6K activity leading to the inhibition of the S6K negative feedback loop to PI3K and the subsequent upregulation of AKT_pT308. More recent data however showed that both AKT_pT308 and AKT_pS473 activity levels decreasing following Zoledronate treatment (figure 6.1). Therefore it was necessary to include Ras upstream of PI3K in order to account for this reduction in AKT_pT308 activity. The final finding of this work was the assumption that a prenylation event must exist upstream of mTORC2. This was also shown in Misra et al 2016 with the observation for a reduction in AKT_pS473 levels. There are number of possible proteins responsible for the inhibition of mTORC2 by Zoledronate including Rac1, RalA, Rab as well as Ras and Rheb [234].

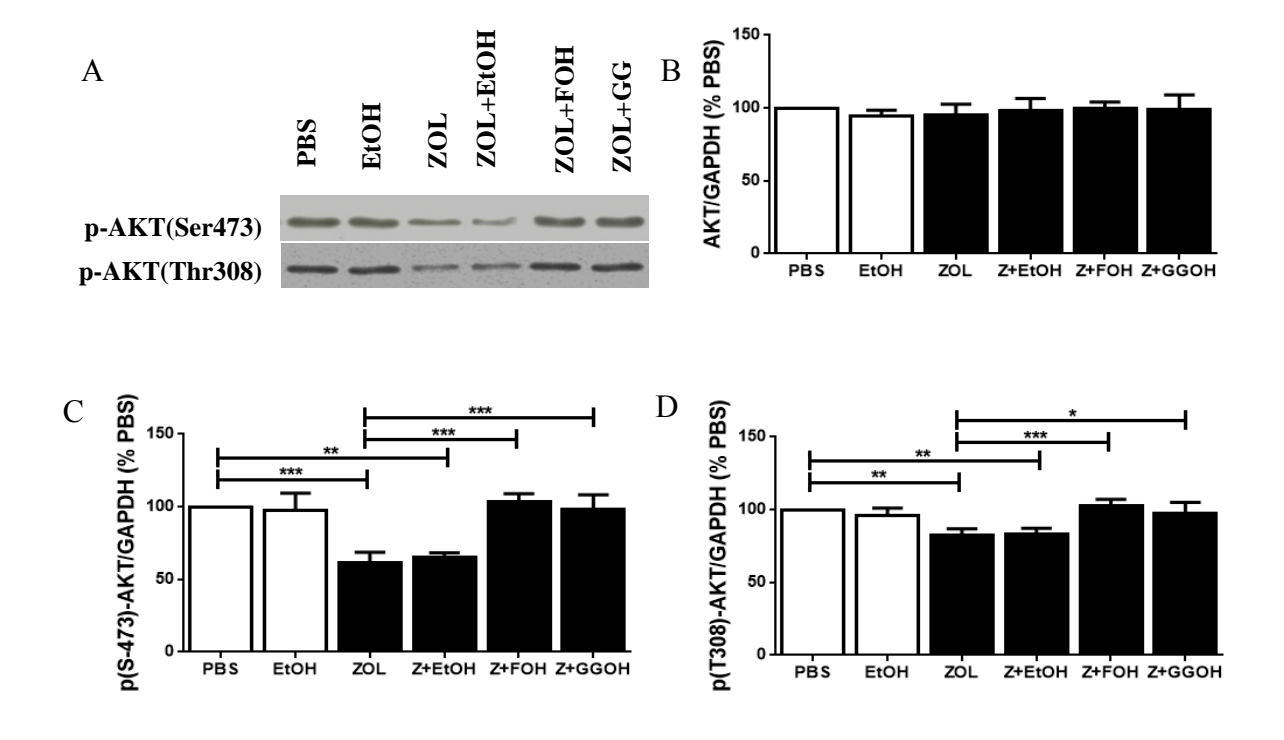


Figure 6.1: Immuno-blotting data examining AKT phosphorylation. Analysis of AKT phosphorylation on Threonine 308 and serine 473 was carried out in MSCs following treatment with 1μM Zoledronate for 72 hours. Signal intensities were quantified and statistics computed (n=3). Image courtesy of Juhi Misra (University of Sheffield) [82].

6.3 Aims

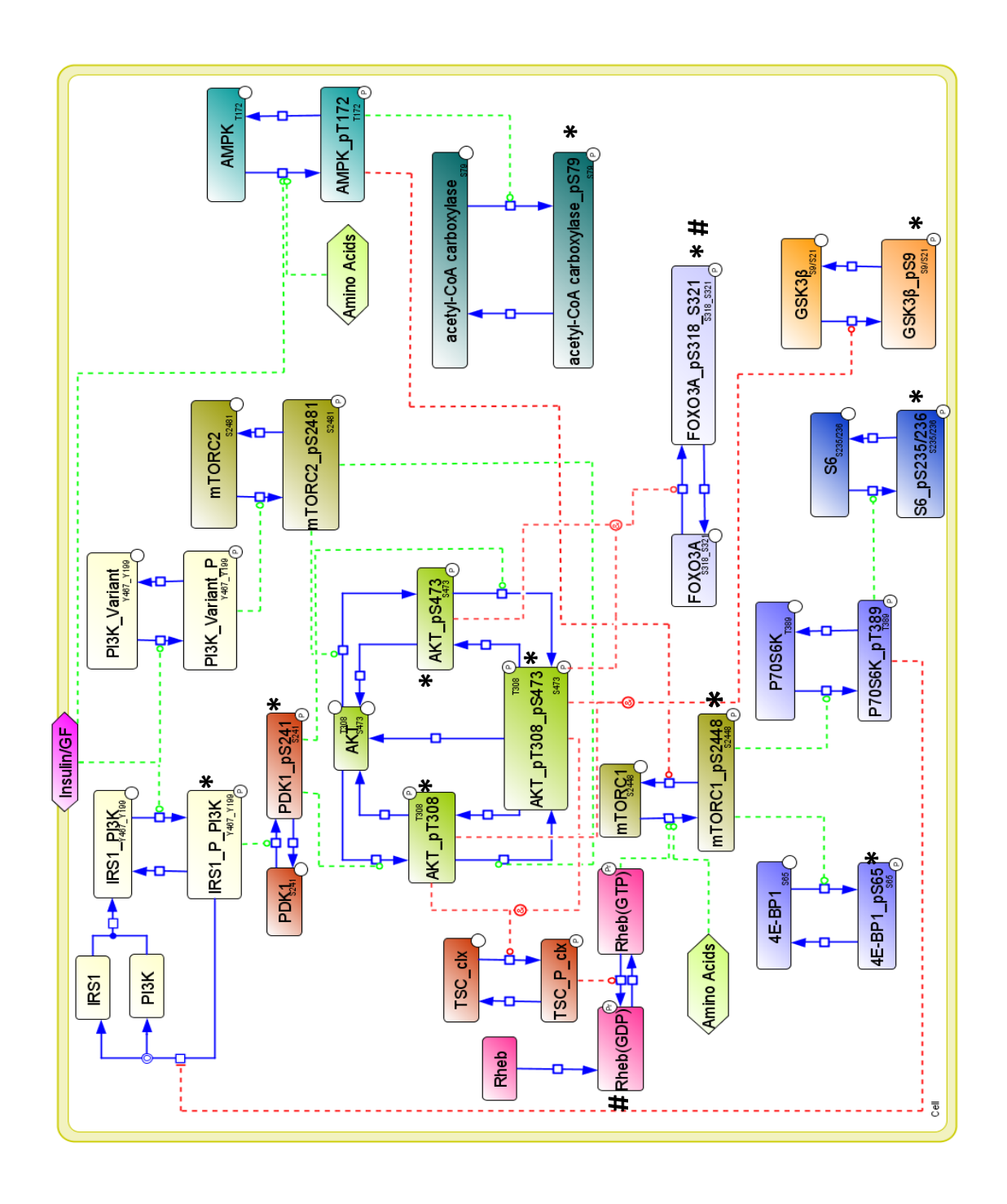
The study aim was to examine the effect of Zoledronate treatment on the dynamics of re-stimulation of the mTOR network. We aim to define using a computational dynamic model how the mTOR network responds in MRC5 fibroblasts and how the mTOR network response differs in human mesenchymal stem cells.

6.4 Results

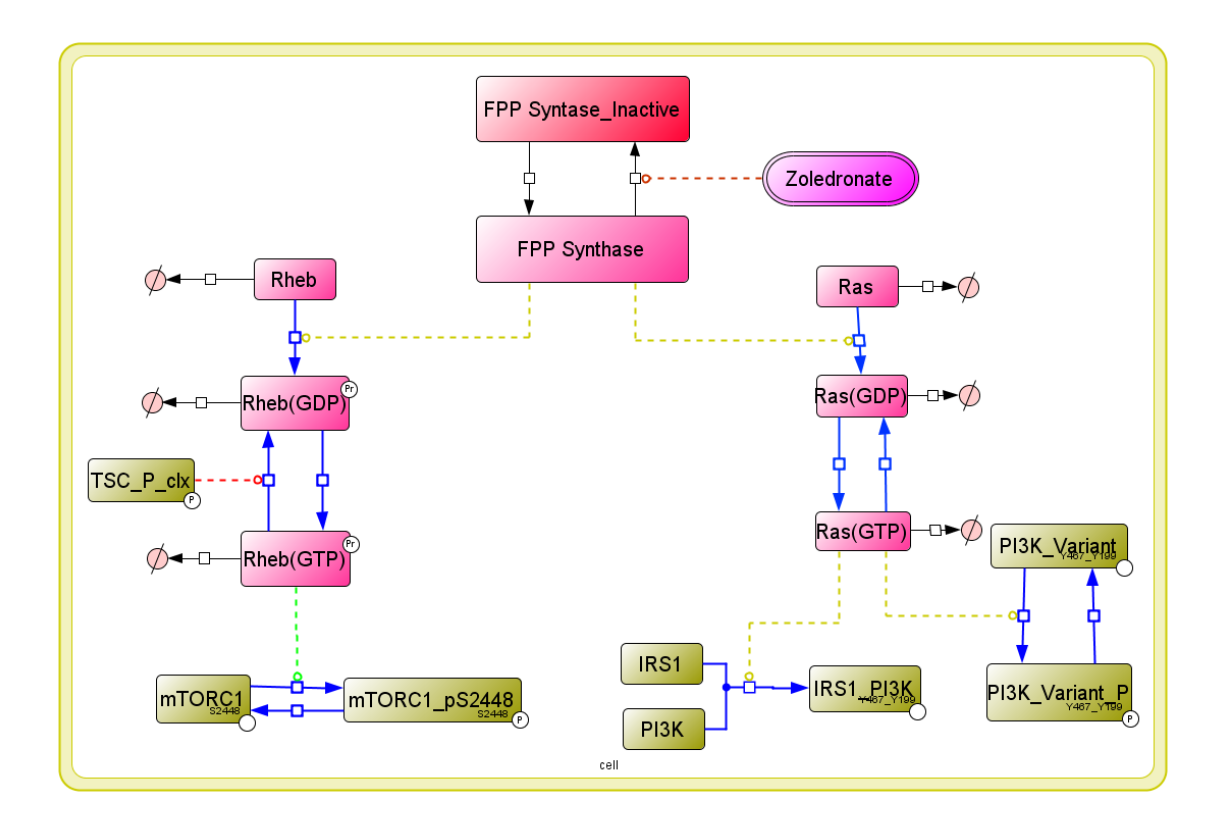
6.4.1 Development of a zoledronate dynamic network model

The model used throughout this section is described in section 4.3.1 and displayed in figure 6.2 (all reactions can be found in appendix B). As described previously the amino acid/nutrient activation of the model will remain as before with a constant level available to the cells assumed. Nutrient signalling activates the model at three separate inputs with PI3K, mTORC1 and AMPK all being activated by nutrient inputs. As before PI3K activation leads to the activation of PDK1 and subsequent activation of AKT on threonine 308. This in turn phosphorylates and inhibits the TSC1/2 complex leading to activation of Rheb(GTP). Rheb in its GTP bound form is then free to activate the mTORC1 complex leading to the activation of the downstream effectors P70S6K_pT389, S6_pS235/236 and 4E-BP1_pS65 with a P70S6K_pT389 feedback loop inhibiting further activation of PI3K by nutrient signalling. In addition to the above a section of the mevalonate network was added to the model based on the assumptions described in section 6.2. A network schematic displaying the mevalonate network and its links to the mTOR network is shown in figure 6.3. As one of the proposed assumptions described in section 6.2 was the need for a prenylation event upstream of mTORC2 further research was carried out investigating which proteins could be responsible. The proteins investigated include Rac1, RalA, Rab as well as Ras and Rheb [234]. With regards to mTORC2 activation there is very little evidence that Rheb has any role in its activation however Ras has been implicated in mTORC2 activation [235]. It has been shown that in invertebrate organisms Ras interacts directly with components of mTORC2 and is required for correct localisation of those components, however this has yet to be shown in mammals [236, 237]. What is known however is that Ras interacts with PI3K which possibly allows it to activate mTORC2 as well as enhancing its activation of AKT phosphorylation and mTORC1 activation [235]. Rac1 appears to act both upstream and downstream of both mTOR complexes surprisingly however its role in mTORC2 regulation is far better understood than its role in

mTORC1 regulation [73, 234]. The guanine exchange factor (GEF) for Rac1 is P-Rex1 which directly interacts with and is activated by mTORC2 leading to increased GTP bound Rac1 [238]. Any decrease in mTORC2 therefore leads to a decrease of around 20-30% GTP bound Rac1. However inhibition of Rac1 leads to a decrease in active mTORC1 and mTORC2 showing that it must act upstream of both TOR complexes. It is believed that Rac1 acts to correctly localise mTOR within the cell as inhibition of Rac1 affects the subcellular localisation of mTOR [239] [240]. In order to interact with mTOR, Rac1 can be in either a GDP or GTP bound state however recent work has shown that following bisphosphonate treatment the level of GTP bound Rac1 increases [240]. It may be interesting to investigate if mTOR localisation is affected by Zoledronate treatment of MSCs as this could provide an insight into how the drugs affect the network. Very little is known about the role that RalA plays in mTORC2 activation. It is known that RalA enhances the interaction of ARF6 with phospholipase D mediating the hydrolysis of phosphatidylcholine which produces phosphatidic acid which is a known mediator if mTORC1 and mTORC2 activation [241-243]. It is not currently known how RalA regulation contributes to mTORC2 activation however it appears to be regulated by nutrient levels with increased GTP binding of RalA under high nutrient conditions leading to increased mTORC1 activation [244-246]. At present there is no evidence in mammals to support the idea that members of the Rab GTPase family can stimulate mTORC2 activation. However work carried out in yeast has shown that the Rab6 homologue Ryh1 controls spTOR2 activation and when expressed in yeast human Rab6 can also activate TORC2 suggesting that the link may be evolutionary conserved [247, 248]. Due to its role in compartment specificity within eukaryotic endomembrane it is possible that Rab6 could control mTOR localisation within the cells however there is currently no evidence to support this idea [249, 250]. Due to the lack of a clear evidence for a prenylated protein that could act upstream of mTORC2 it was decided that Ras should be selected from the G proteins investigated. This was pragmatic decision as it prevented the need for the addition of an additional species within the model whilst satisfying the above evidence.



<u>Figure 6.2: The mTOR network.</u> A SBGN network model diagram displaying the mTOR network. Asterisks mark phospho proteins measured for starvation-restimulation RPPA experiments whilst hashtags mark proteins assayed by imagestream flow cytometry.



<u>Figure 6.3: The effect of Zoledronate on the mTOR network.</u> A SBGN network model diagram displaying the connections between the mevalonate and the mTOR networks. Proteins in Pink and red denote mevalonate proteins; Green proteins represent mTOR related proteins.

6.4.2 Utilising RPPA to produce a calibration dataset following zoledronate treatment

As with the two previous chapters once the network topology had been determined a timecourse dataset was collected using RPPA. As the removal of prenylated proteins within a cell takes three days MRC5 cells were treated with $1\mu M$ Zoledronate for this period of time at which point the Zoledronate was removed and the cells restimulated with standard DMEM as described in sections 2.1.15. As with the two previous datasets the timecourse was designed to allow for the capturing of the immediate dynamics of the mTOR network following removal of Zoledronate. In addition however time points were taken every 24 hours during to Zoledronate treatment to observe the changes in the mTOR network during Zoledronate treatment. Throughout this chapter a total of 17 proteins were analysed consisting of 10 phosphoproteins, 7 total proteins and the house keeping protein α -tubulin (Table 6.1). However during the initial RPPA analysis of Zoledronate treatment on MRC5 cells a total of 9 phospho-proteins and 8 total proteins were analysed. Each of the antibodies used had previously been validated in previous chapters or in the case of GSK3- β had been validated in a separate project.

6.4.3 Zoledronate treatment of MRC5 cells results in cell death at 1µM

The Initial assay of MRC5 cells following Zoledronate treatment is shown in figure 6.4. Following normalisation the expected relative fluorescent level a given protein undergoing RPPA should be above 0.1 to be considered above the background threshold. As can be observed in figure 6.4, whilst there appears to be a dynamic reaction in response to re-stimulation following Zoledronate withdrawal of all proteins with the exception of PDK1_pS241 fail to maintain an expression over the background threshold. It is therefore not possible to assess the effect of Zoledronate withdrawal using this dataset. To complement RPPA, an analysis of the response of both FOXO3A and Rheb to Zoledronate treatment and was carried out using Imagestream flow cytometry. As described above MRC5 cells were treated with 1µM Zoledronate for a period of 72 hours with time points analysed every 24 hours. As can be observed in figure 6.5 following 72 hours Zoledronate all cells in the analysis display autofluorescence characteristic of cell death. As the removal of prenylated proteins from the cell requires 3 days following Zoledronate treatment it was decided that no further analysis of these samples should be performed. Following these results it was decided that a cell death assay should be performed in order to ascertain the level of cell death in

MRC5 cells following Zoledronate treatment. For the purposes of this study three separate concentrations were selected each decreasing 10 fold from the previous. As luM had proved to already lead to cell death in MRC5 cells this concentration was tested along with 0.1µM and 0.01µM Zoledronate. As with the previous timecourse experiments MRC5 cells were treated with Zoledronate at the above concentrations for a period of 72 hours and then a cell count performed with cells stained with Trypan blue allowing for the identification of live and dead cells. The results of this study are shown in figure 6.6. Following treatment with both 1µM and 0.1µM Zoledronate cell death was determined to be 34 and 32 percentage respectively with no statistical significance observed between the two different treatments (P=0.33; 2-way analysis of variance-ANOVA). At the lowest concentration of 0.01 µM Zoledronate cell death was determined to be 20 percentage with a significant difference observed between this treatment and both 1µM and 0.1µM Zoledronate respectively (P=0.0037 and P=0.015 respectively; 2-way ANOVA). As such it was decided that whilst cell death was still relatively high in the 0.01µM Zoledronate treatment samples, that this concentration should be carried forward for further tests using RPPA and Imagestream flow cytometry.

<u>Table 6.1: Reverse Phase Protein Array Antibodies.</u> A list of all antibodies assayed during Zoledronate experiments.

Antibody	Antibody	Source
ACC	GSK3B_pS9_pS21	Cell Signalling Technology
ACC_pS79	mTOR	Cell Signalling Technology
PI3K p85_pY467_Y199,	mTOR_pS2448	Cell Signalling Technology
PTEN_pS380_T382_T383	4E-BP1	Cell Signalling Technology
PDK	4E-BP1_pS65	Cell Signalling Technology
PDK1_pS241	S6_pS235/236	Cell Signalling Technology
AKT	FOXO3A	Cell Signalling Technology
AKT_pT308	FOXO3A_pS318_S321	Cell Signalling Technology
AKT_pS473	A-tubulin	Cell Signalling Technology

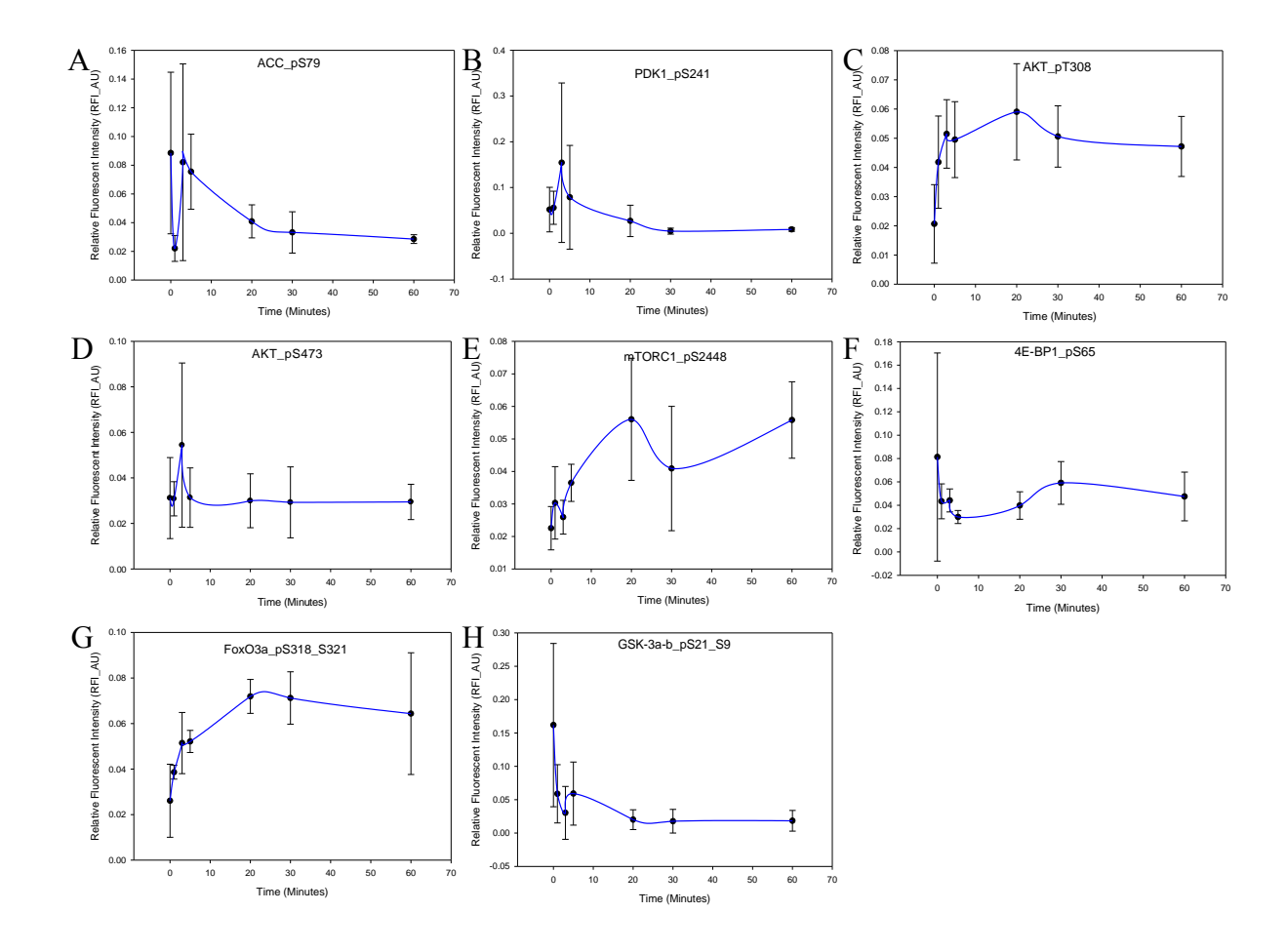


Figure 6.4: Measuring the kinetics of the mTOR network in MRC5 cells. A sixty minute time course following 72 hour Zoledronate treatment (1μM). Cells were re-stimulated at 0 hours and relative fluorescent intensity measured at each time point (n=3) (Mean +/- SEM). (A) ACC_pS79, (B) PDK1_pS24, (C) AKT_pT308, (D) AKT_pS473, (E) mTORC1_pS2448, (F) 4E-BP1_pS65, (G) FOXO3A_pS318_S321, (H) GSK3-β_pS9_pS21.

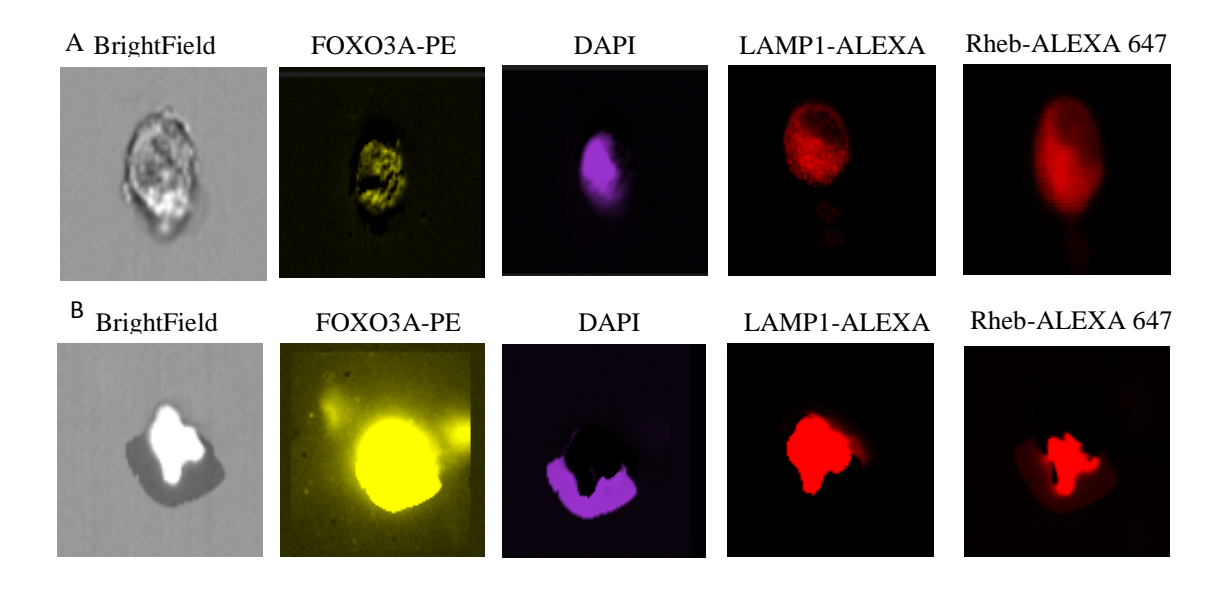


Figure 6.5: Imagestream flow cytometry reveals cell death in MRC5 cells. (A) Untreated MRC5 cells and MRC5 treated with 1μM Zoledronate for 72 hours (B) were stained for FOXO3A, DAPI, LAMP1 and Rheb and analysed using an Amnis Imagestream flow cytometer. (Image representative of 1000 cell events).

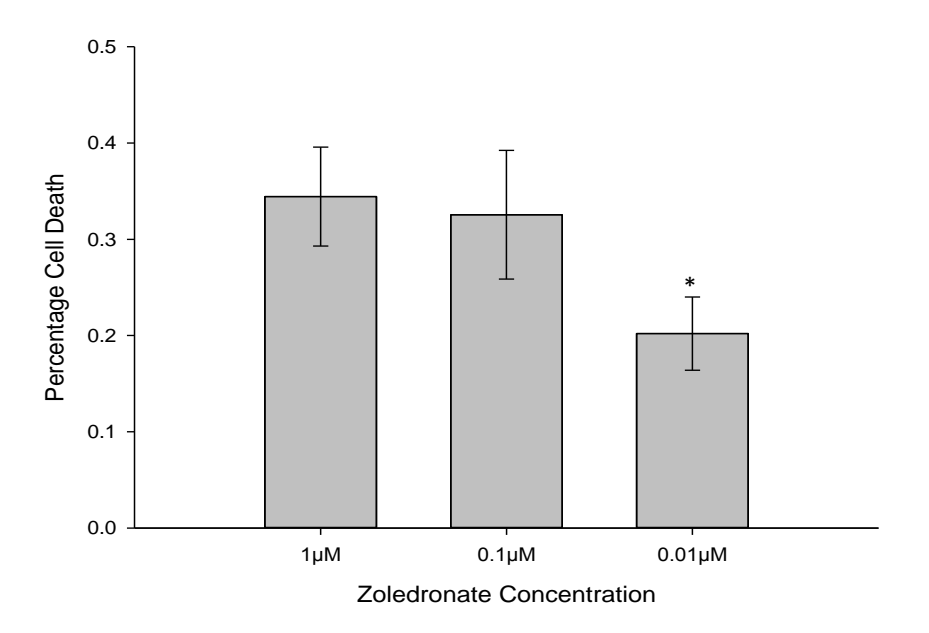


Figure 6.6: Zoledronate cell death assay. MRC5 cells were treated with $1\mu M$ $0.1\mu M$ and $0.01\mu M$ Zoledronate. Percentage cell death was calculated (n=3) (Mean +/- SEM).

6.4.4 Treatment of MRC5 cells with $0.01\mu M$ zoledronate followed by nutrient re-stimulation results in clear dynamic signalling profiles.

Following the results obtained by the cell death assay a second time course was produced using MRC5 cells treated with 0.01μM Zoledronate. This was carried out exactly as described as above and is shown in figure 6.7. In contrast to the previous dataset the raw RFI values obtained for this data all displayed values between 0.1 and above with the exception of GSK3-β_pS9_pS21 (figure 6.7 K) (the values shown in figure 6.7 are the normalised values not raw RFi values). As can been seen in figure 6.7 there is a clear flow of information through the network with an initial increase observed in all observables with the exceptions of AKT_pS473, FOXO3A_pS318_S321 and S6_pS235/236 (figure 6.7 F, I and J). Following a decrease between the 3 and 10 minutes time points there is then an increase for all observables with AKT_pS473 and S6_pS235/236 again proving to be the exceptions (figure 6.7 F and J). However in the case of these two observables there is an earlier increase at the 10 minute time point with a decrease in signalling observed by 20 minutes.

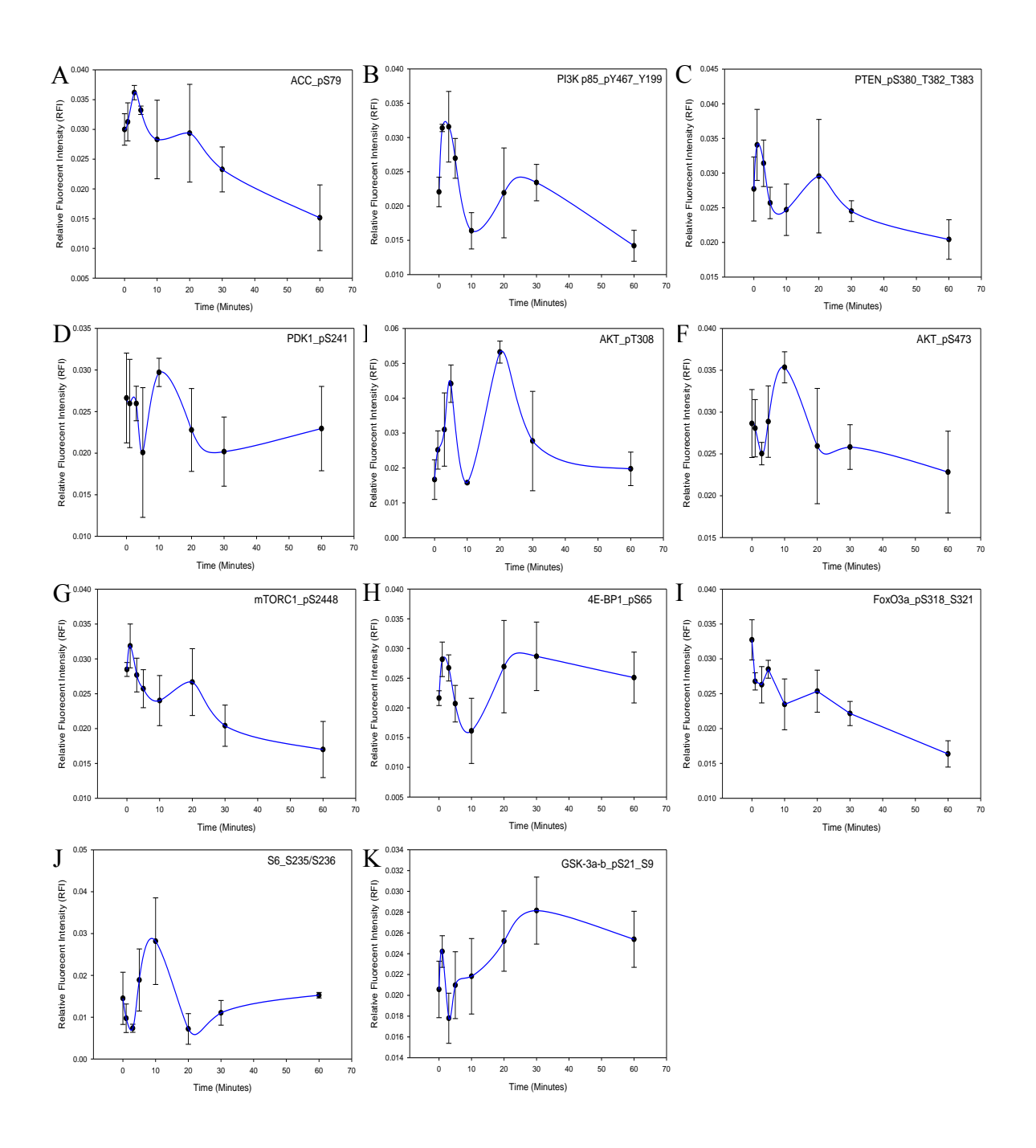


Figure 6.7: Measuring the dynamics of the mTOR network in MRC5 cells. A sixty minute time course following 72 hour Zoledronate treatment (0.01μM). Cells were re-stimulated at 0 hours and relative fluorescent intensity measured at each time point (n=3) (Mean +/- SEM). (A) ACC_pS79, (B) PI3K_P85_pY467_Y199, (C) PTEN_pS380_T382_T383, (D) PDK1_pS241, (E) AKT_pT308, (F) AKT_pS473, (G) mTORC1_pS2448, (H) 4E-BP1_pS65, (I) FOXO3A_pS318_S321, (J) S6_pS235/236, (K) GSK3- β _pS9_pS21.

6.4.5 Parameter estimation

As with the starvation re-stimulation and Rapamycin models following generation of the second calibration dataset using RPPA, parameter estimations were carried out for the first 60 minutes of the timecourse. The data was normalised as previously described with all proteins measured normalised to the housekeeping protein α-tubulin and then the control time point 0 set to a value of 1 and all subsequent time points divided by this value. This would allow for a direct comparison between not only the MRC5 and MSC cells, but also between treatments, as it would provide a simplified kinetic profile from an arbitrary initial value. As with the previous models a total number of 10000 runs were then performed using a computational cluster with the genetic algorithm used as described in section 2.2.2. The time length for these runs was variable as they were dependent on how the cluster was being used on a given day by multiple users. In addition to the set-up described above all prenylated species were set to have an initial starting value of 0 to represent the effect of Zoledronate on the model. As described in section 4.3.3 the residual sum of squares (RSS) value was used to determine a "goodness of fit" due to the scale of the data being used. As in previous chapters the python package Pycotools was used to ascertain the best fitting parameters from the parameter estimations. An updated version of this package was available for this work which allowed for a far more in depth analysis of the data it was decided that this should be carried out for the work presented here.

6.4.6 Existing model is capable of fitting MRC5 dataset in response to zoledronate withdrawal

As can be seen in figure 6.8 the model was able to achieve an acceptable fit to the data for 7 out of the 10 observables measured (RSS=0.738134). The three observables that could not be fitted were PTEN_pS380_T382_T383, PDK1_pS241 and 4E-BP1_pS65 (figure 6.8 C, D + H). This further confirms that the model was incapable of fitting both PTEN_pS380_T382_T383 and 4E-BP_pS65 using the current topology and known activation mechanisms. For PDK1_pS241 whilst it had proved possible to fit this observable for the MRC5 starvation-restimulation data it had not been possible to do so for both the Rapamycin and Zoledronate data. This suggests that there are mechanisms governing PDK1_pS241 activity not included in the model which are affected by Rapamycin and Zoledronate treatment in MRC5 cells. In addition to investigating the parameter estimation which provided the 'best fit' to the data it was also possible to

view how the model fit differed across repeats by plotting a time course ensemble using the Pycotools python package (figure 6.9). As can be seen in figure 6.9 there is very little difference between the top ten ranked parameter estimations with each of the parameter sets resulting in a model fit close to the overall mean model simulation (dark blue line). This also holds true for the three observables which the model is unable to fit, further supporting the need to further investigate the mechanisms governing the activity of these proteins. Figure 6.9 K, displays the RSS value for each parameter estimation ranked in order of 'best fit' and suggests that the parameter estimations have not found a minimum RSS value. This is to be expected however as the purpose of the second round of parameter estimations using the Hooke and Jeeves algorithm is to find a local minima for the model parameters. In addition to allowing for the analysis of time course ensembles it is also possible to analyse the overall spread of each parameter fitted by the parameter estimations (figure 6.10). For each parameter within the estimation there is a limited set of values that may be used, in the case of all parameter estimations carried out in this work those limits were $1e^{-6} - 1e^4$ with each parameter able to be any value between those two values. The less variation a parameter displays between the upper and lower limits the more confidence can be placed upon the models ability to fit that parameter value. Across the full 10000 parameter estimations the majority of parameters estimated display a large variation in values (figure 6.10 A). However upon refinement to the top 100 parameter estimations there are few sections of the model which continue to display a large variation. These parameters are primarily involved in the mevalonate network section of the model suggesting that more data are required to inform the model fit for this part of the model topology (figure 6.10 B).

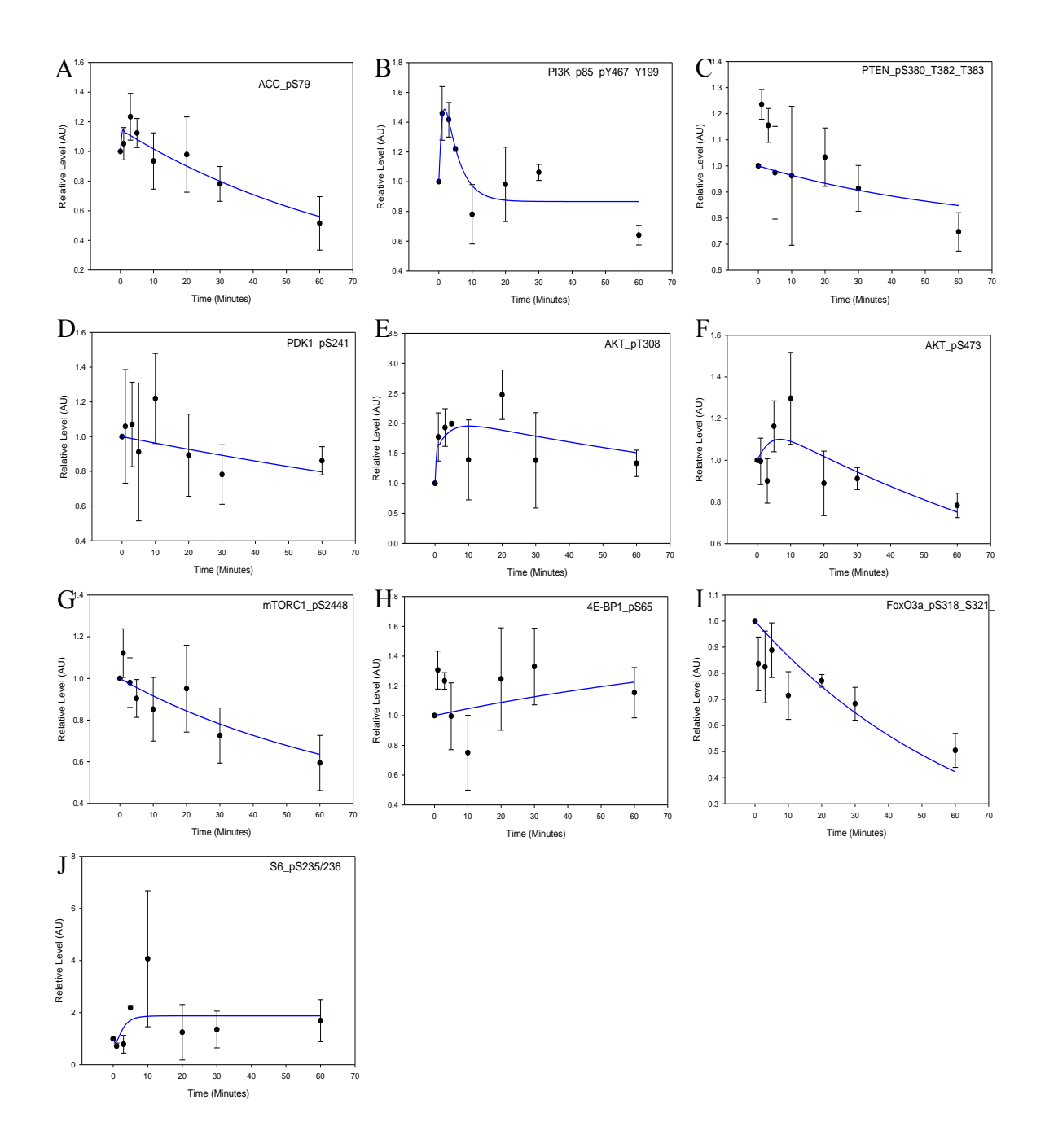


Figure 6.8: Time course simulations from the model compared to Zoledronate withdrawal data in MRC5 cells. The model displayed in figure 6.2 was calibrated using the RPPA data shown in figures 6.7. A parameter estimation consisting of 59 parameters in total was performed using the genetic algorithm (10000 runs). The residual sum of squares between the experimental data (Black +/- SEM) and the simulated data (Blue) was calculated as 0.738134 with a good fit achieved.

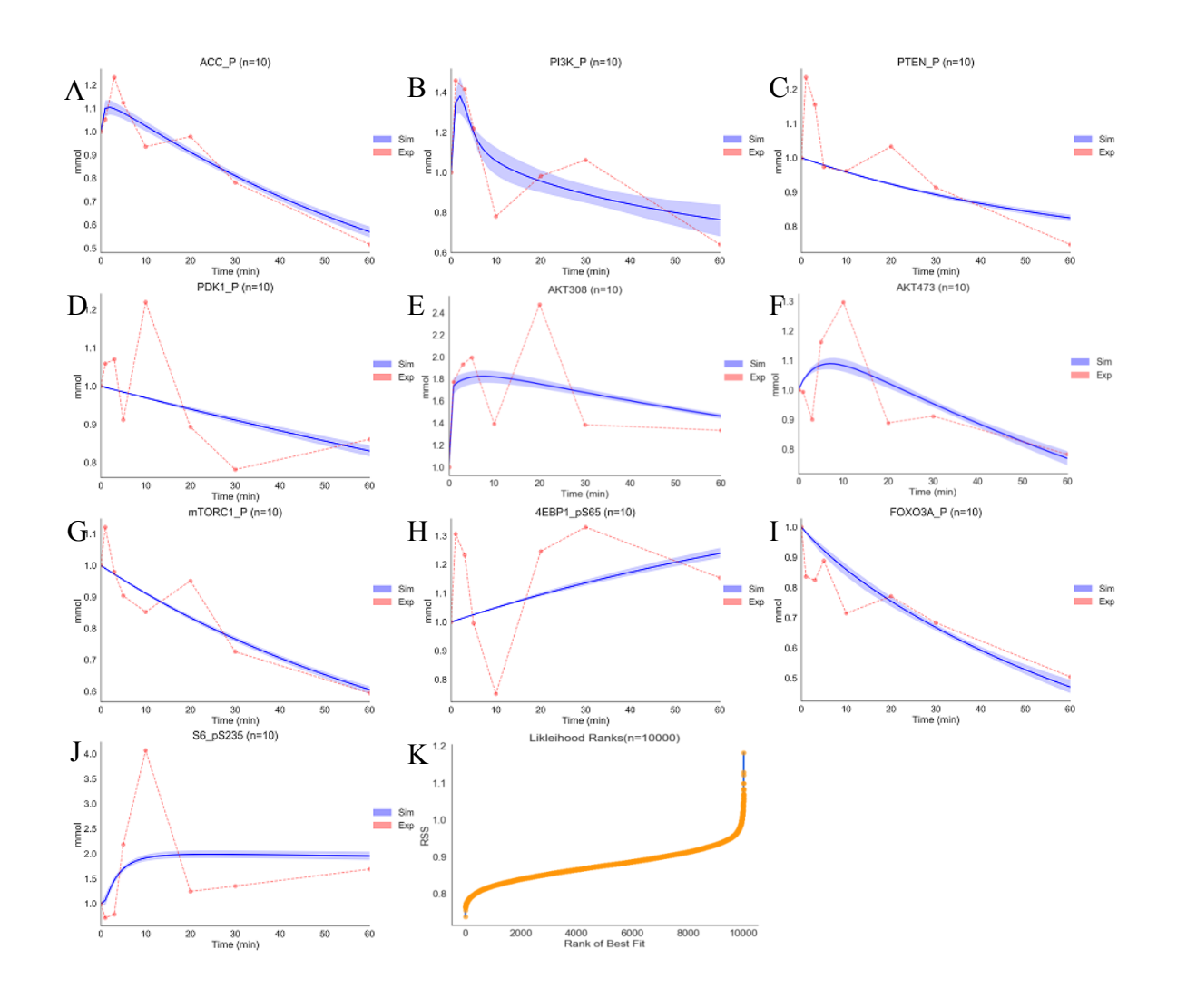


Figure 6.9: Time course ensemble for the top 10 genetic algorithm parameter estimations in MRC5 cells. (A-J) A time course ensemble was computed using the python package Pycotools. The top ten ranked parameter estimations from 10000 were inserted into the model shown in figure 6.2 and a time course simulation performed. The mean value for each time point in each of the 10 simulations was then plotted (dark blue line) and 95% confidence intervals calculated (light blue area). (K) The RSS value for each of the 10000 parameter estimations was ranked.

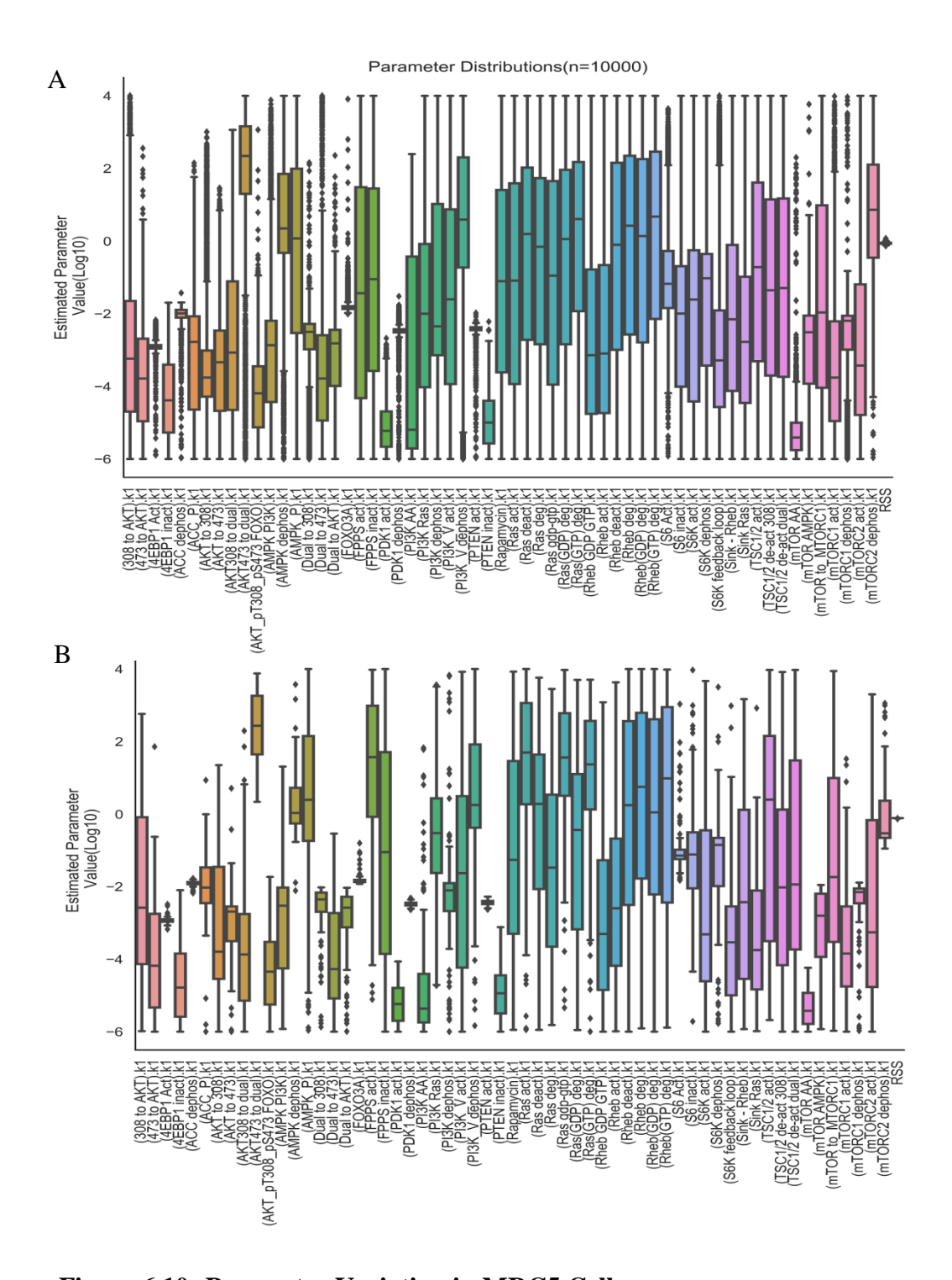


Figure 6.10: Parameter Variation in MRC5 Cells. Boxplots displaying the variation of each parameter estimated within the lower (1e-6) and upper limit (1000) bound of 10000 (A) and top 100 (B) parameter estimations using the genetic algorithm in MRC5 cells.

6.4.7 Modelling difference in MRC5 and MSC

As carried out previously following the calibration of the model using the MRC5 dataset a second time course was performed using MSCs. As in previous chapters this time course was carried out using the same points as for the MRC5 dataset and is shown in figure 6.11. A comparison between the MRC5 and MSC kinetic following restimulation can be seen in figure 6.12. There is a clear dynamic behaviour observed throughout the dataset with an initial decrease observed for all proteins excluding ACC_pS79. Unfortunately the mTORC_pS2448 read out displayed background level fluorescence and therefore could not be used in parameter estimations figure 6.11 G). Following the initial decrease in signalling there is an increase in activity across the time course up to the 10 minute time point with a decrease observed at either 10 or 20 minutes for all proteins. Following this there is an increase for all proteins except PDK1_pS241, 4E-BP1_pS65, S6_pS235/236 and GSK3-β pS9 S21 at 30 minutes (figure 6.11 D, H and K). All proteins display a decrease in signalling at the 60 minute time point. Interestingly the ACC_pS79 time course follows a very similar kinetic profile to that observed in starvation-restimulation in MRC5 cells with an increase in signalling occurring over the first 5-10 minutes and then decreasing to baseline signalling after 30 minutes (figure 6.11 A).

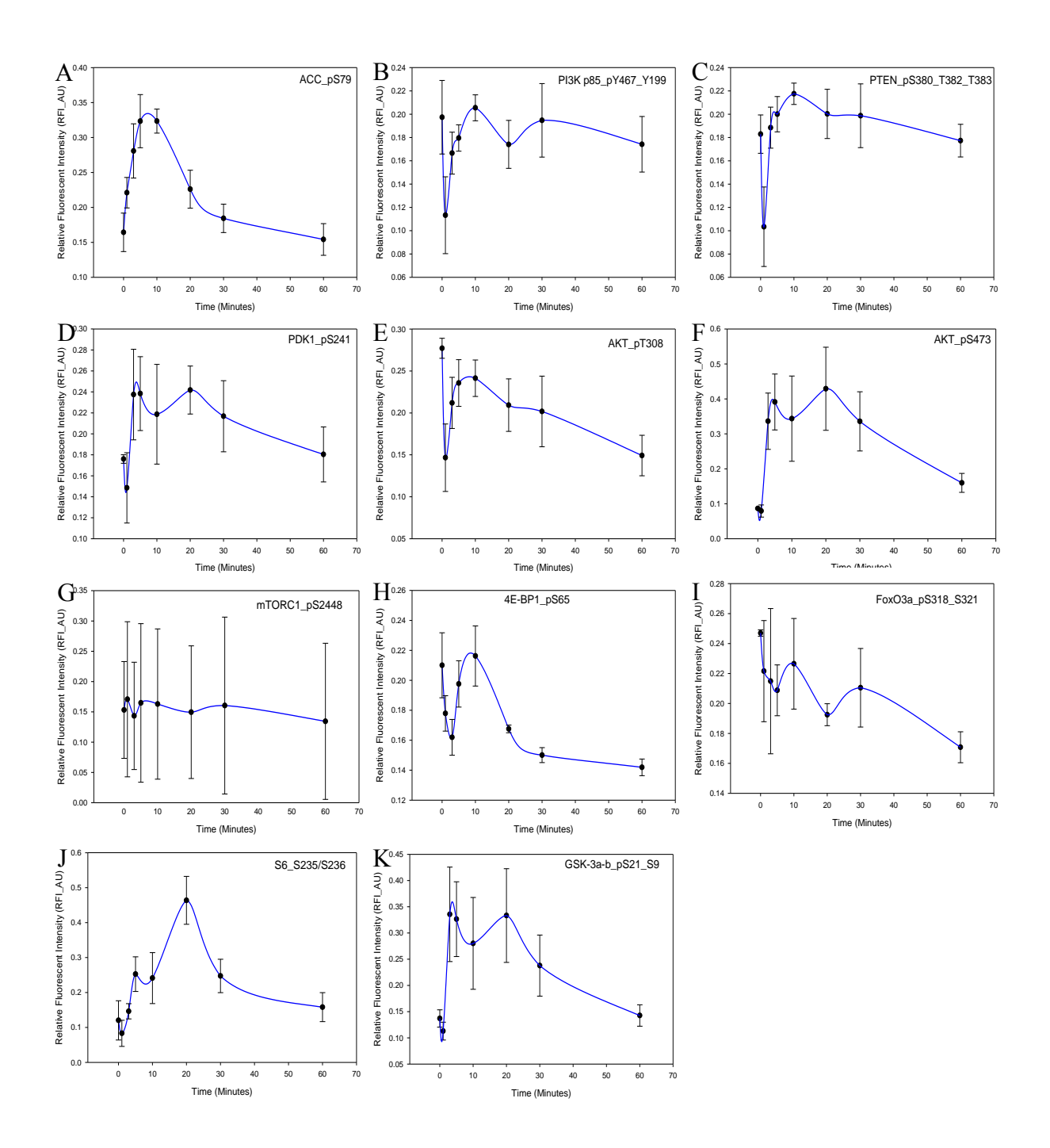


Figure 6.11: Measuring the Kinetics of the mTOR Network in MSC Cells. A sixty minute time course following 72 hour Zoledronate treatment (1μM). Cells were re-stimulated at 0 hours and relative fluorescent intensity measured at each time point (n=3) (Mean +/- SEM). (A) ACC_pS79, (B) PI3K_P85_pY467_Y199, (C) PTEN_pS380_T382_T383, (D) PDK1_pS241, (E) AKT_pT308, (F) AKT_pS473, (G) mTORC1_pS2448, (H) 4E-BP1_pS65, (I) FOXO3A_pS318_S321, (J) S6_pS235/236, (K) GSK3-β_pS9_pS21.

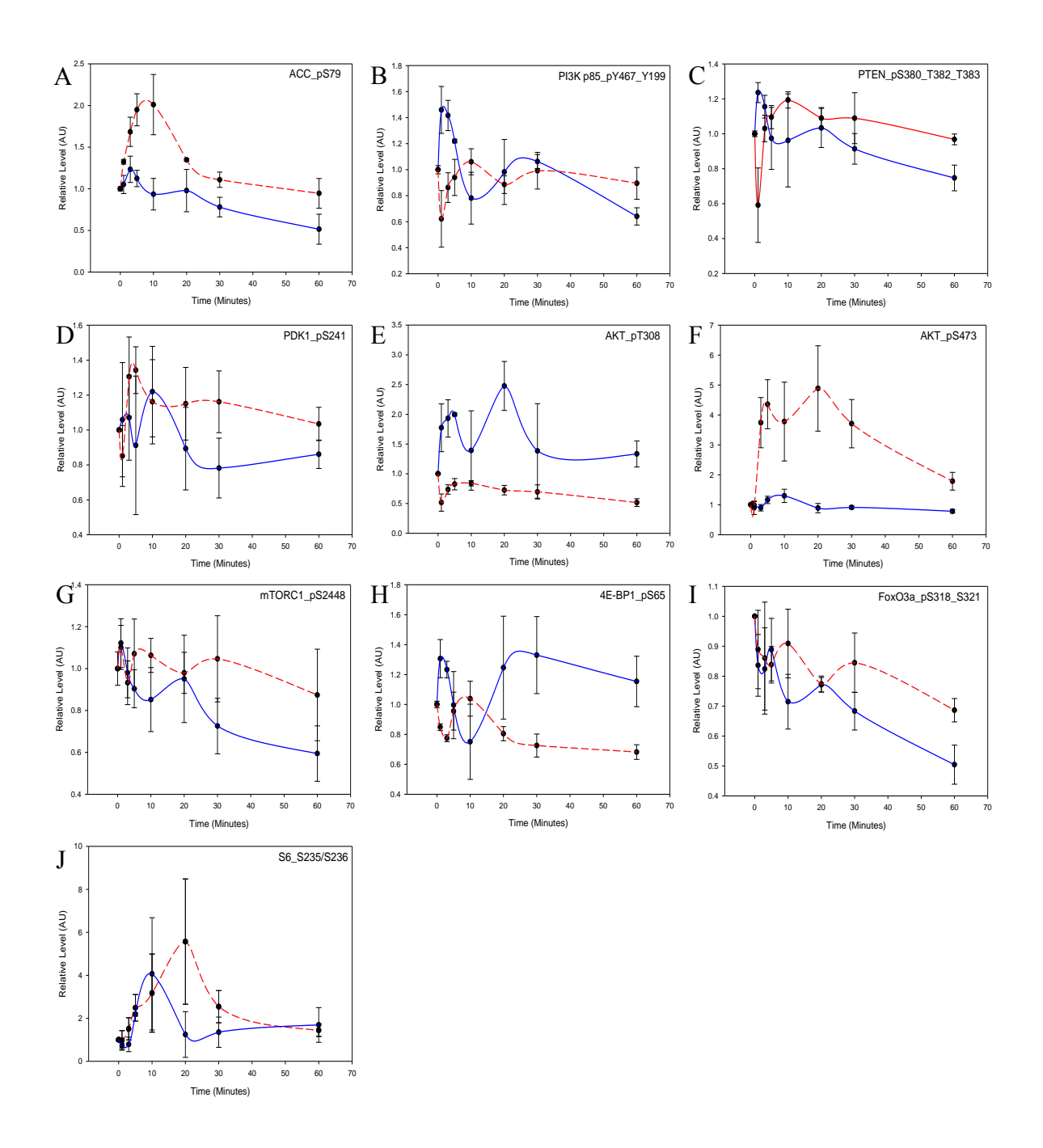


Figure 6.12: A comparison of MRC5 vs MSC outputs following Zoledronate withdrawal. A sixty minute time course following 72 hour Zoledronate treatment for both MRC5
(Blue) and MSC (Red) cells. Cells were re-stimulated at 0 hours and relative fluorescent intensity measured at each time point (n=3) (Mean +/- SEM). (A) ACC_pS79, (B) PI3K_p85_pY467_pY199, (C)
PTEN_pS380_pT382_pT383, (D) PDK1_pS241, (E) AKT_pT308, (F) AKT_pS473, (G)
mTORC1_pS2448, (H) 4E-BP1_pS65, (I) FOXO3A_pS318_pS321 and (J) S6_pS235/236.

6.4.8 Pycotools analysis reveals similar parameter constraints for both MRC5 and MSC parameter estimations

Prior to analysis using the Hooke and Jeeves algorithm, analysis using the Pycotools python package was carried out for the MSC parameter estimations carried out using the genetic algorithm. Time course ensembles were carried out as described above for examining the variation between the top ten ranked parameter fits (figure 6.13). As was observed for the MRC5 dataset the time course ensembles revealed very little variation between these fits with extremely small confidence intervals (light blue area) surround each mean value for the ten parameter estimations (dark blue line figure 6.13). As was also true for the MRC5 genetic algorithm, using the genetic algorithm for the MSC dataset failed to find the local minima (figure 6.13 J). However as discussed above as the Hooke and Jeeves algorithm was subsequently applied to these values the fit achieved using the genetic algorithm can be said to be acceptable (figure 6.13 A-I). Upon analysing the variation for each parameter value it became clear that as for the MRC5 dataset, the top 100 fits led to a significant reduction in variation for a number of parameters analysed (figure 6.14). Using this approach it was also possible to analyse how each parameter value was varying in both the MRC5 and MSC parameter estimations for the top 100 parameter estimations (figure 6.15). This revealed that two sections of the topology displayed a large variation in values for both parameter estimations. These were the reaction parameters for the Rheb and Ras prenylation reactions and the reaction parameters for the TSC1/2 complex reactions. As there is currently no data covering these parts of the topology this is to be expected. In addition to these parameters a number of other parameters governing AKT activity displayed differential fitting between the two parameter estimations. A reason for this is possibly that this section of the network is extremely complex with a large number of reactions existing to govern AKT activity across its four possible species within the model. A number of parameters however displayed very similar behaviour in terms of constraint across both parameter estimations. These reactions were largely involved in mTORC1 and mTORC2 activity in addition to those parameters governing PI3K activity. Despite the large amount of data covering these reactions it is interesting that the model appears to always converge upon a similar parameter value for these parameters for two separate parameter optimisation problems.

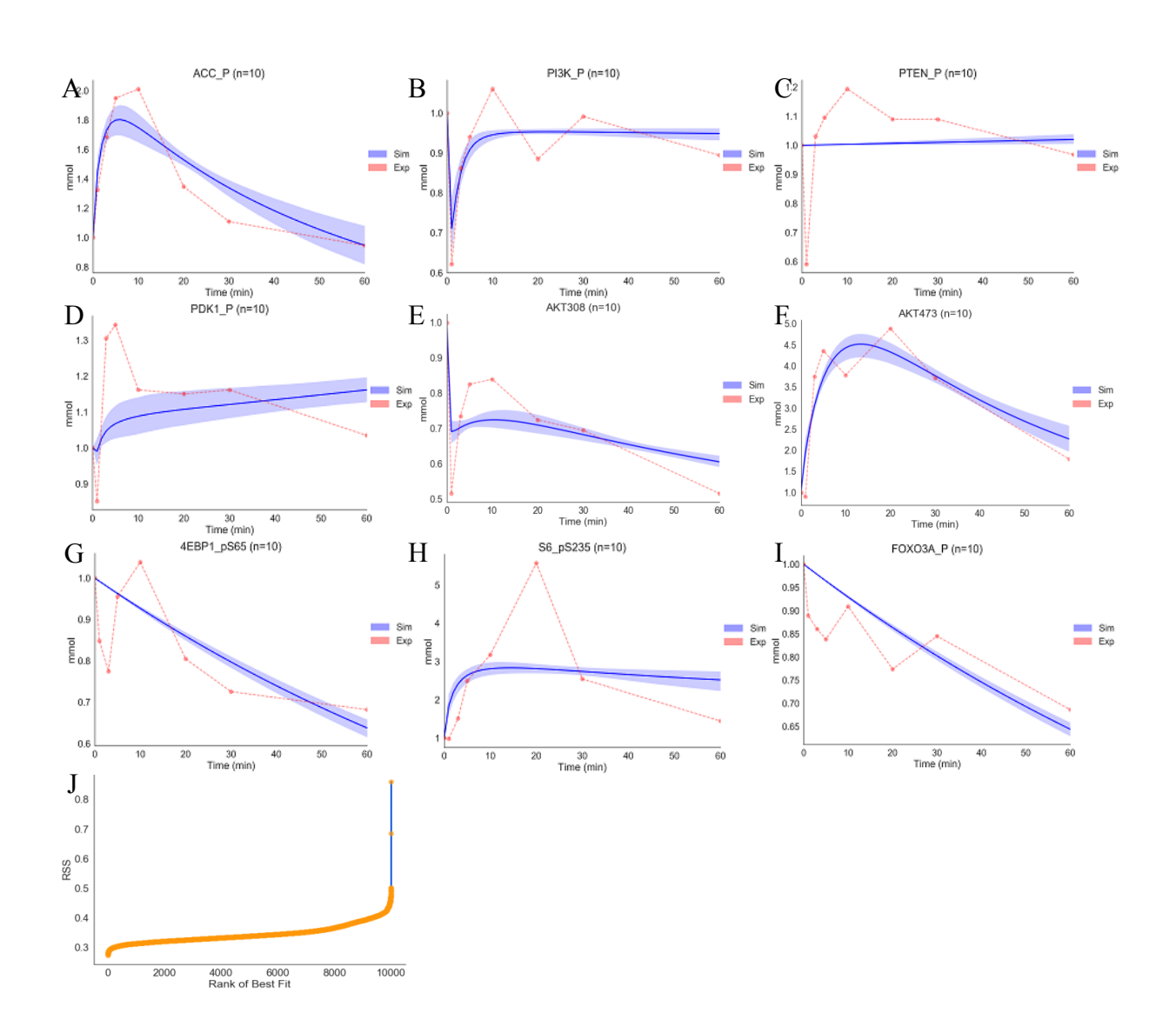


Figure 6.13: Time course ensemble for top 10 genetic algorithm parameter estimations in MSC cells. (A-I) A time course ensemble was computed using the python package Pycotools. The top ten ranked parameter estimations from 10000 were inserted into the model shown in figure 6.2 and a time course simulation performed. The mean value for each time point in each of the 10 simulations was then plotted (dark blue line) and 95% confidence intervals calculated (light blue area). (J) the RSS value for each of the 10000 parameter estimations was ranked

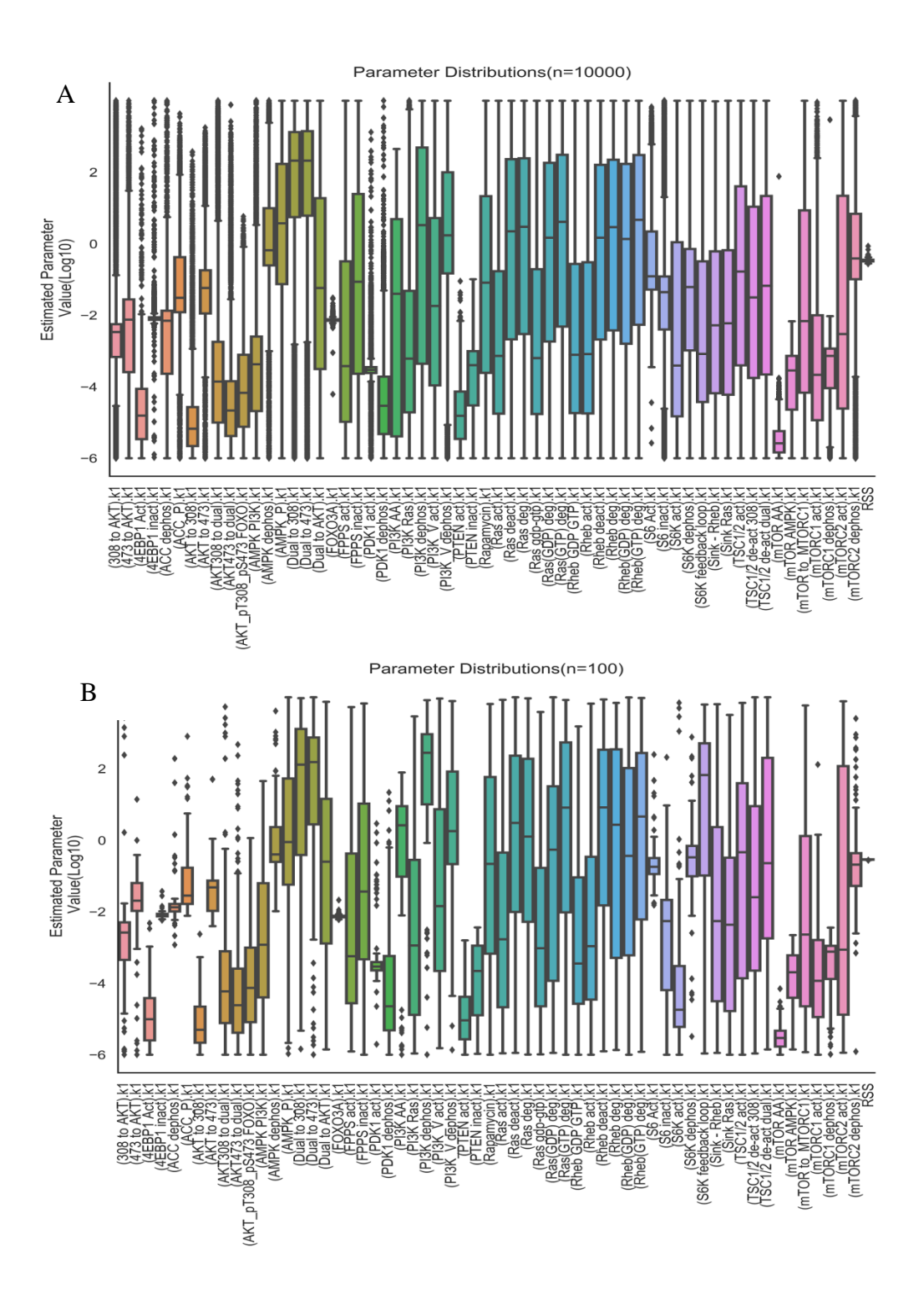


Figure 6.14: Parameter Variation in MSCs. Boxplots displaying the variation of each parameter estimated within the lower (1e-6) and upper limit (1000) bound of 10000 (A) and top 100 (B) parameter estimations using the genetic algorithm in MSCs.

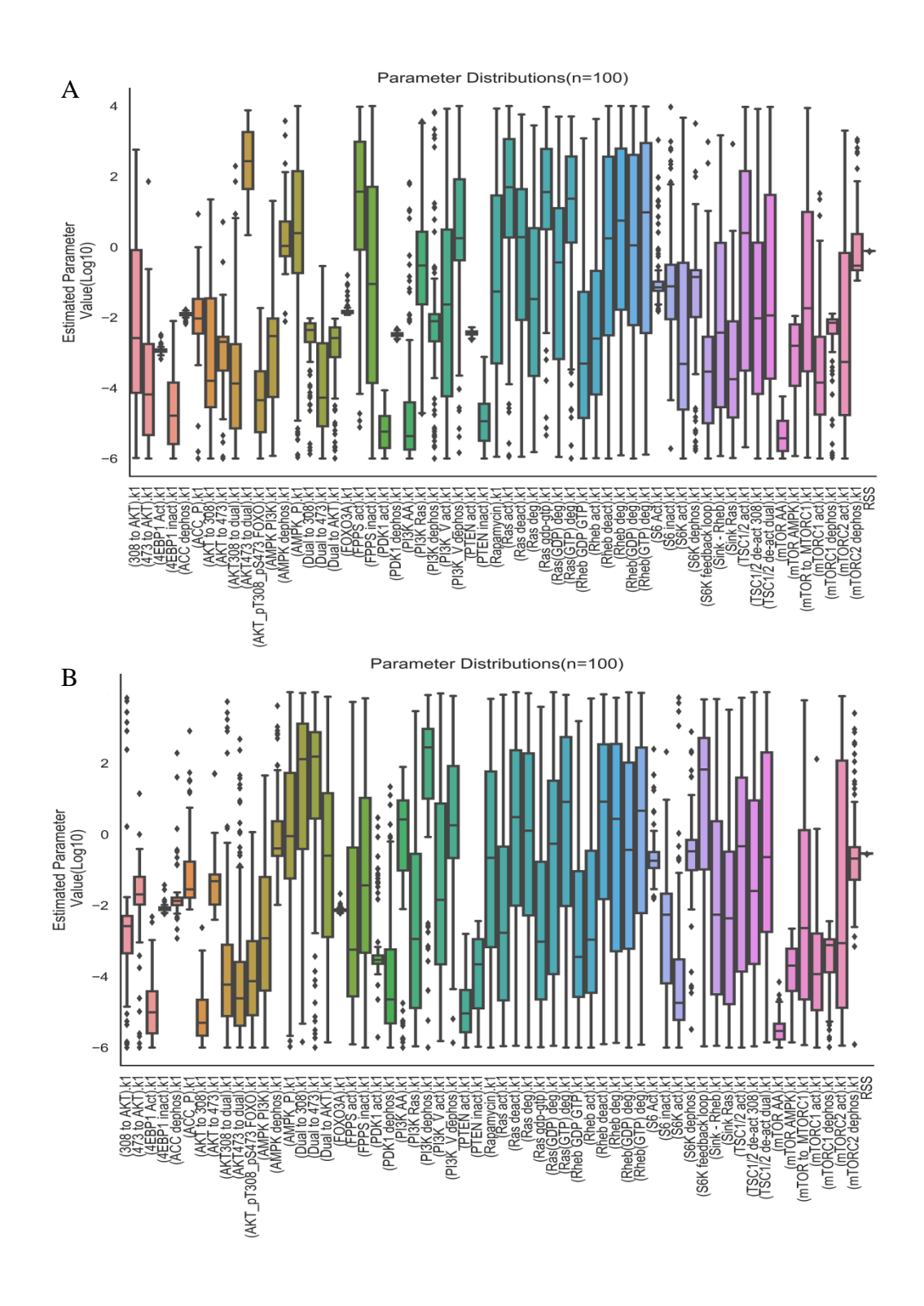


Figure 6.15: Parameter variation between MRC5 and MSC cells. Boxplots displaying the variation of each parameter estimated within the lower (1e-6) and upper limit (1000) bound in the top 100 ranked parameter estimations in MRC5 cells (A) MSCs (B).

6.4.9 Hooke and Jeeves

As in the previous chapters a comparison testing the ability of the calibrated MRC5 model to fit the MSC data was carried out. The MRC5 dataset was removed and replaced with the MSC dataset. A set of 100 parameter estimations using the Hooke and Jeeves algorithm was then performed using the reaction parameter values obtained by the best fit to the MRC5 dataset as the initial reaction parameter values. In addition a set of 100 parameter estimations was also carried out as above for the MRC5 dataset. This resulted in an improved fit with an RSS value of 0.70 however as expected little improvement was observed for the observables that could not be fitted using the genetic algorithm (figure 6.16). Applying the Hooke and Jeeves algorithm to the MRC5 calibrated model using the MSC dataset resulted in an improved fit (RSS = 0.383181) with the model capable of reproducing a similar fit to that observed using the genetic algorithm (RSS = 0.272978) (figure 6.17). This was true for all observables fitted with the exception of 4E-BP1_pS65 whose fit using the genetic algorithm could not be replicated using the Hooke and Jeeves algorithm (figure 6.17 H).

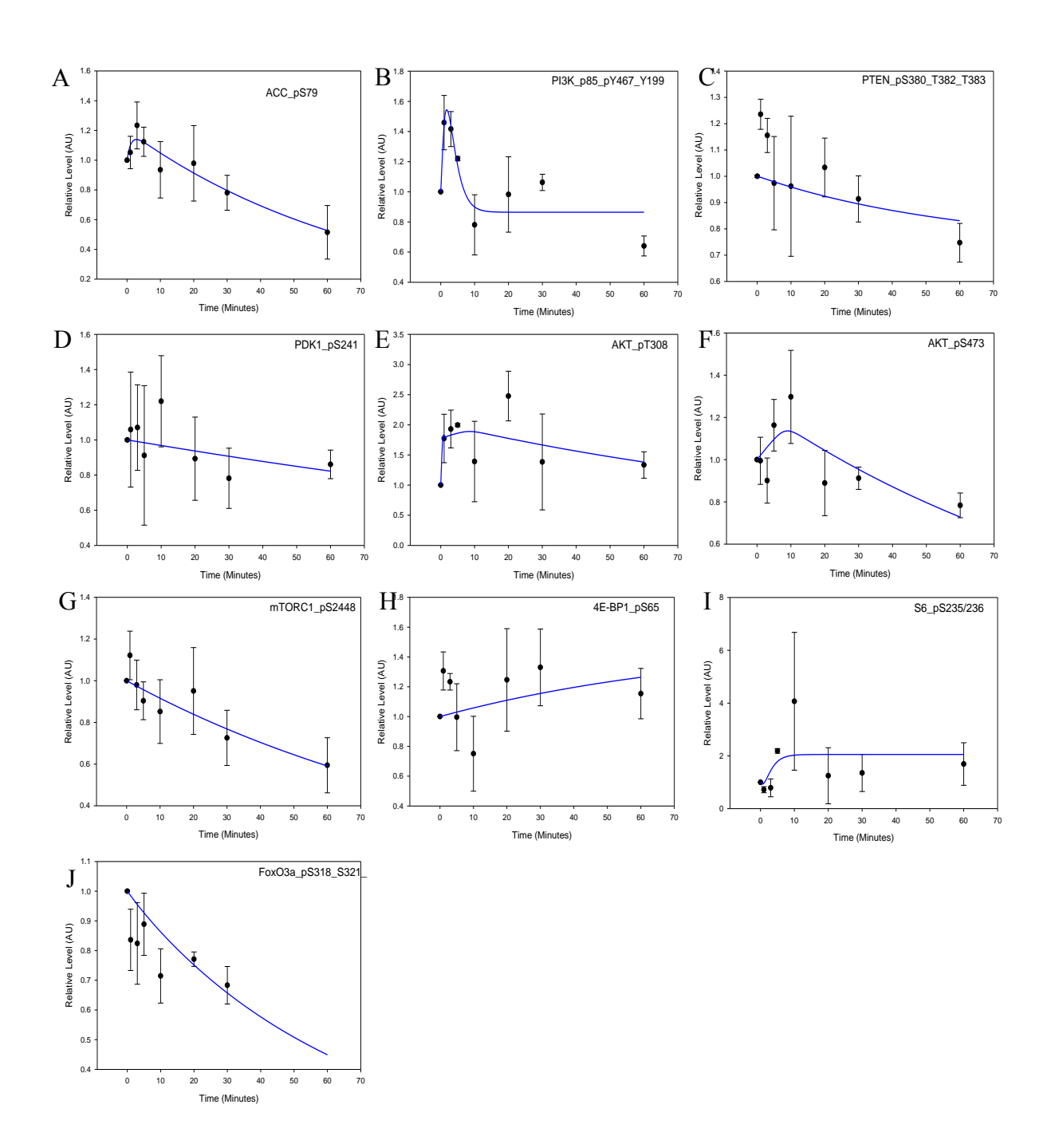


Figure 6.16: Time course simulations from the model compared to re-stimulation data utilizing the local Hooke and Jeeves algorithm. The model displayed in figure 6.2 was calibrated using the re-simulated RPPA data shown in figures 6.7. A parameter estimation consisting of 59 parameters in total was performed using the local algorithm Hooke and Jeeves (100 runs). The Residual sum of squares between the experimental data (Black +/- SEM) and the simulated data (Blue) was calculated as 0.701168.

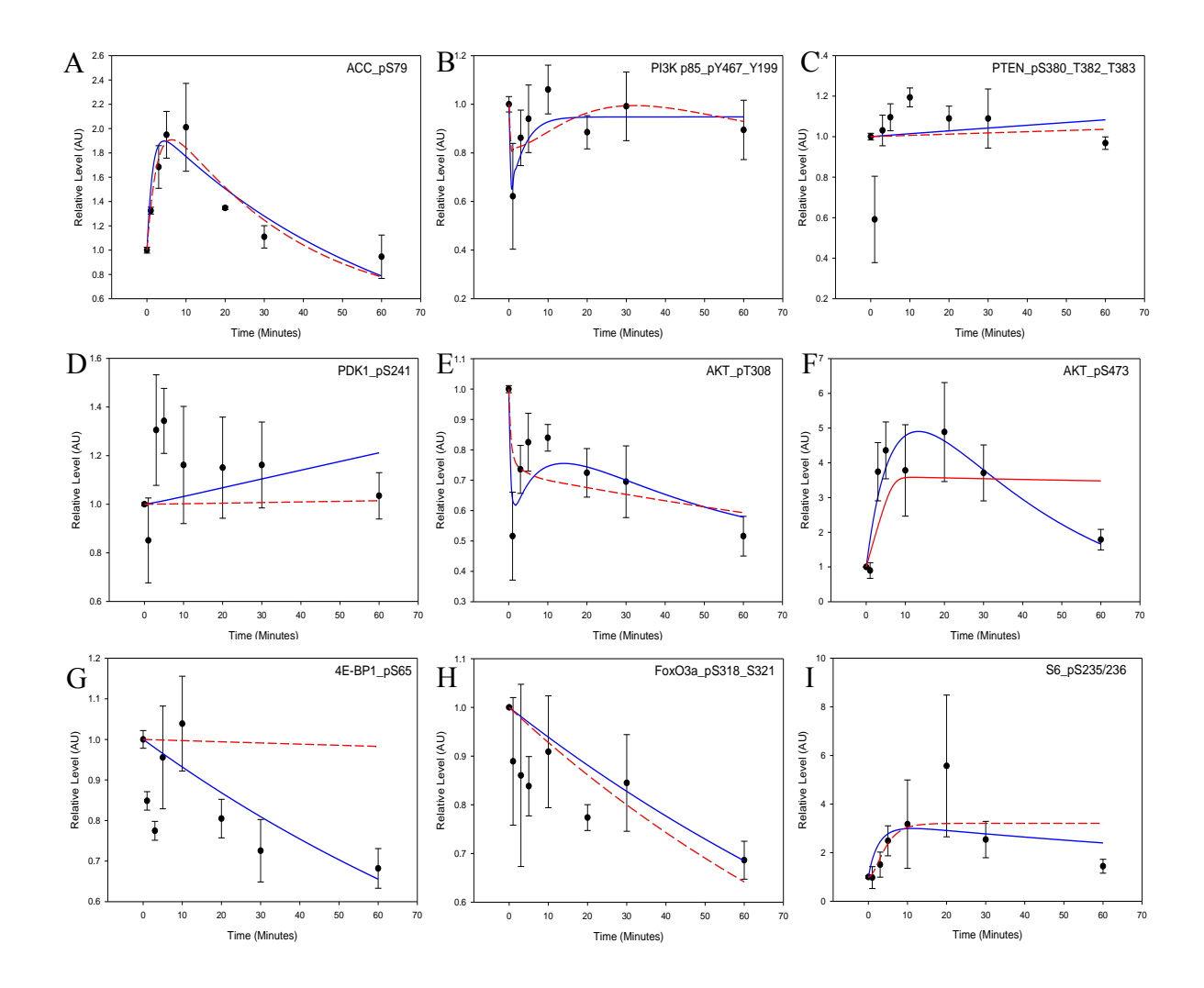


Figure 6.17: Genetic vs Hooke and Jeeves fit for MSC. The model displayed in figure 6.2 was calibrated using the RPPA data shown in figure 6.11. A parameter estimation consisting of 59 parameters in total was performed using the genetic algorithm (1000 runs) (Blue) randomising the initial parameter values and the Hooke and Jeeves algorithm (100 runs) (Red) using previously obtained parameter values form the MRC5 data fit. The Residual sum of squares between the experimental data (Black +/- SEM) and the simulated data (Genetic-Blue, Hooke and Jeeves-Red) was calculated as 0.27 (genetic) and 0.38 (Hooke and Jeeves).

<u>Table 6.2: Residual sum of squares value for each model.</u> The residual sum of squares for each model fitted to the experimental data for both MRC5 and MSC datasets. The lower the RSS value, the closer the fit between the model simulations and the corresponding dataset. Corresponding figure number also shown.

Parameter Estimation	Residual Sum of	Figure No.		
Squares				
MRC5 Genetic Fit	0.738134	6.8		
MRC5 Hooke and Jeeves	0.701168	6.16		
MSC Genetic Fit	0.272978	6.11		
MSC Hooke and Jeeves	0.383181	6.17		

6.5 A comparison between zoledronate withdrawal and starvationrestimulation and rapamycin withdrawal.

As in the previous chapter a comparison was carried out between the MRC5 and MSC datasets for both Zoledronate withdrawal and starvation-restimulation and Zoledronate withdrawal and Rapamycin withdrawal (figure 6.18 and 6.19). There are a number of differences between the response to Zoledronate withdrawal and starvationrestimulation in MRC5 cells (figure 6.18 A-J). In particular the responses of ACC_pS79 and AKT_pS473 are of interest (figure 6.18 A + F). Following starvation-restimulation there is an increase in ACC_pS79 signalling over the first 10 minutes of the time course before a decrease back to initial levels. This peak does not exist within the Zoledronate data with a very slight increase observed in the first minute before a gradual decline. The AKT_pS473 kinetic profiles are similar in both the starvation-restimulation and Zoledronate datasets however the level of activity varies greatly with a far greater response observed following starvation-restimulation (figure 6.18 F). Within the MSC datasets there is far less variation between the observables (figure 6.18 K-T). However the response of ACC_pS79 to each treatment varies greatly as it does for the MRC5 datasets. Interestingly there is a reversal in the difference between the treatments with a similar peak in ACC_pS79 activity within the Zoledronate withdrawal MSC data observed whereas there is no peak observed in the starvation-restimulation data (figure 6.18 K). Upon comparing Zoledronate withdrawal and Rapamycin withdrawal in MC5 cells there are few similarities (figure 6.19 A-I). The exception to this is the response of the AKT_pT308 observable whose kinetic profile is very similar in response to both treatments (figure 6.19 E). Within the MSC datasets there are a number of observables which display similar behaviour in response to Zoledronate and Rapamycin Withdrawal (figure 6.19 J-R). In PI3K_P85_pY467_Y199, particular the PTEN_pS390_T382_T383, and 4E-BP1_pS65 all display similar kinetic profiles from the 1 minute time point onwards (figure 6.19 K, L + Q). Interestingly the profiles for the two AKT phosphosites measured display similar kinetic profiles between each treatment however the relative response to each treatment differs greatly. In response to Zoledronate withdrawal there is far greater activation of AKT_pS473 whilst in response to Rapamycin treatment there is a far greater activation of AKT_pT308 (figure 6.19 N + O). This supports the data shown in figure 6.1 that Zoledronate treatment leads to a greater inhibition of AKT_pS473 than AKT_T308.

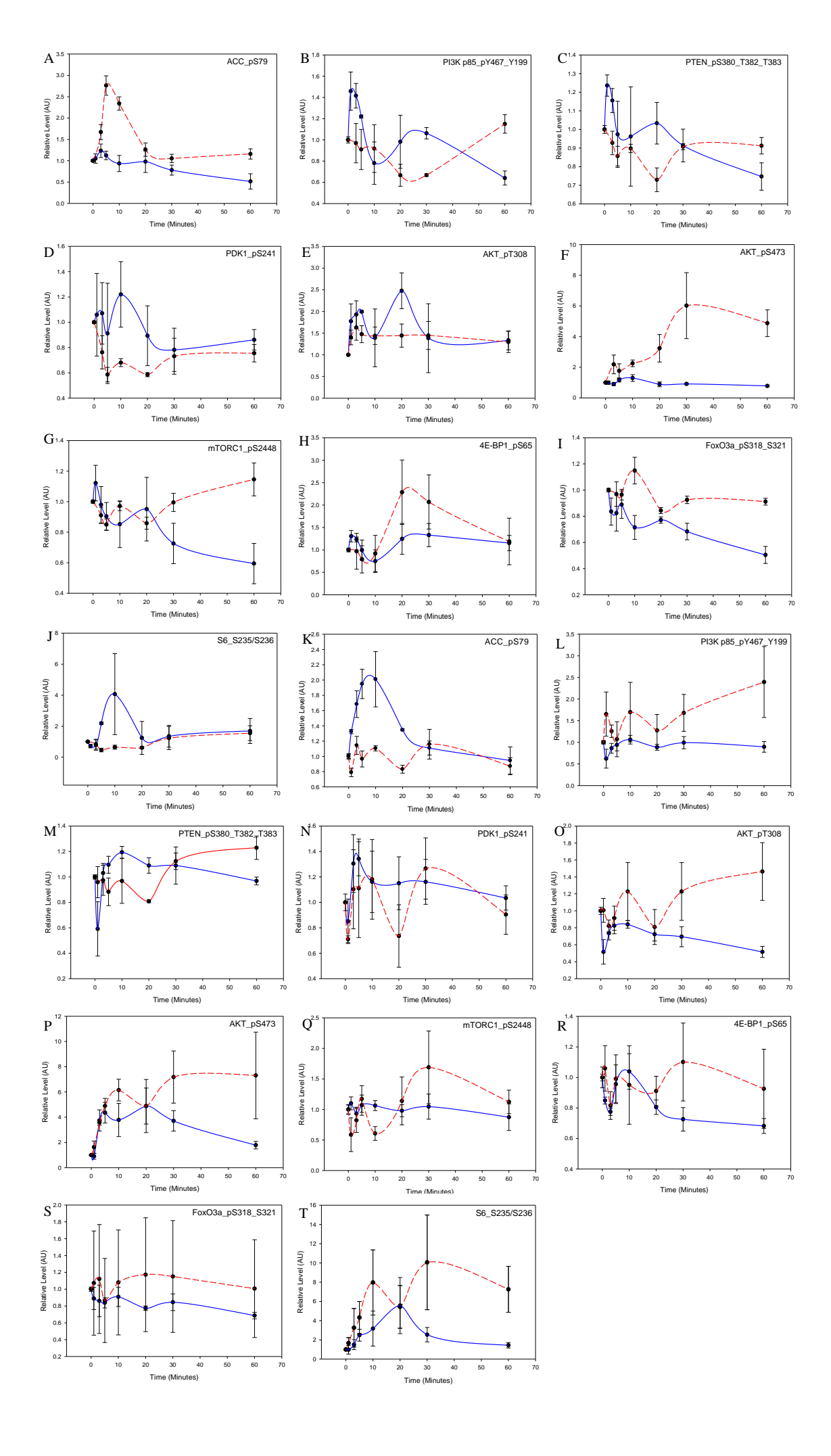


Figure 6.18: A comparison of mTOR kinetics following Zoledronate withdrawal an d starvation-restimulation in MRC5 and MSC cells. A sixty minute time course following 72 hour Zoledronate treatment (Blue) and starvation-restimulation (Red). Cells were re-stimulated at 0 hours and relative fluorescent intensity measured at each time point (n=3) (Mean +/- SEM) in MRC5 cells (A) ACC_pS79, (B) PI3K_p85_pY467_pY199, (C) PTEN_pS380_pT382_pT383, (D) PDK1_pS241, (E) AKT_pT308, (F) AKT_pS473, (G) mTORC1_pS2448, (H) 4E-BP1_pS65, (I) FOXO3A_pS318_pS321 and (J) S6_pS235/236. In MSCs (K) ACC_pS79, (L) PI3K_p85_pY467_pY199, (M) PTEN_pS380_pT382_pT383, (N) PDK1_pS241, (O) AKT_pT308, (P) AKT_pS473, (Q) mTORC1_pS2448, (R) 4E-BP1_pS65, (S) FOXO3A_pS318_pS321 and (T) S6_pS235/236. (previous page).

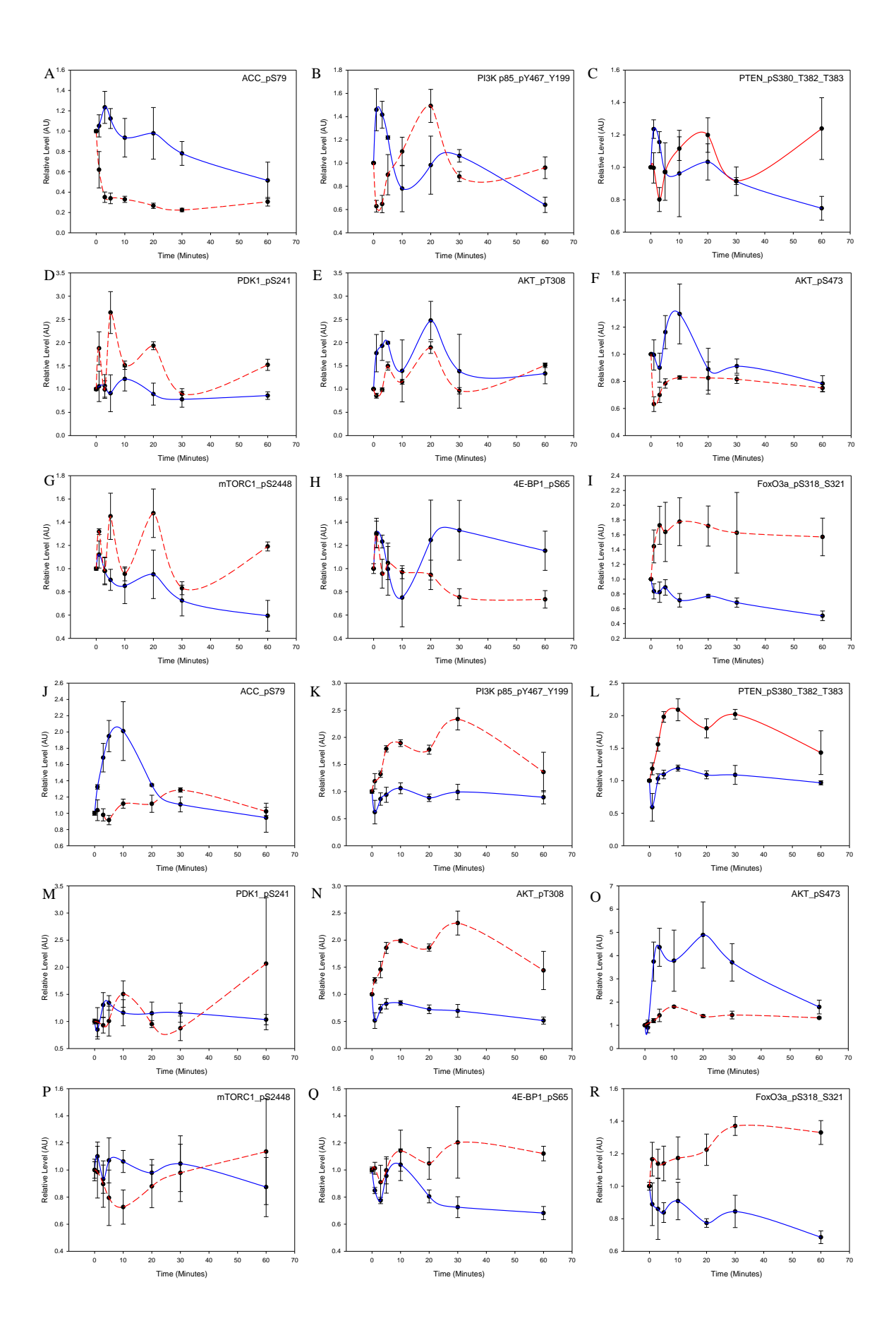


Figure 6.19: A comparison of mTOR kinetics following Zoledronate withdrawal and Rapamycin withdrawak in MRC5 and MSC cells. A sixty minute time course following 72 hour Zoledronate treatment (Blue) and Rapamycin (Red). Cells were re-stimulated at 0 hours and relative fluorescent intensity measured at each time point (n=3) (Mean +/- SEM) in MRC5 cells AKT_pT308, (F) AKT_pS473, (G) mTORC1_pS2448, (H) 4E-BP1_pS65 and (I) FOXO3A_pS318_pS321.In MSCs (K) ACC_pS79, (K) PI3K_p85_pY467_pY199, (L) PTEN_pS380_pT382_pT383, (M) PDK1_pS241, (N) AKT_pT308, (O) AKT_pS473, (P) mTORC1_pS2448, (Q) 4E-BP1_pS65 and (R) FOXO3A_pS318_pS321. (Previous page).

6.6 Image flow cytometry fails to show correlation between DAPI – FOXO3A and Rheb-LAMP1

As in the previous chapters imagestream flow cytometry was used to analyse the response of FOXO3A and Rheb cellular localisation following Zoledronate treatment and withdrawal. The timecourse used during the imagestream flow cytometry assays differed from those obtained using the RPPA and from the two previous treatments with time points taken at the following times 0 hour (untreated), 24 hours post treatment, 48 hours post treatment, 72 hours post treatment, 5 minutes post restimulation, 15 minutes post restimulation, 30 minutes post restimulation, and 60 minutes post restimulation. As carried out previously LAMP1-Alexa-488 and DAPI were also stained for in order to allow for lysosomal and nuclear localisation comparison as in the previous chapter. In addition the template and correlation matrix previously created for the analysis of both serum starvation-restimulation and Rapamycin treatment was used for the analysis of Zoledronate treatment allowing for a standard set of analysis conditions across all three treatments. A representative image of cells following 72 hours Zoledronate treatment in shown in figure 6.20. As in the previous chapter a single cell population was selected and out of focus cell images removed from the analysis prior to analysi of colocalisation between FOXO3A- DAPI and Rheb-LAMP1 (figure 6.20 A-D). Whilst the number of cell and the imaging of DAPI in the final analysis of the previous two experiments had proved problematic this was not the case with ~1800 cells per time point obtained following Zoledronate treatment. It was therefore possible to analyse the data shown in table 6.3. Upon inspection however it was determined that nether FOXO3A-DAPI or Rheb-LAMP1 display a positive correlation (Pearson's' correlation co-efficient) (figure 6.21).

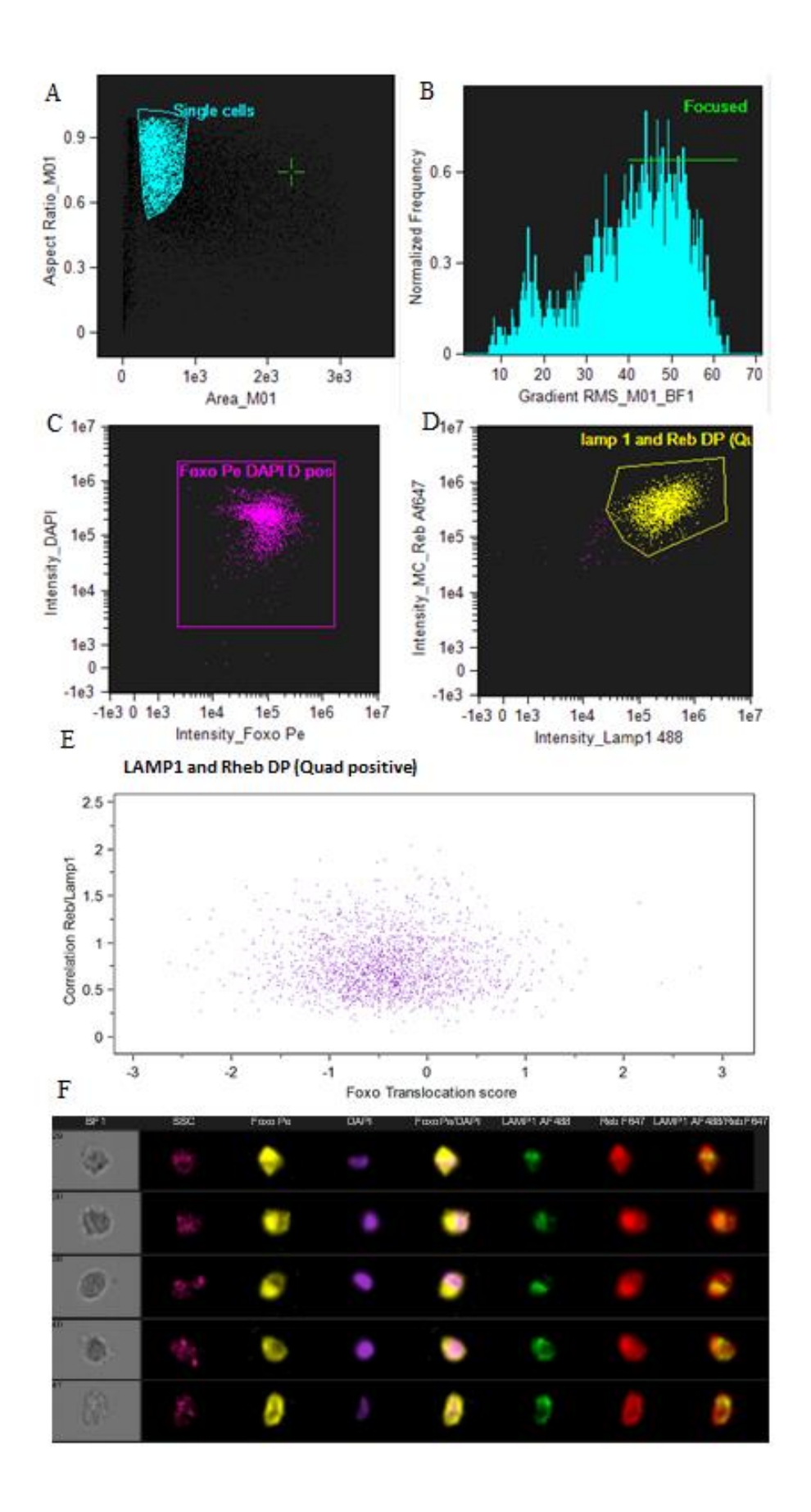


Figure 6.20: Image flow cytometry fails to show correlation between DAPI – FOXO3A and Rheb-LAMP1. Representative image displaying image flow cytometry analysis of untreated cells following 72 hour Zoledronate treatment (0.01μM), (A) A single cell population was selected, (B) followed by the removal of images that were not in focus. (C) Nuclear localisation correlation was analysed for FOXO3A and DAPI, in addition to (D) correlation analysis of RHEB and LAMP1. (E) Population analysis displaying correlation between DAPI-FOXO3A and Rheb-LAMP1 (Pearson's correlation co-efficient). (F) Representative image of in focus single cell population for 72 hour Zoledronate (0.01μM) treated cells.

<u>Table 6.3: Image flow cytometry time course correlation</u>. Correlation values for each time point assayed for FOXO3A-DAPI (FD) and Rheb-LAMP1 (RL) (Pearson's correlation co-efficient; all values are non-significant P>0.05)

Time Point	FOXO3A-DAPI	Rheb-LAMP1	P-value
	Pearson's correlation	Pearson's correlation	FD/RL
	co-efficient	co-efficient	
0 hours	-0.3104	0.7639	0.79/0.45
24 hours treated	-0.3365	0.7557	0.78/0.46
48 hours treated	-0.2176	0.856	0.87/0.34
72 hours treated	-0.4275	0.7226	0.72/0.49
5 minutes restimulated	-0.4246	0.7874	0.72/0.43
15 minutes restimulated	-0.4228	0.8008	0.72/0.41
30 minutes restimulated	-0.4196	0.7818	0.73/0.43
60 minutes restimulated	-0.3574	0.8024	0.77/0.41

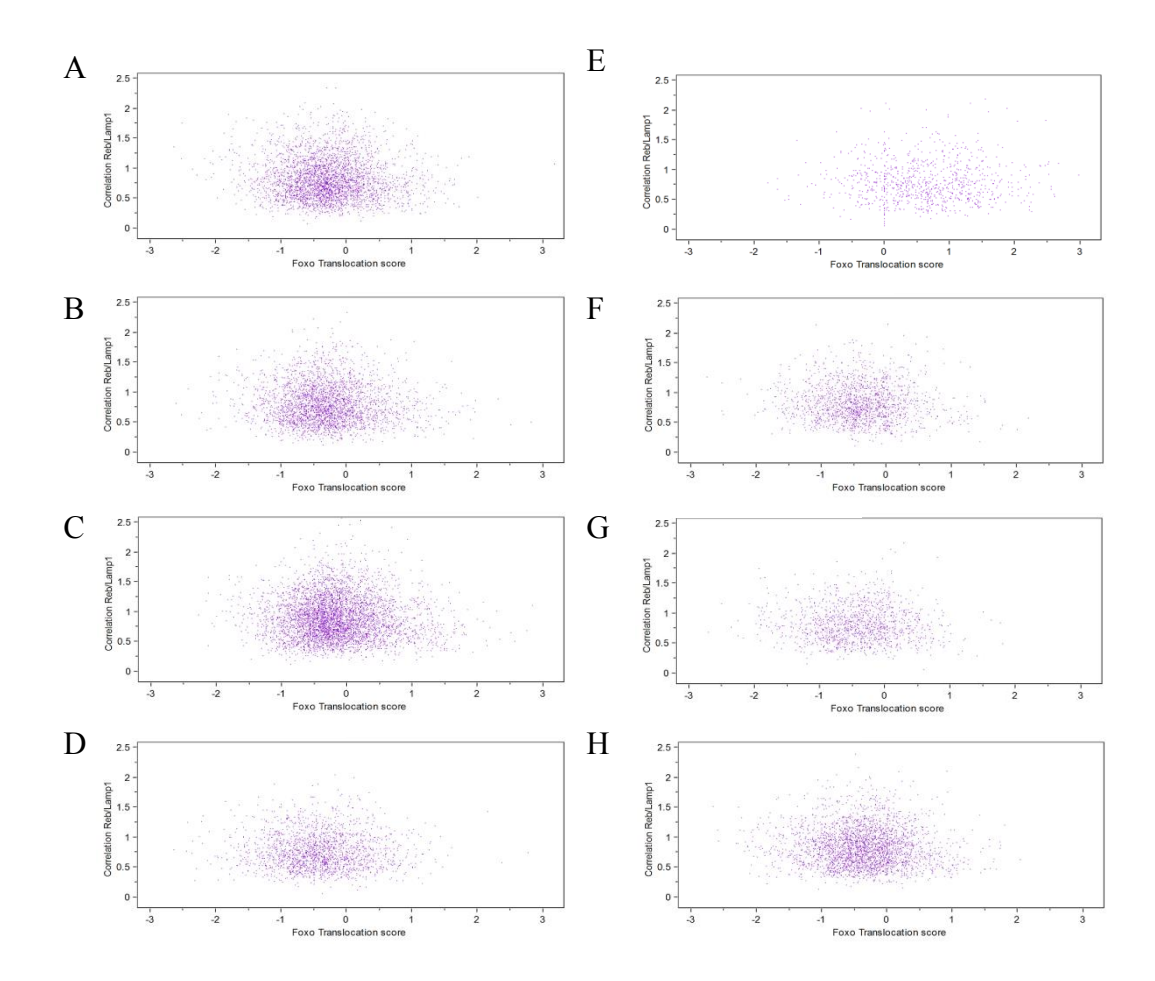


Figure 6.21: Image flow cytometry time course correlation. Population analysis displaying correlation between DAPI-FOXO3A and Rheb-LAMP1, (Pearson's correlation co-efficient), (A) 0 hour untreated cells, (B) 24 hours Zoledronate treated cells, (C) 48 hours Zoledronate treated cells, (D) 72 hours Zoledronate treated cells, (E) 5 minutes re-stimulated cells, (F) 15 minutes re-stimulated cells, (G) 30 minutes re-stimulated cells, (H) 60 minutes re-stimulated cells.

6.7 Discussion

The aims of the work presented here were to define a dynamic model capable of representing the mTOR networks response to Zoledronate Withdrawal. To calibrate this model in both MRC5 and MSCs using reverse phase protein arrays. To use imagestream flow cytometry to analyse the cellular localisation of key proteins within the mTOR network. And to identify how MRC5 fibroblasts and MSCs differ in their response to Zoledronate Withdrawal. Through the computational dynamic modelling approach described above this has been achieved. The model presented proved capable of simulating the response of both MRC5 and MSCs in response to restimulation following a period of Zoledronate treatment.

As with the two previous chapters RPPA was utilised to create a time course dataset capable of calibrating a dynamic model of the mTOR network. Initial attempts to carry this out in MRC5 cells failed to produce a time course suitable for the calibration of the model above. However subsequent analysis revealed that MRC5 cells are far more sensitive to Zoledronate treatment than expected. In order to address this a 100 fold reduction in Zoledronate concentration was required. This resulted in a significant reduction is cell death and the ability to produce a high quality calibration dataset using RPPA. In addition imagestream flow cytometry analysis of MRC5 cells treated using this concentration displayed normal cell morphology. As it has previously been observed that MSCs do not undergo cell death at 1µM Zoledronate it was not necessary to perform a cell death assay on these cells [82]. Following Zoledronate withdrawal a consistent kinetic profile was observed throughout the time course with a clear flow of information through the mTOR network observed. It proved possible to assay a total of 17 proteins using RPPA for both MRC5 and MSCs although one antibody per RPPA assay failed. This can however be appears to a consequence of antibody failure as opposed to a failure of the RPPA methodology.

Following parameter estimation with the genetic algorithm it proved possible to fit seven out of the ten observables assayed in the MRC5 dataset and eight out of the nine observables assayed in the MSC dataset. As with the previous chapter it did not prove possible to fit the PTEN_pS380_T382_T383 or PDK1_pS241 observables in the MRC5 dataset. Suggesting that the model at present does not sufficiently capture the regulatory mechanisms which control the activation of these proteins. In addition it did not prove possible to obtain a fit for 4E-BP1_pS65 in any of the three treatments analysed in

MRC5 cells suggesting that a more in depth analysis of mTORC1 regulation of 4E-BP1 activity is required. As this would likely require the construction of second dynamic model to analyse possible regulatory frameworks for 4E-BP1 this was not attempted in this work [251] [252].

A key factor throughout this work has been the reaction of the ACC_pS79 observable as a read out of AMPK activity. Following Zoledronate withdrawal there is again an interesting response observed for this protein. In MRC5 cells there is an initial increase ACC_pS79 phosphorylation followed by a decrease over the remainder of the time course. This size of this peak is extremely small when compared to the relative changes observed for both starvation-restimulation and Rapamycin withdrawal. In contrast however a transient peak is observed in the MSC dataset which follows the same pattern as the peak observed in MRC5 cells following starvation-restimulation. Given the apparent regulatory constrictions placed on AMPK activity observed in MSCs in the previous two treatments this is a very interesting observation and suggests that Zoledronate in MSCs could have a similar effect to that observe with starvationrestimulation in MRC5 cells. Upon comparison of the response of MRC5 cells to Zoledronate withdrawal and starvation-restimulation it is apparent that a number of differences exist. In particular as already described the reaction of ACC_pS79 differs greatly between these treatments. In addition whilst the kinetic profile of the AKT_pS473 observable is very similar between the treatments there is a far larger level of activation observed following starvation-restimulation than in Zoledronate treatment. The same can be said when comparing Zoledronate withdrawal to Rapamycin withdrawal in MRC5 cells with very few similarities observed with the exception of the AKT_pT308 observable whose kinetic profile is extremely similar in response to both treatments.

As was the case in the previous chapter the response of MSCs to Zoledronate withdrawal and starvation-restimulation is far less varied with a number of profiles displaying similar behaviour. As previously described the ACC_pS79 observable is the exception to this with large increase in phosphorylation observed in response to Zoledronate withdrawal but not starvation-restimulation. Upon comparison of Zoledronate withdrawal to Rapamycin withdrawal in MSCs this pattern repeats itself with a large number of kinetic profiles displaying similar behaviour. There is a greater level of activation in the Rapamycin withdrawal dataset among the observables

upstream of mTORC1 when compared to Zoledronate withdrawal with PDK1_pS241 again proving to be the exception to this. In contrast there is far greater level of activation observed in the mTORC2 dependent AKT_pS473 variable in response to Zoledronate withdrawal compared to Rapamycin withdrawal. This is not unexpected however as the Rapamycin treatment protocol used above was designed not to elicit chronic inhibition of the mTOR network and therefore mTORC2 should have remained active over the length of the time course. The contrasting differences of the AKT phosphosites in response to Zoledronate withdrawal and Rapamycin withdrawal however provides further evidence of RPPAs ability to provide consistent data which can be used to calibrate dynamic models.

Within this chapter it proved possible to perform in depth analysis of the data obtained during the parameter estimations using the genetic algorithm by utilising the Pycotools python package. Our analysis revealed that the top estimation profiles obtained during the parameter estimations all followed the same kinetic profile with extremely tight confidence intervals in both the MRC5 and MSC parameter estimations. In addition whilst the analysis of the total number of runs for both estimations revealed a large variation in parameter values per parameter. The top 100 estimations displayed far less variation with a number of parameters being tightly constrained to a small set of values. Interestingly a comparison of the level of parameter variation between the cell types revealed that the same parameters for each cell type were being constrained by the model and more significantly a number of these parameters were being constrained to similar values. This analysis also identified two areas in which the model struggled to constrain parameters. These were identified as reaction parameters relating to the TSC1/2 complex and the parameters concerned with Ras and Rheb protein production and degradation. In order to assist the model in fitting these parameters further experimental data should be produced and added to the parameter estimations.

Whilst it did not prove possible to analyse the correlation between either FOXO3A-DAPI or Rheb-LAMP1 using imagestream flow cytometry in this study the results above indicate that this should be possible with experimental refinement. Whilst FOXO3A phosphorylation does not always correspond to activity or indeed to nuclear localisation it is possible that a different result would be obtained if total FOXO3A was assayed in place of FOXO3A_pS253. The lack of correlation between Rheb-LAMP1 is harder to explain. Whilst it was expected that Rheb localisation at the lysosome would

be disrupted following Zoledronate treatment the lack of correlation in the untreated samples suggests that there is no change in correlation across the time course. This could possibly be due to non-specific binding of the antibody concerned resulting in an inability of the analysis software to determine a correct correlation.

Overall the aims of this work have been met with a dynamic model capable of reproducing the response of both MRC5 cells and MSCs to Zoledronate withdrawal. Due to the level of cell death observed in MRC5 cells the initial concentration of Zoledronate used was required to be reduced resulting in the production of a consistent kinetic profile using RPPA. As in previous chapters problems arose in the fitting of the PTEN, PDK1 and 4E-BP1 observables assayed suggesting that further regulation of these proteins is required within the model. A comparison between the three treatments revealed that whilst large differences occur in MRC5 cells a number of similarities exist in MSCs. In addition whilst the observed output for ACC_pS79 in starvationrestimulation and Rapamycin withdrawal led to similar profiles the ACC pS79 kinetic profile for Zoledronate withdrawal displayed more similarity to that of the MRC5 starvation-restimulation. In depth analysis of the parameter estimations for both cell types revealed very little variation between the top parameter ensembles with similar parameter groups being constrained or unconstrained in both estimations. Imagestream analysis was unable to capture the dynamics expected following Zoledronate treatment however this may be obtained following further refinement of the experimental process.

7. Discussion

7.1 Summary

The study aims and objectives have been largely met. Our initial hypothesis was as follows, that due to the fact that both starvation-restimulation and Zoledronate treatment leads to the inhibition of both mTOR complexes, the response in both MRC5 cells and MSCs should be similar between these two treatments. However as acute treatment of Rapamycin leads only to the inhibition of mTORC1, this treatment would therefore lead to a separate response to the other treatments analysed. This hypothesis has been largely proven to be true with both the response of the mTOR network to restimulation following starvation and Zoledronate withdrawal being dependent upon AMPK. Following Rapamycin treatment however the response of the mTOR network was found to be largely dependent upon the P70S6K negative feedback loop. However whilst AMPK may be the key regulatory component following both starvation-restimulation and Zoledronate withdrawal this appears to occur through two distinct mechanisms.

A total of three methodologies have been investigated and their suitability to provide accurate time course data assessed. Whilst further investigation is warranted, RPPA proved capable of producing accurate and reproducible time course data capable for calibrating a dynamic model of the mTOR network. The second methodology assessed, intracellular flow cytometry was capable of producing the time course data required however the limitations associated with this technology made it unsuitable in comparison to both western blots and RPPA. The final methodology assessed was imagestream flow cytometry. Whilst this methodology suffers from the same drawbacks as intracellular flow cytometry it provides a powerful analysis tool for cellular localisation and further investigation is warranted into its ability to provide the data required for network calibration. Upon restimulation following a period of serum starvation the response of MRC5 cells is dependent upon AMPK signalling with an increase in ACC_pS79 observed. This is not observed in MSCs raising the possibility that AMPK signalling is placed under stringent regulation in MSCs compared to MRC5. Whilst the kinetics of the mTOR network following starvation-restimulation depend upon AMPK ACC signalling our model revealed this not to be the case following Rapamycin withdrawal. The P70S6K feedback loop was identified as the key signalling reaction in MRC5 cells following Rapamycin withdrawal with a change in network topology required in order to achieve an acceptable model fit. As with the starvationrestimulation data the data obtained following Rapamycin withdrawal data for MSCs

displayed far less variation when compared to the MRC5 dataset. However PDK1 was identified as differentially regulated in both MRC5 and MSCs following Rapamycin withdrawal. As with the two previous MSC datasets the data obtained following Zoledronate withdrawal displayed less variation compared to MRC5 cells. Following parameter estimation with both MRC5 and MSC datasets for Zoledronate withdrawal a number of parameters showed similar constraints in their values following fitting with the genetic algorithm. Two areas of the network were also identified were the estimation algorithms could not pin down a refined set of parameter values. This project again demonstrated the significant power in using an integrative experimental and computational approach to analyse biological signalling networks. Using the same initial topology with minimal alterations, it was possible to analyse how the mTOR network is affected during restimulation following three separate life extending treatments. This would not have been possible using a purely experimental approach, and indeed the unbiased model calibration performed served to highlight a number of observables whose kinetic behaviour could not be explained by the model selected.

7.1.1 Summary of key findings

- Reverse Phase proteins arrays provide a high quality medium through-put alternative to western blotting
- Following serum starvation, AMPK signalling is the pivotal section of the mTOR networks response in MRC5 cells but not in MSCs
- Following Rapamycin withdrawal, mTOR signalling is dependent upon the P70S6K negative feedback loop
- Following Zoledronate withdrawal there is an activation of AMPK signalling in MSCs but not in MRC5 cells
- Imagestream flow cytometry did not prove capable in this study of providing colocalisation timecourse data for either Rheb or FOXO3a

7.2 Key study observations

7.2.1 Reverse phase protein arrays provide a high quality medium through-put alternative to western blotting

The work carried out in chapter 3 cleary indicated the suitability of RPPA to produce large scale datasets required for the calibration of dynamic models. Building upon this the subsequent chapters in this work proved that this data could be used to achieve the

calibration of a dynamic model of the mTOR network for two cell types across three separate treatments. Comparison of the data obtained in MRC5 cells in chapter 4 to previously published work examining the effect of amino acid deprivation on the mTOR network revealed similar kinetic profiles for the AMPK read out ACC_pS79 and for both AKT_pT308 and AKT_pS473 [172]. In addition to this, recent research has utilised RPPA to calibrate a dynamic model of cytokine regulation of osteogenesis with the aim of providing a therapeutic tool for future research [195]. Whilst this project has achieved a large amount of success in using RPPA in dynamic modelling there are a number of limitations associated with this methodology. As previously discussed antibody availability is the primary limitation associated with RPPA, whilst this did not prove particularly problematic in this project due to the extensive research previously carried out on the mTOR network there were certain proteins that could not be assayed. Amongst these AMPK_pT172, P70S56K_pT389, TSC2_pT1462 and PRAS40_pS183 would be of particular interest to assay. In addition although the previous work supports our findings using RPPA for starvation-restimulation validation work is still required using western blots to verify the findings presented in this work.

7.2.2 Dynamic modelling reveals the importance of AMPK signalling in response to starvation-restimulation in MRC5 fibroblasts but not MSCs

Recent work has revealed the interplay between AMPK and mTOR signalling following restimulation with amino acids [172]. The work presented in chapter 4 further supports these findings with the ACC_pS79 data proving to have the largest effect on fitting the MRC5 data to the model. This resulted in the requirement for the removal of baseline AMPK and ACC phosphorylation from the model fitting. The reason for the inability of the model to fit the data with a baseline activation of AMPK within the model is likely due to the complex regulation of AMPK itself. As the primary focus of this work was on the identification of differences between life extending treatments it was decided that additional modelling of potential regulatory mechanisms should not be undertaken as the identification of AMPKs importance in starvation-restimulation satisfied the original objectives. Interestingly in MSCs the transient peak observed in the literature for AMPK_pT172 and in the MRC5 data for ACC_pS79 was not observed. This suggests that this section of the network differs between the MSCs and differentiated MRC5 cells. It is possible that the stringent regulation placed on stem cells compared with

differentiated cells could account for this difference. However recent research showing that AMPK can act to bypass the inhibitory effect of caloric restriction in intestinal stem cells taken from mice suggests that under periods of caloric restriction stem cells possess protective mechanisms in order to prevent proliferation or differentiation under sub-optimal conditions [209]. As AMPK regulation of mTOR was not the primary focus of this work the AMPK-mTOR network connections presented here represent an abstracted version of the work presented in Dalle Pezze et al 2016. As such further analysis is required to elucidate the mechanisms governing AMPK activity during starvation-restimulation and how this differs between stem cells and differentiated cells.

7.2.3 mTOR signalling following rapamycin withdrawal is dependent upon the P70S6K negative feedback loop

Rapamycin was included in this study as it is considered to be the 'gold standard' in terms of pharmalogically extending lifespan. In addition previous work produced by at the University of Sheffield had used Rapamycin in comparison studies with Zoledronate [82]. It is however not considered to be a particularly clean drug with many off target effects [219]. This was also shown to be the case in this study with a large amount of variation observed in the MRC5 dataset. Interestingly this variation was not observed in the MSC dataset further supporting the idea that a set of extremely stringent regulatory mechanisms exist in stem cells which are absent in differentiated cells [253]. In addition, in response to Rapamycin withdrawal the P70S6K negative feedback loop was identified as the key section of the mTOR signalling network with a disconnect observed between the responses of proteins upstream of mTORC1 and downstream of MTORC1. As it was not possible to assay the activity of P70S6K directly using RPPA it will be necessary in future to assay this protein and to ascertain as to whether the above assumption is correct. In addition to providing a standard drug treatment with which to compare Zoledronate to, Rapamycin also served to act as a comparison treatment between total and partial mTOR inhibition. It would be of interest to take this work further by investigating the response of both MRC5 and MSCs to chronic Rapamycin treatment targeting the mTORC2 complex in addition to the mTORC1 complex.

7.2.4 Zoledronate withdrawal leads to an activation of the AMPK signalling pathway in MSCs but not MRC5 cells

The recent finding that Zoledronate treatment leads to lifespan extension in MSCs supports a growing body of evidence that Zoledronate and other N-BPs act to extend lifespan and inhibit DNA damage [124]. In addition it has been found that the treatment of MSCs with Zoledronate for a period of three days is sufficient to achieve lifespan extension through the mTOR network [82]. The work presented here aimed at building upon these findings and establishing the mechanistic reaction of the mTOR network to Zoledronate withdrawal. Treatment of MRC5 cells with Zoledronate at 1µM resulted in cell death and with high levels of cell death not observed at 0.01 µM. Indeed the cytotoxicity of Zoledronate in fibroblasts is ill-defined with little to no data available for MRC5 fibroblasts [254]. This therefore meant that it was not possible to cross reference this finding with other research. The model used in this work proved capable of fitting the majority of the data produced by the RPPA following Zoledronate withdrawal on the first attempt. However a number of observables could not be fitted with the current model topology. These included PTEN, PDK1 and 4E-BP1, whilst it was possible to obtain a fit for both PTEN and PDK1 for the starvation-restimulation MRC5 dataset this was not possible for either the Rapamycin withdrawal or Zoledronate withdrawal datasets. The regulation of PTEN has yet to be fully elucidated and therefore the defining of extra regulatory reactions for this protein and its relationship with the mTOR network would be better suited to an individual project. Whilst the reactions governing PDK1 activation have previously been defined, how this regulation is affected by Rapamycin and Zoledronate treatment has yet to be investigated [51]. Possibly the most interesting observation regarding the kinetics of Zoledronate withdrawal occurs in MSCs with an increase in phosphorylation of ACC_pS79 observed. This occurs over the same time frame as the transient peak observed in response to starvation-restimulation in MRC5 cells. Given the finding that the phosphorylation of ACC_pS79 does not increase following starvation-restimulation or Rapamycin withdrawal in MSCs and the relative importance of AMPK signalling in MSC proliferation and differentiation this finding is very surprising. When the remainder of the observables assayed were compared across treatments the reaction of the mTOR network in MSCs was similar with the exception of ACC_pS79. This suggests that whilst Zoledronate treatment and withdrawal exerts a similar response by the mTOR network to all three treatments this is not the case with the AMPK network.

Indeed recent research has suggested that prenylation of LKB1, a primary activator of AMPK affects its localisation within the cell [255]. It is as yet unknown whether or not the prenylation inhibition affects the activity of LKB1. Whilst research has been carried out investigating the role of AMPK in bone metabolism this does not appear to include the research into the effect of bisphosphonates on AMPK activation.

7.2.5 Imagestream

The ability of imagestream flow cytometry to analyse cellular localisation and to produce data capable of calibrating a dynamic model has been explored throughout the work presented here. The data collected showed that this methodology is an extremely powerful tool capable of analysing in detail the cellular localisation of proteins within the cell. Whilst the result obtained in this work did not show co-localisation for either of the protein analysed this is likely due to the need to refine the experimental process. Indeed FOXO3A localisation has previously been measured successfully using this technology [256]. This suggests that it would be possible to refine and optimise the protocols used throughout this work in order to successfully measure FOXO3A nuclear localisation. Whilst Rheb was also assayed for each treatment it localisation was not expected to be altered by either starvation-restimulation of Rapamycin treatment. The lack of correlation with the lysosomal marker LAMP1 prior to Zoledronate treatment suggests possible non-specific binding form the antibody used. Imagestream flow cytometry whilst a very powerful analysis tool presents a number of difficulties which need to be overcome in order for this technology to become a frequently utilised tool in dynamic modelling. Aside from the problems discussed above there is also the difficulty in producing small time points required to observe fast acting signalling events. This is because cells a required to remain intact (as opposed to lysed for western blots or RPPA) throughout flow cytometry protocols. This raises the question of how to inhibit further signalling once a sample is removed for analysis. In this work cells were treated with ice cold PBS and culture medium in order to overcome this problem however due to this smaller time points were not attempted. Due to the reasons discussed above it has not proved possible to validate imagestream flow cytometry as a methodology for producing time course data required for the calibration of dynamic models although this may prove possible with further analysis.

7.3 Limitations and future study

7.3.1 Technical

Throughout this work a number of technical challenges arose particularly concerning generation of time course calibration data. The RPPA has proved successful with regards to generating the large amount of time course data required for this work. It is however a relatively new and largely untested technology in field of systems biology and dynamic modelling. As such in addition to performing assays of proteins which currently cannot be measured using RPPA such as P70S6K and TSC2_ pT1462 it will also be necessary to perform validation experiments confirming the findings present above. Of particular interest is the response of ACC_pS79 to Zoledronate withdrawal. As recent research has shown that the AMPK activator LKB1 possesses a post translation farnesylation modification the activation of AMPK may not only be of biological interest but also could serve as a read-out of protein prenylation in Zoledronate treated cells. One of the key findings of this work was that the response of ACC_pS79 to both serum starvation-restimulation in MRC5 cells and in response to Zoledronate withdrawal is very similar. This however appears to be controlled through two distinct mechanisms with amino acids acting activate AMPK in MRC5 cells upon restimulation and with the re-prenylation of LKB1 in MSCs following Zoledronate withdrawal. Further investigation of these mechanisms and in particular how they affect by bisphosphonate treatment will be of primary importance in further work. The lack of this response in MRC5 cells following Zoledronate withdrawal is interesting. As it did not prove possible to confirm de-prenylation using imagestream flow cytometry it will be necessary to confirm this by western blots in MRC5 cells.

In addition to RPPA the work presented here also attempted to utilise flow cytometry as an alternative to western blotting. This proved only partially successful when using a standard flow cytometer. In addition to this there were a number of technical limitations associated with this technology which could not be overcome. When producing time course data it is of utmost importance to prevent further cell signalling from taking place after the designated time point. Whilst in Western blotting and RPPA this achieved by the use of a lysis buffer in flow cytometry it is required that the cells remain intact throughout the process. It was therefore necessary to attempt to inhibit cell signalling by carrying out the flow cytometry procedure at ice cold temperatures. As the flow cytometry procedure used here prior to cell fixation took between 10-15 minutes

depending upon sample numbers an argument can be made that that cellular signalling could still be occurring during this period. Therefore the data collected would not be representative of the time points being analysed.

The primary focus of the Imagestream flow cytometry was to investigate the cellular localisation of both FOXO3A and Rheb in response to each treatment. Whilst the analysis of intracellular localisation proved possible further refinement is required in order to analyse if time course data can be produced using this methodology. As such further optimisation should be performed analysing the localisation of total FOXO3A and investigating alternative antibodies for Rheb and possibly Ras.

7.3.2 Computational

The work presented above was ideally suited to an integrated computational modelling study. Indeed without this approach it would not have proved possible to identify a number of key sections within the mTOR network in response to each treatment. The modelling approach above is one that has been used on a number of previous investigations by our group [171, 172, 203, 233]. There were however two key changes presented here compared to previous work, 1) the model topology could only undergo minor changes between treatments and this therefore meant that, 2) data was removed from datasets to identify key areas within the network topology. Due to time constraints and the time required to produce data for each treatment, it was necessary to carry out the computational modelling work for each treatment individually. This therefore meant that once the network topology was in place it could only undergo minor changes with these usually relating to initial concentrations representing the changes between each treatment. An alternative methodology which could be used in future studies would be to attempt to fit all the data presented here for each cell type in one model. This would require presenting the model with all three datasets representing each treatment and performing parameter estimations. It may therefore be possible to identify a single parameter set capable of fitting the restimulation data for each treatment in both cell types.

Throughout this work the python package Pycotools was used to analyse the data obtained from the parameter estimations in Copasi. In chapter 6 an updated version of this package was available and proved capable of providing in depth analysis of the parameter estimations obtained in response to Zoledronate withdrawal. The work

presented in this chapter displays only a small number of analysis tools available within this package. It would be interesting to apply these analysis techniques to the data obtained in chapters 4 and 5. In addition at present the Pycotools package is still in the development phase and in future a number of other analysis tools are expected to be available including sensitivity analysis and identifiability which could be used to analyse the parameter estimations presented in chapters 4, 5 and 6.

7.3.3 Biological

The network used throughout this work represents an abstracted version of the mTOR network and is by no means a complete representation of this network. Indeed there are a number of signalling networks associated with the mTOR network not described here of which three are of particular interest given the findings above. These include the DNA damage response, MSC proliferation and differentiation and the process of autophagy. Initial work on this project included the building and refining of both a DNA damage response (DDR) network adapted from Procter et al 2008 and a model of MSC differentiation (osteogenesis) [134, 257, 258].

The relationship between Zoledronate treatment and the DNA damage repair mechanisms and how these relate to decreased mortality and lifespan extension have only broadly been explored [82, 118, 124]. However this area is coming under increased scrutiny as researchers investigate the repurposing of pharmaceuticals already available to patients. Given the connections between the mTOR network and the DDR described in section 1.5.2 and the findings that Zoledronate inhibits the mTOR network and its withdrawal in MSCs elicits a similar response in AMPK signalling to that observed for starvation-restimulation in MRC5 cells, this warrants future work into the connections between Zoledronate treatment and the DDR. The work presented here would provide the framework for this to be carried out. As already stated a DDR module has already been defined using a previously published model and connected into the model used throughout this work. It would be possible to simulate the predicted response to DNA damage for each treatment and cell type using the calibrated model described above. This could then be tested against experimental data produced using RPPA with irradiation used to induce DNA damage following each treatment and time course produced in the same manner as above. Model predictions could then be compared to the experimental data allowing for the evaluation of the models ability to fit the DDR data.

Zoledronate treatment is only prescribed to patients that have already developed osteoporosis with the aim of inhibiting bone resorption. This however only acts to bring bone resorption and bone formation back into balance and one of the primary aims of osteoporosis research is how to maintain bone formation whilst preventing bone resorption with age. Whilst this was not a primary aim of this work it was something which was discussed and a differentiation network was developed with this aim in mind. The mTOR network has a number of functions one of which is cellular growth. As Zoledronate inhibits mTOR signalling this also inhibits cellular growth, proliferation and differentiation. Linking the mTOR model discussed throughout this work with a model of proliferation/differentiation would allow for the analysis of how each treatment in MSCs affects the differentiation process. As with the DDR experimental data could then be collected using RPPA to examine if the model is capable of reproducing the cellular response of MSCs during differentiation following each of the treatments discussed above.

7.4 Research impact

The impact of this research on ageing lies primarily in its focus on the mTOR network. How this network is regulated and how this regulation changes with age is one of the primary focuses of ageing research. The aim of this work was to build upon previous work exploring the interconnection of three separate life extending treatments with the mTOR network and to explore how the response observed in the mTOR network differs between each treatment. It has proved possible to show an increase in AMPK signalling following serum-starvation which is consistent with previously published data. In addition this reaction was observed in MSCs following Zoledronate treatment. This is likely to be due the de-prenylation of LKB1 upstream of AMPK. This work has further highlighted the importance of AMPK signalling in ageing research with further work required to elucidate the important role that this protein plays in lifespan extension.

8. Bibliography

- 1. Rodríguez-Rodero, S., et al., *Aging Genetics and Aging*. Aging and Disease, 2011. **2**(3): p. 186-195.
- 2. Bloom, D.E., D. Canning, and G. Fink, *Implications of population ageing for economic growth*. Oxford Review of Economic Policy, 2010. **26**(4): p. 583-612.
- 3. Weinert, B.T. and P.S. Timiras, *Invited Review: Theories of aging.* Journal of Applied Physiology, 2003. **95**(4): p. 1706-1716.
- 4. Smith, M.A., et al., *Radical AGEing in Alzheimer's disease.* Trends in Neurosciences, 1995. **18**(4): p. 172-176.
- 5. Campisi, J., *Cancer and ageing: rival demons?* Nature Reviews Cancer, 2003. **3**: p. 339.
- 6. Longo Valter, D., et al., *Interventions to Slow Aging in Humans: Are We Ready?* Aging Cell, 2015. **14**(4): p. 497-510.
- 7. Kenyon, C.J., *The genetics of ageing.* Nature, 2010. **464**(7288): p. 504-512.
- 8. Lewis, K.N., N.D. Rubinstein, and R. Buffenstein, A window into extreme longevity; the circulating metabolomic signature of the naked mole-rat, a mammal that shows negligible senescence. GeroScience, 2018.
- 9. Hulbert, A.J., et al., *Life and Death: Metabolic Rate, Membrane Composition, and Life Span of Animals.* Physiological Reviews, 2007. **87**(4): p. 1175-1213.
- 10. Kirkwood, T.B.L. and S.N. Austad, *Why do we age?* Nature, 2000. **408**(6809): p. 233-238.
- 11. Kirkwood, T.B.L., *Evolution of ageing*. Nature, 1977. **270**(5635): p. 301-304.
- 12. Weismann, A., E.B. Poulton, and A.E. Shipley, *Essays upon heredity and kindred biological problems*. Vol. 1. 1891: Clarendon press.
- 13. Gavrilov, L.A. and N.S. Gavrilova, *Evolutionary Theories of Aging and Longevity.* TheScientificWorldJOURNAL, 2002. **2**.
- 14. Kirkwood, T.B.L., *New science for an old problem.* Trends in Genetics, 2002. **18**(9): p. 441-442.
- 15. Kowald, A. and T.B.L. Kirkwood, *Can aging be programmed? A critical literature review.* Aging Cell, 2016. **15**(6): p. 986-998.
- 16. Hill, K., et al., *Mortality rates among wild chimpanzees*. Journal of Human Evolution, 2001. **40**(5): p. 437-450.
- 17. Medawar, P.B., *An unsolved problem of biology. 1952.* HK Lewis & Co., London, 1957.
- 18. Walker, F.O., *Huntington's disease*. The Lancet, 2007. **369**(9557): p. 218-228.
- 19. Williams, G.C., *Pleiotropy, Natural Selection, and the Evolution of Senescence.* Evolution, 1957. **11**(4): p. 398-411.
- 20. Kirkwood, T.B., Evolution of ageing. Nature, 1977. 270.
- 21. Phelan, J.P. and S.N. Austad, *Natural selection, dietary restriction, and extended longevity*. 1988.
- 22. Berry, R.J. and F.H. Bronson, *Life history and bioeconomy of the house mouse.* Biological Reviews, 1992. **67**(4): p. 519-550.
- 23. Kirkwood, T.B.L., *Understanding the odd science of aging.* Cell, 2005. **120**(4): p. 437-447.
- 24. Reznick, D., et al., *The evolution of senescence in natural populations of guppies* (*Poecilia reticulata*): a comparative approach. Experimental Gerontology, 2001. **36**(4): p. 791-812.
- 25. Reznick, D.N., et al., *Effect of extrinsic mortality on the evolution of senescence in guppies.* Nature, 2004. **431**: p. 1095.
- 26. Bryant, Michael J. and D. Reznick, *Comparative Studies of Senescence in Natural Populations of Guppies*. The American Naturalist, 2004. **163**(1): p. 55-68.
- 27. Soto, A.M. and C. Sonnenschein, *The somatic mutation theory of cancer: growing problems with the paradigm?* BioEssays, 2004. **26**(10): p. 1097-1107.

- 28. Shammas, M.A., *Telomeres, lifestyle, cancer, and aging*. Current Opinion in Clinical Nutrition and Metabolic Care, 2011. **14**(1): p. 28-34.
- 29. Epel, E.S., et al., *Accelerated telomere shortening in response to life stress.* Proceedings of the National Academy of Sciences of the United States of America, 2004. **101**(49): p. 17312-17315.
- 30. Von Zglinicki, T., *Role of Oxidative Stress in Telomere Length Regulation and Replicative Senescence*. Annals of the New York Academy of Sciences, 2000. **908**(1): p. 99-110.
- 31. Evans, A. and N. Neuman, *The Mighty Mitochondria*. Trends in Biochemical Sciences. **41**(3): p. 205-206.
- 32. Passos, J.F., T. von Zglinicki, and T.B.L. Kirkwood, *Mitochondria and ageing: winning and losing in the numbers game*. BioEssays, 2007. **29**(9): p. 908-917.
- 33. Gallage, S. and J. Gil, *Mitochondrial Dysfunction Meets Senescence*. Trends in Biochemical Sciences, 2016. **41**(3): p. 207-209.
- 34. Green, D.R., L. Galluzzi, and G. Kroemer, *Mitochondria and the Autophagy–Inflammation–Cell Death Axis in Organismal Aging.* Science, 2011. **333**(6046): p. 1109.
- 35. López-Otín, C., et al., *The Hallmarks of Aging*. Cell, 2013. **153**(6): p. 1194-1217.
- 36. Rossi, D.J., C.H.M. Jamieson, and I.L. Weissman, *Stems Cells and the Pathways to Aging and Cancer.* Cell. **132**(4): p. 681-696.
- 37. Li, Z., et al., *Impaired DNA double-strand break repair contributes to the age-associated rise of genomic instability in humans.* Cell Death Differ, 2016. **23**(11): p. 1765-1777.
- 38. Chandel, N.S., et al., *Metabolic regulation of stem cell function in tissue homeostasis and organismal ageing.* Nat Cell Biol, 2016. **18**(8): p. 823-832.
- 39. Branicky, R. and S. Hekimi, *Proteostasis or Aging: Let the CHIPs Fall Where They May.* Developmental Cell, 2017. **41**(2): p. 126-128.
- 40. Ben-Zvi, A., E.A. Miller, and R.I. Morimoto, *Collapse of proteostasis represents an early molecular event in Caenorhabditis elegans aging.* Proceedings of the National Academy of Sciences, 2009.
- 41. Bar-Peled, L. and D.M. Sabatini, *Regulation of mTORC1 by amino acids*. Trends in Cell Biology, 2014. **24**(7): p. 400-406.
- 42. Laplante, M. and David M. Sabatini, *mTOR Signaling in Growth Control and Disease*. Cell, 2012. **149**(2): p. 274-293.
- 43. Vadlakonda, L., et al., *The paradox of Akt -mTOR interactions*. Frontiers in Oncology, 2013 **3**
- 44. Haar, E.V., et al., *Insulin signalling to mTOR mediated by the Akt/PKB substrate PRAS40.* Nat Cell Biol, 2007. **9**(3): p. 316-323.
- 45. Shamji, A.F., P. Nghiem, and S.L. Schreiber, *Integration of Growth Factor and Nutrient Signaling: Implications for Cancer Biology.* Molecular Cell, 2003. **12**(2): p. 271-280.
- 46. Luo, J., B.D. Manning, and L.C. Cantley, *Targeting the PI3K-Akt pathway in human cancer: Rationale and promise.* Cancer Cell, 2003. **4**(4): p. 257-262.
- 47. Lam, K., et al., *The phosphatidylinositol 3-kinase serine kinase phosphorylates IRS-1. Stimulation by insulin and inhibition by Wortmannin.* Journal of Biological Chemistry, 1994. **269**(32): p. 20648-52.
- 48. Akinleye, A., et al., *Phosphatidylinositol 3-kinase (PI3K) inhibitors as cancer therapeutics*. Journal of Hematology & Oncology, 2013. **6**(1): p. 88.
- 49. Mora, A., et al., *PDK1*, the master regulator of AGC kinase signal transduction. Seminars in Cell & Developmental Biology, 2004. **15**(2): p. 161-170.
- 50. Stephens, L., et al., *Protein Kinase B Kinases That Mediate Phosphatidylinositol 3,4,5-Trisphosphate-Dependent Activation of Protein Kinase B.* Science, 1998. **279**(5351): p. 710-714.
- 51. Calleja, V., et al., *Acute regulation of PDK1 by a complex interplay of molecular switches.* Biochem Soc Trans, 2014. **42**(5): p. 1435-40.

- 52. Huang, J., et al., *The TSC1-TSC2 Complex Is Required for Proper Activation of mTOR Complex 2.* Molecular and Cellular Biology, 2008. **28**(12): p. 4104-4115.
- 53. Inoki, K., et al., *TSC2 Integrates Wnt and Energy Signals via a Coordinated Phosphorylation by AMPK and GSK3 to Regulate Cell Growth.* Cell, 2006. **126**(5): p. 955-968.
- 54. Marshall, C.B., et al., Characterization of the Intrinsic and TSC2-GAP-Regulated GTPase Activity of Rheb by Real-Time NMR. Sci. Signal., 2009. **2**(55): p. ra3-.
- Martin, T.D., et al., Ral and Rheb GTPase activating proteins integrate mTOR and GTPase signaling in aging, autophagy, and tumor cell invasion. Mol Cell, 2014. **53**(2): p. 209-20.
- 56. Bai, X., et al., *Rheb Activates mTOR by Antagonizing Its Endogenous Inhibitor, FKBP38.* Science, 2007. **318**(5852): p. 977-980.
- 57. Alain, T., et al., eIF4E/4E-BP Ratio Predicts the Efficacy of mTOR Targeted Therapies. Cancer Research, 2012. **72**(24): p. 6468-6476.
- 58. Menon, S., et al., Spatial Control of the TSC Complex Integrates Insulin and Nutrient Regulation of mTORC1 at the Lysosome. Cell, 2014. **156**(4): p. 771-785.
- 59. Hsieh, C.-T., et al., *Ceramide inhibits insulin-stimulated Akt phosphorylation through activation of Rheb/mTORC1/S6K signaling in skeletal muscle*. Cellular Signalling, 2014. **26**(7): p. 1400-1408.
- 50. Zhang, J., et al., S6K Directly Phosphorylates IRS-1 on Ser-270 to Promote Insulin Resistance in Response to TNF- α Signaling through IKK2. Journal of Biological Chemistry, 2008. **283**(51): p. 35375-35382.
- 61. Hara, K., et al., Amino Acid Sufficiency and mTOR Regulate p70 S6 Kinase and eIF-4E BP1 through a Common Effector Mechanism. Journal of Biological Chemistry, 1998. **273**(23): p. 14484-14494.
- 62. Wang, X., et al., *Amino acid availability regulates p70 S6 kinase and multiple translation factors.* Biochem J, 1998. **334 (Pt 1)**: p. 261-7.
- 63. Sancak, Y., et al., *The Rag GTPases Bind Raptor and Mediate Amino Acid Signaling to mTORC1*. Science, 2008. **320**(5882): p. 1496-1501.
- 64. Kim, E., et al., Regulation of TORC1 by Rag GTPases in nutrient response. Nat Cell Biol, 2008. **10**(8): p. 935-945.
- 65. Bar-Peled, L., et al., Ragulator Is a GEF for the Rag GTPases that Signal Amino Acid Levels to mTORC1. Cell, 2012. **150**(6): p. 1196-1208.
- 66. Sancak, Y., et al., Ragulator-Rag Complex Targets mTORC1 to the Lysosomal Surface and Is Necessary for Its Activation by Amino Acids. Cell, 2010. **141**(2): p. 290-303.
- 67. Forgac, M., Vacuolar ATPases: rotary proton pumps in physiology and pathophysiology. Nat Rev Mol Cell Biol, 2007. **8**(11): p. 917-929.
- 68. Bar-Peled, L., et al., A Tumor Suppressor Complex with GAP Activity for the Rag GTPases That Signal Amino Acid Sufficiency to mTORC1. Science, 2013. **340**(6136): p. 1100-1106.
- 69. Panchaud, N., M.-P. Péli-Gulli, and C. De Virgilio, *Amino Acid Deprivation Inhibits TORC1 Through a GTPase-Activating Protein Complex for the Rag Family GTPase Gtr1*. Vol. 6. 2013. ra42-ra42.
- 70. Shimobayashi, M. and M.N. Hall, *Making new contacts: the mTOR network in metabolism and signalling crosstalk.* Nat Rev Mol Cell Biol, 2014. **15**(3): p. 155-162.
- 71. Beauchamp, E.M. and L.C. Platanias, *The evolution of the TOR pathway and its role in cancer*. Oncogene, 2013. **32**(34): p. 3923-3932.
- 72. Sarbassov, D.D., et al., *Prolonged Rapamycin Treatment Inhibits mTORC2 Assembly and Akt/PKB*. Molecular Cell, 2006. **22**(2): p. 159-168.
- 73. Jacinto, E., et al., *Mammalian TOR complex 2 controls the actin cytoskeleton and is rapamycin insensitive*. Nat Cell Biol, 2004. **6**(11): p. 1122-1128.

- 74. Zinzalla, V., et al., *Activation of mTORC2 by Association with the Ribosome*. Cell, 2011. **144**(5): p. 757-768.
- 75. Betz, C. and M.N. Hall, *Where is mTOR and what is it doing there?* The Journal of Cell Biology, 2013. **203**(4): p. 563-574.
- 76. Hagiwara, A., et al., *Hepatic mTORC2 Activates Glycolysis and Lipogenesis through Akt, Glucokinase, and SREBP1c.* Cell Metabolism, 2012. **15**(5): p. 725-738.
- 77. Sarbassov, D.D., et al., *Phosphorylation and Regulation of Akt/PKB by the Rictor-mTOR Complex.* Science, 2005. **307**(5712): p. 1098-1101.
- 78. Mizunuma, M., et al., *mTORC2-SGK-1* acts in two environmentally responsive pathways with opposing effects on longevity. Aging Cell, 2014. **13**(5): p. 869-878.
- 79. Liu, P., et al., Sin1 phosphorylation impairs mTORC2 complex integrity and inhibits downstream Akt signalling to suppress tumorigenesis. Nat Cell Biol, 2013. **15**(11): p. 1340-1350.
- 80. Dalle Pezze, P., et al., A dynamic network model of mTOR signaling reveals TSC-independent mTORC2 regulation. Sci Signal, 2012. **5**.
- 81. Kaeberlein, M., *mTOR Inhibition: From Aging to Autism and Beyond.* Scientifica (Cairo), 2013. **2013**: p. 849186.
- 82. Misra, J., et al., *Zoledronate Attenuates Accumulation of DNA Damage in Mesenchymal Stem Cells and Protects Their Function.* Stem Cells (Dayton, Ohio), 2016. **34**(3): p. 756-767.
- 83. Cornu, M., V. Albert, and M.N. Hall, *mTOR in aging, metabolism, and cancer.* Current Opinion in Genetics & Development, 2013. **23**(1): p. 53-62.
- 84. Carlson, M.E. and I.M. Conboy, Loss of stem cell regenerative capacity within aged niches. Aging Cell, 2007. **6**(3): p. 371-82.
- 85. Sharpless, N.E. and R.A. DePinho, *How stem cells age and why this makes us grow old.* Nat Rev Mol Cell Biol, 2007. **8**(9): p. 703-713.
- 86. Armstrong, L., et al., *Concise Review: The Epigenetic Contribution to Stem Cell Ageing: Can We Rejuvenate Our Older Cells?* STEM CELLS, 2014. **32**(9): p. 2291-2298.
- 87. Bentzinger, C.F. and M.A. Rudnicki, *Rejuvenating aged muscle stem cells.* Nat Med, 2014. **20**(3): p. 234-235.
- 88. Rossi, D.J., et al., *Cell intrinsic alterations underlie hematopoietic stem cell aging.* Proceedings of the National Academy of Sciences of the United States of America, 2005. **102**(26): p. 9194-9199.
- 89. Rossi, D.J., et al., *Deficiencies in DNA damage repair limit the function of haematopoietic stem cells with age.* Nature, 2007. **447**(7145): p. 725-729.
- 90. Le Grand, F. and M.A. Rudnicki, *Skeletal muscle satellite cells and adult myogenesis*. Current Opinion in Cell Biology, 2007. **19**(6): p. 628-633.
- 91. Zhou, S., et al., *Age-related intrinsic changes in human bone-marrow-derived mesenchymal stem cells and their differentiation to osteoblasts*. Aging Cell, 2008. **7**(3): p. 335-343.
- 92. Naylor, K. and R. Eastell, *Bone turnover markers: use in osteoporosis.* Nat Rev Rheumatol, 2012. **8**(7): p. 379-389.
- 93. Rosen, C.J. and M.L. Bouxsein, *Mechanisms of Disease: is osteoporosis the obesity of bone?* Nat Clin Pract Rheum, 2006. **2**(1): p. 35-43.
- 94. Kawai, M., F.J.A. de Paula, and C.J. Rosen, *New insights into osteoporosis: the bone–fat connection.* Journal of Internal Medicine, 2012. **272**(4): p. 317-329.
- 95. Smink, J.J. and A. Leutz, *Instruction of mesenchymal cell fate by the transcription factor C/EBP6*. Gene, 2012. **497**(1): p. 10-17.
- 96. Kim, E.-K., et al., *Human mesenchymal stem cell differentiation to the osteogenic or adipogenic lineage is regulated by AMP-activated protein kinase.* Journal of Cellular Physiology, 2012. **227**(4): p. 1680-1687.

- 97. Fakhry, M., et al., *Molecular mechanisms of mesenchymal stem cell differentiation towards osteoblasts.* World J Stem Cells, 2013. **5**(4): p. 136-48.
- 98. Pantovic, A., et al., Coordinated time-dependent modulation of AMPK/Akt/mTOR signaling and autophagy controls osteogenic differentiation of human mesenchymal stem cells. Bone, 2013. **52**(1): p. 524-531.
- 99. Reid, I.R., *Osteoporosis treatment: Focus on safety.* European Journal of Internal Medicine, 2013. **24**(8): p. 691-697.
- 100. Rachner, T.D., S. Khosla, and L.C. Hofbauer, *Osteoporosis: now and the future.* The Lancet, 2011. **377**(9773): p. 1276-1287.
- 101. Antonio Herrera, A.L.-E., Jesús Mateo, Jorge Gil, Elena Ibarz and Luis Gracia., *Male osteoporosis: A review*. World J Orthop, 2012. **12**(3): p. 223-234.
- 102. Makridis, K.G., et al., The effect of osteoporotic treatment on the functional outcome, re-fracture rate, quality of life and mortality in patients with hip fractures: A prospective functional and clinical outcome study on 520 patients. Injury, 2015. **46**(2): p. 378-383.
- 103. Mobasheri, A., *The Future of Osteoarthritis Therapeutics: Targeted Pharmacological Therapy.* Current Rheumatology Reports, 2013. **15**(10): p. 1-13.
- 104. Dominguez, L., et al., *Physiology of the aging bone and mechanisms of action of bisphosphonates*. Biogerontology, 2011. **12**(5): p. 397-408.
- 105. Jobke, B., et al., Bisphosphonate-osteoclasts: Changes in osteoclast morphology and function induced by antiresorptive nitrogen-containing bisphosphonate treatment in osteoporosis patients. Bone, 2014. **59**(0): p. 37-43.
- 106. Eriksen, E.F., A. Díez-Pérez, and S. Boonen, *Update on long-term treatment with bisphosphonates for postmenopausal osteoporosis: A systematic review.* Bone, 2014. **58**(0): p. 126-135.
- 107. Dunford, J.E., et al., *Inhibition of Protein Prenylation by Bisphosphonates Causes Sustained Activation of Rac, Cdc42, and Rho GTPases.* Journal of Bone and Mineral Research, 2006. **21**(5): p. 684-694.
- 108. Berndt, N., A.D. Hamilton, and S.M. Sebti, *Targeting protein prenylation for cancer therapy*. Nat Rev Cancer, 2011. **11**(11): p. 775-791.
- 109. Kimmel, D.B., *Mechanism of Action, Pharmacokinetic and Pharmacodynamic Profile, and Clinical Applications of Nitrogen-containing Bisphosphonates.* Journal of Dental Research, 2007. **86**(11): p. 1022-1033.
- 110. Alakangas, A., et al., *Alendronate Disturbs Vesicular Trafficking in Osteoclasts*. Calcified Tissue International, 2002. **70**(1): p. 40-47.
- 111. Pavlos, N.J., et al., *Rab3D Regulates a Novel Vesicular Trafficking Pathway That Is Required for Osteoclastic Bone Resorption.* Molecular and Cellular Biology, 2005. **25**(12): p. 5253-5269.
- 112. Yoshida, T., et al., Geranylgeranyl-pyrophosphate (GGPP) synthase is down-regulated during differentiation of osteoblastic cell line MC3T3M-E1. Febs Letters, 2006. **580**(22): p. 5203-5207.
- 113. Yoshida, T., et al., Geranylgeranyl pyrophosphate (GGPP) and its synthase (GGPPS) promote proliferation but impair differentiation in mouse pre-osteoblastic MC3T3-E1 cells. Endocrine Journal, 2010. **57**: p. S486-S486.
- 114. Asanuma, M., et al., Supply of geranylgeranyl pyrophosphate (GGPP) by GGPP synthase is critical to control proliferation and differentiation in osteoblast cell line, MC3T3-E1 cells. Journal of Pharmacological Sciences, 2003. **91**: p. 164p-164p.
- 115. Kavanagh, K.L., et al., *The molecular mechanism of nitrogen-containing bisphosphonates as antiosteoporosis drugs.* Proceedings of the National Academy of Sciences, 2006. **103**(20): p. 7829-7834.

- 116. Basso, F.G., et al., *Zoledronic Acid Inhibits Human Osteoblast Activities*. Gerontology, 2013. **59**(6): p. 534-541.
- 117. Ibrahim, T., et al., *Cisplatin in combination with zoledronic acid: a synergistic effect in triple-negative breast cancer cell lines.* Int J Oncol, 2013. **42**(4): p. 1263-70.
- 118. Moriceau, G., et al., *Zoledronic Acid Potentiates mTOR Inhibition and Abolishes the Resistance of Osteosarcoma Cells to RAD001 (Everolimus): Pivotal Role of the Prenylation Process.* Cancer Research, 2010. **70**(24): p. 10329-10339.
- 119. Pearce, T., et al., Bone metastases from prostate, breast and multiple myeloma: differences in lesion conspicuity at short-tau inversion recovery and diffusion-weighted MRI. The British Journal of Radiology, 2012. **85**(1016): p. 1102-1106.
- 120. Espinoza, I., et al., *CCN1*, a Candidate Target for Zoledronic Acid Treatment in Breast Cancer. Molecular Cancer Therapeutics, 2011. **10**(5): p. 732-741.
- 121. Lyles, K.W., et al., *Zoledronic Acid and Clinical Fractures and Mortality after Hip Fracture*. New England Journal of Medicine, 2007. **357**(18): p. 1799-1809.
- 122. Wolfe, F., et al., *Bisphosphonate use is associated with reduced risk of myocardial infarction in patients with rheumatoid arthritis.* Journal of Bone and Mineral Research, 2013. **28**(5): p. 984-991.
- 123. Center, J.R., et al., *Osteoporosis Medication and Reduced Mortality Risk in Elderly Women and Men.* The Journal of Clinical Endocrinology & Metabolism, 2011. **96**(4): p. 1006-1014
- 124. Varela, I., et al., Combined treatment with statins and aminobisphosphonates extends longevity in a mouse model of human premature aging. Nat Med, 2008. **14**(7): p. 767-772.
- 125. Chen, H., et al., *Role of SIRT1 and AMPK in mesenchymal stem cells differentiation*. Ageing Research Reviews, 2014. **13**(0): p. 55-64.
- 126. Kasai, T., et al., *Osteoblast differentiation is functionally associated with decreased AMP kinase activity.* Journal of Cellular Physiology, 2009. **221**(3): p. 740-749.
- 127. Calkhoven, C.F., C. Müller, and A. Leutz, *Translational control of C/EBPα and C/EBP6 isoform expression*. Genes & Development, 2000. **14**(15): p. 1920-1932.
- 128. Smink, J.J., et al., *Transcription factor C/EBP6 isoform ratio regulates osteoclastogenesis through MafB*. Vol. 28. 2009. 1769-1781.
- 129. Tominaga, H., et al., *CCAAT/Enhancer-binding Protein & Promotes Osteoblast Differentiation by Enhancing Runx2 Activity with ATF4*. Molecular Biology of the Cell, 2008. **19**(12): p. 5373-5386.
- 130. Gutierrez, S., et al., CCAAT/Enhancer-binding Proteins (C/EBP) θ and δ Activate Osteocalcin Gene Transcription and Synergize with Runx2 at the C/EBP Element to Regulate Bone-specific Expression. Journal of Biological Chemistry, 2002. **277**(2): p. 1316-1323.
- 131. Harding, H.P., et al., *An Integrated Stress Response Regulates Amino Acid Metabolism and Resistance to Oxidative Stress.* Molecular Cell, 2003. **11**(3): p. 619-633.
- 132. Grandy, R., et al., *The Ric-8B Gene Is Highly Expressed in Proliferating Preosteoblastic Cells and Downregulated during Osteoblast Differentiation in a SWI/SNF- and C/EBP6-Mediated Manner.* Molecular and Cellular Biology, 2011. **31**(14): p. 2997-3008.
- 133. Villagra, A., et al., Chromatin Remodeling and Transcriptional Activity of the Bone-specific Osteocalcin Gene Require CCAAT/Enhancer-binding Protein β-dependent Recruitment of SWI/SNF Activity. Journal of Biological Chemistry, 2006. **281**(32): p. 22695-22706.
- 134. Hata, K., et al., A CCAAT/Enhancer Binding Protein β Isoform, Liver-Enriched Inhibitory Protein, Regulates Commitment of Osteoblasts and Adipocytes. Molecular and Cellular Biology, 2005. **25**(5): p. 1971-1979.

- 135. Bae, E.J. and S.G. Kim, Enhanced CCAAT/Enhancer-Binding Protein β-Liver-Enriched Inhibitory Protein Production by Oltipraz, Which Accompanies CUG Repeat-Binding Protein-1 (CUGBP1) RNA-Binding Protein Activation, Leads to Inhibition of Preadipocyte Differentiation. Molecular Pharmacology, 2005. **68**(3): p. 660-669.
- 136. Byun, M.R., et al., *Canonical Wnt signalling activates TAZ through PP1A during osteogenic differentiation*. Cell Death Differ, 2014. **21**(6): p. 854-863.
- 137. Clevers, H., K.M. Loh, and R. Nusse, *An integral program for tissue renewal and regeneration: Wnt signaling and stem cell control.* Science, 2014. **346**(6205).
- 138. Bennett, C.N., et al., *Regulation of osteoblastogenesis and bone mass by Wnt10b.* Proceedings of the National Academy of Sciences of the United States of America, 2005. **102**(9): p. 3324-3329.
- 139. Morvan, F., et al., Deletion of a Single Allele of the Dkk1 Gene Leads to an Increase in Bone Formation and Bone Mass. Journal of Bone and Mineral Research, 2006. **21**(6): p. 934-945.
- 140. Kang, S., et al., Wnt Signaling Stimulates Osteoblastogenesis of Mesenchymal Precursors by Suppressing CCAAT/Enhancer-binding Protein α and Peroxisome Proliferator-activated Receptor γ. Journal of Biological Chemistry, 2007. **282**(19): p. 14515-14524.
- 141. Garinis, G.A., et al., *DNA damage and ageing: new-age ideas for an age-old problem.*Nat Cell Biol, 2008. **10**(11): p. 1241-1247.
- 142. Papaioannou, T.G., et al., *Arterial ageing: Major nutritional and life-style effects*. Ageing Research Reviews, 2017. **37**(Supplement C): p. 162-163.
- 143. Bousquet, P.A., et al., *Abstract 1782: Reactive oxygen species (ROS) and mitochondrial DNA (mtDNA) damage in tumor hypoxia, poor radiotherapy response, and metastatic progression of rectal cancer.* Cancer Research, 2017. **77**(13 Supplement): p. 1782-1782.
- 144. Heydari, A.R., et al., *Caloric restriction and genomic stability*. Nucleic Acids Research, 2007. **35**(22): p. 7485-7496.
- 145. Guo, Z., et al., Effects of age and food restriction on oxidative DNA damage and antioxidant enzyme activities in the mouse aorta. Mechanisms of Ageing and Development, 2001. **122**(15): p. 1771-1786.
- 146. Tran, H., et al., DNA Repair Pathway Stimulated by the Forkhead Transcription Factor FOXO3a Through the Gadd45 Protein. Science, 2002. **296**(5567): p. 530-534.
- 147. Chung, Y.M., et al., *FOXO3 signalling links ATM to the p53 apoptotic pathway following DNA damage.* Nat Commun, 2012. **3**: p. 1000.
- Hu, T., et al., Reprogramming ovarian and breast cancer cells into non-cancerous cells by low-dose metformin or SN-38 through FOXO3 activation. Sci. Rep., 2014. **4**.
- 149. Sulli, G., R. Di Micco, and F.d.A. di Fagagna, *Crosstalk between chromatin state and DNA damage response in cellular senescence and cancer.* Nature Reviews Cancer, 2012. **12**: p. 709.
- 150. Kitano, H., Systems Biology: A Brief Overview. Science, 2002. 295(5560): p. 1662-1664.
- 151. Kohl, P., et al., *Systems Biology: An Approach.* Clinical Pharmacology & Therapeutics, 2010. **88**(1): p. 25-33.
- 152. Bruggeman, F.J. and H.V. Westerhoff, *The nature of systems biology.* Trends in Microbiology, 2007. **15**(1): p. 45-50.
- 153. Westerhoff, H.V. and B.O. Palsson, *The evolution of molecular biology into systems biology.* Nature Biotechnology, 2004. **22**: p. 1249.
- 154. Werner, T., *Regulatory networks: Linking microarray data to systems biology.* Mechanisms of Ageing and Development, 2007. **128**(1): p. 168-172.
- 155. Kiyatkin, A., et al., SCAFFOLDING PROTEIN GAB1 SUSTAINS EPIDERMAL GROWTH FACTOR-INDUCED MITOGENIC AND SURVIVAL SIGNALING BY MULTIPLE POSITIVE FEEDBACK LOOPS. The Journal of biological chemistry, 2006. **281**(29): p. 19925-19938.

- 156. Bio-itworld.com, Horizons.
- 157. van Riel, N.A.W., *Dynamic modelling and analysis of biochemical networks:* mechanism-based models and model-based experiments. Briefings in Bioinformatics, 2006. **7**(4): p. 364-374.
- 158. Rodriguez-Fernandez, M., P. Mendes, and J.R. Banga, *A hybrid approach for efficient and robust parameter estimation in biochemical pathways.* Biosystems, 2006. **83**(2): p. 248-265.
- 159. DiStefano, J. and J.J. DiStefano, *Dynamic Systems Biology Modeling and Simulation*. 2013: Academic Press.
- 160. Hucka, M., et al., *The systems biology markup language (SBML): a medium for representation and exchange of biochemical network models.* Bioinformatics, 2003. **19**(4): p. 524-531.
- 161. Horn, F. and R. Jackson, *General mass action kinetics*. Archive for Rational Mechanics and Analysis, 1972. **47**(2): p. 81-116.
- 162. Hoops, S., et al., *COPASI—a COmplex PAthway Simulator*. Bioinformatics, 2006. **22**(24): p. 3067-3074.
- 163. Horstemeyer, M.F., *Multiscale Modeling: A Review*, in *Practical Aspects of Computational Chemistry: Methods, Concepts and Applications*, J. Leszczynski and M.K. Shukla, Editors. 2010, Springer Netherlands: Dordrecht. p. 87-135.
- 164. Brennan, T., M. Fink, and B. Rodriguez, *Multiscale modelling of drug-induced effects on cardiac electrophysiological activity.* European Journal of Pharmaceutical Sciences, 2009. **36**(1): p. 62-77.
- 165. Kitano, H., Computational systems biology. Nature, 2002. **420**(6912): p. 206-210.
- 166. Navlakha, S. and Z. Bar-Joseph, *Algorithms in nature: the convergence of systems biology and computational thinking.* Molecular Systems Biology, 2011. **7**(1).
- 167. Mendes, P., et al., *Computational modeling of biochemical networks using COPASI*. Methods Mol Biol, 2009. **500**.
- 168. Székely, T. and K. Burrage, *Stochastic simulation in systems biology*. Computational and Structural Biotechnology Journal, 2014. **12**(20-21): p. 14-25.
- 169. Le Novère, N., *Quantitative and logic modelling of molecular and gene networks.*Nature Reviews Genetics, 2015. **16**: p. 146.
- 170. Villaverde, A.F. and J.R. Banga, *Reverse engineering and identification in systems biology: strategies, perspectives and challenges.* Journal of The Royal Society Interface, 2014. **11**(91).
- 171. Sonntag, A.G., et al., A modelling–experimental approach reveals insulin receptor substrate (IRS)-dependent regulation of adenosine monosphosphate-dependent kinase (AMPK) by insulin. FEBS Journal, 2012. **279**(18): p. 3314-3328.
- 172. Dalle Pezze, P., et al., A systems study reveals concurrent activation of AMPK and mTOR by amino acids. 2016. **7**: p. 13254.
- 173. Smith, G.R. and D.P. Shanley, *Computational modelling of the regulation of Insulin signalling by oxidative stress.* BMC Systems Biology, 2013. **7**(1): p. 1-19.
- Jain, P. and U.S. Bhalla, Signaling logic of activity-triggered dendritic protein synthesis: an mTOR gate but not a feedback switch. PLoS Comput Biol, 2009. **5**.
- 175. Borisov, N., et al., Systems-level interactions between insulin-EGF networks amplify mitogenic signaling. Mol Syst Biol, 2009. **5**.
- 176. Caron, E., et al., *A comprehensive map of the mTOR signaling network*. Molecular Systems Biology, 2010. **6**(1).
- 177. Araujo, R.P., L.A. Liotta, and E.F. Petricoin, *Proteins, drug targets and the mechanisms they control: the simple truth about complex networks.* Nat Rev Drug Discov, 2007. **6**(11): p. 871-80.

- 178. Matsuoka, Y., et al., *Modeling and Simulation Using CellDesigner*, in *Transcription Factor Regulatory Networks: Methods and Protocols*, E. Miyamoto-Sato, et al., Editors. 2014, Springer New York: New York, NY. p. 121-145.
- 179. Novere, N.L., et al., *The Systems Biology Graphical Notation*. Nat Biotech, 2009. **27**(8): p. 735-741.
- 180. Peng, H., et al., A systematic modeling study on the pathogenic role of p38 MAPK activation in myelodysplastic syndromes. Molecular BioSystems, 2012. **8**(4): p. 1366-1374.
- 181. Volkmer, B. and M. Heinemann, *Condition-Dependent Cell Volume and Concentration of Escherichia coli to Facilitate Data Conversion for Systems Biology Modeling*. PLOS ONE, 2011. **6**(7): p. e23126.
- 182. and C.L. Paweletz CP, Bichsel VE, et al., Reverse phase protein microarrays which capture disease progression show activation of pro-survival pathways at the cancer invasion front. Oncogene., 2001. **20**(16): p. 1981–1989.
- 183. Creighton, C.J. and S. Huang, *Reverse phase protein arrays in signaling pathways: a data integration perspective.* Drug Design, Development and Therapy, 2015. **9**: p. 3519-3527.
- 184. Boellner, S. and K.-F. Becker, *Reverse Phase Protein Arrays—Quantitative Assessment of Multiple Biomarkers in Biopsies for Clinical Use.* Microarrays, 2015. **4**(2): p. 98-114.
- 185. Centre, M.A. MD Anderson Centre RPPA Core Facility.
- 186. Honda, K., et al., *Proteomic Approaches to the Discovery of Cancer Biomarkers for Early Detection and Personalized Medicine.* Japanese Journal of Clinical Oncology, 2013. **43**(2): p. 103-109.
- 187. Jameson, G.S., et al., A pilot study utilizing multi-omic molecular profiling to find potential targets and select individualized treatments for patients with previously treated metastatic breast cancer. Breast Cancer Research and Treatment, 2014. 147(3): p. 579-588.
- 188. Faratian, D., et al., Systems biology reveals new strategies for personalizing cancer medicine and confirms the role of PTEN in resistance to trastuzumab. Cancer Res, 2009.
- 189. Cosma, A., G. Nolan, and B. Gaudilliere, *Mass cytometry: The time to settle down.* Cytometry Part A, 2017. **91**(1): p. 12-13.
- 190. Blasi, T., et al., *Label-free cell cycle analysis for high-throughput imaging flow cytometry*. Nature Communications, 2016. **7**: p. 10256.
- 191. Patterson, J.O., M. Swaffer, and A. Filby, *An Imaging Flow Cytometry-based approach to analyse the fission yeast cell cycle in fixed cells.* Methods, 2015. **82**(Supplement C): p. 74-84.
- 192. Henson, M.A., *Dynamic modeling and control of yeast cell populations in continuous biochemical reactors.* Computers & Chemical Engineering, 2003. **27**(8): p. 1185-1199.
- 193. Chen, C., et al., *mTOR Regulation and Therapeutic Rejuvenation of Aging Hematopoietic Stem Cells.* Science signaling, 2009. **2**(98): p. ra75-ra75.
- 194. Delgoffe, G.M., et al., *The mTOR Kinase Differentially Regulates Effector and Regulatory T Cell Lineage Commitment*. Immunity, 2009. **30**(6): p. 832-844.
- 195. Tan, H., et al., A systems biology approach to studying the molecular mechanisms of osteoblastic differentiation under cytokine combination treatment. npj Regenerative Medicine, 2017. **2**(1): p. 5.
- 196. Kenyon, C., *The Plasticity of Aging: Insights from Long-Lived Mutants.* Cell, 2005. **120**(4): p. 449-460.
- 197. Johnson, S.C., P.S. Rabinovitch, and M. Kaeberlein, *mTOR is a key modulator of ageing and age-related disease*. Nature, 2013. **493**(7432): p. 338-345.

- 198. Zoncu, R., A. Efeyan, and D.M. Sabatini, *mTOR: from growth signal integration to cancer, diabetes and ageing.* Nat Rev Mol Cell Biol, 2011. **12**(1): p. 21-35.
- 199. Kenyon, C., et al., A C. elegans mutant that lives twice as long as wild type. Nature, 1993. **366**(6454): p. 461-464.
- 200. Blagosklonny, M.V., *Calorie restriction: Decelerating mTOR-driven aging from cells to organisms (including humans)*. Cell Cycle, 2010. **9**(4): p. 683-688.
- 201. Kim, Y.C. and K.-L. Guan, *mTOR: a pharmacologic target for autophagy regulation.* The Journal of Clinical Investigation, 2015. **125**(1): p. 25-32.
- 202. Salminen, A. and K. Kaarniranta, *Regulation of the aging process by autophagy*. Trends in Molecular Medicine, 2009. **15**(5): p. 217-224.
- 203. Dalle Pezze, P., et al., *Dynamic Modelling of Pathways to Cellular Senescence Reveals Strategies for Targeted Interventions.* PLoS Comput Biol, 2014. **10**(8): p. e1003728.
- 204. Hay, N., *Interplay between FOXO, TOR, and Akt.* Biochimica et biophysica acta, 2011. **1813**(11): p. 1965-1970.
- 205. Feehan, R.P. and L.M. Shantz, *Negative regulation of the FOXO3a transcription factor* by mTORC2 induces a pro-survival response following exposure to ultraviolet-B irradiation. Cellular Signalling, 2016. **28**(8): p. 798-809.
- 206. Acosta-Jaquez, H.A., et al., *Site-Specific mTOR Phosphorylation Promotes mTORC1-Mediated Signaling and Cell Growth.* Molecular and Cellular Biology, 2009. **29**(15): p. 4308-4324.
- 207. Herzig, S. and R.J. Shaw, *AMPK: guardian of metabolism and mitochondrial homeostasis.* Nature Reviews Molecular Cell Biology, 2017.
- 208. Kodiha, M., et al., Localization of AMP kinase is regulated by stress, cell density, and signaling through the MEK→ERK1/2 pathway. American Journal of Physiology Cell Physiology, 2007. 293(5): p. C1427-C1436.
- 209. Igarashi, M. and L. Guarente, *The unexpected role of mTORC1 in intestinal stem cells during calorie restriction*. Cell Cycle, 2017. **16**(1): p. 1-2.
- 210. Kahan, B.D., *Sirolimus: a comprehensive review.* Expert Opinion on Pharmacotherapy, 2001. **2**(11): p. 1903-1917.
- 211. Sehgal, S.N., H. Baker, and C. Vezina, *Rapamycin (AY-22,989), a new antifungal antibiotic. II. Fermentation, isolation and characterization.* J Antibiot (Tokyo), 1975. **28**(10): p. 727-32.
- 212. Douros, J. and M. Suffness, *New antitumor substances of natural origin.* Cancer Treatment Reviews, 1981. **8**(1): p. 63-87.
- 213. Seto, B., *Rapamycin and mTOR: a serendipitous discovery and implications for breast cancer.* Clinical and Translational Medicine, 2012. **1**(1): p. 29.
- 214. Huang, S. and P.J. Houghton, *Targeting mTOR signaling for cancer therapy.* Curr Opin Pharmacol, 2003. **3**.
- 215. Oldham, S., et al., *Genetic and biochemical characterization of dTOR, the Drosophila homolog of the target of rapamycin.* Genes Dev, 2000. **14**.
- 216. Vilella-Bach, M., et al., *The FKBP12-Rapamycin-binding Domain Is Required for FKBP12-Rapamycin-associated Protein Kinase Activity and G1 Progression*. Journal of Biological Chemistry, 1999. **274**(7): p. 4266-4272.
- 217. Miller, T.W., et al., Mutations in the phosphatidylinositol 3-kinase pathway: role in tumor progression and therapeutic implications in breast cancer. Breast Cancer Res, 2011. **13**.
- 218. Margariti, N., et al., "Overcoming breast cancer drug resistance with mTOR inhibitors". Could it be a myth or a real possibility in the short-term future? Breast Cancer Res Treat, 2011. **128**.
- 219. Rizzieri, D.A., et al., A Phase 2 Clinical Trial of Deforolimus (AP23573, MK-8669), a Novel Mammalian Target of Rapamycin Inhibitor, in Patients with Relapsed or

- Refractory Hematologic Malignancies. Clinical Cancer Research, 2008. **14**(9): p. 2756-2762.
- 220. Harrison, D.E., et al., *Rapamycin fed late in life extends lifespan in genetically heterogeneous mice*. Nature, 2009. **460**(7253): p. 392-5.
- 221. Li, J., Sang G. Kim, and J. Blenis, *Rapamycin: One Drug, Many Effects*. Cell Metabolism, 2014. **19**(3): p. 373-379.
- 222. Ehninger, D., F. Neff, and K. Xie, *Longevity, aging and rapamycin*. Cellular and Molecular Life Sciences, 2014. **71**(22): p. 4325-4346.
- 223. Bjedov, I., et al., *Mechanisms of Life Span Extension by Rapamycin in the Fruit Fly Drosophila melanogaster.* Cell Metabolism, 2010. **11**(1): p. 35-46.
- 224. Pazhanisamy, S.K., *Stem cells, DNA damage, ageing and cancer.* Hematology/Oncology and Stem Cell Therapy, 2009. **2**(3): p. 375-384.
- 225. Schuld, N.J., et al., *The Chaperone Protein SmgGDS Interacts with Small GTPases Entering the Prenylation Pathway by Recognizing the Last Amino Acid in the CAAX Motif.* Journal of Biological Chemistry, 2014. **289**(10): p. 6862-6876.
- 226. Senaratne, S.G., J.L. Mansi, and K.W. Colston, *The bisphosphonate zoledronic acid impairs membrane localisation and induces cytochrome c release in breast cancer cells.*Br J Cancer, 2002. **86**(9): p. 1479-1486.
- 227. Wagner, R.J., et al., Lovastatin induces VSMC differentiation through inhibition of Rheb and mTOR. American Journal of Physiology Cell Physiology, 2010. **299**(1): p. C119-C127.
- 228. Jiang, H. and P.K. Vogt, *Constitutively active Rheb induces oncogenic transformation*. Oncogene, 2008. **27**(43): p. 5729-5740.
- Tucci, P., Caloric restriction: is mammalian life extension linked to p53? Aging-Us, 2012. **4**(8): p. 525-534.
- 230. Yilmaz, O.H., et al., mTORC1 in the Paneth cell niche couples intestinal stem-cell function to calorie intake. Nature, 2012. **486**(7404): p. 490-U87.
- 231. Cerletti, M., et al., Short-Term Calorie Restriction Enhances Skeletal Muscle Stem Cell Function. Cell Stem Cell, 2012. **10**(5): p. 515-519.
- 232. Honjoh, S., et al., Signalling through RHEB-1 mediates intermittent fasting-induced longevity in C-elegans. Nature, 2009. **457**(7230): p. 726-U6.
- 233. Dalle Pezze, P., et al., A Dynamic Network Model of mTOR Signaling Reveals TSC-Independent mTORC2 Regulation. Sci. Signal., 2012. **5**(217): p. ra25-.
- 234. Durán, R.V. and M.N. Hall, Regulation of TOR by small GTPases. Vol. 13. 2012. 121-128.
- 235. Gan, X., et al., Evidence for Direct Activation of mTORC2 Kinase Activity by Phosphatidylinositol 3,4,5-Trisphosphate. Journal of Biological Chemistry, 2011. **286**(13): p. 10998-11002.
- 236. Lee, S., et al., *TOR Complex 2 Integrates Cell Movement during Chemotaxis and Signal Relay in Dictyostelium.* Molecular Biology of the Cell, 2005. **16**(10): p. 4572-4583.
- 237. Lee, S., et al., A Novel Ras-interacting Protein Required for Chemotaxis and Cyclic Adenosine Monophosphate Signal Relay inDictyostelium. Molecular Biology of the Cell, 1999. **10**(9): p. 2829-2845.
- 238. Hernández-Negrete, I., et al., *P-Rex1 Links Mammalian Target of Rapamycin Signaling to Rac Activation and Cell Migration*. Journal of Biological Chemistry, 2007. **282**(32): p. 23708-23715.
- 239. Saci, A., Lewis C. Cantley, and Christopher L. Carpenter, *Rac1 Regulates the Activity of mTORC1 and mTORC2 and Controls Cellular Size*. Molecular Cell, 2011. **42**(1): p. 50-61.
- 240. Takahara, T. and T. Maeda, *Evolutionarily conserved regulation of TOR signalling*. Journal of Biochemistry, 2013. **154**(1): p. 1-10.

- 241. Toschi, A., et al., *Regulation of mTORC1 and mTORC2 Complex Assembly by Phosphatidic Acid: Competition with Rapamycin.* Molecular and Cellular Biology, 2009. **29**(6): p. 1411-1420.
- 242. Fang, Y., et al., *Phosphatidic Acid-Mediated Mitogenic Activation of mTOR Signaling*. Science, 2001. **294**(5548): p. 1942-1945.
- 243. Xu, L., et al., *Elevated Phospholipase D Activity in H-Ras- but Not K-Ras-Transformed Cells by the Synergistic Action of RalA and ARF6.* Molecular and Cellular Biology, 2003. **23**(2): p. 645-654.
- 244. Xu, L., et al., *Phospholipase D Mediates Nutrient Input to Mammalian Target of Rapamycin Complex 1 (mTORC1).* Journal of Biological Chemistry, 2011. **286**(29): p. 25477-25486.
- 245. Sun, Y., et al., *Phospholipase D1 is an effector of Rheb in the mTOR pathway.* Proceedings of the National Academy of Sciences, 2008. **105**(24): p. 8286-8291.
- 246. Maehama, T., et al., *RalA Functions as an Indispensable Signal Mediator for the Nutrient-sensing System.* Journal of Biological Chemistry, 2008. **283**(50): p. 35053-35059.
- 247. Tatebe, H., et al., *Rab-Family GTPase Regulates TOR Complex 2 Signaling in Fission Yeast*. Current Biology, 2010. **20**(22): p. 1975-1982.
- 248. Tatebe, H., *Rab small GTPase emerges as a regulator of TOR complex 2.* Small GTPases, 2010. **1**(3): p. 180-182.
- Zerial, M. and H. McBride, *Rab proteins as membrane organizers*. Nat Rev Mol Cell Biol, 2001. **2**(2): p. 107-117.
- 250. Fernandes, H., et al., *Structural aspects of Rab6-effector complexes*. Biochem Soc Trans, 2009. **37**(Pt 5): p. 1037-41.
- 251. Qin, X., B. Jiang, and Y. Zhang, *4E-BP1*, a multifactor regulated multifunctional protein. Cell Cycle, 2016. **15**(6): p. 781-786.
- 252. Gardner, T.W., et al., *Phosphatase control of 4E-BP1 phosphorylation state is central for glycolytic regulation of retinal protein synthesis.* American Journal of Physiology Endocrinology And Metabolism, 2015. **309**(6): p. E546-E556.
- 253. Ito, K. and K. Ito, Metabolism and the Control of Cell Fate Decisions and Stem Cell Renewal, in Annual Review of Cell and Developmental Biology. 2016. p. 399-409.
- 254. Tanaka, Y., et al., In vitro cytotoxicity of zoledronate (nitrogen-containing bisphosphonate: NBP) and/or etidronate (non-NBP) in tumour cells and periodontal cells. Archives of Oral Biology, 2013. **58**(6): p. 628-637.
- 255. Houde, Vanessa P., et al., *Investigation of LKB1 Ser(431) phosphorylation and Cys(433) farnesylation using mouse knockin analysis reveals an unexpected role of prenylation in regulating AMPK activity.* Biochemical Journal, 2014. **458**(Pt 1): p. 41-56.
- 256. Thompson, M.G., et al., *FOXO3–NF-κB RelA Protein Complexes Reduce Proinflammatory Cell Signaling and Function.* The Journal of Immunology, 2015. **195**(12): p. 5637-5647.
- 257. Proctor, C. and D. Gray, *Explaining oscillations and variability in the p53-Mdm2 system*. BMC Systems Biology, 2008. **2**(1): p. 75.
- 258. Kim, M., et al., Age-related alterations in mesenchymal stem cells related to shift in differentiation from osteogenic to adipogenic potential: Implication to age-associated bone diseases and defects. Mechanisms of Ageing and Development, 2012. 133(5): p. 215-225.

9. Appendices

9.1 Appendix A

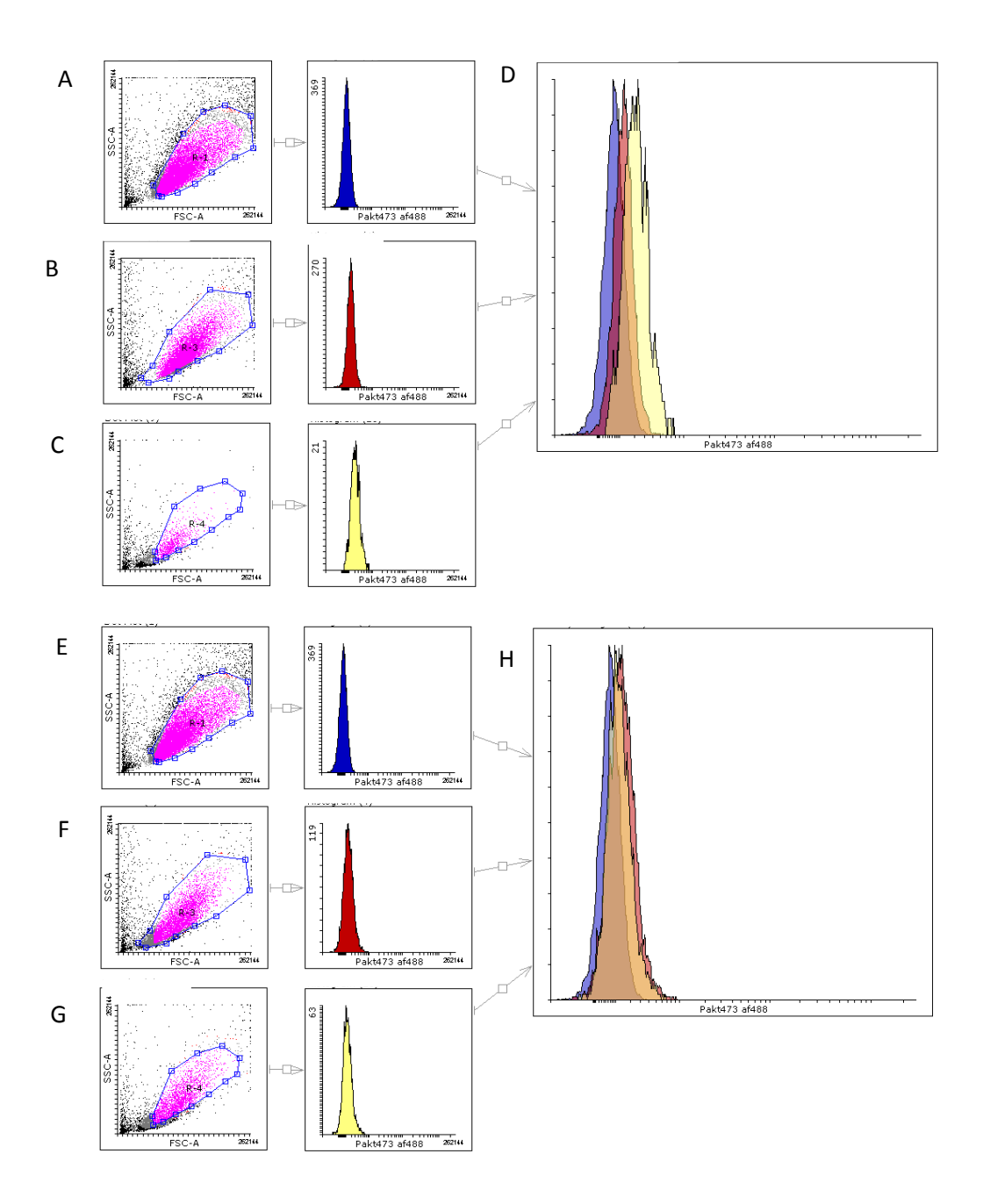


Figure A1: AKT_pT308 signalling. MRC5 cells were treated with 50μM Torin1 for 24 hours with samples taken at 0 hours and 24 hours. (A+E) unstained sample (B) 50μM Torin1 0 hours, (C) 50μM Torin1 24 hours, (D) Overlay histogram displaying a comparison for each time point, (F) Untreated sample 0 hours, (G) Untreated sample 24 hours, (H) Overlay histogram displaying a comparison for each time point.

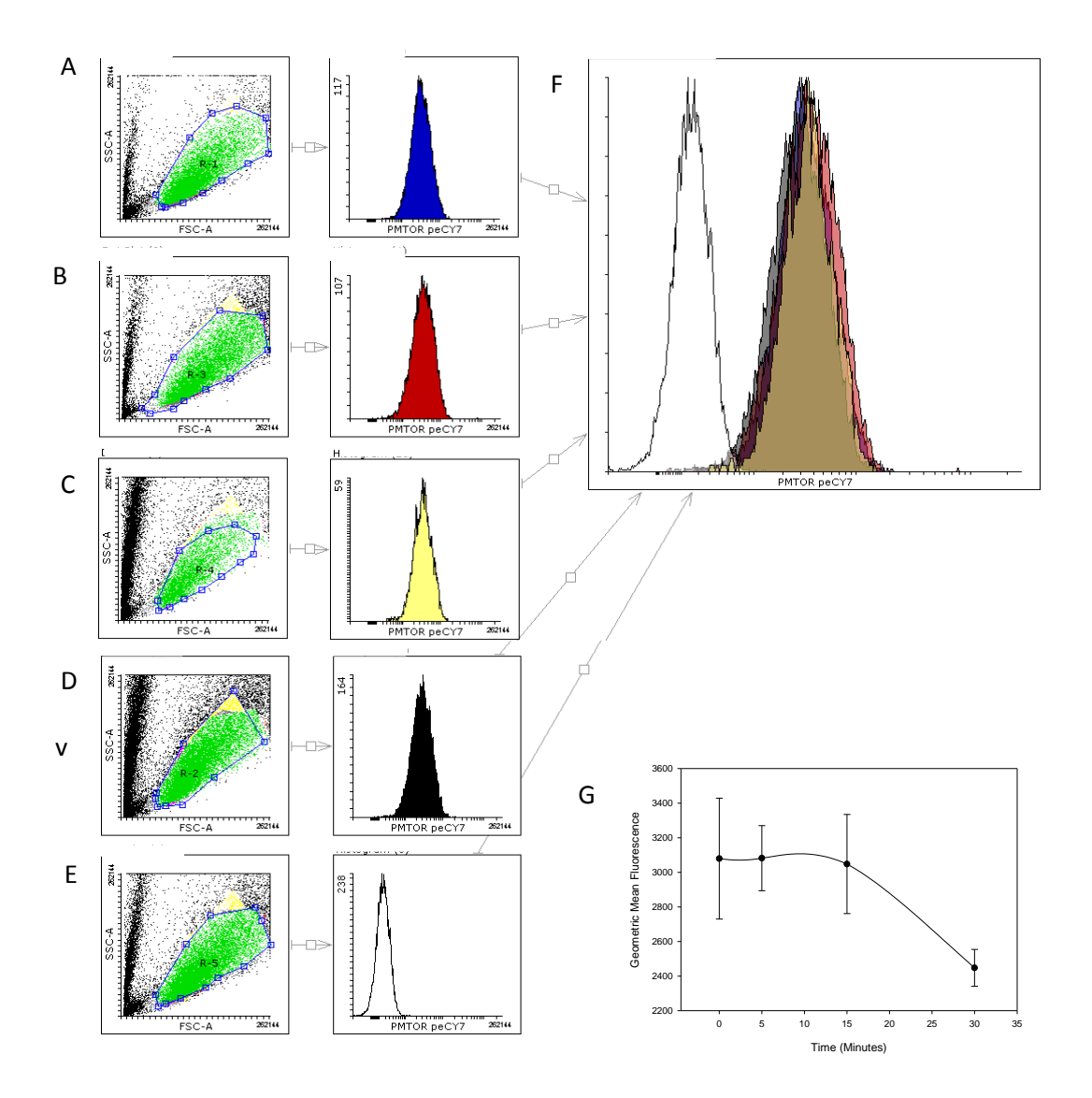


Figure A2: Intracellular flow cytometry is not capable of producing calibration time course data for a dynamic model for mTORC1_pS2448. Cells were serum starved overnight and then re-stimulated with FBS and L-Glutamine containing media with time points collected after (A) 0 minutes, (B) 5 minutes, (C) 15 minutes and (D) 30 minutes (n=3) representative of 1 repeat shown. (F) Overlay histogram displaying a comparison for each time point. (G) The average Geometric mean for each time point plotted against time.

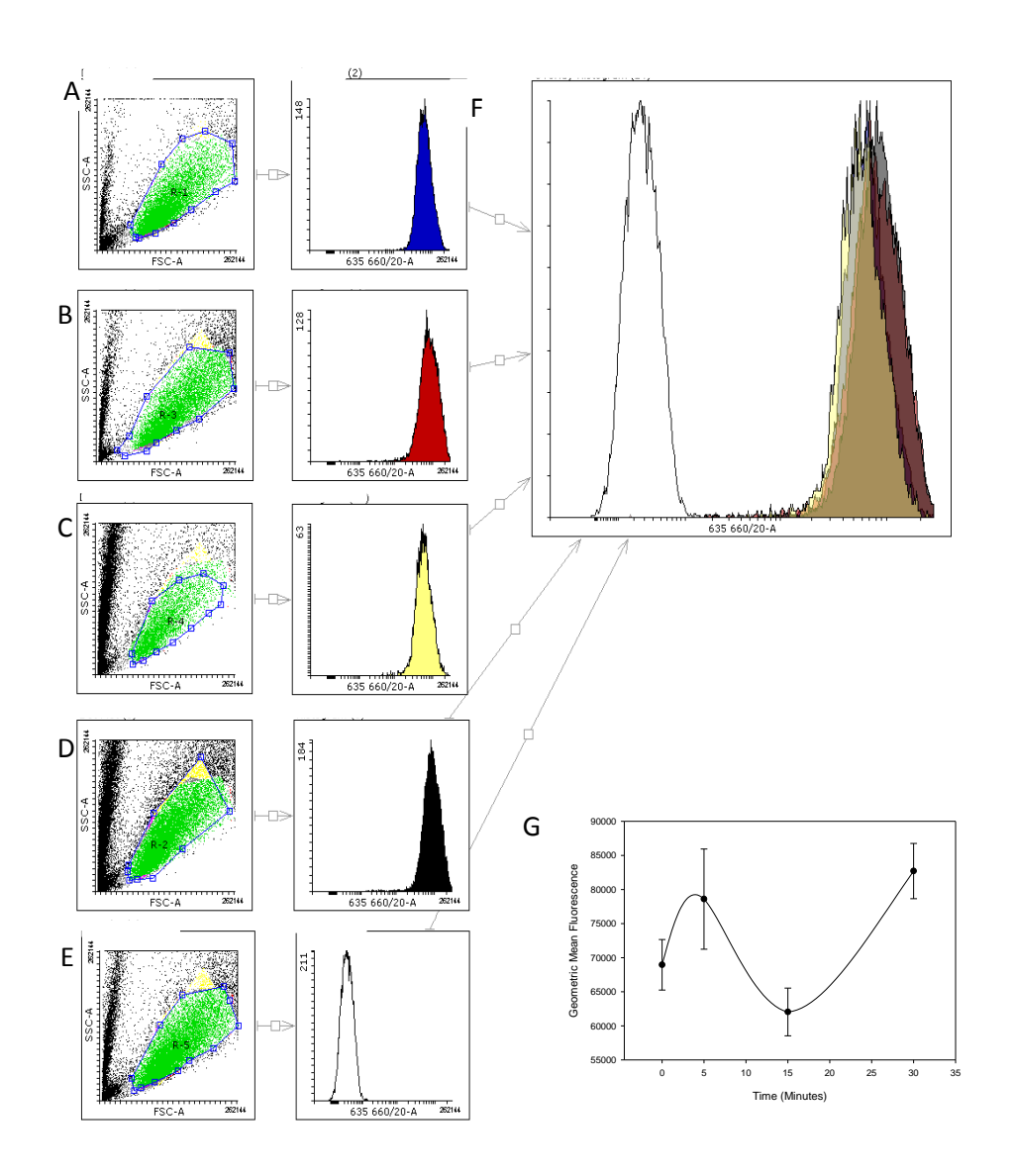


Figure A3: Intracellular flow cytometry is not capable of producing calibration time course data for a dynamic model for AKT_pS473. Cells were serum starved overnight and then re-stimulated with FBS and L-Glutamine containing media with time points collected after (A) 0 minutes, (B) 5 minutes, (C) 15 minutes and (D) 30 minutes (n=3) representative of 1 repeat shown. (F) Overlay histogram displaying a comparison for each time point. (G) The average Geometric mean for each time point plotted against time.

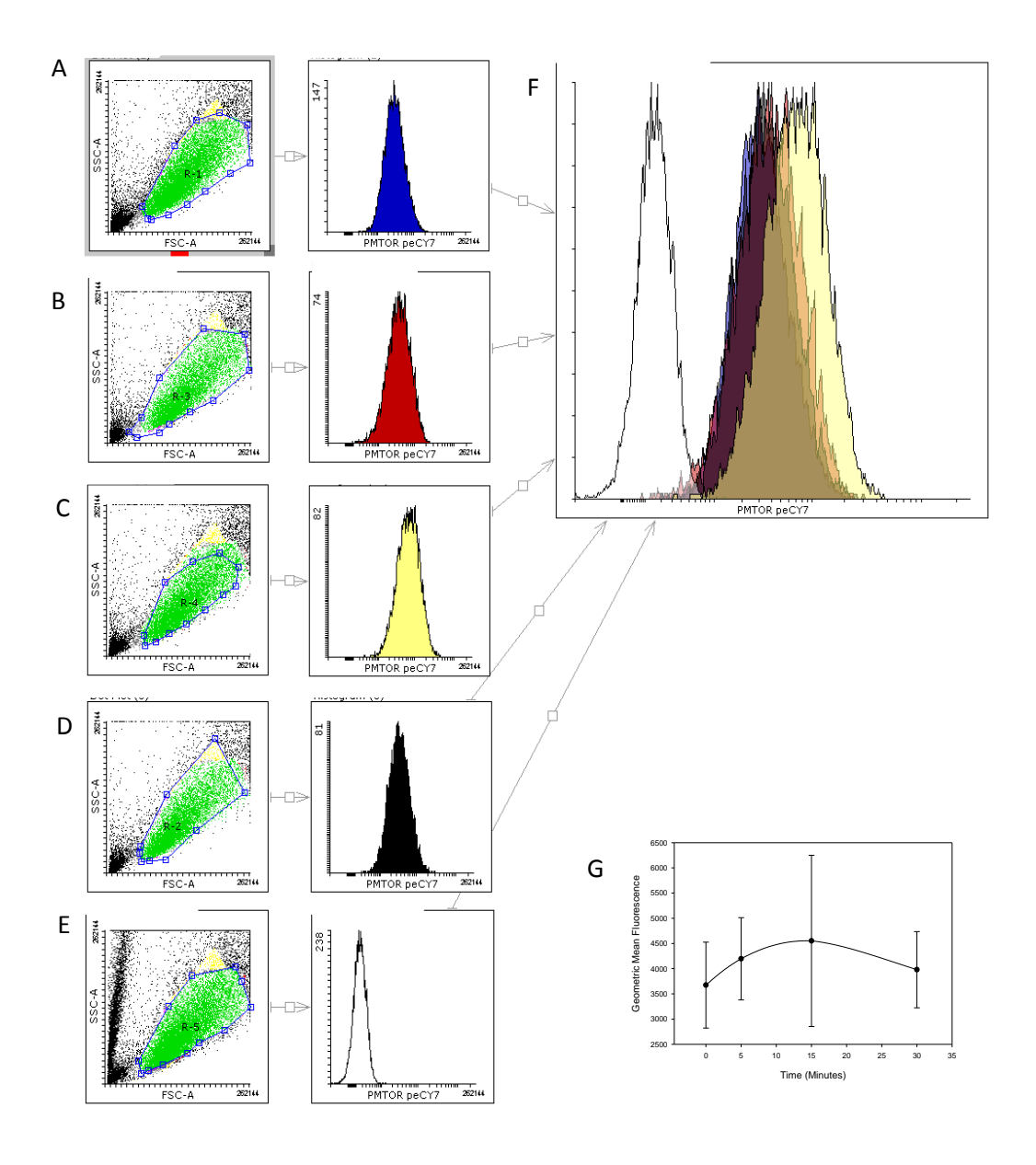


Figure A4: Insulin treatment enhances the capable of Intracellular flow cytometry to produce calibration time course data for a dynamic model for mTORC1 pS2448. Cells were serum starved overnight and then re-stimulated with FBS and L-Glutamine media supplemented with 100nM insulin with time points collected after (A) 0 minutes, (B) 5 minutes, (C) 15 minutes and (D) 30 minutes (n=3) representative of 1 repeat shown. (F) Overlay histogram displaying a comparison for each time point. (G) The average Geometric mean for each time point plotted against time.

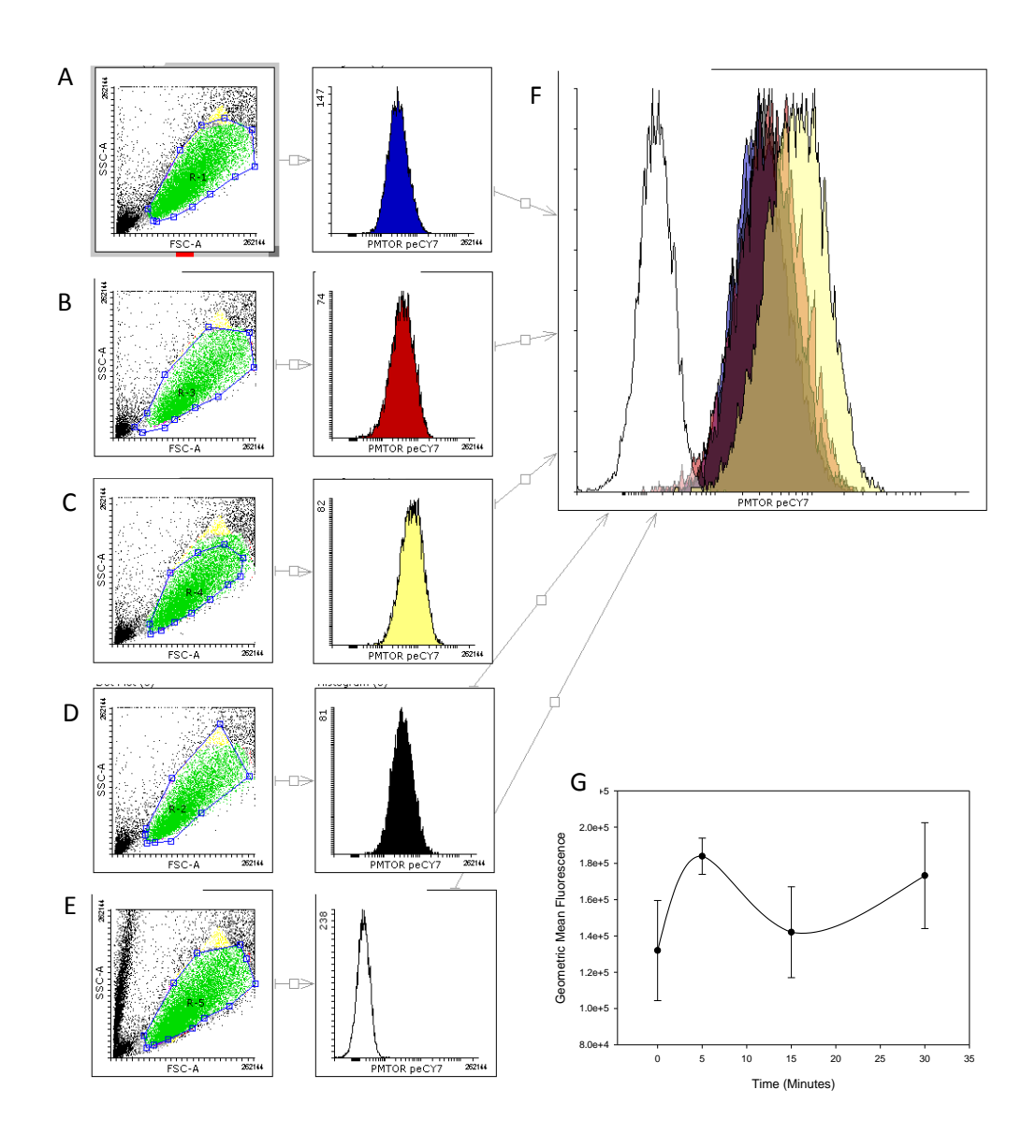


Figure A5: Insulin treatment enhances the capable of Intracellular flow cytometry to produce calibration time course data for a dynamic model for AKT_pS473. Cells were serum starved overnight and then re-stimulated with FBS and L-Glutamine media supplemented with 100nM insulin with time points collected after (A) 0 minutes, (B) 5 minutes, (C) 15 minutes and (D) 30 minutes (n=3) representative of 1 repeat shown. (F) Overlay histogram displaying a comparison for each time point. (G) The average Geometric mean for each time point plotted against time.

9.2 Appendix B

Table B1: Initial Concentrations for starvation-restimulation model

compartment ml	1
AA mmol/ml	10
PI3K mmol/ml	10
PI3K_P mmol/ml	1
S6K_P mmol/ml	1
PDK1 mmol/ml	10
PDK1_P mmol/ml	1
AKT mmol/ml	20
AKT_pT308 mmol/ml	0.5
AKT_pS473 mmol/ml	0.5
mTORC2_P mmol/ml	1
AKT_pT308_pS473	
mmol/ml	0.5
PI3K_V mmol/ml	10
PI3K_V_P mmol/ml	1
mTORC2 mmol/ml	5
TSC1/2 mmol/ml	5
TSC1/2_P mmol/ml	1
Rheb mmol/ml	5
Rheb(GTP) mmol/ml	1
mTORC1 mmol/ml	5
mTORC1_P mmol/ml	1
Rapamycin mmol/ml	0
S6K mmol/ml	5
FPPS mmol/ml	5
Ras(GTP) mmol/ml	1
Ras mmol/ml	5
FPPS_i mmol/ml	0
Zol mmol/ml	0
Ras(GDP) mmol/ml	2
Rheb(GDP) mmol/ml	2
Sink mmol/ml	0.1
FOXO3A mmol/ml	5
FOXO3A_P mmol/ml	1
AMPK mmol/ml	5
AMPK_P mmol/ml	1
ACC mmol/ml	5
ACC P mmol/ml	0
mTOR mmol/ml	0
4EBP1 mmol/ml	5
4EBP1_pS65 mmol/ml	1
	1

PTEN mmol/ml	0
PTEN_P mmol/ml	1
S6 mmol/ml	5
S6_pS235 mmol/ml	1
AKT473	1
AKT308	1

Table B2 – Final parameter values Starvation-restimulation genetic algorithm MRC5 cells

PI3K AA	7.32E-05
PI3K dephos	1.95E-05
S6K feedback loop	3.47E-05
PDK1 act	0.04562
PDK1 dephos	0.624943
AKT -> 308	6.20E-06
AKT308 -> dual	7541.31
AKT -> 473	1.49E-06
AKT473 -> dual	7681.41
Dual -> AKT	0.002034
Dual -> 308	1.01E-05
Dual -> 473	8.89E-06
308 -> AKT	0.00066
473 -> AKT	0.01001
PI3K_V act	384.059
PI3K_V dephos	1.94E-05
mTORC2 act	1.75E-06
mTORC2 dephos	0.000242
TSC1/2 de-act 308	6.02E-06
TSC1/2 de-act dual	63.8319
TSC1/2 act	0.159927
Rheb deact	0.024202
Rheb act	0.000949
mTORC1 act	0.00039
mTORC1 dephos	1.31E-05
S6K act	0.022449
S6K dephos	2.50E-06
PI3K Ras	2.18E-05
Ras act	856.741
FPPS inact	10000
FPPS act	10000
Ras deact	117.929
Ras gdp-gtp	0.000147
Rheb GDP GTP	3.51E-06
Rheb deg	0.000797

Rheb(GDP) deg	0.009059
Rheb(GTP) deg	56.2759
Ras deg	0.000365
Ras(GDP) deg	0.000672
Ras(GTP) deg	4.15865
Sink - Rheb	0.112345
Sink Ras	0.00349
AKT_pT308_pS473 FOXO	2.61E-05
FOXO3A	0.001366
AMPK dephos	0.659257
AMPK_P	7.38403
AMPK PI3K	0.031079
ACC_P	0.047271
ACC dephos	0.136097
PTEN act	0.01853
Rapamycin	0.062519
mTOR -> MTORC1	0.000488
4EBP1 Act	0.004473
4EBP1 inact	0.000765
PTEN inact	0.020089
S6 Act	0.012627
S6 inact	0.174259
mTOR AA	0.000126
mTOR AMPK	0.017255
	-

 $Table\ B3-Final\ parameter\ values\ Starvation-restimulation\ Hooke\ and\ Jeeves\ MRC5\ cells$

PI3K AA	0.000107
PI3K dephos	1.00E-06
S6K feedback loop	1.03E-06
PDK1 act	0.050029
PDK1 dephos	0.678169
AKT -> 308	7.00E-06
AKT308 -> dual	0.001318
AKT -> 473	0.002157
AKT473 -> dual	59.6159
Dual -> AKT	0.007048
Dual -> 308	1.20E-05
Dual -> 473	0.406246
308 -> AKT	2.98E-06
473 -> AKT	0.737759
PI3K_V act	0.018645
PI3K_V dephos	3.53299
mTORC2 act	1.31272

mTORC2 dephos	0.034439
TSC1/2 de-act 308	10.153
TSC1/2 de-act dual	8.86E-05
TSC1/2 act	0.003557
Rheb deact	429.299
Rheb act	3.99E-05
mTORC1 act	1.06E-06
mTORC1 dephos	5.83E-06
S6K act	0.022104
S6K dephos	1.00E-06
PI3K Ras	5.57E-05
Ras act	815.83
FPPS inact	10000
FPPS act	10000
Ras deact	0.000226
Ras gdp-gtp	3.68E-05
Rheb GDP GTP	2.36E-05
Rheb deg	0.000371
Rheb(GDP) deg	6.16E-06
Rheb(GTP) deg	211.892
Ras deg	3.50E-05
Ras(GDP) deg	10.7584
Ras(GTP) deg	0.142144
Sink - Rheb	8.22E-05
Sink Ras	4.71E-05
AKT_pT308_pS473 FOXO	1.44E-05
FOXO3A	0.002287
AMPK dephos	2.49068
AMPK_P	0.01548
AMPK PI3K	0.034879
ACC_P	2.05622
ACC dephos	1.22348
PTEN act	0.020961
Rapamycin	0.062519
mTOR -> MTORC1	0.000937
4EBP1 Act	0.003089
4EBP1 inact	0.000177
PTEN inact	0.039305
S6 Act	0.01669
S6 inact	0.234351
mTOR AA	0.00017
mTOR AMPK	0.018407

 $Table\ B4-Final\ parameter\ values\ Starvation-restimulation\ genetic\ algorithm\ MSCs$

PI3K AA	4.78E-05
PI3K dephos	3.69E-05
S6K feedback loop	8.87E-06
PDK1 act	0.000201
PDK1 dephos	1.99E-05
AKT -> 308	0.000495
AKT308 -> dual	1.09E-06
AKT -> 473	0.077915
AKT473 -> dual	0.000152
Dual -> AKT	5.10446
Dual -> 308	96.4466
Dual -> 473	42.443
308 -> AKT	5.16E-05
473 -> AKT	0.006095
PI3K_V act	0.021595
PI3K_V dephos	21.0726
mTORC2 act	8.42E-06
mTORC2 dephos	0.036055
TSC1/2 de-act 308	3.30068
TSC1/2 de-act dual	0.002608
TSC1/2 act	0.010819
Rheb deact	0.061057
Rheb act	352733
mTORC1 act	0.034379
mTORC1 dephos	2.19078
S6K act	2.13E-06
S6K dephos	8.79E-05
PI3K Ras	0.004699
Ras act	11.8046
FPPS inact	508201
FPPS act	10212.8
Ras deact	0.022624
Ras gdp-gtp	3.92797
Rheb GDP GTP	0.007522
Rheb deg	0.073574
Rheb(GDP) deg	1.21E-05
Rheb(GTP) deg	416.765
Ras deg	1.85E-06
Ras(GDP) deg	14.48
Ras(GTP) deg	5.57015
Sink - Rheb	301276
Sink Ras	6.14E-06
AKT_pT308_pS473	2.78979
-	

FOXO	
FOXO3A	0.000516
AMPK dephos	0.072417
AMPK_P	0.007556
AMPK PI3K	0.000305
ACC_P	0.000885
ACC dephos	0.000338
PTEN act	1.06E-06
Rapamycin	0.062519
mTOR -> MTORC1	12236.1
4EBP1 Act	1.97E-06
4EBP1 inact	0.003185
PTEN inact	17.2284
S6 Act	0.155236
S6 inact	0.002656
mTOR AA	0.02246
mTOR AMPK	0.03304

Table B5 – Final parameter values Starvation-restimulation Hooke and Jeeves MSCs

PI3K AA 0.004624 PI3K dephos 0.013564 S6K feedback loop 0.032947 PDK1 act 1.00E-06 PDK1 dephos 1.00E-06 AKT -> 308 0.000882 AKT308 -> dual 5118.06 AKT -> 473 0.002151 AKT473 -> dual 1.00E-06 Dual -> AKT 1.00E-06 Dual -> 308 0.003408 Dual -> 473 0.007984 308 -> AKT 1.00E-06 473 -> AKT 0.003854 PI3K_V act 9596.25 PI3K_V dephos 0.000556 mTORC2 act 0.002781 mTORC2 dephos 0.010132 TSC1/2 de-act 308 0.001008 TSC1/2 de-act dual 4510.86 TSC1/2 act 18.3166 Rheb deact 5.23133 Rheb act 0.208629 mTORC1 act 4.29E-05		
S6K feedback loop 0.032947 PDK1 act 1.00E-06 PDK1 dephos 1.00E-06 AKT -> 308 0.000882 AKT308 -> dual 5118.06 AKT -> 473 0.002151 AKT473 -> dual 1.00E-06 Dual -> AKT 1.00E-06 Dual -> 308 0.003408 Dual -> 473 0.007984 308 -> AKT 1.00E-06 473 -> AKT 0.003854 PI3K_V act 9596.25 PI3K_V dephos 0.000556 mTORC2 act 0.002781 mTORC2 dephos 0.010132 TSC1/2 de-act 308 0.001008 TSC1/2 de-act dual 4510.86 Rheb deact 5.23133 Rheb act 0.208629	PI3K AA	0.004624
PDK1 act 1.00E-06 PDK1 dephos 1.00E-06 AKT -> 308 0.000882 AKT 308 -> dual 5118.06 AKT -> 473 0.002151 AKT473 -> dual 1.00E-06 Dual -> AKT 1.00E-06 Dual -> 308 0.003408 Dual -> 473 0.007984 308 -> AKT 1.00E-06 473 -> AKT 0.003854 PI3K_V act 9596.25 PI3K_V dephos 0.000556 mTORC2 act 0.002781 mTORC2 dephos 0.010132 TSC1/2 de-act 308 0.001008 TSC1/2 de-act dual 4510.86 TSC1/2 act 18.3166 Rheb deact 5.23133 Rheb act 0.208629	PI3K dephos	0.013564
PDK1 dephos 1.00E-06 AKT -> 308 0.000882 AKT308 -> dual 5118.06 AKT -> 473 0.002151 AKT473 -> dual 1.00E-06 Dual -> AKT 1.00E-06 Dual -> 308 0.003408 Dual -> 473 0.007984 308 -> AKT 1.00E-06 473 -> AKT 0.003854 PI3K_V act 9596.25 PI3K_V dephos 0.000556 mTORC2 act 0.002781 mTORC2 dephos 0.010132 TSC1/2 de-act 308 0.001008 TSC1/2 de-act dual 4510.86 TSC1/2 act 18.3166 Rheb deact 5.23133 Rheb act 0.208629	S6K feedback loop	0.032947
AKT -> 308	PDK1 act	1.00E-06
AKT308 -> dual 5118.06 AKT -> 473 0.002151 AKT473 -> dual 1.00E-06 Dual -> AKT 1.00E-06 Dual -> 308 0.003408 Dual -> 473 0.007984 308 -> AKT 1.00E-06 473 -> AKT 0.003854 PI3K_V act 9596.25 PI3K_V dephos 0.000556 mTORC2 act 0.002781 mTORC2 dephos 0.010132 TSC1/2 de-act dual 4510.86 TSC1/2 act 18.3166 Rheb deact 5.23133 Rheb act 0.0028629	PDK1 dephos	1.00E-06
AKT -> 473 0.002151 AKT473 -> dual 1.00E-06 Dual -> AKT 1.00E-06 Dual -> 308 0.003408 Dual -> 473 0.007984 308 -> AKT 1.00E-06 473 -> AKT 0.003854 PI3K_V act 9596.25 PI3K_V dephos 0.000556 mTORC2 act 0.002781 mTORC2 dephos 0.010132 TSC1/2 de-act 308 0.001008 TSC1/2 de-act dual 4510.86 TSC1/2 act 18.3166 Rheb deact 5.23133 Rheb act 0.208629	AKT -> 308	0.000882
AKT473 -> dual 1.00E-06 Dual -> AKT 1.00E-06 Dual -> 308 0.003408 Dual -> 473 0.007984 308 -> AKT 1.00E-06 473 -> AKT 0.003854 PI3K_V act 9596.25 PI3K_V dephos 0.000556 mTORC2 act 0.002781 mTORC2 dephos 0.010132 TSC1/2 de-act 308 0.001008 TSC1/2 de-act dual 4510.86 TSC1/2 act 18.3166 Rheb deact 5.23133 Rheb act 0.208629	AKT308 -> dual	5118.06
Dual -> AKT 1.00E-06 Dual -> 308 0.003408 Dual -> 473 0.007984 308 -> AKT 1.00E-06 473 -> AKT 0.003854 PI3K_V act 9596.25 PI3K_V dephos 0.000556 mTORC2 act 0.002781 mTORC2 dephos 0.010132 TSC1/2 de-act 308 0.001008 TSC1/2 de-act dual 4510.86 TSC1/2 act 18.3166 Rheb deact 5.23133 Rheb act 0.208629	AKT -> 473	0.002151
Dual -> 308 0.003408 Dual -> 473 0.007984 308 -> AKT 1.00E-06 473 -> AKT 0.003854 PI3K_V act 9596.25 PI3K_V dephos 0.000556 mTORC2 act 0.002781 mTORC2 dephos 0.010132 TSC1/2 de-act 308 0.001008 TSC1/2 de-act dual 4510.86 TSC1/2 act 18.3166 Rheb deact 5.23133 Rheb act 0.208629	AKT473 -> dual	1.00E-06
Dual -> 473 0.007984 308 -> AKT 1.00E-06 473 -> AKT 0.003854 PI3K_V act 9596.25 PI3K_V dephos 0.000556 mTORC2 act 0.002781 mTORC2 dephos 0.010132 TSC1/2 de-act 308 0.001008 TSC1/2 de-act dual 4510.86 TSC1/2 act 18.3166 Rheb deact 5.23133 Rheb act 0.208629	Dual -> AKT	1.00E-06
308 -> AKT 1.00E-06 473 -> AKT 0.003854 PI3K_V act 9596.25 PI3K_V dephos 0.000556 mTORC2 act 0.002781 mTORC2 dephos 0.010132 TSC1/2 de-act 308 0.001008 TSC1/2 de-act dual 4510.86 TSC1/2 act 18.3166 Rheb deact 5.23133 Rheb act 0.208629	Dual -> 308	0.003408
473 -> AKT 0.003854 PI3K_V act 9596.25 PI3K_V dephos 0.000556 mTORC2 act 0.002781 mTORC2 dephos 0.010132 TSC1/2 de-act 308 0.001008 TSC1/2 de-act dual 4510.86 TSC1/2 act 18.3166 Rheb deact 5.23133 Rheb act 0.208629	Dual -> 473	0.007984
PI3K_V act 9596.25 PI3K_V dephos 0.000556 mTORC2 act 0.002781 mTORC2 dephos 0.010132 TSC1/2 de-act 308 0.001008 TSC1/2 de-act dual 4510.86 TSC1/2 act 18.3166 Rheb deact 5.23133 Rheb act 0.208629	308 -> AKT	1.00E-06
PI3K_V dephos 0.000556 mTORC2 act 0.002781 mTORC2 dephos 0.010132 TSC1/2 de-act 308 0.001008 TSC1/2 de-act dual 4510.86 TSC1/2 act 18.3166 Rheb deact 5.23133 Rheb act 0.208629	473 -> AKT	0.003854
mTORC2 act 0.002781 mTORC2 dephos 0.010132 TSC1/2 de-act 308 0.001008 TSC1/2 de-act dual 4510.86 TSC1/2 act 18.3166 Rheb deact 5.23133 Rheb act 0.208629	PI3K_V act	9596.25
mTORC2 dephos 0.010132 TSC1/2 de-act 308 0.001008 TSC1/2 de-act dual 4510.86 TSC1/2 act 18.3166 Rheb deact 5.23133 Rheb act 0.208629	PI3K_V dephos	0.000556
TSC1/2 de-act 308 0.001008 TSC1/2 de-act dual 4510.86 TSC1/2 act 18.3166 Rheb deact 5.23133 Rheb act 0.208629	mTORC2 act	0.002781
TSC1/2 de-act dual 4510.86 TSC1/2 act 18.3166 Rheb deact 5.23133 Rheb act 0.208629	mTORC2 dephos	0.010132
TSC1/2 act 18.3166 Rheb deact 5.23133 Rheb act 0.208629	TSC1/2 de-act 308	0.001008
Rheb deact 5.23133 Rheb act 0.208629	TSC1/2 de-act dual	4510.86
Rheb act 0.208629	TSC1/2 act	18.3166
	Rheb deact	5.23133
mTORC1 act 4.29E-05	Rheb act	0.208629
	mTORC1 act	4.29E-05

mTORC1 dephos	0.0051
S6K act	0.053437
S6K dephos	3.76E-06
PI3K Ras	0.006521
Ras act	1.00E-06
FPPS inact	10000
FPPS act	10000
Ras deact	1.00E-06
Ras gdp-gtp	0.006999
Rheb GDP GTP	0.000609
Rheb deg	0.325024
Rheb(GDP) deg	1.97464
Rheb(GTP) deg	7202.45
Ras deg	0.017321
Ras(GDP) deg	0.00148
Ras(GTP) deg	1.00E-06
Sink - Rheb	35.2241
Sink Ras	1.87393
AKT_pT308_pS473 FOXO	0.00029
FOXO3A	1.00E-06
AMPK dephos	0.388339
AMPK_P	1.00E-06
AMPK PI3K	11.6022
ACC_P	0.0107
ACC dephos	0.576476
PTEN act	13.0413
Rapamycin	0.062519
mTOR -> MTORC1	0.000488
4EBP1 Act	1.00E-06
4EBP1 inact	0.00087
PTEN inact	22.5255
S6 Act	0.165683
S6 inact	1.00E-06
mTOR AA	0.000235
mTOR AMPK	1.00E-06

Table B6: Initial Concentrations for Rapamycin withdrawal model

	1
compartment ml	1
AA mmol/ml	1
PI3K mmol/ml	1
S6K_P mmol/ml	1
PDK1 mmol/ml	10
PDK1_P mmol/ml	1
AKT mmol/ml	20
AKT_pT308 mmol/ml	0.5
AKT_pS473 mmol/ml	0.5
mTORC2_P mmol/ml	1
AKT_pT308_pS473	0.5
mmol/ml	0.5
PI3K_V mmol/ml	10
PI3K_V_P mmol/ml	1
mTORC2 mmol/ml	5
TSC1/2 mmol/ml	5
TSC1/2_P mmol/ml	1
Rheb(GTP) mmol/ml	1
mTORC1 mmol/ml	0.5
mTORC1_P mmol/ml	0
Rapamycin mmol/ml	10
S6K mmol/ml	5
FPPS mmol/ml	5
Ras(GTP) mmol/ml	1
Ras mmol/ml	5
FPPS_i mmol/ml	0
Zol mmol/ml	0
Ras(GDP) mmol/ml	2
Rheb(GDP) mmol/ml	1
Sink mmol/ml	0.1
FOXO3A mmol/ml	5
FOXO3A_P mmol/ml	1
AMPK mmol/ml	5
AMPK P mmol/ml	1
ACC mmol/ml	5
ACC_P mmol/ml	1
mTOR mmol/ml	4.5
4EBP1 mmol/ml	5
4EBP1_pS65 mmol/ml	1
PTEN mmol/ml	1
PTEN P mmol/ml	1
S6 mmol/ml	5
	_
S6_pS235 mmol/ml	1

PI3K_IRS1 mmol/ml	1
PI3K_P_IRS1 mmol/ml	1
IRS1 mmol/ml	1
AKT473	1
AKT308	1

Table B7 – Final parameter values Rapamycin withdrawal genetic algorithm MRC5 cells

PI3K AA	0.000579
PI3K dephos	0.000136
S6K feedback loop	3.51E-06
PDK1 act	1.47E-05
PDK1 dephos	0.142666
AKT to 308	0.004035
AKT308 to dual	0.000168
AKT to 473	0.000672
AKT473 to dual	0.00139
Dual to AKT	0.000288
Dual to 308	8418.14
Dual to 473	4636.26
308 to AKT	9.22E-06
473 to AKT	0.000241
PI3K_V act	1.79E-06
PI3K_V dephos	2075.45
mTORC2 act	0.002991
mTORC2 dephos	0.082018
TSC1/2 de-act 308	1.81E-06
TSC1/2 de-act dual	0.000202
TSC1/2 act	0.261072
Rheb deact	3.72E-05
mTORC1 act	5.19E-05
mTORC1 dephos	9.08019
S6K act	0.000958
S6K dephos	2681.39
PI3K Ras	3.70E-06
Ras act	0.060602
FPPS inact	1.65142
FPPS act	2.95E-05
Ras deact	713.229
Ras gdp-gtp	1.61E-06
Rheb GDP GTP	0.009122
Ras deg	1.35E-05
Ras(GDP) deg	0.209463
Ras(GTP) deg	1.28E-06

Sink Ras	0.023571
AKT_pT308_pS473	
FOXO	3764.42
FOXO3A	0.000305
AMPK dephos	5.39E-05
AMPK_P	137.285
AMPK PI3K	0.000611
ACC_P	0.004745
ACC dephos	0.62987
PTEN act	6.06E-05
Rapamycin	1.56E-05
mTOR to MTORC1	8.74E-06
4EBP1 Act	5.34E-06
4EBP1 inact	0.004426
PTEN inact	0.002513
S6 Act	7.39065
S6 inact	1.17E-05
mTOR AA	33.0747
mTOR AMPK	0.000224
IRS1	13.1569

Table B8 – Final parameter values Rapamycin withdrawal Hooke and Jeeves MRC5 cells

PI3K AA	0.132441
PI3K dephos	0.010805
S6K feedback loop	70.5347
PDK1 act	1.40E-06
PDK1 dephos	0.276583
AKT to 308	0.009844
AKT308 to dual	0.000733
AKT to 473	4.11E-05
AKT473 to dual	1.75E-06
Dual to AKT	2.04767
Dual to 308	31.784
Dual to 473	37.4038
308 to AKT	3.64E-05
473 to AKT	1.00E-06
PI3K_V act	9.84E-05
PI3K_V dephos	29.1312
mTORC2 act	9.58E-06
mTORC2 dephos	22.4142
TSC1/2 de-act 308	9181.55
TSC1/2 de-act dual	4.25398

TSC1/2 act	5.38E-06
Rheb deact	5.86E-05
mTORC1 act	4.42223
mTORC1 dephos	2.47222
S6K act	3.15E-06
S6K dephos	87.6397
PI3K Ras	0.002709
Ras act	9.81E-06
FPPS inact	29.1555
FPPS act	1.04E-06
Ras deact	0.000152
Ras gdp-gtp	0.234431
Rheb GDP GTP	71.292
Ras deg	177.692
Ras(GDP) deg	0.00109
Ras(GTP) deg	0.000204
Sink Ras	1.64268
AKT_pT308_pS473 FOXO	19.6364
FOXO3A	3.23E-06
AMPK dephos	1.28E-05
AMPK_P	1.00E-06
AMPK PI3K	1.00E-06
ACC_P	0.036404
ACC dephos	0.722306
PTEN act	3.59E-06
Rapamycin	3.31E-05
mTOR to MTORC1	1.00E-06
4EBP1 Act	1.00E-06
4EBP1 inact	0.005499
PTEN inact	0.003442
S6 Act	0.000144
S6 inact	0.000407
mTOR AA	7.61E-05
IRS1	0.000548
	•

 $Table\ B9-Final\ parameter\ values\ Rapamycin\ with drawal\ genetic\ algorithm\ MSCs$

	1
PI3K AA	0.332282
PI3K dephos	3.30E-06
S6K feedback loop	0.165603
PDK1 act	0.00063
PDK1 dephos	2.71E-05
AKT to 308	2.87E-06
AKT308 to dual	0.071091
AKT to 473	0.005981
AKT473 to dual	1.13763
Dual to AKT	0.004386
Dual to 308	0.00064
Dual to 473	2.54E-05
308 to AKT	7.49E-06
473 to AKT	8.70E-05
PI3K_V act	0.000327
PI3K_V dephos	1.96E-05
mTORC2 act	1.82E-06
mTORC2 dephos	0.218211
TSC1/2 de-act 308	2.00E-06
TSC1/2 de-act dual	0.105091
TSC1/2 act	29.7399
Rheb deact	3.19263
mTORC1 act	3.88E-06
mTORC1 dephos	0.002966
S6K act	0.009964
S6K dephos	2.69034
PI3K Ras	1.29E-06
Ras act	174.723
FPPS inact	25.2475
FPPS act	2.64E-06
Ras deact	0.099762
Ras gdp-gtp	0.001148
Rheb GDP GTP	1.49E-05
Ras deg	92.63
Ras(GDP) deg	0.002218
Ras(GTP) deg	0.000133
Sink Ras	4.86E-06
AKT_pT308_pS473 FOXO	0.001048
FOXO3A	0.00043
AMPK dephos	0.095855
AMPK_P	0.820254
AMPK PI3K	0.000257
4 MVII 1X 1 IJIX	0.000237

ACC_P	0.0005
ACC dephos	0.000261
PTEN act	0.54544
Rapamycin	0.058941
mTOR to MTORC1	0.082049
4EBP1 Act	0.001096
4EBP1 inact	8.56E-06
PTEN inact	0.452548
S6 Act	0.002236
S6 inact	4.31E-06
mTOR AA	0.024123
mTOR AMPK	0.097957
IRS1	1.01E-06

 $Table\ B10-Final\ parameter\ values\ Rapamycin\ with drawal\ Hooke\ and\ Jeeves\ MSCs$

PI3K AA	0.039248
PI3K dephos	0.018773
S6K feedback loop	1.00E-06
PDK1 act	6.85E-05
PDK1 dephos	1.00E-06
AKT to 308	0.00207
AKT308 to dual	0.007322
AKT to 473	0.000266
AKT473 to dual	8.12E-05
Dual to AKT	1.00E-06
Dual to 308	6.18064
Dual to 473	124.531
308 to AKT	0.000103
473 to AKT	2.53E-05
PI3K_V act	1.06E-06
PI3K_V dephos	392.228
mTORC2 act	5.24E-05
mTORC2 dephos	0.011764
TSC1/2 de-act 308	0.117525
TSC1/2 de-act dual	35.5129
TSC1/2 act	4.70E-05
Rheb deact	0.000707
mTORC1 act	0.224946
mTORC1 dephos	0.363499
S6K act	6.56E-06
S6K dephos	134.328
PI3K Ras	0.114347
Ras act	0.00013

FPPS inact 29.1555 FPPS act 1.04E-06 Ras deact 1.00E-06 Ras gdp-gtp 0.357557 Rheb GDP GTP 1223.29 Ras deg 2277.82 Ras(GDP) deg 1.00E-06 Ras(GTP) deg 1.00E-06 Sink Ras 10.4657 AKT_pT308_pS473 FOXO FOXO3A 1.00E-06 AMPK dephos 2.85E-05 AMPK_P 4.52E-05 ACC_P 0.015762 ACC dephos 0.067668 PTEN act 1.01E-06 Rapamycin 3.31E-05 mTOR to MTORC1 4.91E-05 4EBP1 Act 4.82E-05 4EBP1 inact 1.00E-06 PTEN inact 0.172623 S6 Act 0.000144 S6 inact 0.001098 IRS1 1.00E-06		
Ras deact 1.00E-06 Ras gdp-gtp 0.357557 Rheb GDP GTP 1223.29 Ras deg 2277.82 Ras(GDP) deg 1.00E-06 Ras(GTP) deg 1.00E-06 Sink Ras 10.4657 AKT_pT308_pS473 9.24225 FOXO3A 1.00E-06 AMPK dephos 2.85E-05 AMPK_P 4.52E-05 AMPK PI3K 1.00E-06 ACC_P 0.015762 ACC dephos 0.067668 PTEN act 1.01E-06 Rapamycin 3.31E-05 mTOR to MTORC1 4.91E-05 4EBP1 Act 4.82E-05 4EBP1 inact 1.00E-06 PTEN inact 0.172623 S6 Act 0.000144 S6 inact 0.000407 mTOR AA 0.001098	FPPS inact	29.1555
Ras gdp-gtp 0.357557 Rheb GDP GTP 1223.29 Ras deg 2277.82 Ras(GDP) deg 1.00E-06 Ras(GTP) deg 1.00E-06 Sink Ras 10.4657 AKT_pT308_pS473 9.24225 FOXO3A 1.00E-06 AMPK dephos 2.85E-05 AMPK_P 4.52E-05 AMPK PI3K 1.00E-06 ACC_P 0.015762 ACC dephos 0.067668 PTEN act 1.01E-06 Rapamycin 3.31E-05 mTOR to MTORC1 4.91E-05 4EBP1 Act 4.82E-05 4EBP1 inact 1.00E-06 PTEN inact 0.172623 S6 Act 0.000144 S6 inact 0.000407 mTOR AA 0.001098	FPPS act	1.04E-06
Rheb GDP GTP 1223.29 Ras deg 2277.82 Ras(GDP) deg 1.00E-06 Sink Ras 10.4657 AKT_pT308_pS473 9.24225 FOXO 9.24225 FOXO3A 1.00E-06 AMPK dephos 2.85E-05 AMPK_P 4.52E-05 AMPK PI3K 1.00E-06 ACC_P 0.015762 ACC dephos 0.067668 PTEN act 1.01E-06 Rapamycin 3.31E-05 mTOR to MTORC1 4.91E-05 4EBP1 Act 4.82E-05 4EBP1 inact 1.00E-06 PTEN inact 0.172623 S6 Act 0.000144 S6 inact 0.000407 mTOR AA 0.001098	Ras deact	1.00E-06
Ras deg 2277.82 Ras(GDP) deg 1.00E-06 Ras(GTP) deg 1.00E-06 Sink Ras 10.4657 AKT_pT308_pS473 9.24225 FOXO3A 1.00E-06 AMPK dephos 2.85E-05 AMPK_P 4.52E-05 AMPK PI3K 1.00E-06 ACC_P 0.015762 ACC dephos 0.067668 PTEN act 1.01E-06 Rapamycin 3.31E-05 mTOR to MTORC1 4.91E-05 4EBP1 Act 4.82E-05 4EBP1 inact 1.00E-06 PTEN inact 0.172623 S6 Act 0.000144 S6 inact 0.000407 mTOR AA 0.001098	Ras gdp-gtp	0.357557
Ras(GDP) deg 1.00E-06 Ras(GTP) deg 1.00E-06 Sink Ras 10.4657 AKT_pT308_pS473 9.24225 FOXO3A 1.00E-06 AMPK dephos 2.85E-05 AMPK_P 4.52E-05 AMPK PI3K 1.00E-06 ACC_P 0.015762 ACC dephos 0.067668 PTEN act 1.01E-06 Rapamycin 3.31E-05 mTOR to MTORC1 4.91E-05 4EBP1 Act 4.82E-05 4EBP1 inact 1.00E-06 PTEN inact 0.172623 S6 Act 0.000144 S6 inact 0.000407 mTOR AA 0.001098	Rheb GDP GTP	1223.29
Ras(GTP) deg 1.00E-06 Sink Ras 10.4657 AKT_pT308_pS473 9.24225 FOXO3A 1.00E-06 AMPK dephos 2.85E-05 AMPK_P 4.52E-05 AMPK PI3K 1.00E-06 ACC_P 0.015762 ACC dephos 0.067668 PTEN act 1.01E-06 Rapamycin 3.31E-05 mTOR to MTORC1 4.91E-05 4EBP1 Act 4.82E-05 4EBP1 inact 1.00E-06 PTEN inact 0.172623 S6 Act 0.000144 S6 inact 0.000407 mTOR AA 0.001098	Ras deg	2277.82
Sink Ras 10.4657 AKT_pT308_pS473 9.24225 FOXO3A 1.00E-06 AMPK dephos 2.85E-05 AMPK_P 4.52E-05 AMPK PI3K 1.00E-06 ACC_P 0.015762 ACC dephos 0.067668 PTEN act 1.01E-06 Rapamycin 3.31E-05 mTOR to MTORC1 4.91E-05 4EBP1 Act 4.82E-05 4EBP1 inact 1.00E-06 PTEN inact 0.172623 S6 Act 0.000144 S6 inact 0.000407 mTOR AA 0.001098	Ras(GDP) deg	1.00E-06
AKT_pT308_pS473 FOXO 9.24225 FOXO3A 1.00E-06 AMPK dephos 2.85E-05 AMPK_P 4.52E-05 AMPK PI3K 1.00E-06 ACC_P 0.015762 ACC dephos 0.067668 PTEN act 1.01E-06 Rapamycin 3.31E-05 mTOR to MTORC1 4.91E-05 4EBP1 Act 4.82E-05 4EBP1 inact 1.00E-06 PTEN inact 0.172623 S6 Act 0.000144 S6 inact 0.000407 mTOR AA 0.001098	Ras(GTP) deg	1.00E-06
FOXO 9.24225 FOXO3A 1.00E-06 AMPK dephos 2.85E-05 AMPK_P 4.52E-05 AMPK PI3K 1.00E-06 ACC_P 0.015762 ACC dephos 0.067668 PTEN act 1.01E-06 Rapamycin 3.31E-05 mTOR to MTORC1 4.91E-05 4EBP1 Act 4.82E-05 4EBP1 inact 1.00E-06 PTEN inact 0.172623 S6 Act 0.000144 S6 inact 0.000407 mTOR AA 0.001098		10.4657
AMPK dephos 2.85E-05 AMPK_P 4.52E-05 AMPK PI3K 1.00E-06 ACC_P 0.015762 ACC dephos 0.067668 PTEN act 1.01E-06 Rapamycin 3.31E-05 mTOR to MTORC1 4.91E-05 4EBP1 Act 4.82E-05 4EBP1 inact 1.00E-06 PTEN inact 0.172623 S6 Act 0.000144 S6 inact 0.000407 mTOR AA 0.001098		9.24225
AMPK_P 4.52E-05 AMPK PI3K 1.00E-06 ACC_P 0.015762 ACC dephos 0.067668 PTEN act 1.01E-06 Rapamycin 3.31E-05 mTOR to MTORC1 4.91E-05 4EBP1 Act 4.82E-05 4EBP1 inact 1.00E-06 PTEN inact 0.172623 S6 Act 0.000144 S6 inact 0.000407 mTOR AA 0.001098	FOXO3A	1.00E-06
AMPK PI3K 1.00E-06 ACC_P 0.015762 ACC dephos 0.067668 PTEN act 1.01E-06 Rapamycin 3.31E-05 mTOR to MTORC1 4.91E-05 4EBP1 Act 4.82E-05 4EBP1 inact 1.00E-06 PTEN inact 0.172623 S6 Act 0.000144 S6 inact 0.000407 mTOR AA 0.001098	AMPK dephos	2.85E-05
ACC_P 0.015762 ACC dephos 0.067668 PTEN act 1.01E-06 Rapamycin 3.31E-05 mTOR to MTORC1 4.91E-05 4EBP1 Act 4.82E-05 4EBP1 inact 1.00E-06 PTEN inact 0.172623 S6 Act 0.000144 S6 inact 0.000407 mTOR AA 0.001098	AMPK_P	4.52E-05
ACC dephos 0.067668 PTEN act 1.01E-06 Rapamycin 3.31E-05 mTOR to MTORC1 4.91E-05 4EBP1 Act 4.82E-05 4EBP1 inact 1.00E-06 PTEN inact 0.172623 S6 Act 0.000144 S6 inact 0.000407 mTOR AA 0.001098	AMPK PI3K	1.00E-06
PTEN act 1.01E-06 Rapamycin 3.31E-05 mTOR to MTORC1 4.91E-05 4EBP1 Act 4.82E-05 4EBP1 inact 1.00E-06 PTEN inact 0.172623 S6 Act 0.000144 S6 inact 0.000407 mTOR AA 0.001098	ACC_P	0.015762
Rapamycin 3.31E-05 mTOR to MTORC1 4.91E-05 4EBP1 Act 4.82E-05 4EBP1 inact 1.00E-06 PTEN inact 0.172623 S6 Act 0.000144 S6 inact 0.000407 mTOR AA 0.001098	ACC dephos	0.067668
mTOR to MTORC1 4.91E-05 4EBP1 Act 4.82E-05 4EBP1 inact 1.00E-06 PTEN inact 0.172623 S6 Act 0.000144 S6 inact 0.000407 mTOR AA 0.001098	PTEN act	1.01E-06
4EBP1 Act 4.82E-05 4EBP1 inact 1.00E-06 PTEN inact 0.172623 S6 Act 0.000144 S6 inact 0.000407 mTOR AA 0.001098	Rapamycin	3.31E-05
4EBP1 inact 1.00E-06 PTEN inact 0.172623 S6 Act 0.000144 S6 inact 0.000407 mTOR AA 0.001098	mTOR to MTORC1	4.91E-05
PTEN inact 0.172623 S6 Act 0.000144 S6 inact 0.000407 mTOR AA 0.001098	4EBP1 Act	4.82E-05
S6 Act 0.000144 S6 inact 0.000407 mTOR AA 0.001098	4EBP1 inact	1.00E-06
S6 inact 0.000407 mTOR AA 0.001098	PTEN inact	0.172623
mTOR AA 0.001098	S6 Act	0.000144
	S6 inact	0.000407
IRS1 1.00E-06	mTOR AA	0.001098
	IRS1	1.00E-06

Table B11: Initial Concentrations for Zoledronate withdrawal model

compartment ml	1
AA mmol/ml	10
PI3K mmol/ml	10
PI3K_P mmol/ml	1
S6K_P mmol/ml	1
PDK1 mmol/ml	10
PDK1_P mmol/ml	1
AKT mmol/ml	20
AKT_pT308 mmol/ml	0.5
AKT_pS473 mmol/ml	0.5
mTORC2_P mmol/ml	1
AKT_pT308_pS473	
mmol/ml	0.5
PI3K_V mmol/ml	10
PI3K_V_P mmol/ml	1

mTORC2 mmol/ml	5
TSC1/2 mmol/ml	5
TSC1/2_P mmol/ml	1
Rheb mmol/ml	5
Rheb(GTP) mmol/ml	0
mTORC1 mmol/ml	1
mTORC1_P mmol/ml	0
Rapamycin mmol/ml	0
S6K mmol/ml	5
FPPS mmol/ml	0
Ras(GTP) mmol/ml	0
Ras mmol/ml	5
FPPS_i mmol/ml	5
Zol mmol/ml	0
Ras(GDP) mmol/ml	0
Rheb(GDP) mmol/ml	0
Sink mmol/ml	0.1
FOXO3A mmol/ml	5
FOXO3A_P mmol/ml	1
AMPK mmol/ml	5
AMPK_P mmol/ml	1
ACC mmol/ml	5
ACC_P mmol/ml	1
mTOR mmol/ml	4
4EBP1 mmol/ml	5
4EBP1_pS65 mmol/ml	1
	1
PTEN mmol/ml	
PTEN mmol/ml PTEN_P mmol/ml	1
	5
PTEN_P mmol/ml	
PTEN_P mmol/ml S6 mmol/ml	5

 $Table\ B12-Final\ parameter\ values\ Zoledronate\ with drawal\ genetic\ algorithm\ MRC5\ cells$

PI3K AA	10.4001
PI3K dephos	1216.33
S6K feedback loop	4.90E-05
PDK1 act	3.57E-06
PDK1 dephos	0.003823
AKT to 308	0.010672
AKT308 to dual	3.16E-05
AKT to 473	0.000538
AKT473 to dual	296.786

	1
Dual to AKT	1.70E-06
Dual to 308	0.007599
Dual to 473	2.00E-06
308 to AKT	0.234654
473 to AKT	1.00E-06
PI3K_V act	4.92E-05
PI3K_V dephos	0.362583
mTORC2 act	1158.02
mTORC2 dephos	646.646
TSC1/2 de-act 308	9.20E-05
TSC1/2 de-act dual	1100.51
TSC1/2 act	0.084502
Rheb deact	43.8892
Rheb act	0.004139
mTORC1 act	0.001158
mTORC1 dephos	0.004717
S6K act	0.468937
S6K dephos	1.69E-06
PI3K Ras	3521.54
Ras act	0.000172
FPPS inact	2.08E-06
FPPS act	892.643
Ras deact	1.13178
Ras gdp-gtp	46.2456
Rheb GDP GTP	1.55E-05
Rheb deg	4700.51
Rheb(GDP) deg	1.00E-06
Rheb(GTP) deg	3208.74
Ras deg	0.248693
Ras(GDP) deg	0.457122
Ras(GTP) deg	0.001709
Sink - Rheb	8.43E-06
Sink Ras	0.001199
AKT_pT308_pS473 FOXO	4.87E-05
FOXO3A	0.014741
AMPK dephos	8.33287
AMPK_P	3.07E-05
AMPK PI3K	1.40E-06
ACC_P	0.269707
ACC dephos	0.209707
PTEN act	0.003468
Rapamycin	0.003408
mTOR to MTORC1	4.32E-06
4EBP1 Act	0.000979

4EBP1 inact	3.60E-05
PTEN inact	7.33E-05
S6 Act	0.071001
S6 inact	0.93514
mTOR AA	9.85E-06
mTOR AMPK	0.00413

Table B13 – Final parameter values Zoledronate withdrawal Hooke and Jeeves MRC5 cells

PI3K dephos 12 S6K feedback loop 4.9 PDK1 act 3.5	0.4001 216.33
S6K feedback loop 4.9 PDK1 act 3.5	
PDK1 act 3.5	OF 05
	0E-05
PDK1 daphos	7E-06
LDIVI debitos 0.0	03823
AKT to 308 0.0	10672
AKT308 to dual 3.1	6E-05
AKT to 473 0.0	00538
AKT473 to dual 29	96.786
Dual to AKT 1.7	0E-06
Dual to 308 0.0	07599
Dual to 473 2.0	0E-06
308 to AKT 0.2	34654
473 to AKT 1.0	0E-06
PI3K_V act 4.9	2E-05
PI3K_V dephos 0.3	62583
mTORC2 act	158.02
mTORC2 dephos 64	16.646
TSC1/2 de-act 308 9.2	0E-05
TSC1/2 de-act dual 11	100.51
TSC1/2 act 0.0	84502
Rheb deact 43	3.8892
Rheb act 0.0	04139
mTORC1 act 0.0	01158
mTORC1 dephos 0.0	04717
S6K act 0.4	68937
S6K dephos 1.6	9E-06
PI3K Ras 35	521.54
Ras act 0.0	00172
FPPS inact 2.0	8E-06
FPPS act 89	92.643
Ras deact 1.	13178
Ras gdp-gtp 46	5.2456
	5E-05
Rheb deg 47	700.51

Rheb(GDP) deg	1.00E-06
Rheb(GTP) deg	3208.74
Ras deg	0.248693
Ras(GDP) deg	0.457122
Ras(GTP) deg	0.001709
Sink - Rheb	8.43E-06
Sink Ras	0.001199
AKT_pT308_pS473 FOXO	4.87E-05
FOXO3A	0.014741
AMPK dephos	8.33287
AMPK_P	3.07E-05
AMPK PI3K	1.40E-06
ACC_P	0.269707
ACC dephos	0.01239
PTEN act	0.003468
Rapamycin	0.000878
mTOR to MTORC1	4.32E-06
4EBP1 Act	0.000979
4EBP1 inact	3.60E-05
PTEN inact	7.33E-05
S6 Act	0.071001
S6 inact	0.93514
mTOR AA	9.85E-06
mTOR AMPK	0.00413

 $Table\ B14-Final\ parameter\ values\ Zoledronate\ with drawal\ genetic\ algorithm\ MSCs$

PI3K AA	5.84151
PI3K dephos	618.028
S6K feedback loop	348.027
PDK1 act	0.000386
PDK1 dephos	1.62E-05
AKT to 308	8.24E-05
AKT308 to dual	5.00E-05
AKT to 473	0.008321
AKT473 to dual	0.100706
Dual to AKT	0.211206
Dual to 308	0.000812
Dual to 473	1.62717
308 to AKT	0.004431
473 to AKT	0.098522
PI3K_V act	0.000839
PI3K_V dephos	18.8424
mTORC2 act	845.079

mTORC2 dephos	0.034216
TSC1/2 de-act 308	0.562312
TSC1/2 de-act dual	0.000376
TSC1/2 act	6.07E-06
Rheb deact	0.054503
Rheb act	0.000133
mTORC1 act	0.00152
mTORC1 dephos	0.001098
S6K act	0.000221
S6K dephos	0.315642
PI3K Ras	0.153496
Ras act	0.001214
FPPS inact	0.300568
FPPS act	1190.82
Ras deact	2.37E-06
Ras gdp-gtp	2.09E-06
Rheb GDP GTP	0.123998
Rheb deg	747.199
Rheb(GDP) deg	3.83E-06
Rheb(GTP) deg	1115.69
Ras deg	9.16E-06
Ras(GDP) deg	7756.62
Ras(GTP) deg	0.06171
Sink - Rheb	6.09E-06
Sink Ras	795.293
AKT_pT308_pS473 FOXO	1.37E-06
FOXO3A	0.006307
AMPK dephos	0.40362
AMPK_P	2.83346
AMPK PI3K	1.00E-06
ACC_P	0.023975
ACC dephos	0.016203
PTEN act	1.17E-06
Rapamycin	1063.53
mTOR to MTORC1	6.81E-06
4EBP1 Act	1.15E-05
4EBP1 inact	0.007112
PTEN inact	0.001443
S6 Act	0.180538
S6 inact	0.005768
mTOR AA	4.97E-06
mTOR AMPK	8.52E-05
·	

 $Table\ B15-Final\ parameter\ values\ Zoledronate\ with drawal\ Hooke\ and\ Jeeves\ MSCs$

Г	1
PI3K AA	0.065762
PI3K dephos	8.18931
S6K feedback loop	1.00E-06
PDK1 act	2.56E-05
PDK1 dephos	1.00E-06
AKT to 308	0.020567
AKT308 to dual	0.000179
AKT to 473	0.003339
AKT473 to dual	1.00E-06
Dual to AKT	2.73E-06
Dual to 308	0.005259
Dual to 473	1.00E-06
308 to AKT	1.64447
473 to AKT	4.50E-06
PI3K_V act	1.01E-06
PI3K_V dephos	1.15903
mTORC2 act	2795.12
mTORC2 dephos	1.46504
TSC1/2 de-act 308	6.52E-05
TSC1/2 de-act dual	870.35
TSC1/2 act	0.096328
Rheb deact	28.5273
Rheb act	0.005602
mTORC1 act	0.00119
mTORC1 dephos	0.001169
S6K act	0.317022
S6K dephos	3.47E-06
PI3K Ras	9979.49
Ras act	0.000934
FPPS inact	2.08E-06
FPPS act	364.313
Ras deact	0.085705
Ras gdp-gtp	1.00E-06
Rheb GDP GTP	2.60E-05
Rheb deg	2421.94
Rheb(GDP) deg	1.25E-06
Rheb(GTP) deg	4144.52
Ras deg	0.04414
Ras(GDP) deg	0.057875
Ras(GTP) deg	0.00108
Sink - Rheb	8.91E-06
Sink Ras	0.001327
AKT_pT308_pS473	0.000351
	0.000001

FOXO	
FOXO3A	0.008369
AMPK dephos	0.207029
AMPK_P	6.78E-05
AMPK PI3K	2.66E-06
ACC_P	0.090173
ACC dephos	0.02306
PTEN act	1.00E-06
Rapamycin	0.000878
mTOR to MTORC1	1.07E-06
4EBP1 Act	1.00E-06
4EBP1 inact	0.000296
PTEN inact	0.000617
S6 Act	0.043336
S6 inact	0.226229
mTOR AA	1.00E-06
mTOR AMPK	1.00E-06

Table B16 – Reactions common to all models

Model Reactions	COPASI reaction
AKT phosphorylation pT308	PDK1_P + AKT -> PDK1_P + AKT_pT308
AKT phosphorylation pS473	AKT + mTORC2_P -> AKT_pS473 + mTORC2_P
4E-BP1 phosphorylation pS65	mTORC1_P + 4EBP1 -> mTORC1_P + 4EBP1_pS6
4E-BP1 dephosphorylation	4EBP1_pS65 -> 4EBP1
ACC phosphorylation pS79	$AMPK_P + ACC \rightarrow AMPK_P + ACC_P$
ACC dephosphorylation	ACC_P -> ACC
AKT dephosphorylation pT308	AKT_pT308 -> AKT
AKT dephosphorylation pS473	AKT_pS473 -> AKT
AKT pT308 phosphorylation to dual	AKT_pT308 + mTORC2_P -> AKT_pT308_pS473 - mTORC2_P AKT_pS473 + PDK1_P -> AKT_pT308_pS473 +
AKT pS473 phosphorylation to dual	PDK1_P
FOXO3A phosphorylation	AKT_pT308_pS473 + FOXO3A -> AKT_pT308_pS473 + FOXO3A_P
AMPK phosphorylation pT172	$AMPK + AA \rightarrow AMPK_P + AA$
AKMPK dephosphorylation pT172	$AMPK_P + ACC_P \rightarrow Sink + ACC_P$
PI3K dephosphorylation via ACC	$PI3K_P + ACC_P \rightarrow PI3K + ACC_P$
AKT Dual dephosphorylation to pT308	AKT_pT308_pS473 -> AKT_pT308
AKT Dual dephosphorylation to pS473	AKT_pT308_pS473 -> AKT_pS473
AKT Dual dephosphorylation to AKT	AKT_pT308_pS473 -> AKT
FOXO3A dephosphorylation	FOXO3A_P -> FOXO3A
mTORC1 phosphorylation pS2448 via Amino acids	$mTORC1 + AA \rightarrow mTORC1_P + AA$
mTORC1 dephosphorylation via AMPK	$mTORC1_P + ACC_P -> mTORC1 + ACC_P$
mTORC1 phosphorylation pS2448 via Rheb(GTP)	Rheb(GTP) + mTORC1 -> Rheb(GTP) + mTORC1_
mTORC1 dephosphorylation	mTORC1_P -> mTORC1
mTORC2 phosphorylation via PI3K_Varient	PI3K_V_P + mTORC2 -> PI3K_V_P + mTORC2_I
mTORC2 dephosphorylation	mTORC2_P -> mTORC2
PDK1 phosphorylation via PI3K	PI3K_P + PDK1 -> PI3K_P + PDK1_P
PDK1 dephosphorylation	PDK1_P -> PDK1
PI3K phosphorylation via Amino acids	$PI3K + AA \rightarrow PI3K_P + AA$
PI3K dephosphorylation	PI3K_P -> PI3K PI3K_V + AA + Ras(GTP) -> PI3K_V_P + AA +
PI3K_Varient phosphorylation via Amino acids + Ras	Ras(GTP)
PI3K_Varient dephosphorylation	$PI3K_V_P \rightarrow PI3K_V$
PTEN dephosphorylation via ACC	$PTEN_P + ACC_P \rightarrow PTEN + ACC_P$
PTEN phosphorylation	PTEN -> PTEN_P
Ras prenylation via FPPS	$Ras + FPPS \rightarrow Ras(GDP) + FPPS$
Ras degradation	Ras -> Sink
Ras GDP->GTP	Ras(GDP) -> Ras(GTP)
Ras GDP degradation	Ras(GDP) -> Sink
Ras GTP degradation	Ras(GTP) -> Sink
Rheb prenylation via FPPS	$Rheb + FPPS \rightarrow Rheb(GDP) + FPPS$
Rheb GTP inhibition via TSC1/2	TSC1/2 + Rheb(GTP) -> TSC1/2 + Rheb
Rheb degradation	Rheb -> Sink
Rheb GDP->GTP	Rheb(GDP) -> Rheb(GTP)
Rheb GDP degradation	Rheb(GDP) -> Sink
Rheb GTP degradation	Rheb(GTP) -> Sink
S6 phosphorylation via P70S6K	S6K_P + S6 -> S6_pS235 + S6K_P

S6 dephosphorylation	S6_pS235 -> S6
P70S6K phosphorylation via mTORC1	$mTORC1_P + S6K -> mTORC1_P + S6K_P$
P70S6K dephosphorylation	S6K_P -> S6K
PI3K dephosphorylation via P70S6K	PI3K_P + S6K_P -> PI3K + S6K_P
Ras formation	Sink -> Ras
Rheb Formation	Sink -> Rheb
TSC1/2 dephosphorylation	TSC1/2_P -> TSC1/2
TSC1/2 phosphorylation via AKT_pT308	AKT_pT308 + TSC1/2 -> AKT_pT308 + TSC1/2_P AKT_pT308_pS473 + TSC1/2 -> AKT_pT308_pS473
TSC1/2 phosphorylation via AKT_Dual	+ TSC1/2_P

Table 17 – Reactions specific to Zoledronate and Rapamycin models

Zoledronate specific model reactions	COPASI reaction
FPPS activation	FPPS_i -> FPPS
FPPS inhibition via Zoledronate	Zol + FPPS -> Zol + FPPS_i
Rapamycin specific model reactions	COPASI reaction
mTOR complex formation	mTOR -> mTORC1
mTOR complex inhibition via Rapamycin	mTORC1 + Rapamycin -> mTOR + Rapamycin

Table B18 – Reaction function forms for starvation-restimulation models

d([PI3K]·V _{compartment})	(200 005 00500 511)	d ([mTORC1_P]·V compartment)	= + V _{compartment} '(0.000389836 '["Rheb(GTP)"] '[mTORC1])
d <i>t</i>	= -V _{compartment} ·(7.32e-005 ·[PI3K] ·[AA])	d <i>t</i>	
	+ V _{compartment} · (1.95e-005 · [PI3K_P])		- V compartment '(1.31e-005 '[mTORC1_P])
	+ V _{compertment} *(3.47e-005 *[PI3K_P] *[S6K_P])		+ V _{compartment} · (0.000126073 · [mTORC1] · [AA])
	- V compartment '(2.18e-005 '[PI3K] '[AA] '["Ras(GTP)"])		- V compartment · (0.0172548 · [mTORC1_P] · [ACC_P])
	+ V _{compertment} ·(0.0310793 ·[PI3K_P] ·[ACC_P])	d ([S6K]· V _{compartment})	= -V _{compartment} ·(0.0224493 ·[mTORC1_P] ·[S6K])
d ([PI3K_P] · V compartment)	= + V _{compertment} · (7.32e-005 · [PI3K] · [AA])	d <i>t</i>	+V _{compartment} '(2.5e-006 '[S6K_P])
d <i>t</i>	- V compartment (1.95e-005 [PI3K_P])	d ([FPPS] · V compartment)	compartment (2.55 000 [50K_1])
	- V compartment (1.93e-903 [PI3K_P]) - V compartment (3.47e-905 [PI3K_P] [S6K_P])	d t	= -V _{compartment} ·(10000 ·[ZoI] ·[FPPS])
	+ V _{compartment} (2.18e-005 [PI3K]-[J3K]-[] (3RE-F))		+ V _{compartment} ·(10000 ·[FPPS_i])
	- V compartment (0.0310793 ·[PI3K_P] ·[ACC_P])	$d(["Ras(GTP)"] \cdot V_{compartment})$	
d([S6K_P]·V _{compartment})		d <i>t</i>	= -V _{compartment} (117.929 · ["Ras(GTP)"])
d £	= +V _{compartment} ·(0.0224493 ·[mTORC1_P] ·[S6K])		+ V _{compartment} ·(0.000146788 · ["Ras(GDP)"])
	- V _{compartment} ·(2.5e-006 ·[S6K_P])		- V compartment '(4.15865 '["Ras(GTP)"])
d([PDK1]·V _{compartment})		d([Ras]· V _{compartment})	= -V _{compartment} ·(856.741 ·[Ras] ·[FPPS])
d <i>t</i>	= -V _{compartment} (0.0456201 ·[PI3K_P] ·[PDK1])	d t	+ V compartment (117.929 · ["Ras(GTP)"])
	+ V _{compartment} ·(0.624943 ·[PDK1_P])		- V compartment (17.929 [Ras(GTP)])
d ([PDK1_P] · V compartment)	= + V _{compartment} · (0.0456201 · [PI3K_P] · [PDK1])		+ V _{compartment} (0.00348969 · [Sink])
d <i>t</i>	- V compartment (0.624943 · [PDK1_P])	d([FPPS_i]·V _{compartment})	
d ([AKT] · V compartment)		d t	= +V _{compartment} ·(10000 ·[ZoI] ·[FPPS])
d t	= $+V_{compartment}$ (0.000660378 [AKT_pT308])		- V _{compartment} ·(10000 ·[FPPS_i])
	+ V _{compartment} ·(0.0100104 ·[AKT_pS473])	$d(["Ras(GDP)"] \cdot V_{compartment})$	
	-V _{compartment} ·(6.2e-006 ·[PDK1_P] ·[AKT])	d <i>t</i>	= + V _{compartment} ·(856.741 ·[Ras] ·[FPPS])
	 - V_{compartment} (1.49e-006 [AKT] [mTORC2_P]) 		- V _{compartment} · (0.000146788 · ["Ras(GDP)"])
	+ V _{compertment} ·(0.00203374 ·[AKT_pT308_pS473])		- V _{compartment} · (0.000672359 · ["Ras(GDP)"])
$d \big([AKT_pT308] \cdot \mathcal{V}_{compartment} \big)$	= +V _{compartment} '(1.01e-005 '[AKT_pT308_pS473])	d (["Rheb(GDP)"] · V compartment)	= +V _{compartment} (0.000949145 '[Rheb] '[FPPS])
d <i>t</i>		d <i>t</i>	-V _{compartment} '(3.51e-006 · ["Rheb(GDP)"])
	-V _{compartment} ·(0.000660378 ·[AKT_pT308])		- V compartment '(0.00905857 ["Rheb(GDP)"])
	+ V compartment '(6.2e-006 '[PDK1_P] [AKT])	d ([FOXO3A] · V compartment)	compartment (0.00303037 [Ricb(GDF)])
AVEAUT -CATOLIV	- V compartment '(7541.31 '[AKT_pT308] '[mTORC2_P])	d t	= -V _{compartment} ·(2.61e-005 ·[AKT_pT308_pS473] ·[FOXO3A])
d([AKT_pS473]·V _{compartment})	= +V _{compartment} ·(8.89e-006·[AKT_pT308_pS473])		+ V _{compartment} ·(0.00136611 ·[FOXO3A_P])
ŭ.	- V _{compartment} ·(0.0100104 ·[AKT_pS473])	$d([FOXO3A_P] \cdot V_{compartment})$	
	+ V _{compartment} ·(1.49e-006 ·[AKT] ·[mTORC2_P])	d t	= + V _{compartment} ·(2.61e-005 ·[AKT_pT308_pS473] ·[FOXO3A])
	-V _{compartment} · (7681.41 · [AKT_pS473] · [PDK1_P])		- V _{compartment} · (0.00136611 · [FOXO3A_P])
$d([mTORC2_P] \cdot V_{compartment})$	= +V _{compartment} '(1.75e-006 ·[PI3K_V_P] ·[mTORC2])	d([AMPK] · V compartment)	= - V _{compartment} '(7.38403 '[AMPK] '[AA])
d <i>t</i>		d <i>t</i> d ([AMPK_P] · V compartment)	
	- V compartment * (0.000242127 * [mTORC2_P])	d t	= -V _{compartment} (0.659257 [AMPK_P] [ACC_P])
d([AKT_pT308_pS473]·V _{compartment}) = -V _{compartment} '(1.01e-005 '[AKT_pT308_pS473])		+ V _{compartment} ·(7.38403 ·[AMPK] ·[AA])
u t	-V _{compartment} ·(8.89e-006 ·[AKT_pT308_pS473])	d([ACC]·V _{compartment})	= -V _{compartment} ·(0.047271 ·[AMPK_P] ·[ACC])
	+ V _{compartment} · (7541.31 · [AKT_pT308] · [mTORC2_P])	d <i>t</i>	
	+ V _{compartment} · (7681.41 · [AKT_pS473] · [PDK1_P])	12/2022/22/23	+ V _{compartment} · (0.136097 · [ACC_P])
	-V _{compartment} ·(0.00203374 ·[AKT_pT308_pS473])	d([ACC_P]·V _{compartment})	= +V _{compartment} '(0.047271 '[AMPK_P] '[ACC])
$d \big([PI3K_V] \cdot \mathcal{V}_{compartment} \big)$		ū t	- V _{compartment} · (0.136097 · [ACC_P])
d <i>t</i>	= -V _{compartment} '(384.059 '[PI3K_V] '[AA] '["Ras(GTP)"])	$d([mTOR] \cdot V_{compartment})$	
	+ V _{compartment} ·(1.94e-005 ·[PI3K_V_P])	d t	= +V _{compartment} ·(0.0625194 ·[mTORC1] ·[Rapamycin])
d ([PI3K_V_P]·V _{compartment})	= +V _{compartment} ·(384.059 ·[PI3K_V] ·[AA] ·["Ras(GTP)"])		- V compartment *(0.000487867 *[mTOR])
αr	- V _{compartment} *(1.94e-005 *[PI3K_V_P])	d ([4EBP1] · V compartment)	= -V _{compartment} ·(0.00447304 ·[mTORC1_P] ·[4EBP1])
d ([mTORC2] · V compartment)	compertment	d <i>t</i>	
d t	= -V _{compartment} ·(1.75e-006 ·[PI3K_V_P] ·[mTORC2])	4/[4EDD1 =C6E].1/	+ V _{compartment} ·(0.000765057·[4EBP1_pS65])
	+ V _{compartment} (0.000242127 [mTORC2_P])	d ([4EBP1_pS65] · V compartment)	= +V _{compartment} '(0.00447304 '[mTORC1_P] '[4EBP1])
d ([TSC1/2] · V compartment)	= -V _{compartment} ·(6.02e-006·[AKT_pT308]·[TSC1/2])	u.	- V _{compartment} · (0.000765057 · [4EBP1_pS65])
d <i>t</i>		d ([PTEN] · V compartment)	
	-V _{compartment} ·(63.8319 ·[AKT_pT308_pS473] ·[TSC1/2])	d <i>t</i>	= + V _{compartment} *(0.0185298 *[PTEN_P] *[ACC_P])
A/FTSC1/2 PT-1/	+ V _{compertment} ·(0.159927 ·[TSC1/2_P])		- V compartment *(0.0200894 *[PTEN])
d ([TSC1/2_P]·V _{compartment})	= +V _{compartment} ·(6.02e-006 ·[AKT_pT308] ·[TSC1/2])	d ([PTEN_P] · V compartment)	= -V _{compartment} ·(0.0185298 ·[PTEN_P] ·[ACC_P])
αt	+ V _{compertment} ·(63.8319 ·[AKT_pT308_pS473] ·[TSC1/2])	d <i>t</i>	
	- V _{compartment} · (0.159927 · [TSC1/2_P])	40001.17	+ V _{compartment} · (0.0200894 · [PTEN])
d ([Rheb] * V compartment)		d ([S6] · V compartment)	= -V _{compartment} ·(0.0126269 ·[S6K_P] ·[S6])
d <i>t</i>	= + V _{compartment} · (0.0242015 · [TSC1/2] · ["Rheb(GTP)"])		+ V _{compartment} ·(0.174259 ·[S6_pS235])
	- V _{compartment} · (0.000949145 · [Rheb] · [FPPS])	$d ([S6_pS235] \cdot V_{compartment})$	
	-V _{compartment} ·(0.000796665 ·[Rheb])	d t	= + V _{compartment} · (0.0126269 · [S6K_P] · [S6])
	+ V _{compartment} · (0.112345 · [Sink])		- V _{compartment} ·(0.174259 ·[S6_pS235])
d (["Rheb(GTP)"] · V compartment)	= -V _{compartment} ·(0.0242015 ·[TSC1/2] ·["Rheb(GTP)"])		3 = [AKT_pS473] + [AKT_pT308_pS473]
d <i>t</i>	+ V _{compartment} · (3.51e-006 · ["Rheb(GDP)"])	AKT30	8 = [AKT_pT308]+[AKT_pT308_pS473]
	-V _{compartment} (56.2759 ["Rheb(GTP)"])		
d ([mTORC1] · V compartment)			
d t	= $-V_{compartment} \cdot (0.000389836 \cdot ["Rheb(GTP)"] \cdot [mTORC1])$		
	$+V_{compartment} \cdot (1.31e-005 \cdot [mTORC1_P])$		
	- V _{compartment} ·(0.0625194 ·[mTORC1] ·[Rapamycin])		
	+ V _{compartment} ·(0.000487867 ·[mTOR])		
	-V _{compartment} ·(0.000126073 ·[mTORC1] ·[AA])		
	$+ V_{compartment} \cdot (0.0172548 \cdot [mTORC1_P] \cdot [ACC_P])$		

Table B19 – Reaction function forms for Rapamycin withdrawal models

d ([PI3K] · V compertment)		d (["Ras(GTP)"] · V compertment)	
d t	= +V _{compartment} '(k1 _("PI3K dephos") '[PI3K_P_IRS1] '[PTEN])	d t	= -V compartment '(k1("Ras deact") '["Ras(GTP)"])
	+ V _{compartment} (k1 _("S6K feedback loop") [PI3K_P_IRS1] [S6K_P]) - V _{compartment} (k1 _(IRS1) [IRS1] [PI3K])		+ V _{compartment} '(k1 _("Ras gdp-gtp") '["Ras(GDP)"]) - V _{compartment} '(k1 _{("Ras(GTP) deg")} '["Ras(GTP)"])
$d([S6K_P] \cdot V_{compartment})$		$d([Ras] \cdot V_{compertment})$	
d t	= $+V_{compartment} \cdot (k1_{("S6K act")} \cdot [mTORC1_P] \cdot [S6K])$	d <i>t</i>	= - V compartment (k1("Ras act") [Ras] [FPPS])
	- V compartment '(k1 _("S6K dephos") '[S6K_P])		+ V compartment (k1("Ras deact") ["Ras(GTP)"])
d ([PDK1] · V compartment)	= -V _{compartment} ·(k1 _("PDK1 act") ·[PI3K_P_IRS1] ·[PDK1])		- V compartment '(k1 _("Ras deg") '[Ras]) + V compartment '(k1 _("Sink Rain") '[Sink])
ű i	+V _{compartment} (k1 _["PDK1 dephos"] [PDK1_P])	$d\big([FPPS_i] \cdot \mathcal{V}_{compartment} \big)$	
d ([PDK1_P] · V compartment)	= +V _{compartment} '(K1 _("PDK1 act") '[PI3K_P_IRS1] '[PDK1])	d t	= +V _{compartment} '(k1 _("FPPS inact") '[ZoI] '[FPPS])
d <i>t</i>	-V compartment ('K1("PDK1 act") ('PDK1_P])	d (FPDes(CDD)#1-1/	- V compartment '(k1 _("FPPS act") '(FPPS_II))
$d([AKT] \cdot V_{compartment})$		d (["Ras(GDP)"] · V compartment)	= +V _{compartment} (k1 _("Ras act") [Ras] [FPPS])
d t	= + V _{compartment} (k1 _("308 to AKT") '[AKT_pT308])		-V _{compartment} (k1 _{("Ras gdp-gtp")"} ["Ras(GDP)"])
	+ V _{compartment} '(k1 _("473 to AKT") '[AKT_pS473])		-V _{compartment} (k1 _{("Ras(GDP) deg")} ["Ras(GDP)"])
	- V _{compartment} '(k1 _("AKT to 308") '[PDK1_P] '[AKT]) - V _{compartment} '(k1 _("AKT to 473") '[AKT] '[mTORC2_P])	d(["Rheb(GDP)"] · V compertment)	= +V _{compartment} (k1 _("Rheb deact") [TSC1/2] ["Rheb(GTP)"])
	+ V _{compartment} (K1 _("Dual to AKT") [AKT_pT308_pS473])		$-V_{\text{compartment}} \cdot (k1_{(\text{"Rheb GDP GTP"})} \cdot [\text{"Rheb(GDP)"}])$
d([AKT_pT308]·V _{compertment})		$d([FOXO3A] \cdot V_{compartment})$	= -V _{compartment} (k1 _("AKT_pT308_pS473_FOXO") [AKT_pT308_pS473] [FOXO3A])
d t	= + V _{compartment} (k1 _("Dual to 308") [AKT_pT308_pS473])	d t	+ V _{compartment} (k1 _(FOXO3A) '[FOXO3A_P])
	- V compartment '(K1 _("308 to AKT") '(AKT_pT308)) + V compartment '(K1 _("AKT to 308") '(PDK1_P] '[AKT])	d ([FOXO3A_P] · V compartment)	
	-V compartment (K1("AKT to 308") [*AKT_pT308] [mTORC2_P])	d t	= $+V_{\text{compartment}}$ ($k1_{\text{("AKT_pT308_pS473 FOXO")}}$ [AKT_pT308_pS473] [FOXO3A]
d ([AKT_pS473]·V _{compartment})		10.00	- V _{compartment} '(k1 _(FOXO3A) '[FOXO3A_P])
d <i>t</i>	= + V _{compartment} (k1 _("Dual to 473") [AKT_pT308_pS473])	d ([AMPK] · V compartment)	= -V _{compartment} ·(k1 _(AMPK,P) ·[AMPK] ·[AA])
	- V compartment (K1 _("473 to AKT") '[AKT_pS473]) + V compartment (K1 _("4KT to 473") '[AKT] *[mTORC2_P])	d ([AMPK_P]·V compartment)	V
	-V compartment (k1("AKT to 493") [AKT_pS473] [PDK1_P])	d <i>t</i>	= -V _{compartment} ·(k1 _("AMPK dephas") ·[AMPK_P] ·[ACC_P])
$d([mTORC2_P] \cdot V_{compartment})$		d/[ACC]:I/	+ V compartment '(k1 _(AMPK,P) '[AMPK] ·[AA])
d <i>t</i>	= + V compartment '(k1 _["mTORC2 act"] '[PI3K_V_P] ·[mTORC2])	d ([ACC] · V compartment) d t	= -V _{compartment} (k1 _(ACC_P) ·[AMPK_P] ·[ACC])
d([AKT_pT308_pS473]·V _{compartment}	- V compartment (k1("mTORC2 dephos") [mTORC2_P])		$+V_{compartment} \cdot (k1_{("ACC dephos")} \cdot [ACC_P])$
d t	compartment (KL("Dual to 308") [AKT_p1300_p3173])	d ([ACC_P] · V compartment) d t	= +V _{compartment} ·(k1 _(ACC,P) ·[AMPK_P]·[ACC])
	-V _{compartment} (k1 _("Dual to 473") [AKT_pT308_pS473])	u	-V compartment (k1 _("ACC dephas") '[ACC_P])
	+ V _{compartment} '(k1 _("AKT308 to duel") '[AKT_pT308] '[mTORC2_P]) + V _{compartment} '(k1 _("AKT473 to duel") '[AKT_pS473] '[PDK1_P])	$d([mTOR] \cdot V_{compartment})$	= + V compartment (k1 _(Rapamycin) ·[mTORC1] ·[Rapamycin])
	- V compartment (K1("Dual to AKI") [AKT_pT308_pS473])	d <i>t</i>	
$d([PI3K_V] \cdot V_{compartment})$	= -V _{compartment} (k1 _("PSIK_V ect") [PI3K_V] [AA] ["Ras(GTP)"])	$d([4EBP1] \cdot V_{compartment})$	- V compartment (K1("mTOR to MTORC1") '[mTOR])
d <i>t</i>	+ V compartment (K1(*PIJK,V dephos*) (PIJK_V_P])	d t	= - V compertment '(k1("4EBP1 Act") '[mTORC1_P] '[4EBP1])
d([PI3K_V_P]·V _{compartment})		d ([4EBP1_pS65] · V compartment)	+ V compartment (k1 _("4EBP1 inact") [4EBP1_pS65])
d t	= $+V_{compartment} \cdot (k1_{["PI3K_V act")} \cdot [PI3K_V] \cdot [AA] \cdot ["Ras(GTP)"])$	d (= $+V_{compartment} \cdot (k1_{("4EBP1 Act")} \cdot [mTORC1_P] \cdot [4EBP1])$
d ([mTORC2] · V compartment)	- V compartment (k1("FEIK_V dephos") [PI3K_V_P])	75056 51100000111445	-V compartment (k1 _("4EBP1 inact") [4EBP1_pS65])
d t	= $-V_{compartment}$ (k1 _("mTORC2 act") ·[PI3K_V_P] ·[mTORC2])	d ([PTEN] · V compartment)	= +V _{compartment} (k1 _("PTEN act") :[PTEN_P] ·[S6K_P])
	+ V compartment '(k1 _("mTORC2 dephos") '[mTORC2_P])		-V _{compartment} (k1 _("PTEN inact") [PTEN])
d ([TSC1/2] · V compartment)	= -V _{compartment} '(k1 _("TSC1/2 de-act 308") '[AKT_pT308] ·[TSC1/2])	d ([PTEN_P] · V compartment)	= -V _{compartment} ·(k1 _("PTEN ect") ·[PTEN_P] ·[S6K_P])
	-V_compartment '(k1 _("TSC1/2 de-act dual") '[AKT_pT308_pS473] '[TSC1/2])	d <i>t</i>	+ V compartment (K1("PTEN inact") [PTEN])
	+ V _{compartment} '(k1 _("TSC1/2 act") '[TSC1/2_P])	$d([S6], V_{compartment})$	
d([TSC1/2_P]·V _{compartment})	= +V _{compartment} ·(k1 _("TSC1/2 de-act 308") ·[AKT_pT308] ·[TSC1/2])	d <i>t</i>	= -V _{compertment} (k1 _("56 Act") [S6K_P] [S6])
u i	+ V compertment (k1(TSC1/2 de-ect dual") (AKT_pT308_pS473) (TSC1/2))	d ([S6_pS235] · V _{comportment})	+ V _{compartment} (k1 _("S6 inact") ·[S6_pS235])
	-V _{compartment} ·(k1 _("TSC1/2 act") ·[TSC1/2_P])	d t	= +V _{compartment} '(k1 _("56 Act") '[S6K_P] · [S6])
d (["Rheb(GTP)"] · V compartment)	= -V _{compartment} ·(k1 _("Rheb deact") ·[TSC1/2] ·["Rheb(GTP)"])		-V _{compartment} ·(k1 _("S6 inect") ·[S6_pS235])
ű i	+ V _{compartment} (k1 _("Rheb GDP GTP") ["Rheb(GDP)"])	d([PI3K_IRS1]·V _{compartment})	= -V _{compartment} '(k1 _("PSIK AA") '[PI3K_IRS1] '[AA])
d ([mTORC1] · V compartment)	= -V _{compartment} (k1 _("mTORC1 act") '["Rheb(GTP)"] '[mTORC1])		-V _{compartment} ·(k1 _("PEIX Ras") ·[PI3K_IRS1] · [AA] · ["Ras(GTP)"])
d <i>t</i>			+ V _{compartment} (k1 _("AMPK PEIK") ·[PI3K_P_IRS1] ·[ACC_P])
	+ V _{compartment} '(k1 _("mTORC1 dephoe") '[mTORC1_P]) - V _{compartment} '(k1 _(Raparmycin) '[mTORC1] '[Rapamycin])	4/fbtak b tbctl/1/	+V _{compertment} '(k1 _(IRS1) '[IRS1] '[PI3K])
	+ V _{compartment} (k1 _("mTOR to MTORC1") [mTOR])	d([PI3K_P_IRS1]·V _{compartment}) d t	= $+V_{compartment}$ ($k1_{("PI3K,AA")}$ [PI3K_IRS1] [AA])
	- V compartment '(k1 _("mTOR AA") '[mTORC1] '[AA])		-V _{compartment} '(k1 _("PEIK dephos") '[PI3K_P_IRS1] · [PTEN])
d/fmTODC1 DI-I/	+V _{compartment} '(k1 _("mTOR AMPK") ·[mTORC1_P] ·[ACC_P])		 V_{compartment} (k1_("S6K feedback loop") '[PI3K_P_IRS1] '[S6K_P])
d ([mTORC1_P]· V compartment)	$= + V_{\text{compartment}} \cdot (k1_{[\text{"mTORC1 act"})} \cdot [\text{"Rheb(GTP)"}] \cdot [\text{mTORC1}])$		+ V compartment (k1 _("PI3K Ras") [PI3K_IRS1] [AA] ["Ras(GTP)"]) - V compartment (k1 _("AMMX PI3K") [PI3K_P_IRS1] [ACC_P])
	- V compartment (k1("mTORC1_dephos") [mTORC1_P])	d ([IRS1] · V compartment)	
	+ V _{compartment} ·(k1 _("mTOR AA") ·[mTORC1]·[AA])	d t	= +V _{compartment} '(k1 _("PIJK dephos") '[PIJK_P_IRS1] '[PTEN])
d(IS6KI+V)	- V _{compartment} '(k1 _("mTOR AMPK") '[mTORC1_P] ·[ACC_P])		+ V compartment (k1 ("S6K feedback loop") [PI3K_P_IRS1] [S6K_P])
$\frac{d([S6K] \cdot V_{compartment})}{dt}$	= $-V_{compartment}$ (k1 _("S&K ect") ·[mTORC1_P]·[S6K])	AKT47	-V _{compartment} (K1 _(IRS1) ·[IRS1] ·[PI3K]) 3 = [AKT_pS473] + [AKT_pT308_pS473]
	+ V compartment '(k1("S6K dephos") '[S6K_P])		B = [AKT_pT308] + [AKT_pT308_pS473]
d ([FPPS] · V compartment)	= -V _{compartment} (k1 _("FPPS inact") '[Zol] '[FPPS])		
u.	+ V compartment (k1("FPPS act") [FPPS_i])		

Table B20 - Reaction function forms for Zoledronate withdrawal models

